


All-Loop Singularities of Scattering Amplitudes in Massless Planar Theories

Igor Prlina,¹ Marcus Spradlin,^{1,2} and Stefan Stanojevic¹

¹*Department of Physics, Brown University, Providence, Rhode Island 02912, USA*

²*School of Natural Sciences, Institute for Advanced Study, Princeton, New Jersey 08540, USA*

 (Received 29 May 2018; published 21 August 2018)

In massless quantum field theories the Landau equations are invariant under graph operations familiar from the theory of electrical circuits. Using a theorem on the Y - Δ reducibility of planar circuits we prove that the set of first-type Landau singularities of an n -particle scattering amplitude in any massless planar theory, at any finite loop order, is a subset of those of a certain n -particle $\lfloor (n-2)^2/4 \rfloor$ -loop “ziggurat” graph. We determine this singularity locus explicitly for $n = 6$ and find that it corresponds precisely to the vanishing of the symbol letters familiar from the hexagon bootstrap in supersymmetric Yang-Mills (SYM) theory. Further implications for SYM theory are discussed.

DOI: [10.1103/PhysRevLett.121.081601](https://doi.org/10.1103/PhysRevLett.121.081601)

Introduction.—For over half a century, much has been learned from the study of singularities of scattering amplitudes in quantum field theory, an important class of which are encoded in the Landau equations [1]. This Letter combines two simple statements to arrive at a general result about such singularities. The first is based on the long appreciated and exploited analogy between Feynman diagrams and electrical circuits [2–5]. In massless field theories, the sets of solutions to the Landau equations are invariant under the elementary graph operations familiar from circuit theory, including the Y - Δ transformation that replaces a triangle subgraph with a trivalent vertex or vice versa. The second is a theorem of Gitler [6], who proved that all relevant (specified below) planar graphs can be Y - Δ reduced to a class we call ziggurats (Fig. 2).

We conclude that the n -particle $\lfloor (n-2)^2/4 \rfloor$ -loop ziggurat graph encodes all possible first-type Landau singularities of any n -particle amplitude at any finite loop order in any massless planar theory. In Sec. VI, we discuss several interesting implications of our result for planar $\mathcal{N} = 4$ supersymmetric Yang-Mills (SYM) theory, which provided the motivation for this work [7–10].

Landau graphs and singularities.—The Landau equations encapsulate the singularity structure of scattering amplitudes via Landau graphs. In planar quantum field theories, the exclusive focus of this Letter, we need only consider plane graphs. An L -loop m -point plane Landau graph is a plane graph with $L + 1$ faces and m distinguished vertices, called terminals, that lie on a common

face called the unbounded face. Henceforth, we use “vertex” only for those that are not terminals, and “face” only for the L faces that are not the unbounded face.

Each edge j is assigned a four-momentum vector q_j , the analog of electric current. At each vertex, the vector sum of incoming momenta equals that of the outgoing momenta (current conservation). This constraint is not applied at terminals, which are the locations where a circuit can be probed by connecting external sources or sinks of current. In field theory, these correspond to the momenta carried by incoming or outgoing particles. If we label the terminals $a = 1, \dots, m$ (in cyclic order around the unbounded face) and let P_a denote the four-momentum flowing into the graph at terminal a , then energy-momentum conservation requires that $\sum_a P_a = 0$, and it implies that precisely L of the q_j 's are linearly independent.

Our interest lies in understanding the loci in P_a -space on which amplitudes may have singularities. A Landau graph is said to have Landau singularities of the first type (LS) at values of P_a for which the Landau equations [1]

$$\alpha_j q_j^2 = 0 \quad \text{for each edge } j, \quad \text{and} \quad (1)$$

$$\sum_{\text{edges } j \in \mathcal{F}} \alpha_j q_j = 0 \quad \text{for each face } \mathcal{F} \quad (2)$$

admit solutions for the Feynman parameters α_j (omitting the trivial solution where all $\alpha_j = 0$). In Eq. (1), we omitted a term proportional to m_j^2 that would be present in massive theories.

The Landau equations generally admit several branches of solutions. The leading LS of a graph \mathcal{G} are those associated to branches having $q_j^2 = 0$ for all j (regardless of whether any of the α_j 's are zero). LS associated to branches on which one or more of the q_j^2 are not zero (in which case the

Published by the American Physical Society under the terms of the Creative Commons Attribution 4.0 International license. Further distribution of this work must maintain attribution to the author(s) and the published article's title, journal citation, and DOI. Funded by SCOAP³.

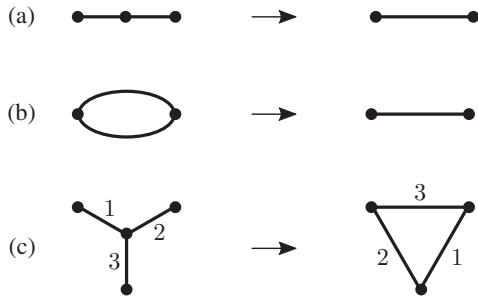


FIG. 1. Elementary circuit moves that preserve solution sets of the massless Landau equations: (a) series reduction, (b) parallel reduction, and (c) Y - Δ reduction.

corresponding α_j 's must necessarily vanish) can be interpreted as leading singularities of a relaxed graph, obtained from \mathcal{G} by contracting the edges associated to the vanishing α_j 's.

A graph is called c connected if it remains connected after the removal of any $c - 1$ vertices. The set of LS for a 1-connected graph is the union of those associated to each 2-connected component since the Landau equations completely decouple. Therefore, we can confine our attention to 2-connected graphs.

Elementary circuit operations.—We call Eq. (2) the Kirchhoff conditions in recognition of their circuit analog where the α_j 's play the role of resistances. The analog of the on shell conditions (1) is mysterious, but a remarkable feature of massless theories is that: The graph moves that are familiar from elementary electrical circuit theory preserve the solution sets of Eqs. (1) and (2), and hence, the sets of LS in any massless field theory.

Series reduction [Fig. 1(a)] removes any vertex of degree two. Since $q_2 = q_1$ by momentum conservation, the Landau equations are trivially preserved if the two edges with Feynman parameters α_1, α_2 are replaced by a single edge carrying momentum $q' = q_1 = q_2$ and Feynman parameter $\alpha' = \alpha_1 + \alpha_2$.

Parallel reduction [Fig. 1(b)] collapses any bubble subgraph. It is easy to verify (see e.g., Appendix A.1 of [8]) the Landau equations are preserved if the two edges of the bubble are replaced by a single edge carrying momentum $q' = q_1 + q_2$ and Feynman parameter $\alpha' = \alpha_1\alpha_2/(\alpha_1 + \alpha_2)$.

The Y - Δ reduction [Fig. 1(c)] replaces a vertex of degree three (a “ Y ”) with a triangle subgraph (a “ Δ ”) or vice versa. Generically, the Feynman parameters α_i of the Δ are related to those of the Y , which we call β_i , by

$$\beta_1 = \frac{\alpha_2\alpha_3}{\alpha_1 + \alpha_2 + \alpha_3}, \quad \text{and cyclic.} \quad (3)$$

On branches where one or more of the parameters vanish, this relation must be suitably modified. For example, if a branch of solutions for a graph containing a Y has $\beta_1 = \beta_2 = 0$ but β_3 nonzero, then the corresponding branch for the reduced graph has $\alpha_3 = 0$ but α_1, α_2 nonzero.

The invariance of the Kirchhoff conditions (2) under Y - Δ reduction follows straightforwardly from these Feynman

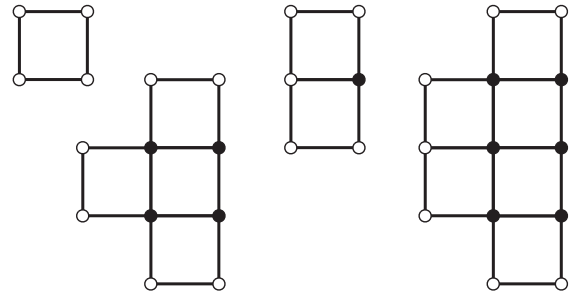


FIG. 2. The four-, six-, five-, and seven-terminal ziggurat graphs. The open circles are terminals, and the filled circles are vertices. The pattern continues in the obvious way, but note, there is an essential difference between ziggurat graphs with an even or odd number of terminals in that only the latter have a terminal of degree three.

parameter assignments. The invariance of the on shell conditions (1) is nontrivial, and it follows from the analysis in Appendix A.2 of [8].

The proof of the crucial theorem of [6] that we employ in the next section relies on three additional, relatively simple moves, that trivially preserve the essential content of the Landau equations. These are (d) the deletion of a “tadpole” (edges that connect a vertex or terminal to itself), (e) the deletion of a “hanging propagator” (a vertex of degree one and the edge connected to it), and (f) the contraction of an edge connected to a terminal of degree one (called “FP assignment” [11]). The last of these is, strictly speaking, not completely trivial at the level of the Landau equations; it just removes an otherwise uninteresting bubble singularity.

Reduction of planar graphs.—The reduction of graphs under circuit operations is a well-studied problem in the mathematical literature. When it is declared that a certain subset of vertices are to be considered terminals (which may not be removed by series or Y - Δ reduction) the corresponding problem is called terminal Y - Δ reducibility. Aspects of this problem have been studied in [11–16], including an application to Feynman diagrams in [17]. For our purpose, the key result comes from the Ph.D. thesis of I. Gitler [6], who proved that any planar 2-connected graph with m terminals lying on the same face can be reduced to a graph of the kind shown in Fig. 2, which we call ziggurat graphs, or to a minor thereof. We denote the m -terminal ziggurat graph by \mathcal{T}_m , and note that, a minor of a graph \mathcal{G} is any graph that can be obtained from \mathcal{G} by a sequence of edge contractions and/or edge deletions.

An edge contraction corresponds to a relaxation, while an edge deletion corresponds to setting the associated q_j to zero. Therefore, the LS associated to any minor of a graph \mathcal{G} are a subset of those associated to \mathcal{G} . Consequently, we do not need to explicitly enumerate all minors of \mathcal{T}_m ; their LS are already contained in the set of singularities of \mathcal{T}_m itself.

It is conventional to discuss scattering amplitudes for a fixed number n of external particles, each of which carries some momentum p_i that in massless theories satisfies

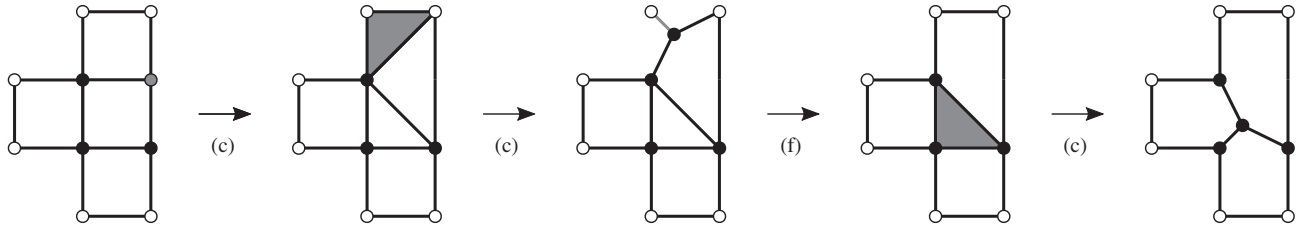


FIG. 3. The six-terminal zigurat graph can be reduced to a three-loop graph by a sequence of three Y - Δ reductions and one FP assignment. In each case the vertex, edge, or face to be transformed is highlighted in gray.

$p_i^2 = 0$. These individual particles are denoted graphically by attaching a total of n external edges to the terminals, with at least one per terminal. Any graph with $m \leq n$ terminals is potentially relevant to finding the Landau singularities of an n -particle amplitude. However, if $m < n$, then \mathcal{T}_m is a minor of \mathcal{T}_n , so the LS of the former are a subset of those of the latter. Therefore, to find the LS of an n -particle amplitude, it suffices to find those of the n -terminal zigurat graph \mathcal{T}_n with precisely one external edge attached to each terminal. We call this the n -particle zigurat graph and finally summarize: The first-type Landau singularities of an n -particle scattering amplitude in any massless planar field theory are a subset of those of the n -particle zigurat graph.

While the LS of the zigurat graph exhaust the set of singularities that may appear in any massless planar theory, we cannot rule out the possibility that in certain special theories, the actual set of singularities may be smaller because of a cancellation between the contributions of different graphs to a given amplitude. We discuss this further in Sec. VI.

The Y - Δ reduction changes (and generally reduces) the number of faces of a graph, so the above statement does not hold at a fixed loop order L ; rather it is an all-order relation about the full set of LS of n -particle amplitudes. Since the n -particle zigurat graph has $L = \lfloor (n-2)^2/4 \rfloor$ faces, a single computation at $\lfloor (n-2)^2/4 \rfloor$ -loop order suffices to expose all possible Landau singularities of any n -particle amplitude.

This bound is unnecessarily high. Gitler's theorem does not imply that zigurat graphs cannot be reduced to graphs of a lower loop order, and in general, this is possible: Figure 3 shows that \mathcal{T}_6 can be reduced to a three-loop wheel graph whose 6-particle avatar we show in Fig. 4. Zigurat graphs with more than six terminals can also be further reduced, but we have not found a lower bound on the loop order that can be obtained for a general n .

Landau analysis of the wheel.—Here, we analyze the Landau equations for the graph shown in Fig. 4. The six external edges carry momenta p_1, \dots, p_6 subject to $\sum_i p_i = 0$ and $p_i^2 = 0$ for each i . Using momentum conservation at each vertex, the momentum q_j carried by each internal edge can be expressed in terms of the p_i and three other linearly independent momenta, which we

take to be l_r , for $r = 1, 2, 3$, as shown in the figure. Initially, we consider the leading LS, for which we impose the on shell conditions

$$\begin{aligned} (l_1 - p_1)^2 = l_1^2 = (l_1 + p_2)^2 = 0, \\ (l_2 - p_3)^2 = l_2^2 = (l_2 + p_4)^2 = 0, \\ (l_3 - p_5)^2 = l_3^2 = (l_3 + p_6)^2 = 0, \\ (l_1 + p_2 - l_2 + p_3)^2 = 0, \\ (l_2 + p_4 - l_3 + p_5)^2 = 0, \\ (l_3 + p_6 - l_1 + p_1)^2 = 0. \end{aligned} \quad (4)$$

For generic p_i , there are 16 discrete solutions for the l_r 's, which we denote by $l_r^*(p_i)$. To enumerate these solutions, it is technically helpful to use momentum twistor variables [18], in which case the solutions can be associated with on shell diagrams [19]. Although the analysis is still applicable to general massless planar theories, in the special context of SYM theory, two cut solutions have MHV support, twelve NMHV, and two NNMHV.

The Kirchhoff conditions are

$$\begin{aligned} 0 = \alpha_1(l_1 - p_1) + \alpha_2 l_1 + \alpha_3(l_1 + p_2) \\ + \alpha_{10}(l_3 + p_6 - l_1 + p_1) + \alpha_{11}(l_1 + p_2 - l_2 + p_3), \\ 0 = \alpha_4(l_2 - p_3) + \alpha_5 l_2 + \alpha_6(l_2 + p_4) \\ + \alpha_{11}(l_1 + p_2 - l_2 + p_3) + \alpha_{12}(l_2 + p_4 - l_3 + p_5), \\ 0 = \alpha_7(l_3 - p_5) + \alpha_8 l_3 + \alpha_9(l_3 + p_6) \\ + \alpha_{12}(l_2 + p_4 - l_3 + p_5) + \alpha_{10}(l_3 + p_6 - l_1 + p_1). \end{aligned} \quad (5)$$

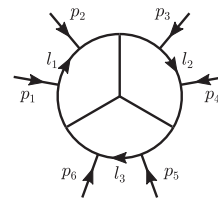


FIG. 4. The three-loop six-particle wheel graph. The leading LS of this graph exhaust all possible LS of six-particle amplitudes in any massless planar field theory, to any finite loop order.

Nontrivial solutions to this 12×12 linear system exist only if the associated Kirchhoff determinant $K(p_i, l_r)$ vanishes. By evaluating K on each solution $l_r = l_r^*(p_i)$, the condition for the existence of a nontrivial solution to the Landau equations can be expressed entirely in terms of the external momenta. Using

$$u = \frac{s_{12}s_{45}}{s_{123}s_{345}}, \quad v = \frac{s_{23}s_{56}}{s_{234}s_{123}}, \quad w = \frac{s_{34}s_{61}}{s_{345}s_{234}}, \quad (6)$$

where $s_{i\dots j} = (p_i + \dots + p_j)^2$, we find that $K(p_i, l_r^*(p_i)) = 0$ can only be satisfied if an element of

$$S = \left\{ u, v, w, 1-u, 1-v, 1-w, \frac{1}{u}, \frac{1}{v}, \frac{1}{w} \right\} \quad (7)$$

vanishes. Therefore, the three-loop six-particle wheel graph has LS on the locus

$$\mathcal{S} = \bigcup_{s \in S} \{s = 0\}. \quad (8)$$

It is straightforward to analyze all subleading LS corresponding to relaxations. We refer the reader to [7,8,10] where this type of analysis has been carried out in detail in several examples. We find no additional LS beyond those that appear at leading order. We conclude that the LS of any six-particle amplitude in any massless planar field theory, at any finite loop order, are given by Eqs. (7) and (8), or a proper subset thereof.

Second-type singularities.—The LS studied here do not exhaust all possible singularities of amplitudes in quantum field theories. There also exist “second-type” singularities [20,21], sometimes called “non-Landauian” [22]. These arise in loop integrals as pinch singularities at infinite loop momentum, and they are encoded in a modified version of Eqs. (1) and (2).

In the next section, we consider the special case of the SYM theory, which possesses a remarkable dual conformal symmetry [23–25], implying that there is no invariant notion of “infinity” in momentum space. We therefore expect that second-type singularities should be absent in any dual conformal invariant theory [7]. Because zigurat graphs are manifestly dual conformal invariant, the LS of the zigurat graphs should capture the entire “dual conformally invariant part” of the singularity structure of all massless planar theories; this means the singularity loci that do not involve the infinity twistor.

Planar SYM theory.—In Sec. III, we acknowledged that in certain theories, the actual set of singularities of amplitudes may be strictly smaller than that of the zigurat graphs due to cancellations. Contrary to the expectation that SYM theory might seem the most promising candidate to exhibit such cancellations, we now argue that: Perturbative amplitudes in SYM theory exhibit first-type Landau singularities on all such loci that are possible in any massless planar field theory.

Our results suggest that this statement is true separately in each helicity sector. Specifically, for any fixed n and any $0 \leq k \leq n-4$, there is a finite value of $L_{n,k}$, such that the singularity locus of the L -loop n -particle N^k MHV amplitude is identical to that of the n -particle zigurat graph for all $L \geq L_{n,k}$. In order to verify this claim, it suffices to construct an n -particle on shell diagram with N^k MHV support that has the same LS as the n -particle zigurat graph; or equivalently, to write down a corresponding configuration of lines inside the amplituhedron [26] $\mathcal{A}_{n,k,L}$ for some sufficiently high L .

To see that this is plausible, note that, the appearance of a given singularity at some fixed k and L implies the existence of the same singularity at lower k but higher L by performing the opposite of parallel reductions—doubling one or more edges of the relevant graph to make bubbles. For example, while one-loop MHV amplitudes do not have singularities of three-mass box type, two-loop MHV amplitudes do [27]. Similarly, while two-loop MHV amplitudes do not have singularities of the four-mass box type, we expect that three-loop MHV and two-loop NMHV amplitudes do. (Our analysis is silent on the question of whether the symbol alphabets of these amplitudes contain square roots; see Sec. VII of [9].)

It is simple to convert the n -particle zigurat graph into a valid on shell diagram with MHV support by doubling each internal edge into a bubble. In this way, it is easy to write an explicit mutually positive configuration of lines inside the MHV amplituhedron. While this construction suffices to demonstrate the claim, it is overkill; we expect MHV support to be reached at a much lower loop level than this argument would require, as can be checked on a case by case basis for a small n .

Symbol alphabets.—Let us comment on the connection of our work to symbol alphabets. All of the singularities tabulated in Eq. (8) are known to appear in both MHV and NMHV six-particle amplitudes, starting at the two-loop order [28,29]. Indeed, the hypothesis that there are no new singularity loci at any higher loop order (which we now consider to be proven) underlies a bootstrap program that has made it possible for impressive explicit computations of six-particle amplitudes in SYM theory [29–35]. An analogous program for $n=7$ has allowed for the computation of symbols of seven-particle amplitudes [36,37].

The hexagon bootstrap involves, in addition to the quantities appearing in Eq. (7), three particular algebraic functions y_u, y_v, y_w that also vanish only on the same locus \mathcal{S} . This highlights the fact that the connection between LS and symbol alphabets is somewhat indirect. Knowledge of the former tells us about the locus where symbol letters vanish [38] or have branch points (see Sec. VII of [9]). In order to determine what the symbol letters of an amplitude actually are away from these loci, it seems necessary to invoke some other kind of structure; cluster algebras may have a role to play here [39,40].

Conclusion.—We leave several questions for future work. What is the minimum loop order to which the n -particle ziggurat graph can be reduced? Can one characterize LS for an arbitrary n , generalizing the result for $n = 6$ in Sec. IV? It is possible to classify second-type singularities, even if only in certain theories? The graph moves reviewed in Sec. II preserve the LS even for nonplanar graphs; are there results on nonplanar Y - Δ reducibility (see e.g., [41,42]) that may be useful for nonplanar (but still massless) theories?.

The ziggurat graphs, and those to which they can be reduced, might warrant further study for their own sake. They generalize those studied in [43,44], and they are particular cases of the graphs that have attracted recent interest, e.g., in [45,46], in the context of “fishnet” theories. We have only looked at their singularity loci; it would be interesting to explore the structure of their cuts, perhaps in connection with the coaction studied in [47–51].

In SYM theory, the technology might exist to address more detailed questions. For a general n and k , what is the minimum loop order at which the Landau singularities of the n -particle N^k MHV amplitude saturate? Is there a direct connection between Landau singularities, ziggurat graphs, and cluster algebras? For amplitudes of a generalized polylogarithm type, what are the actual symbol letters for a general n , k , and loop order? How do LS manifest themselves in general amplitudes that are of more complicated functional type?.

We are grateful to C. Colbourn for correspondence, to N. Arkani-Hamed for stimulating discussions, to J. Bourjaily for helpful comments on the draft, and to T. Dennen, J. Stankowicz, and A. Volovich for collaboration on closely related work. We are especially indebted to I. Gitler for sending us the relevant portion of his Ph.D. thesis. This work was supported in part by the US Department of Energy under contract No. DE-SC0010010 Task A and the Simons Fellowship Program in Theoretical Physics (MS).

[1] L. D. Landau, *Nucl. Phys.* **13**, 181 (1959).
 [2] J. Mathews, *Phys. Rev.* **113**, 381 (1959).
 [3] T. T. Wu, *Phys. Rev.* **123**, 678 (1961).
 [4] T. T. Wu, *Phys. Rev.* **123**, 689 (1961).
 [5] J. Bjorken and S. Drell, *Relativistic Quantum Fields* (McGraw-Hill, New York, 1965).
 [6] I. Gitler, Delta-Wye-Delta Transformations: Algorithms and Applications,” Ph.D. Thesis, University of Waterloo, 1991.
 [7] T. Dennen, M. Spradlin, and A. Volovich, *J. High Energy Phys.* **03** (2016) 069.
 [8] T. Dennen, I. Prlina, M. Spradlin, S. Stanojevic, and A. Volovich, *J. High Energy Phys.* **06** (2017) 152.
 [9] I. Prlina, M. Spradlin, J. Stankowicz, S. Stanojevic, and A. Volovich, *J. High Energy Phys.* **05** (2018) 159.
 [10] I. Prlina, M. Spradlin, J. Stankowicz, and S. Stanojevic, *J. High Energy Phys.* **04** (2018) 049.
 [11] I. Gitler and F. Sagols, *Network* **57**, 174 (2011).

[12] S. B. Akers, *Oper. Res.* **8**, 311 (1960).
 [13] T. A. Feo and J. S. Provan, *Oper. Res.* **41**, 572 (1993).
 [14] Y. C. Verdière, I. Gitler, and D. Vertigan, *Commentarii mathematici Helvetici* **71**, 144 (1996).
 [15] D. Archdeacon, C. J. Colbourn, I. Gitler, and J. S. Provan, *J. Graph Theory* **33**, 83 (2000).
 [16] L. Demasi and B. Mohar, *Proceedings of the Twenty-Sixth Annual ACM-SIAM Symposium on Discrete Algorithms, San Diego, California, 2015* (SIAM, Philadelphia, 2015) pp. 1728–1742.
 [17] A. T. Suzuki, *Can. J. Phys.* **92**, 131 (2014).
 [18] A. Hodges, *J. High Energy Phys.* **05** (2013) 135.
 [19] N. Arkani-Hamed, J. L. Bourjaily, F. Cachazo, A. B. Goncharov, A. Postnikov, and J. Trnka, arXiv:1212.5605.
 [20] D. B. Fairlie, P. V. Landshoff, J. Nuttall, and J. C. Polkinghorne, *J. Math. Phys.* **3**, 594 (1962).
 [21] R. J. Eden, P. V. Landshoff, D. I. Olive, and J. C. Polkinghorne, *The Analytic S-Matrix* (Cambridge University Press, Cambridge, England, 1966).
 [22] R. E. Cutkosky, *J. Math. Phys.* **1**, 429 (1960).
 [23] J. M. Drummond, J. Henn, V. A. Smirnov, and E. Sokatchev, *J. High Energy Phys.* **01** (2007) 064.
 [24] L. F. Alday and J. M. Maldacena, *J. High Energy Phys.* **06** (2007) 064.
 [25] J. M. Drummond, J. Henn, G. P. Korchemsky, and E. Sokatchev, *Nucl. Phys.* **B828**, 317 (2010).
 [26] N. Arkani-Hamed and J. Trnka, *J. High Energy Phys.* **10** (2014) 030.
 [27] S. Caron-Huot, *J. High Energy Phys.* **12** (2011) 066.
 [28] A. B. Goncharov, M. Spradlin, C. Vergu, and A. Volovich, *Phys. Rev. Lett.* **105**, 151605 (2010).
 [29] L. J. Dixon, J. M. Drummond, and J. M. Henn, *J. High Energy Phys.* **01** (2012) 024.
 [30] L. J. Dixon, J. M. Drummond, and J. M. Henn, *J. High Energy Phys.* **11** (2011) 023.
 [31] L. J. Dixon, J. M. Drummond, M. von Hippel, and J. Pennington, *J. High Energy Phys.* **12** (2013) 049.
 [32] L. J. Dixon, J. M. Drummond, C. Duhr, M. von Hippel, and J. Pennington, *Proc. Sci.*, LL2014 (2014) 077.
 [33] L. J. Dixon and M. von Hippel, *J. High Energy Phys.* **10** (2014) 065.
 [34] L. J. Dixon, M. von Hippel, and A. J. McLeod, *J. High Energy Phys.* **01** (2016) 053.
 [35] S. Caron-Huot, L. J. Dixon, A. McLeod, and M. von Hippel, *Phys. Rev. Lett.* **117**, 241601 (2016).
 [36] J. M. Drummond, G. Papathanasiou, and M. Spradlin, *J. High Energy Phys.* **03** (2015) 072.
 [37] L. J. Dixon, J. Drummond, T. Harrington, A. J. McLeod, G. Papathanasiou, and M. Spradlin, *J. High Energy Phys.* **02** (2017) 137.
 [38] J. Maldacena, D. Simmons-Duffin, and A. Zhiboedov, *J. High Energy Phys.* **01** (2017) 013.
 [39] J. Golden, A. B. Goncharov, M. Spradlin, C. Vergu, and A. Volovich, *J. High Energy Phys.* **01** (2014) 091.
 [40] J. Drummond, J. Foster, and Ö. Gürdoğan, *Phys. Rev. Lett.* **120**, 161601 (2018).
 [41] D. K. Wagner, *Discrete Appl. Math.* **180**, 158 (2015).
 [42] I. Gitler and G. Sandoval-Angeles, *ENDM* **62**, 129 (2017).
 [43] J. L. Bourjaily, A. J. McLeod, M. Spradlin, M. von Hippel, and M. Wilhelm, *Phys. Rev. Lett.* **120**, 121603 (2018).

- [44] J. L. Bourjaily, Y. H. He, A. J. McLeod, M. von Hippel, and M. Wilhelm, [arXiv:1805.09326](#) [*Phys. Rev. Lett.* (to be published)].
- [45] D. Chicherin, V. Kazakov, F. Loebbert, D. Müller, and D. I. Zhong, *J. High Energy Phys.* **05** (2018) 003.
- [46] B. Basso and L. J. Dixon, *Phys. Rev. Lett.* **119**, 071601 (2017).
- [47] S. Abreu, R. Britto, C. Duhr, and E. Gardi, *J. High Energy Phys.* **10** (2014) 125.
- [48] S. Abreu, R. Britto, C. Duhr, and E. Gardi, *J. High Energy Phys.* **06** (2017) 114.
- [49] S. Abreu, R. Britto, C. Duhr, and E. Gardi, *Phys. Rev. Lett.* **119**, 051601 (2017).
- [50] S. Abreu, R. Britto, C. Duhr, and E. Gardi, *J. High Energy Phys.* **12** (2017) 090.
- [51] S. Abreu, R. Britto, C. Duhr, and E. Gardi, *Proc. Sci., RADCOR2017* (**2018**) 002.

Boundaries of amplituhedra and NMHV symbol alphabets at two loops

I. Prlina,^a M. Spradlin,^{a,b} J. Stankowicz^{a,c} and S. Stanojevic^a

^a*Department of Physics, Brown University,
Providence RI 02912, U.S.A.*

^b*School of Natural Sciences, Institute for Advanced Study,
Princeton NJ 08540, U.S.A.*

^c*Kavli Institute for Theoretical Physics, University of California,
Santa Barbara CA 93106, U.S.A.*

E-mail: igor_prlina@brown.edu, marcus_spradlin@brown.edu,
james_stankowicz@brown.edu, stefan_stanojevic@brown.edu

ABSTRACT: In this sequel to [3] we classify the boundaries of amplituhedra relevant for determining the branch points of general two-loop amplitudes in planar $\mathcal{N} = 4$ super-Yang-Mills theory. We explain the connection to on-shell diagrams, which serves as a useful cross-check. We determine the branch points of all two-loop NMHV amplitudes by solving the Landau equations for the relevant configurations and are led thereby to a conjecture for the symbol alphabets of all such amplitudes.

KEYWORDS: Scattering Amplitudes, Supersymmetric Gauge Theory

ARXIV EPRINT: [1712.08049](https://arxiv.org/abs/1712.08049)

Contents

1	Introduction	1
2	Classification of two-loop boundaries	2
2.1	Identifying the relevant boundaries	3
2.2	Merging one-loop boundaries	4
2.3	Planarity from positivity	4
2.4	Establishing the lower bound on helicity	6
3	Presentation of the results	8
3.1	Resolutions	8
3.2	Relaxations	10
3.3	Closing comments	11
4	The connection with on-shell diagrams	15
4.1	On-shell diagrams	16
4.2	Examples at one and two loops	17
5	Landau singularities of two-loop NMHV amplitudes	21
5.1	Computational approaches	22
5.2	A sample two-loop diagram	24
5.3	Two-loop NMHV symbol alphabets	28
5.4	Eight-point example	30
6	Conclusion	31
A	Notation	32
B	Twistor diagrams to Landau diagrams	33

1 Introduction

It has been a long-standing goal to determine scattering amplitudes in quantum field theory from knowledge of their analytic structure coupled with other basic physical and mathematical input. In planar $\mathcal{N} = 4$ super-Yang-Mills theory (which we refer to as SYM theory), the current state of the art for carrying out explicit computations of multi-loop amplitudes is a bootstrap program that relies fundamentally on assumptions about the location of branch points of certain amplitudes.

The aim of the research program initiated in [1, 2] for MHV amplitudes and generalized to non-MHV amplitudes in [3] (to which this paper should be considered a sequel) is to

provide an *a priori* derivation of the set of branch points for any given amplitude. For sufficiently simple amplitudes in SYM theory¹ this information can go a long way by leading to natural guesses for the *symbol alphabets* [4] of various amplitudes. The possibility to do so exists because of the simple fact pointed out in [5] that the locus in the space of external data $\text{Conf}_n(\mathbb{P}^3)$ where the symbol letters of a given amplitude vanish should be the same as the locus where the corresponding Landau equations [6, 7] admit solutions. A slight refinement of this statement, to account for the fact that amplitudes in general have algebraic branch cuts in addition to logarithmic cuts, was discussed in section 7 of [3].

The hexagon bootstrap program, which has succeeded in computing all six-point amplitudes through five loops [8–12], relies on the hypothesis that these amplitudes can have branch points only at fifteen specific loci in the space of external data $\text{Conf}_6(\mathbb{P}^3)$. Similarly the heptagon bootstrap [13], which has revealed the symbols of the seven-point four-loop MHV and three-loop NMHV amplitudes [14], assumes 49 particular branch points. Ultimately we may hope for an all-loop proof of these hypotheses about six- and seven-point amplitudes, but in this paper we focus on the less ambitious goal of deriving the singularity loci for all two-loop NMHV amplitudes in SYM theory. The result, summarized in section 5.3, leads to a natural conjecture for the symbol alphabets of these amplitudes which we hope may be employed in the near future by bootstrappers eager to study this class of amplitudes.

The rest of this paper is organized as follows. In section 2 we develop a procedure for constructing certain boundaries of two-loop amplituhedra by “merging” one-loop configurations of the type classified in the prequel [3]. In section 3 we organize the results according to helicity and codimensionality (the number of on-shell conditions satisfied by each configuration) and discuss some subtleties about overconstrained configurations that require resolution. Section 4 discusses the connection between branches of solutions to on-shell conditions and on-shell diagrams, which provides a useful cross-check of our classification. In section 5 we discuss the analysis of the Landau equations for configurations relevant for NMHV amplitudes and, in eqs. (5.17) and (5.18), we present a conjecture for the symbol alphabets of all two-loop NMHV amplitudes.

2 Classification of two-loop boundaries

In this section we classify certain boundaries of two-loop amplituhedra. This analysis builds heavily on sections 3–5 of [3], and in particular we show how to recycle the one-loop boundaries classified there by “merging” pairs of one-loop boundaries into two-loop boundaries. We find that two different formulations of the amplituhedron — the original formulation in terms of C and D matrices [18], and the reformulation in terms of sign flips [19] — play two complementary roles, exactly as in [3]. Specifically, the former is useful for establishing the existence of boundaries by constructing explicit C and D matrix representatives, while the latter is useful for establishing the non-existence of any other boundaries.

¹General amplitudes lie outside the class of generalized polylogarithm functions that have well-defined symbols, see for example [15–17] for a discussion of this in the context of SYM theory.

Before proceeding let us dispense of some important details that would otherwise overcomplicate our exposition. There is a parity symmetry between $A_{n,k,L}$, the n -point, N^k MHV, L -loop amplitude in SYM theory, and its parity conjugate $A_{n,n-k-4,L}$. For fixed n , amplitudes become increasingly complicated as k is increased from zero, but after $k \sim n/2$ they must begin to decrease in complexity until the upper bound $k = n - 4$. In what follows we will often make use of lower bounds on k , or on constructions that increment k by 1. In making these arguments, we always have in mind that k is sufficiently small compared to n . In other words, unless otherwise stated, we are always working in the “low- k ” regime, to use the terminology of [3]. At the very end of our analysis, once we have all of the desired results in this regime, we appeal to parity symmetry in order to translate low- k results into high- k results. However the details of matching these two regimes near the midpoint $k \sim n/2$ can be quite intricate, even moreso at two loops than it was in the one-loop analysis of [3].

2.1 Identifying the relevant boundaries

In general, a configuration $(Y, \mathcal{L}^{(1)}, \mathcal{L}^{(2)})$ lies on a boundary of a two-loop amplituhedron if at least one item on the following menu is satisfied:

- (1) Y is such that some four-brackets of the form $\langle a \ a+1 \ b \ b+1 \rangle$ vanish,
- (2) $\mathcal{L}^{(1)}$ satisfies some on-shell conditions $\langle \mathcal{L}^{(1)} \ a_1 \ a_1+1 \rangle = \dots = \langle \mathcal{L}^{(1)} \ a_{d_1} \ a_{d_1}+1 \rangle = 0$,
- (3) $\mathcal{L}^{(2)}$ satisfies some on-shell conditions $\langle \mathcal{L}^{(2)} \ b_1 \ b_1+1 \rangle = \dots = \langle \mathcal{L}^{(2)} \ b_{d_2} \ b_{d_2}+1 \rangle = 0$,
- (4) or $\langle \mathcal{L}^{(1)} \ \mathcal{L}^{(2)} \rangle = 0$.

Above and through the remainder of the paper, we always take $\langle ABCD \rangle \equiv [YABCD]$ — what we call projected four-brackets following [19].

For the purpose of finding Landau singularities we are always interested only in loop momenta $(\mathcal{L}^{(1)}, \mathcal{L}^{(2)})$ that exist for generic projected external data, i.e., for generic Y , so we disregard possibility (1) in all that follows. Next, we note that for configurations which do not satisfy (4), the Landau equations decouple into two separate sets of equations on the two individual loop momenta, so there can be no new Landau singularities beyond those already found at one loop. Therefore in all that follows we only consider boundaries on which $\langle \mathcal{L}^{(1)} \ \mathcal{L}^{(2)} \rangle = 0$. The Landau equations similarly degenerate if either d_1 or d_2 (defined in the preceding paragraph) is zero, so we are only interested in configurations with $d_1 d_2 > 0$.

The above considerations motivate us to define an \mathcal{L} -boundary of a two-loop amplituhedron as a configuration $(Y, \mathcal{L}^{(1)}, \mathcal{L}^{(2)})$ for which Y is such that the projected external data are generic, $\langle \mathcal{L}^{(1)} \ \mathcal{L}^{(2)} \rangle = 0$, and each \mathcal{L} satisfies at least one on-shell condition of the form $\langle \mathcal{L} \ a \ a+1 \rangle = 0$. In particular, these conditions imply that both $(Y, \mathcal{L}^{(1)})$ and $(Y, \mathcal{L}^{(2)})$ must lie on boundaries of some one-loop amplituhedra; each of these must therefore be one of the 19 branches tabulated in table 1 of [3].

2.2 Merging one-loop boundaries

The preceding analysis suggests that the boundaries of two-loop amplituhedra can be understood by merging various one-loop boundaries. Let us now see how this works in detail. Suppose that $(Y^{(1)}, \mathcal{L}^{(1)})$ and $(Y^{(2)}, \mathcal{L}^{(2)})$ lie on boundaries of $\mathcal{A}_{n,k_1,1}$ and $\mathcal{A}_{n,k_2,1}$, respectively. Then they can be represented as $Y^{(\alpha)} = C^{(\alpha)}\mathcal{Z}$ and $\mathcal{L}^{(\alpha)} = D^{(\alpha)}\mathcal{Z}$, where for each $\alpha \in \{1, 2\}$, the matrices $C^{(\alpha)}$, $\begin{pmatrix} D^{(\alpha)} \\ C^{(\alpha)} \end{pmatrix}$, and $D^{(\alpha)}$ (as shown in [3]), are all non-negative. In order to streamline the argument we initially consider k_1 and k_2 to be the smallest values of helicity for which boundaries of the desired class exist, and we take each pair $(C^{(\alpha)}, D^{(\alpha)})$ to have the form of one of the 19 branches shown in sections 4.2 through 4.4 of [3]. We will show that such a pair of valid one-loop boundary configurations can be uplifted into a valid two-loop boundary configuration $(C, D^{(1)}, D^{(2)})$ satisfying $\langle \mathcal{L}^{(1)} \mathcal{L}^{(2)} \rangle = 0$ by constructing an appropriate matrix C from $C^{(1)}$ and $C^{(2)}$.

The process of merging two boundaries depends on whether the two loop momenta $\mathcal{L}^{(1)}, \mathcal{L}^{(2)}$ each pass through some common external point Z_i . If they do, then we say that they *manifestly intersect* and the condition that $\langle \mathcal{L}^{(1)} \mathcal{L}^{(2)} \rangle = 0$ is automatically satisfied. In this case we can simply stack the two individual C -matrices on top of each other in order to form

$$C = \begin{pmatrix} C^{(1)} \\ C^{(2)} \end{pmatrix}. \tag{2.1}$$

If, on the other hand, the two loop momenta do not manifestly intersect, then we can still ensure that $\langle \mathcal{L}^{(1)} \mathcal{L}^{(2)} \rangle = [(C\mathcal{Z}) \mathcal{L}^{(1)} \mathcal{L}^{(2)}] = 0$ by adding one additional suitably crafted row to C . Specifically, if $A^{(\alpha)}, B^{(\alpha)}$ are any four points in \mathbb{P}^n such that $\mathcal{L}^{(\alpha)} = (A^{(\alpha)}\mathcal{Z}, B^{(\alpha)}\mathcal{Z})$, then adding a row to C that is any linear combination of these four points will guarantee that $\langle \mathcal{L}^{(1)} \mathcal{L}^{(2)} \rangle = 0$.

In this manner we have constructed a candidate for a configuration on the boundary of $\mathcal{A}_{n,k,2}$ with $k = k_1 + k_2$ in the case of manifest intersection, or $k = k_1 + k_2 + 1$ otherwise. It remains to verify that this configuration is *valid*, which means that C can be chosen so that it and the matrices $\begin{pmatrix} D^{(1)} \\ C \end{pmatrix}$, $\begin{pmatrix} D^{(2)} \\ C \end{pmatrix}$, and $\begin{pmatrix} D^{(1)} \\ D^{(2)} \\ C \end{pmatrix}$ are all non-negative.

2.3 Planarity from positivity

Let us begin by analyzing the non-negativity of the C -matrix shown in eq. (2.1). The nonzero columns of each $C^{(\alpha)}$ (which may be read off from sections 4.3 and 4.4 of [3]) are grouped into clusters corresponding to the sets of contiguous indices appearing in the on-shell conditions satisfied by the corresponding $\mathcal{L}^{(\alpha)}$. For example, for a boundary on which the three-mass triangle on-shell conditions $\langle \mathcal{L}^{(1)} i i+1 \rangle = \langle \mathcal{L}^{(1)} j j+1 \rangle = \langle \mathcal{L}^{(1)} k k+1 \rangle = 0$ are satisfied, the C -matrix is zero except in six columns grouped into three clusters $\{i, i+1\}$, $\{j, j+1\}$ and $\{k, k+1\}$.

When we stack two C -matrices together, the result can be one of two different cases depending on whether or not the clusters of $C^{(1)}$ are cyclically adjacent compared to the

clusters of $C^{(2)}$. If so, then the stacked C -matrix has the schematic form

$$C = \begin{pmatrix} C^{(1)} \\ C^{(2)} \end{pmatrix} = \begin{pmatrix} \cdots 0 \star 0 \star 0 0 0 0 0 \cdots \\ \cdots 0 0 0 0 0 \star 0 \star 0 \cdots \end{pmatrix} \begin{matrix} \} k_1 \text{ rows} \\ \} k_2 \text{ rows} \end{matrix} \quad (2.2)$$

which we call *planar*; otherwise it is of the form

$$C = \begin{pmatrix} C^{(1)} \\ C^{(2)} \end{pmatrix} = \begin{pmatrix} \cdots 0 \star 0 0 0 \star 0 0 0 \cdots \\ \cdots 0 0 0 \star 0 0 0 \star 0 \cdots \end{pmatrix} \begin{matrix} \} k_1 \text{ rows} \\ \} k_2 \text{ rows} \end{matrix}. \quad (2.3)$$

which we call *non-planar*. In eqs. (2.2) and (2.3) each \star is shorthand for one or more contiguous columns (i.e, clusters) of non-zero entries, and we suppress displaying columns shared by the two C -matrices, which are not relevant to our argument. Also as indicated the top (bottom) row is shorthand for k_1 (k_2) rows. Given that our starting point is a pair of matrices $C^{(1)}$, $C^{(2)}$ that are each non-negative, it is clear that the resulting stacked C -matrix has a chance to be non-negative (for certain values of its parameters) only for planar configurations; the minors of eq. (2.3) manifestly have non-definite signs.

In cases when $\mathcal{L}^{(1)}$ and $\mathcal{L}^{(2)}$ do not manifestly intersect we need to add an additional row to C as described in the previous section. This additional row can be considered part of either $C^{(1)}$ or $C^{(2)}$. Since the coefficients in this row can be arbitrary and still preserve $\langle \mathcal{L}^{(1)} \mathcal{L}^{(2)} \rangle = 0$, the coefficients can always be chosen such that the enlarged C -matrix is non-negative. The conclusion that only planar C 's can be made positive still holds.

The nomenclature of ‘planar’ and ‘non-planar’ clusters is appropriate in light of the fact that the locations of the clusters precisely correspond to the sets of indices appearing in on-shell conditions listed in points (2) and (3) at the beginning of section 2.1. In a configuration like eq. (2.2) there exist a, b such that all of the on-shell conditions satisfied by $\mathcal{L}^{(1)}$ lie in the range $\{a, a+1, \dots, b, b+1\}$ while all of the on-shell conditions satisfied by $\mathcal{L}^{(2)}$ lie in the range $\{b, b+1, \dots, a, a+1\}$ (as usual, all indices are always understood mod n). Consequently, the two-loop Landau diagram depicting the merged sets of on-shell conditions (together with the propagator $\langle \mathcal{L}^{(1)} \mathcal{L}^{(2)} \rangle$ shared between the two loops) is planar. By the same argument, a nonplanar configuration such as eq. (2.3) is necessarily associated to a nonplanar Landau diagram.

Now let us consider the non-negative matrices $\begin{pmatrix} D^{(\alpha)} \\ C^{(\alpha)} \end{pmatrix}$ for the two individual initial boundary configurations ($\alpha = 1$ or 2). We require that these matrices stay non-negative when $C^{(\alpha)}$ is replaced by C . By the argument given in section 4.7 of [3], this will be the case if the rows added to $C^{(\alpha)}$ have nonzero entries only in the gaps between clusters of $C^{(\alpha)}$. But this is just another way to phrase the planarity condition described above, so again we see that planarity is enforced, this time by requiring non-negativity of $\begin{pmatrix} D^{(\alpha)} \\ C \end{pmatrix}$.

The final step in establishing the validity of the configuration $(C, D^{(1)}, D^{(2)})$ is checking that the matrix $\begin{pmatrix} D^{(1)} \\ D^{(2)} \\ C \end{pmatrix}$ is non-negative. In the parameterization we have chosen, all of the maximal minors of this matrix actually vanish. If the two loops manifestly intersect this can be checked by looking at the form of the (C, D) matrices tabulated in [3]. If they do not manifestly intersect the analysis is even easier, since in such cases we have included in C a row that is some linear combination of the four rows of $D^{(1)}, D^{(2)}$.

The argument as presented appears to fail if either of the individual one-loop boundaries is MHV, in which case there is no C matrix. However, for MHV boundaries it can be seen from the expressions tabulated in section 4.2 of [3] that the D -matrix serves the same role as the C -matrix played in the above argument. For example, if $k_1 = 0$ so that $C^{(1)}$ is empty, then $C = C^{(2)}$ so the requirement that $\begin{pmatrix} D^{(1)} \\ C \end{pmatrix} = \begin{pmatrix} D^{(1)} \\ C^{(2)} \end{pmatrix}$ must be non-negative requires that the clusters of $D^{(1)}$ be cyclically adjacent compared to the clusters of $C^{(2)}$. If both k_1 and k_2 are zero then C is empty and the same conclusion follows from consideration of the matrix $\begin{pmatrix} D^{(1)} \\ D^{(2)} \end{pmatrix}$. Therefore, in all cases, the various non-negativity conditions imply that the Landau diagram must be planar. This emergent planarity was discussed in context of MHV amplitudes in [20].

In conclusion, we have established that a boundary of $\mathcal{A}_{n,k,2}$ can be constructed by “merging” a boundary of $\mathcal{A}_{n,k_1,1}$ with a boundary of $\mathcal{A}_{n,k_2,1}$, with $k - k_1 - k_2 = 0$ or 1 depending on whether $\mathcal{L}^{(1)}$ and $\mathcal{L}^{(2)}$ manifestly intersect. So far we have considered k_1 and k_2 to saturate the lower bounds shown in table 1 of [3], but once a valid configuration $(C, D^{(1)}, D^{(2)})$ has been constructed as described in this section, it can be lifted to higher values of k by growing the C -matrix according to a suitably modified version of the argument given in section 4.7 of that reference.

2.4 Establishing the lower bound on helicity

We have shown that it is possible to merge two one-loop boundaries with (minimal) helicities k_1 and k_2 in order to generate two-loop boundaries with helicities $k \geq k_1 + k_2$. The merging algorithm we have described cannot generate boundaries with k below this lower bound. In this section we prove that we have not overlooked any potential two-loop boundaries. To do so, we use the formulation of amplituhedra in terms of sign flips [19] (reviewed also in section 2.2 of [3]) in order to prove the lower bound.

The proof is essentially a loop-level version of the factorization argument presented in section 6 of [19] for tree-level amplituhedra. Let $(\mathcal{L}^{(1)}, \mathcal{L}^{(2)})$ be some configuration of loop momenta on some codimension $d_1 + d_2 + 1$ boundary of $\mathcal{A}_{n,k,2}$, satisfying the on-shell conditions

$$\langle \mathcal{L}^{(1)} a_1 a_{1+1} \rangle = \dots = \langle \mathcal{L}^{(1)} a_{d_1} a_{d_1+1} \rangle = 0, \tag{2.4}$$

$$\langle \mathcal{L}^{(2)} b_1 b_{1+1} \rangle = \dots = \langle \mathcal{L}^{(2)} b_{d_2} b_{d_2+1} \rangle = \langle \mathcal{L}^{(1)} \mathcal{L}^{(2)} \rangle = 0, \tag{2.5}$$

with the sets of indices $\{a_1, \dots, a_{d_1}\}$ and $\{b_1, \dots, b_{d_2}\}$ cyclically ordered and with $1 \leq d_1, d_2 \leq 4$ as detailed in [3]. Planarity requires that all of the b 's fall inside an interval between two consecutive a 's; specifically, there exists some j such that $a_j \leq b_i \leq a_{j+1}$ for all i . Once we have identified this value of j , let's backtrack and consider factorization (as described in [19]) on the boundary $\langle \mathcal{L}^{(1)} a_j a_{j+1} \rangle = \langle \mathcal{L}^{(1)} a_{j+1} a_{j+1+1} \rangle = 0$. Then $\mathcal{L}^{(1)}$ passes through some point A on the line $(a_j a_{j+1})$ and some point B on the line $(a_{j+1} a_{j+1+1})$. With $\mathcal{L}^{(1)} = (AB)$ we consider the sets of momentum twistors

$$V = \{A, Z_{a_{j+1}}, \dots, Z_{a_{j+1}}, B\}, \tag{2.6}$$

$$W = \{B, Z_{a_{j+1+1}}, \dots, Z_{a_j}, A\}. \tag{2.7}$$

Thinking of V and W separately as “(projected) external data” for sub-amplituhedra describing two smaller sets of scattering particles,² it follows using arguments analogous to those in section 6 of [19] that they lie in the principal domain for helicities k_V and k_W satisfying $k_V + k_W = k$ where k is the original helicity sector of the (projected) external data $\{Z_i\}$.

Under the assumption that the two-loop configuration $(Y, \mathcal{L}^{(1)}, \mathcal{L}^{(2)})$ is a boundary of $\mathcal{A}_{n,k,2}(Z)$, we prove below the following statements:

- if $\mathcal{L}^{(1)}$ is a solution to the on-shell conditions (2.4) with minimum helicity k_1 , then $k_V \geq k_1$, and similarly,
- if $\mathcal{L}^{(2)}$ is a solution to the on-shell conditions (2.5) with minimum helicity k_2 , then $k_W \geq k_2$.

Once we show this, it follows immediately that the two-loop configuration $(\mathcal{L}^{(1)}, \mathcal{L}^{(2)})$ cannot be a valid boundary unless

$$k = k_V + k_W \geq k_1 + k_2. \tag{2.8}$$

Proof. The minimum values of helicity k_{\min} for which sets of one-loop one-shell conditions admit solutions inside the closure of $\mathcal{A}_{n,k,1}$ were derived in section 4 of [3]. In that analysis, the fact that a set of on-shell conditions does not have valid solutions of a certain type for $k < k_{\min}$ followed from the fact that the non-negativity constraints on the C and $\binom{D}{C}$ matrices required certain sequences of (projected) four-brackets to contain at least k_{\min} sign flips. In analyzing the constraints on the solution $\mathcal{L}^{(1)}$ to eq. (2.4), the relevant sequences of four-brackets are of the form $\langle \alpha \beta \gamma \bullet \rangle$ where α, β and γ are functions of the momentum twistors belonging to the set $S = \{Z_{a_1}, Z_{a_1+1}, \dots, Z_{a_{d_1}}, Z_{a_{d_1}+1}\}$ only, and the required sign flips occur between adjacent entries in S . Note that there are two points $(Z_{a_j}$ and $Z_{a_{j+1}+1})$ in S that lie outside V , the “(projected) external data” for one of the sub-amplituhedra under consideration. However, because A lies on the line $(a_j a_{j+1})$ and B lies on the line $(a_{j+1} a_{j+1}+1)$, we clearly have $(a_j a_{j+1}) = (a_j A)$ and similarly $(a_{j+1} a_{j+1}+1) = (a_{j+1} B)$ so we can choose to express α, β and γ in terms of momentum twistors belonging to

$$S' = \{Z_{a_1}, Z_{a_1+1}, \dots, Z_{a_j}, A, B, Z_{a_{j+1}+1}, \dots, Z_{a_{d_1}}, Z_{a_{d_1}+1}\} \subset V. \tag{2.9}$$

Therefore the abovementioned sequences can all be expressed in terms of the “(projected) external data” associated to the V sub-amplituhedron. Since there are k_1 sign flips in S' , it must be the case that $k_V \geq k_1$. It follows similarly that $k_W \geq k_2$. \square

In eq. (2.8) we derived an inequality $k \geq k_1 + k_2$, and at the end of section 2.2 we explained that two-loop configurations have support starting from $k = k_1 + k_2$ or $k = k_1 + k_2 + 1$. In section 2.2 we effectively defined k_1 and k_2 as the minimum helicities for configurations of loop momenta satisfying sets of disjoint on-shell conditions, not including

²We put “(projected) external data” in quotation marks when it is (projected) external data only for a sub-amplituhedron, not for the full amplituhedron.

the shared propagator. However, in this section the definition of k_2 (only) now includes the shared propagator (cf. eq. (2.5)). Effectively, this means that the k_2 here is the same as in section 2.2 only for manifest intersection, but one greater than the latter in the case of non-manifest intersection.

3 Presentation of the results

It is now a straightforward exercise to explicitly enumerate all possible pairs of one-loop boundaries, using those listed in table 1 of [3], and to determine the minimum value of k such that the merged configuration is a valid boundary of $\mathcal{A}_{n,k,2}$. The resulting set is too large to display in a single figure of the type of figure 1 of [3] (which is a summary of the analogous results at one loop), so we focus first on the maximal codimension boundaries. Each involves a total of $d = 8$ on-shell conditions: the shared condition $\langle \mathcal{L}^{(1)} \mathcal{L}^{(2)} \rangle = 0$ together with seven conditions on the two loop momenta ($d_1 + d_2 = 7$, in the notation of section 2.1).

We find a total of 14 topologically distinct maximal codimension configurations at two loops, which are summarized in figure 1. The figure emphasizes the fact that all 14 varieties of \mathcal{L} -boundaries can be obtained by some sequence of helicity-increasing operations \mathcal{K} (defined in section 5.2 of [3]) acting on just two primitive diagrams, one at MHV level and one at NMHV level. The entirety of this figure should be thought of as the two-loop $d = 8$ analog of the one-loop $d = 4$ column of figure 2 of that reference. In the figure, an arrow labeled by i indicates that the diagram at the end of the arrow can be obtained by acting with \mathcal{K}_i on the diagram at the beginning of the arrow. An arrow carries two labels if the result of acting with two different instances of \mathcal{K} gives topologically equivalent diagrams, in which case only the diagram corresponding to the first label on the arrow is shown. Note that for each diagram, the minimal value of k precisely matches the number of non-MHV intersections.

3.1 Resolutions

In each of the 14 twistor diagrams shown in figure 1, the configuration manifestly exhibits a total of $2n_{\text{filled}} + n_{\text{empty}} = 8$ on-shell conditions, where n_{filled} is the number of filled nodes and n_{empty} is the number of empty nodes (including, in each diagram, the node at the intersection of the two loop momenta).

However, on certain sufficiently high codimension boundaries, additional on-shell conditions can be implied by the others and are therefore “accidentally” satisfied. This phenomenon occurs for the four twistor diagrams in figure 1 that have been drawn with a filled node at the point Z_i and two empty nodes in close proximity (grouped in a faint gray circle in figure 1), representing the four on-shell conditions

$$\langle \mathcal{L}^{(1)} i-1 i \rangle = \langle \mathcal{L}^{(1)} i i+1 \rangle = \langle \mathcal{L}^{(2)} i i+1 \rangle = \langle \mathcal{L}^{(1)} \mathcal{L}^{(2)} \rangle = 0. \tag{3.1}$$

The first three conditions are satisfied by $\mathcal{L}^{(1)} = (Z_i, A)$ and $\mathcal{L}^{(2)} = (\alpha Z_i + (1 - \alpha)Z_{i+1}, B)$ for any points A, B . Then, for generic A and B , the fourth condition in eq. (3.1) implies

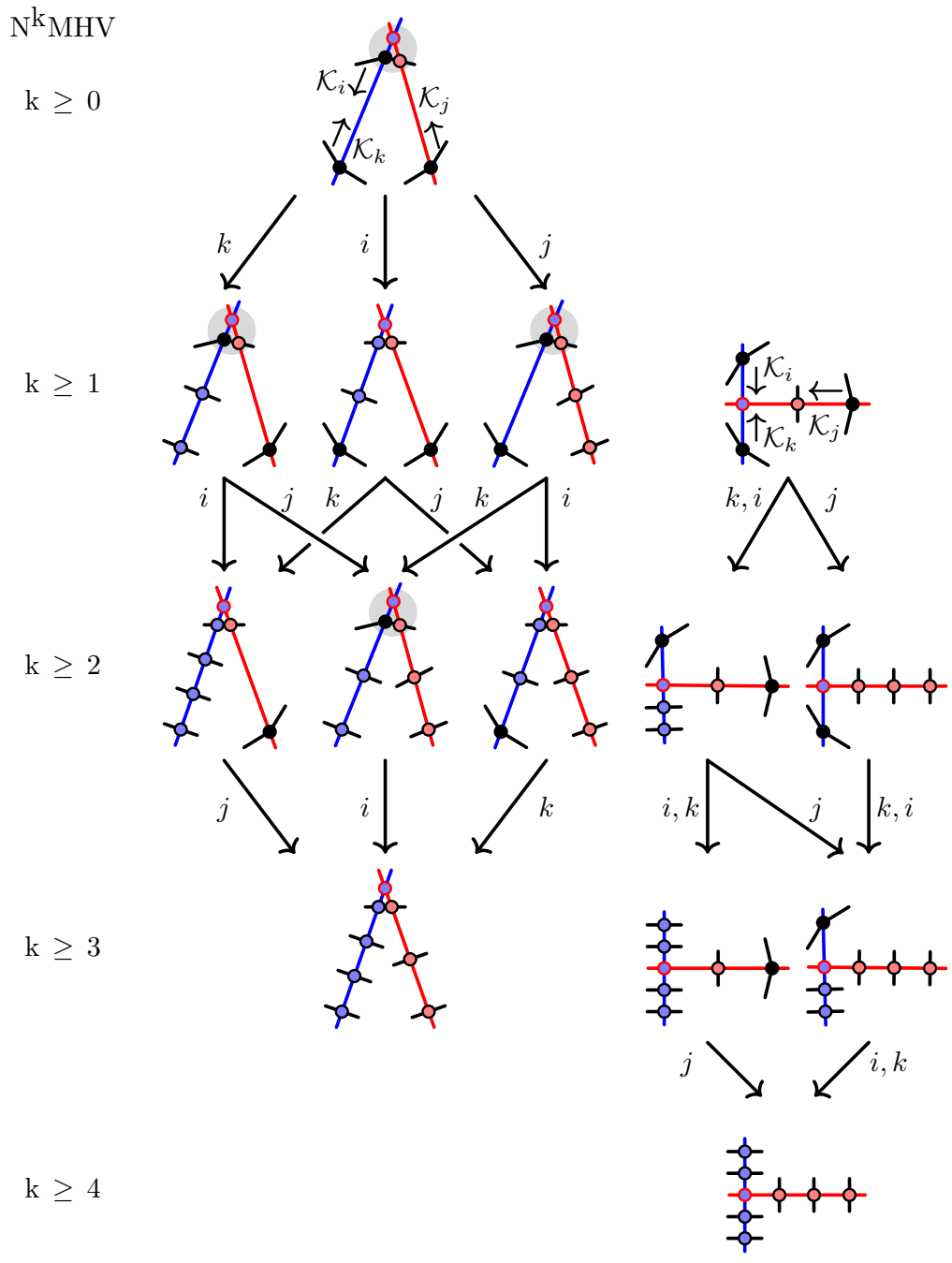


Figure 1. The twistor diagrams depicting the 14 distinct maximal codimension boundaries of two-loop N^k MHV amplituhedra. See the text for more details.

that $\alpha = 1$, so the line $\mathcal{L}^{(2)}$ is forced to pass through the point Z_i . Therefore, configurations of this type satisfy the additional on-shell condition $\langle \mathcal{L}^{(2)} i-1 i \rangle = 0$.

This phenomenon reflects the fact that in general, the on-shell conditions satisfied by a given configuration are not independent: some of them may be implied by the others. In [2] it was found that solving the Landau equations for boundaries of this type was rather subtle,

and required first identifying a suitable minimal subset of independent on-shell conditions, a process called *resolution*. It was suggested that a resolution must satisfy two criteria: (1) the chosen subset of on-shell conditions must imply the full set of conditions satisfied for generic (projected) external data, and (2) the Landau diagram corresponding to the subset must be planar.

The example considered above describes a configuration that satisfies five on-shell conditions, the four shown in eq. (3.1) and also $\langle \mathcal{L}^{(2)} i-1 i \rangle = 0$. There are four possible resolutions that satisfy criterion (1): we can simply omit any one of the conditions except for $\langle \mathcal{L}^{(1)} \mathcal{L}^{(2)} \rangle = 0$. However not all four choices will satisfy criterion (2), depending on the points A and B . For the four configurations appearing in figure 1 that require resolution, there are in each case precisely two valid resolutions: we can omit either $\langle \mathcal{L}^{(2)} i-1 i \rangle = 0$ (as was done in eq. (3.1)), or we can omit $\langle \mathcal{L}^{(1)} i i+1 \rangle = 0$.

In figure 1 we have chosen to always draw a resolved configuration in the four cases where it is necessary. However, in order to avoid clutter we do not draw both resolutions unless they give rise to inequivalent diagrams. There are at least three reasons for preferring the resolved configurations. First of all, it becomes somewhat less clear how to see the action of the three graph operators \mathcal{K} , \mathcal{U} and \mathcal{R} on an unresolved configuration. Also, the need for resolution is an accident that occurs only when both loop momenta lie in the low- k branch of solutions to their respective on-shell conditions (or, by parity symmetry, when they both lie in the high- k branch). If one of them lies in the low- k branch and the other lies in the high- k branch, then for generic (projected) external data only the resolved configuration(s) exist; the “extra” on-shell condition would place restrictions on the external data. Finally, when we turn our attention to finding Landau singularities in section 5, we will always want to work with resolved diagrams since these give us the independent sets of on-shell conditions for which we will need to solve the Landau equations [2].

3.2 Relaxations

All lower-codimension \mathcal{L} -boundaries are relaxations: they can be generated by releasing one or more of the seven on-shell conditions (excepting $\langle \mathcal{L}^{(1)} \mathcal{L}^{(2)} \rangle = 0$, which we always preserve) satisfied on the maximal boundaries. Boundaries of this type can be generated by acting on the twistor diagrams in figure 1 with sequences of the graph operators \mathcal{U} and \mathcal{R} . In this way one could imagine uplifting the figure to a three-dimensional generalization of figure 2 of [3], with the top layer being a copy of figure 1 showing the maximal codimension boundaries ($d = 8$), the next layer showing those with $d = 7$, etc. One novelty compared to the one-loop analysis of [3] is that starting at two loops the relaxation of a boundary is not necessarily still a boundary — this will only be the case if the Landau diagram of the relaxation continues to be planar.

Rather than attempting to draw the aforementioned web of interconnected boundaries in a single figure, we summarize our results in terms of the corresponding Landau diagrams in tables 1–5 grouped according to the minimum helicity for which the configuration is valid, i.e. the minimum k for which $\mathcal{A}_{n,k,2}$ has boundaries of the type shown in the corresponding twistor diagram. Because the maximal codimension singularities have $d_1 + d_2 = 7$, the corresponding Landau diagrams always have the topology of a planar pentagon-box.

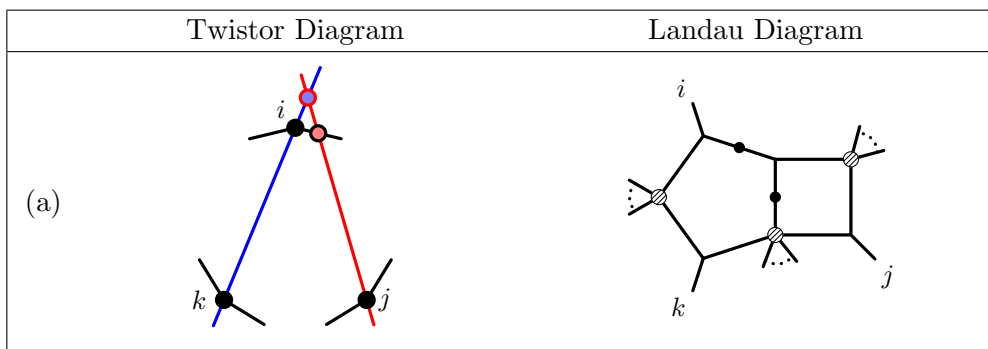


Table 1. The twistor and Landau diagram describing a type (the unique type, for $k = 0$) of resolved maximal codimension boundary of $N^{k \geq 0}$ MHV amplituhedra.

As mentioned above the lower codimension singularities can be obtained by acting on the twistor diagrams with sequences of \mathcal{U} and \mathcal{R} operators. As discussed in section 5.2 of [3], at one loop these operators generate relaxations that respectively preserve or increase, but can never decrease, the minimum helicity for which a configuration is valid. There is however a subtlety with the \mathcal{U} operator at two loops. Recall that $\mathcal{U}_{i,\mp}$ is the “unpinning” operator which acts on a loop momentum \mathcal{L} passing through some point Z_i by relaxing the on-shell condition $\langle \mathcal{L} i i \pm 1 \rangle = 0$. This can have the effect of turning what was a manifest intersection between the two loop momenta into a non-manifest intersection, which requires increasing the minimum helicity by 1.

In the tables we have introduced a new graphical notation in order to account for this phenomenon: a propagator with a black dot denotes an on-shell condition that cannot be relaxed without increasing the minimum helicity for which the configuration is valid. (We also always draw a black dot on the $\langle \mathcal{L}^{(1)} \mathcal{L}^{(2)} \rangle$ propagator, as a reminder that we never want to relax it.) Consider for example the twistor diagram in table 1(a). The two loop momenta manifestly intersect at the point Z_i as explained in the previous section, but this will no longer be the case if we act on this twistor diagram with $\mathcal{U}_{i,-}$. Instead, the configuration would become NMHV rather than MHV (in fact, it would become a relaxation of table 2(d), up to relabeling). For this reason we draw a black dot on the $\langle i i + 1 \rangle$ propagator on the pentagon in the Landau diagram of table 1(a).

3.3 Closing comments

In summary, to get the full list of Landau diagrams at helicity $k = 0, 1, 2, 3, 4$, one must therefore consider all of the Landau diagrams in tables 1 through 5, respectively, together with the diagrams generated therefrom by collapsing any subset of undotted propagators.

In figure 1 and in the tables we have chosen to always draw the loop momentum satisfying $d_1 = 4$ in blue and the one satisfying $d_2 = 3$ in red, but of course the amplituhedron is symmetric under the exchange of any \mathcal{L} 's so in each case both assignments $\mathcal{L}^{(1)}, \mathcal{L}^{(2)}$ and $\mathcal{L}^{(2)}, \mathcal{L}^{(1)}$ describe valid boundaries.

The Landau diagrams in tables 1–5 are always drawn with the understanding that all indicated labels are cyclically ordered: $i < i' < j < j' < j'' < k < k' < k'' < i \pmod{n}$.

	Twistor Diagram	Landau Diagram
(a)		
(b)		
(c)		
(d)		

Table 2. The twistor and Landau diagrams describing types of (resolved, in (a) and (c)) maximal codimension boundaries of $N^{k \geq 1}$ MHV amplituhedra.

However, the ordering of intersections along the red or blue loop momentum lines carries no significance. Therefore, as described in section 5.1 of [3], there is a second type of ambiguity between the two classes of diagrams. For example, the twistor diagram in table 2(a) is agnostic about the cyclic ordering of i , k , and k' ; the two independent choices lead to the Landau diagram shown in the table or to its mirror image. In all of the tables we use primes (and, when necessary, also double primes) to indicate pairs (or triplets) of nodes that can be exchanged, as far as the twistor diagram is concerned. Sometimes, as in the example table 2(a) just considered, an exchange generates a Landau diagram of the same topology, but in other cases it can generate a new topology. For example, exchanging

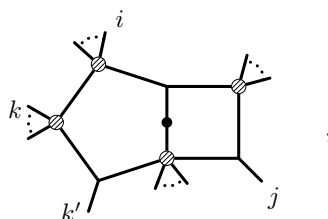
	Twistor Diagram	Landau Diagram
(a)		
(b)		
(c)		
(d)		
(e)		

Table 3. The twistor and Landau diagrams describing types of (resolved, in (b)) maximal codimension boundaries of $N^{k \geq 2}$ MHV amplituhedra.

	Twistor Diagram	Landau Diagram
(a)		
(b)		
(c)		

Table 4. The twistor and Landau diagrams describing types of maximal codimension boundaries of $N^{k \geq 3}$ MHV amplituhedra.

k and k' in the twistor diagram of table 2(b) generates the new Landau diagram



where it is to be understood that $i < j < k' < k < i$.

Let us also note that although when interpreted literally as configurations of intersecting lines in \mathbb{P}^3 most twistor diagrams only depict the low- k branch of solutions to a given set of on-shell conditions, it is clear that additional, higher- k boundaries can be generated by replacing one or both of the \mathcal{L} 's with their parity conjugates. The twistor diagrams appearing in figure 1 and in the five tables can therefore each be thought of as representing four different types of boundaries corresponding to the same Landau diagram.

Finally, we detail, in appendix B, how a partial edge-to-node duality maps between the twistor diagrams on the left and the Landau diagrams on the right of these tables, when the

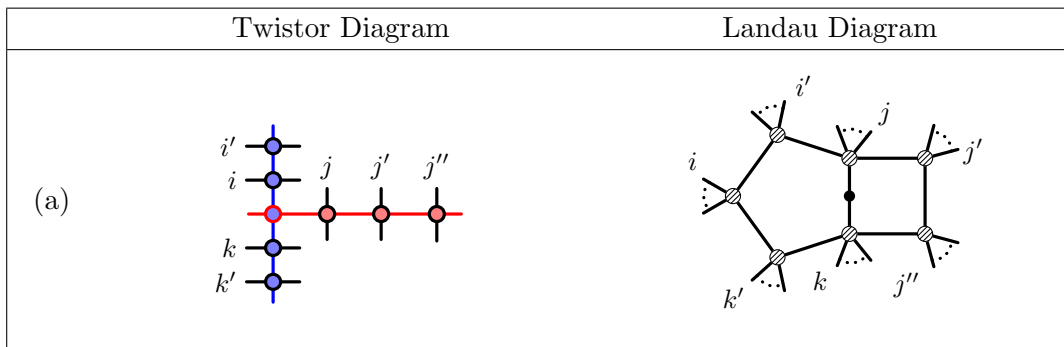


Table 5. The twistor and Landau diagram describing a type of maximal codimension boundary of $N^{k \geq 4}$ MHV amplituhedra.

two diagrams are treated as graphs. On the one hand, it is not surprising that there exists some map between these two classes of graphs, since both are designed to encode the same information. On the other hand, it is intriguing that there is a straightforward map between a generic Landau diagram and the minimum-helicity solution to the on-shell conditions of said diagram in the very particular choice of loop momentum twistor coordinates. This observation is also reminiscent of the map from Feynman integrals to their duals that aided in exploring the dual conformal invariance of SYM theory amplitudes [21–23] but here, enticingly, this partial edge-to-node map is well-defined even on nonplanar graphs.

4 The connection with on-shell diagrams

So far, we have seen that to each boundary of an amplituhedron one can associate a Landau diagram which encodes information about the singularities of the associated amplitude. In this section we explore the connection between Landau diagrams and a class of closely related diagrams that also encode information about an amplitude’s mathematical structure: the on-shell diagrams of [24]. We explain and demonstrate in several examples that for a given amplitude, the information content of certain on-shell diagrams matches the combined information content in the amplituhedron and Landau diagrams. Except possibly for cases of the type discussed in the paragraph following eq. (5.2), we expect our arguments to also hold for amplitudes at higher loop order and higher helicity.

One reason to shift focus to on-shell diagrams is that anything that can be formulated in terms of the on-shell diagrams discussed here potentially generalizes to more general quantum field theories including less supersymmetric theories as well as the full, non-planar super-Yang-Mills theory. The major difference is that in the planar theory, the relevant Landau diagrams can, in principle, be read off from the boundaries of $\mathcal{A}_{n,k,L}$ for arbitrary n , k , and L , while in the non-planar sector there is currently no known supplier of this list of diagrams. Nevertheless, assuming one has a way to generate a representation for a given non-planar amplitude in terms of Feynman integrals, all of the techniques discussed in this section apply equally well to those non-planar integrals.

Putting that ambitious motivation aside, in the rest of this section we stick to planar SYM theory and show in several examples that a given Landau diagram encodes a singu-

larity of an N^k MHV amplitude only if the diagram can be decorated in such a way that it becomes an on-shell diagram associated with an N^k MHV amplitude. We begin with a brief review of on-shell diagrams.

4.1 On-shell diagrams

An *on-shell diagram*, as introduced in [24], is a connected trivalent graph with each node having one of two distinct decorations, traditionally denoted by coloring them black or white. In the application to scattering amplitudes, each edge of the diagram represents an on-shell condition (just like in a Landau diagram) and each black (white) node corresponds to a three-point MHV ($\overline{\text{MHV}}$) tree-level superamplitude. A straightforward generalization allows nodes of higher degree which represent higher-point tree-level superamplitudes. These we depict by a shaded node.

We refer the reader to [24] for details, recalling here only a few basic facts. A *tree-level superamplitude* of *Grassmann weight* κ is a rational function of (projected) external data that is a homogeneous polynomial of degree 4κ in certain Grassmann variables (the fermionic partners of the momentum twistors Z_i). Three-point MHV and $\overline{\text{MHV}}$ amplitudes respectively have $\kappa = 2$ and $\kappa = 1$ while for $n > 3$ an n -point amplitude with helicity k has $\kappa = k + 2$. To each on-shell diagram there is an associated differential form that is obtained by first multiplying together the tree-level superamplitudes represented by each of the diagram's nodes, and then sewing them together according to a set of simple rules that involve integrating over four Grassmann variables for each internal edge (propagator) in the diagram. Such forms are the values of the residue of the amplitude's integrand at specific loci in loop momentum space.

Consider an on-shell diagram δ . Let ι be the number of internal edges of δ , and for each node ν let κ_ν be the Grassmann weight of the tree-level superamplitude at ν . As a result of the rules just reviewed, the total Grassmann weight of δ is

$$\kappa_\delta = \sum_\nu \kappa_\nu - \iota, \tag{4.1}$$

and the total helicity is $k_\delta = \kappa_\delta - 2$.

To assign a *coloring* to a Landau diagram depicting some set of on-shell conditions means to assign to each trivalent node in the diagram either a white or black coloring, and to assign to each node ν of degree $n > 3$ some helicity $k_\nu = \kappa_\nu - 2 \in \{0, \dots, n - 4\}$. Since ι is fixed by the propagator structure of the diagram, and each κ_ν is positive, it is clear from eq. (4.1) that the minimal Grassmann weight of a given Landau diagram results from coloring all trivalent nodes white and from assigning all nodes of higher degree to be MHV ($\kappa_\nu = 2$). In this way we see that the Grassmann weight of an arbitrary coloring of a given Landau diagram is bounded below by

$$\kappa \geq \kappa_{\min} = n_{\text{tri}} + 2n_{\text{high}} - \iota, \tag{4.2}$$

where n_{tri} is the number of trivalent nodes and n_{high} is the number of nodes of degree higher than three. This implies a minimal helicity sector $k_{\min} = \kappa_{\min} - 2$ for which the Landau diagram can be relevant.

If a diagram has n_{tri} trivalent indices, there are $2^{n_{\text{tri}}}$ colorings of the trivalent nodes, but in general some of these may lead to on-shell diagrams that evaluate to zero. In practice we count the number of permissible colorings of a diagram by solving the on-shell conditions implied by the diagram and mapping each resulting solution to a specific coloring (see [24]). As discussed in [25], solving a set of on-shell conditions in momentum twistor space amounts to solving a Schubert problem. At one loop these problems have in general two solutions, while for an L -loop Landau diagram we would in general expect 2^L branches of solutions. Given a solution to a Schubert problem in momentum twistor space, it is straightforward³ to check if a given trivalent node is MHV or $\overline{\text{MHV}}$ by considering the rank of the three momentum-twistor lines at the node. For an MHV node, the three twistors have full rank, while for an $\overline{\text{MHV}}$ node the rank is less than full. This process is illustrated explicitly in several examples in the following section.

In summary, we have reviewed that a given Landau diagram encodes a set of on-shell conditions, and the various branches of solutions to those conditions correspond in general to different minimum helicity sectors. The permissible colorings of a Landau diagram are in one-one correspondence with those branches, and the Grassmann weight κ of each such Landau-turned-on-shell diagram is related to the minimum helicity sector k of the corresponding solution via $\kappa = k + 2$.

This observation provides an alternative way to phrase the Landau-equation-based algorithm we employ to identify singularities of amplitudes, compared for example to the way it is phrased in the conclusion of [2] or in section 2.5 of [3]. For one thing, it means we can identify a singularity of a Landau diagram as a singularity of $N^k\text{MHV}$ amplitudes only if the diagram admits a coloring with total helicity k (equivalently, Grassmann weight $k + 2$). More specifically, when first solving the on-shell conditions (a subset of the Landau equations) for a given Landau diagram, each solution directly indicates, via the test reviewed in the previous paragraph, the helicity sector for which the singularity associated to that solution is relevant. In the on-shell diagram approach this step is the analog in the amplituhedron approach of identifying the values of k for which the momentum twistor solution lies on the boundary of the $N^k\text{MHV}$ amplituhedron. In the amplituhedron-based approach, there is potential for confusion because solving the Kirchhoff conditions (the remaining Landau equations) can lead to solutions for loop momenta that lie outside the $N^k\text{MHV}$ amplituhedron. The on-shell diagram approach bypasses this confusion because the Kirchhoff conditions only further localize a loop momentum solution whose helicity sector has already been identified.

4.2 Examples at one and two loops

We now consider several examples in order to emphasize the following point:

$$\begin{aligned} &\text{A Landau diagram contributes singularities to an } N^k\text{MHV amplitude} \\ &\text{only if the diagram permits a coloring with total Grassmann weight } k + 2. \end{aligned} \tag{4.3}$$

For each of our examples, we also list the values of the loop momenta corresponding to the colorings of the correct Grassmann weight. For the one-loop examples the same

³We thank J. Bourjaily for explaining this point to us.

information can be read off from table 1 of [3]. We will show how the on-shell diagram and amplituhedron-based methods work in tandem to quickly identify the helicity sector for which a given solution to the set of on-shell conditions is relevant.

One-loop two-mass easy box. The on-shell conditions

$$\langle \mathcal{L} i-1 i \rangle = \langle \mathcal{L} i i+1 \rangle = \langle \mathcal{L} j-1 j \rangle = \langle \mathcal{L} j j+1 \rangle = 0 \tag{4.4}$$

admit two solutions, called branches (12) and (13) in [3]. In table 6 we pair the momentum twistor representation of each solution with the associated on-shell diagram, i.e. colored Landau diagram. Having this information accessible will prove useful when considering two loops.

In table 6(a) the minimum Grassmann weight is computed according to eq. (4.2) and found to be

$$\kappa_{\min} = \underbrace{1 + 1}_{\text{white}} + \underbrace{2 + 2}_{\text{higher}} - 4 = 2 \tag{4.5}$$

so that it is an MHV ($k = 2 - 2 = 0$) coloring.

In table 6(b) the minimum Grassmann weight is

$$\kappa_{\min} = \underbrace{2 + 2}_{\text{black}} + \underbrace{2 + 2}_{\text{higher}} - 4 = 4 \tag{4.6}$$

so that it is an N^2 MHV ($k = 4 - 2 = 2$) coloring.

Let us now show how to compute the appropriate node colorings directly from the momentum twistor solutions in table 6. Consider the trivalent node where external label i connects to the loop. The three lines in momentum twistor space defining the trivalent node are $(i-1 i)$, $(i i+1)$, and \mathcal{L}_* , where \mathcal{L}_* is either $(i j)$ or $\bar{i} \cap \bar{j}$. Taking first $\mathcal{L}_* = (i j)$, we seek the dimension of the space spanned by the three momentum-twistor lines. One way to compute this is to ask for the rank of the matrix:

$$\text{rank} \begin{pmatrix} (i-1 i) \\ (i i+1) \\ (i j) \end{pmatrix} = \text{rank} \begin{pmatrix} i-1 & i & i+1 & j \\ 1 & 0 & 0 & 0 \\ 0 & 1 & 0 & 0 \\ 0 & 1 & 0 & 0 \\ 0 & 0 & 1 & 0 \\ 0 & 1 & 0 & 0 \\ 0 & 0 & 0 & 1 \end{pmatrix} = 4 \tag{4.7}$$

which has maximal rank. So the node is MHV, and colored white.

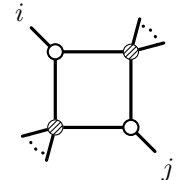
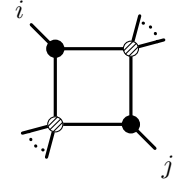
	Coloring	N^k MHV	Twistor Solution
(a)		$k \geq 0$	$\mathcal{L} = (ij)$
(b)		$k \geq 2$	$\mathcal{L} = \bar{i} \cap \bar{j}$

Table 6. Two colorings of the two-mass easy box. Row (a) shows the MHV coloring and momentum twistor solution to the on-shell conditions, and row (b) shows the same for the N^2 MHV solution.

In contrast, consider the other solution $\mathcal{L}_* = \bar{i} \cap \bar{j}$. The analogous matrix is then

$$\text{rank} \begin{pmatrix} (i-1 i) \\ (i i+1) \\ \bar{i} \cap \bar{j} \end{pmatrix} = \text{rank} \begin{pmatrix} i-1 & i & i+1 \\ 1 & 0 & 0 \\ 0 & 1 & 0 \\ 0 & 1 & 0 \\ 0 & 0 & 1 \\ \langle i \bar{j} \rangle & -\langle i-1 \bar{j} \rangle & 0 \\ 0 & \langle i+1 \bar{j} \rangle & -\langle i \bar{j} \rangle \end{pmatrix} = 3 \quad (4.8)$$

which does not have maximal rank. Thus the second solution is encoded in an $\overline{\text{MHV}}$ node at i , colored black. The colorings of the node at j can be computed analogously.

One-loop three-mass box. We perform the same exercise for the three-mass box on-shell conditions

$$\langle \mathcal{L} i-1 i \rangle = \langle \mathcal{L} i i+1 \rangle = \langle \mathcal{L} j j+1 \rangle = \langle \mathcal{L} k k+1 \rangle = 0. \quad (4.9)$$

The solutions of the on-shell conditions are matched to the two on-shell diagram colorings in table 7, and the corresponding minimum Grassmann weights are computed using eq. (4.2). The colorings are also directly calculable from the momentum twistor solutions as in the previous two-mass easy box example. The three-mass box is worth pointing out because in this case neither coloring is MHV, in contrast to the previous example.

Two-loop pentagon-box. We can recycle our knowledge of one-loop solutions to determine the helicity sectors to which a given two-loop Landau diagram contributes its singularities. We consider the pentagon-box of table 2(a) as an exemplar. We solve the pentagon-box on-shell conditions as follows. We first solve the subsystem of four propagators that depend on only $\mathcal{L}^{(2)}$:

$$\langle \mathcal{L}^{(2)} i-1 i \rangle = \langle \mathcal{L}^{(2)} i i+1 \rangle = \langle \mathcal{L}^{(2)} k k+1 \rangle = \langle \mathcal{L}^{(2)} k' k'+1 \rangle = 0 \quad (4.10)$$

	Coloring	N^k MHV	Twistor Solution
(a)		$k \geq 1$	$\mathcal{L} = (i j j+1) \cap (i k k+1)$
(b)		$k \geq 2$	$\mathcal{L} = (A B)$ $A = (j j+1) \cap \bar{i}$ $B = (k k+1) \cap \bar{i}$

Table 7. Two colorings of the three-mass box. Row (a) shows the NMHV coloring and momentum twistor solution to the on-shell conditions, and row (b) shows the same for the N^2 MHV solution.

using either of the two three-mass box solutions shown in table 7, after an appropriate exchange of the external labels in order to match to eq. (4.10). This means there are two branches of colorings: one where the trivalent node at i is white, and one where it is black. The two corresponding solutions $\mathcal{L}_*^{(2)}$ are shown in the first row of table 8. For each choice of $\mathcal{L}_*^{(2)}$ we then solve the remaining four on-shell conditions

$$\langle \mathcal{L}^{(1)} i i+1 \rangle = \langle \mathcal{L}^{(1)} j-1 j \rangle = \langle \mathcal{L}^{(1)} j j+1 \rangle = \langle \mathcal{L}^{(1)} \mathcal{L}_*^{(2)} \rangle. \tag{4.11}$$

These four conditions constitute a two-mass easy box problem, so we can utilize table 6 to identify the two solutions $\mathcal{L}_*^{(1)}$, which color the trivalent nodes of the box either both white or both black. These two solutions are tabulated in the first column of table 8. Altogether the table shows a grid containing a total of four distinct solutions, and the four associated distinct colorings. From this analysis we conclude that only the solution

$$\mathcal{L}_{*,1}^{(2)} = (i k k+1) \cap (i k' k'+1), \quad \mathcal{L}_{*,1}^{(1)} = (j i i+1) \cap (j \mathcal{L}_{*,1}^{(2)}) = (i j) \tag{4.12}$$

shown in the top left of table 8 is relevant to the NMHV sector. This means that when we turn in the following section to the problem of finding singularities of NMHV amplitudes by solving the Landau equations, we can disregard the other three solutions. Were we to attempt an amplituhedron-based answer to this same question, we would find that the other solutions to the on-shell conditions do not lie on a boundary of $\mathcal{A}_{n,1,2}$.

General two-loop pentagon-boxes. By using the same simple counting arguments applied to the results in tables 1–5, it is a straightforward exercise to show that

- the set of Landau diagrams corresponding to the maximal codimension boundaries of $\mathcal{A}_{n,k,2}$ and
- the set of on-shell diagrams of pentagon-box topology that admit an N^k MHV coloring

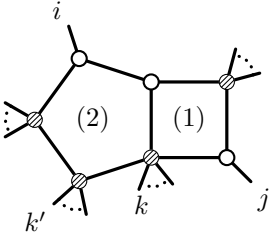
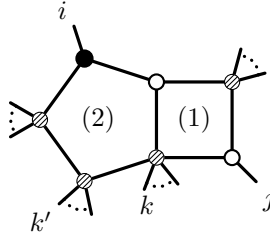
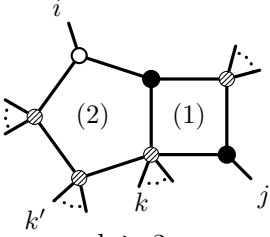
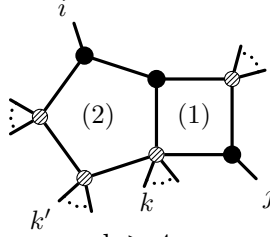
$\mathcal{L}_*^{(1)} \setminus \mathcal{L}_*^{(2)}$	$(i k k+1) \cap (i k' k'+1)$	$((k k+1) \cap \bar{i} (k' k'+1) \cap \bar{i})$
$(i j)$	 $k \geq 1$	 $k \geq 2$
$\bar{i} \cap \bar{j}$	 $k \geq 3$	 $k \geq 4$

Table 8. All permissible colorings of the trivalent nodes of the two-loop pentagon-box Landau diagram from table 2(a). The first row shows the two possible solutions to the three-mass on-shell conditions (eq. (4.10)) satisfied by $\mathcal{L}^{(2)}$, the loop momentum in the pentagon. The first column shows the two possible solutions to the two-mass easy on-shell conditions (eq. (4.11)) satisfied by $\mathcal{L}^{(1)}$, the loop momentum in the box. The cell at the intersection of a row and a column is the colored Landau diagram that results from the two solutions. Also indicated in each cell is the minimum helicity sector of the colored Landau diagram, which is achieved only if the gray nodes are taken to be MHV.

are the same. Specifically, the second set may be constructed by starting with a pentagon-box diagram with no external edges or coloring, then placing all possible combinations of massive and massless edges on nodes of the diagram in all possible ways, and finally enumerating all colorings of the resulting Landau diagrams to identify the minimum possible value of k .

5 Landau singularities of two-loop NMHV amplitudes

Finally we come to step 2 of the algorithm summarized in section 2.5 of [3]: in order to determine the locations of Landau singularities of the two-loop N^k MHV amplitude in SYM theory, we must identify, for each \mathcal{L} -boundary of $\mathcal{A}_{n,k,2}$ tabulated in section 3, the codimension-one loci (if there are any) in $\text{Conf}_n(\mathbb{P}^3)$ on which the corresponding Landau equations admit nontrivial solutions.

The ultimate aim of this project has been to derive (or at least to conjecture) symbol alphabets for two-loop amplitudes. However, as discussed in section 7 of [3], guessing a symbol alphabet from a list of singularity loci can require a nontrivial extrapolation. At one loop the extrapolation is straightforward for all Landau diagrams except the four-mass box.

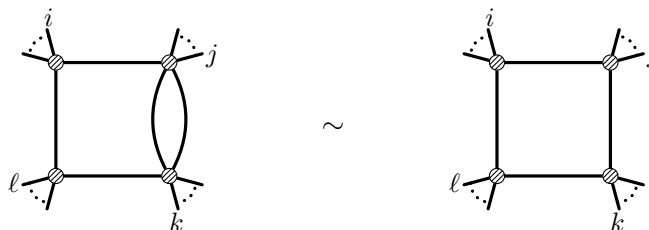


Figure 2. The Landau equations of a Landau diagram containing a bubble are identical to the equations of a Landau diagram with one propagator of the bubble removed. The two-loop four-mass bubble-box on the left is the only Landau diagram with a four-mass box contributing to the branch points of the NMHV amplitude. It has the same well-known branch points as the one-loop four-mass box on the right.

At two loops, four-mass box subdiagrams become prevalent starting at $k = 2$, where they appear in the maximal codimension Landau diagram shown in table 2(e), as well as in many of the relaxations of the other Landau diagrams in table 2. At $k = 1$ there is a single four-mass bubble-box Landau diagram, figure 2, relevant to two-loop NMHV amplitudes. As shown in the appendix of [2], Landau diagrams containing bubble subdiagrams are equivalent to the same diagram with one of the propagators of the bubble removed. So we expect the one-loop four-mass box singularity to reappear as a singularity of the two-loop NMHV amplitude. Though we are only guaranteed from this analysis that the singularities match, we can throw caution to the wind and conjecture that the same symbol entries that appear in the one-loop four-mass box integral appear also in two-loop NMHV amplitudes. Of note here: the four-mass box has support starting at $k = 2$, so there is shared singularity structure between the two-loop NMHV and one-loop N^2 MHV amplitudes.

Having dealt with this single caveat, we restrict our analysis to the remaining NMHV singularities, where we may hope that our approach allows us to read off symbol alphabets directly from lists of singularity loci.

5.1 Computational approaches

Section 2.4 of [3] reviews the Landau equations and section 6 of that reference details the process of solving them in several one-loop examples. Beyond one loop, one approach for seeking solutions is to perform the analysis “one loop at a time”, by considering each one-loop subdiagram and writing down the constraints on the values of other loop and external momenta imposed by the on-shell and Kirchhoff conditions of the subdiagram. After taking the union of those constraints, one may conclude that a solution exists for generic external data, or that the solution exists only when the external data satisfy some set of equations. Solutions of the former type were associated with the infrared singularities of an amplitude in [1], and solutions of the latter type indicate branch points of the amplitude when they live on codimension-one loci in $\text{Conf}_n(\mathbb{P}^3)$.

Here we recall a few basic facts about this loop-by-loop approach, which has been carried out for several cases in [1, 2].

First, as mentioned above, one edge of a bubble subdiagram can always be removed without affecting Landau analysis.

Second, as shown in the appendix of [2], a generic triangle subdiagram has seven different branches of solutions that should be considered separately. All of the solutions demand that the squared sum of momenta on “external” edges attached to at least one of the triangle’s corners vanish, and the seven branches of solutions are classified according to the number of null corners.⁴ There are three branches of “codimension-one” solutions (any one of the three corners vanishing), three branches of “codimension two” (any two of the three corners vanishing) and one of “codimension three” (all corners vanishing). In a Landau diagram analysis, it will often be the case that one of a triangle’s corners is null by fiat; in this case, the solution space will be reduced. For example, a “two-mass” triangle subdiagram has only one codimension-one solution. In the examples we detail in section 5.2, all triangle subdiagrams we describe are of this two-mass variety.

Finally, the Kirchhoff conditions associated to a box subdiagram constitute four homogeneous equations on four Feynman parameters, so the existence of nontrivial solutions requires the vanishing of a certain four-by-four determinant called the *Kirchhoff constraint* for the box. The Kirchhoff constraints for the four different cases of box diagrams are summarized in eqs. (2.7) through (2.11) of [1].

It is worth noting one detail regarding the “one loop at a time” approach. Because the method starts by enumerating the constraints imposed by the existence of nontrivial solutions to the Landau equations of each subdiagram, it will miss the solutions which set all Feynman parameters corresponding to some one-loop subdiagram to zero. However, Landau singularities obtained this way will always be those already present at lower loop order. So the “one loop at a time” approach neglects no novel branch points. We comment on a specific example of this phenomenon in the next section.

Let us also describe a conceptually simpler but computationally less effective alternative approach which we have used as a cross-check on our results. For a given branch of solutions to a set of on-shell conditions, or equivalently, for a given on-shell diagram, one can reduce the Landau equations “all at once” to see whether they impose codimension-one constraints on the external data. This approach is of course usually feasible only with the aid of a computer algebra system such as Mathematica. It also lends itself well to numerical experimentation: one can probe the presence or absence of a putative singularity at some locus $a = 0$ by generating random numeric values for the external data except for one free parameter z , and then reducing the Landau equations to see if the existence of nontrivial solutions forces z to take a value that sets $a = 0$.

Before proceeding to the examples and results, let us address the question: how do we confirm that we have detected all singularities? Starting from the maximal codimension boundaries of the NMHV amplituhedron shown in table 2, we determine all corresponding Landau diagrams keeping in mind the ambiguity mentioned in section 3.3. From there it is straightforward to produce all possible relaxed Landau diagrams. And from the diagrams we compute the singularities using the “one loop at a time” approach outlined above. Once we have a list of potential singularities, we turn to the “all at once” numerical

⁴These corners can be read off as the factors of the Landau singularity locus, for example in the rightmost column of table 1, branch (9), of [3].

probing. Doing so we directly confirm on a diagram-by-diagram basis not only that the set of singularities is correct, but also that there are no additional singularities. We have performed these steps to confirm the NMHV singularities presented in section 5.3.

We will focus only on Landau diagrams that have minimally-NMHV coloring, as defined in section 4.1, or equivalently, diagrams that come from a boundary of a two-loop NMHV amplituhedron. A priori, we cannot dismiss the possibility that a minimally-MHV diagram may have novel singularities coming from an NMHV branch of solutions, but we have explicitly checked that this does not occur in the two-loop NMHV amplitudes we consider here. We will demonstrate our “one loop at a time” approach to solving Landau equations on an example in the next section, and then proceed to list the full set of singularities in section 5.3.

5.2 A sample two-loop diagram

We now turn to the Landau analysis of the boundaries displayed in table 2. The analysis is very similar to that of the many examples that have been considered in [1, 2], to which we refer the reader for additional details. Therefore we only carry out the analysis in detail for the case of table 2(a), and summarize all of the results in the following section.

At maximal codimension the on-shell conditions encapsulated in the Landau diagram of table 2(a) are shown in eqs. (4.10) and (4.11). These have a total of four discrete solutions, as summarized in table 8, but the only one relevant at NMHV order is the one displayed in eq. (4.12). The Landau equations (specifically, the Kirchhoff constraint for the box subdiagram defined by eq. (4.11)) admit a solution only if [1]

$$\langle j(j-1\ j+1)(i\ i+1)\mathcal{L}_*^{(2)} \rangle = 0. \tag{5.1}$$

Substituting in the lower-helicity solution $\mathcal{L}_{*,1}^{(2)}$ and simplifying turns the constraint into

$$\langle i\bar{j} \rangle \langle i(i+1\ j)(k\ k+1)(k'\ k'+1) \rangle = 0. \tag{5.2}$$

Now we must address a subtlety of the result (5.2) that is analogous to the one encountered for the maximal codimension MHV configuration under eq. (3.29) of [2]. Like in that case, the eight-propagator Landau diagram under consideration here, shown in table 2(a), corresponds to a resolution of a configuration that actually satisfies nine on-shell conditions, as reviewed in section 3.1. It was proposed in [2] that we should trust the resulting Landau analysis only to the extent that the eight on-shell conditions imply the ninth for generic external data. Let us note that if we put $\langle \mathcal{L}^{(1)}\mathcal{L}^{(2)} \rangle = 0$ aside for a moment, the NMHV solution to the seven other on-shell conditions is

$$\mathcal{L}^{(2)} = (i\ k\ k+1) \cap (i\ k'\ k'+1), \quad \mathcal{L}^{(1)} = (\alpha Z_i + (1-\alpha)Z_{i+1}, Z_j), \tag{5.3}$$

from which we find

$$\langle \mathcal{L}^{(1)}\mathcal{L}^{(2)} \rangle = (1-\alpha)\langle i(i+1\ j)(k\ k+1)(k'\ k'+1) \rangle. \tag{5.4}$$

Therefore the conclusion that $\alpha = 1$, and hence that the ninth condition $\langle \mathcal{L}^{(1)}\ i-1\ i \rangle = 0$ is also satisfied, actually only follows if $\langle i(i+1\ j)(k\ k+1)(k'\ k'+1) \rangle \neq 0$. This observation

introduces controversy about whether the second quantity on the left-hand side of eq. (5.2) is a valid singularity. However, note that from the on-shell diagram point of view there is no apparent reason why this singularity should be excluded, since the diagram can be assigned a valid NMHV coloring as shown in table 8. Absent a rigorous argument resolving the matter, we remain agnostic about the status of this singularity.

It is easy to see that another solution to the Landau equations with $\mathcal{L}^{(1)} = (i j)$ and $\mathcal{L}^{(2)} = (i k k+1) \cap (i k' k'+1)$ exists if the four Feynman parameters associated to the box subdiagram are set to zero. In this case the box completely decouples and the pentagon subdiagram reduces to a three-mass box, so this branch exists if the external data satisfy the corresponding Kirchhoff constraint

$$\langle i(i-1 i+1)(k k+1)(k' k'+1) \rangle = 0. \tag{5.5}$$

This illustrates the point highlighted in the previous section that the “one loop at a time” approach can miss certain solutions to the Landau equations associated entirely with one-loop subdiagrams. As mentioned, we are only seeking new singularities, whereas eq. (5.5) is already known from one loop.

Next we move on to codimension seven. There are four inequivalent relaxations, which we now discuss in turn. These relaxations result from collapsing any of the undotted propagators of table 2(a). We list only the minimally-NMHV diagrams; see figure 3.

Relaxing $\langle \mathcal{L}^{(2)} i-1 i \rangle = 0$: leads to a double-box Landau diagram, figure 3(a).

There are two Kirchhoff constraints (one per box), one of which is easier to determine than the other. The easier-to-find Kirchhoff constraint comes from the box formed of the $\mathcal{L}^{(1)}$ -dependent propagators (including the shared propagator). It reads

$$\langle j(j-1 j+1)(i i+1) \mathcal{L}_*^{(2)} \rangle = 0, \tag{5.6}$$

where we write $\mathcal{L}_*^{(2)}$ to emphasize the loop momentum is on-shell when all Landau equations are satisfied.

The second Kirchhoff constraint is easiest to find after solving the three $\mathcal{L}^{(1)}$ -dependent on-shell conditions via $\mathcal{L}_{*,1}^{(1)} = (Z_j, B)$, with $B = \alpha Z_i + (1 - \alpha) Z_{i+1}$. Using this form of $\mathcal{L}^{(1)}$ in the $\mathcal{L}^{(2)}$ -dependent propagators (including the shared one) results in

$$\langle \mathcal{L}^{(2)} i B \rangle = \langle \mathcal{L}^{(2)} k k+1 \rangle = \langle \mathcal{L}^{(2)} k' k'+1 \rangle = \langle \mathcal{L}^{(2)} j B \rangle = 0, \tag{5.7}$$

which are now effectively the propagators of a three-mass box. The second Kirchhoff constraint is therefore

$$\langle B(i j)(k k+1)(k' k'+1) \rangle = 0. \tag{5.8}$$

Solving the remaining on-shell and Kirchhoff constraints (recall that the three $\mathcal{L}^{(1)}$ -dependent conditions were solved already) fixes

$$\mathcal{L}_{*,1}^{(2)} = (A k k+1) \cap (A k' k'+1), \quad A = (i i+1) \cap \bar{j}, \quad \text{and} \tag{5.9}$$

$$B = (i i+1) \cap (j \mathcal{L}_{*,1}^{(2)}). \tag{5.10}$$

This constraint on B turns eq. (5.8) into a codimension-one constraint on the external data:

$$\langle A(ij)(kk+1)(k'k'+1) \rangle = 0, \quad A = (ii+1) \cap \bar{j}, \quad (5.11)$$

which is a new, genuinely two-loop, singularity.

Relaxing $\langle \mathcal{L}^{(1)} j-1j \rangle = 0$: leads to a pentagon-triangle Landau diagram, figure 3(b).

There is a single codimension-one branch for the triangle subdiagram since there is an on-shell line at one of its corners. This branch leads to Landau equations with a solution locus that is a Kirchhoff constraint of three-mass box type:

$$\langle i(i-1i+1)(kk+1)(k'k'+1) \rangle = 0. \quad (5.12)$$

We do not focus on these already familiar singularities.

Following any codimension-two branch of the triangle subdiagram leads to Landau singularities that exist only on codimension-two loci in the space of external data, which are not of interest to us.

Following the single codimension-three branch for the triangle leads to a branch of solutions to the Landau equations that exists only if

$$\langle i(jj+1)(kk+1)(k'k'+1) \rangle = 0, \quad (5.13)$$

which is a new type of singularity.

Relaxing $\langle \mathcal{L}^{(1)} ii+1 \rangle = 0$: leads to a pentagon-triangle Landau diagram, figure 3(c).

There is again a single codimension-one branch for the triangle subdiagram leading to an effective decoupling of the two loop momenta and an overall Landau constraint of the same form (up to relabeling) as eq. (5.12).

Following the codimension-two branches for the triangle subdiagram uncovers constraints of codimension higher than one on the external data, which cannot sensibly be associated with branch points.

Following the codimension-three branch for the triangle subdiagram leads to the same Landau singularity as in eq. (5.13) (up to relabeling).

At codimension six there are three inequivalent relaxations, shown in figure 4, that do not reduce the Landau diagram to an MHV one. Collapsing any of the undotted propagators of a box subdiagram in figure 4 results in a minimally-MHV Landau diagram, as one of the external labels would necessarily drop out. Any additional relaxations of a propagator in a triangle subdiagram of figure 4 will yield a bubble subdiagram, which cannot yield a new singularity as we have already emphasized.

Relaxing both $\langle \mathcal{L}^{(1)} ii+1 \rangle = \langle \mathcal{L}^{(2)} i-1i \rangle = 0$: leads to a box-triangle Landau diagram, figure 4(a).

The single codimension-one branch of the triangle leads to the effective decoupling of the two loops and results in Landau singularities at Mandelstam-type loci:

$$\langle ii+1kk+1 \rangle \langle ii+1k'k'+1 \rangle \langle kk+1k'k'+1 \rangle = 0. \quad (5.14)$$

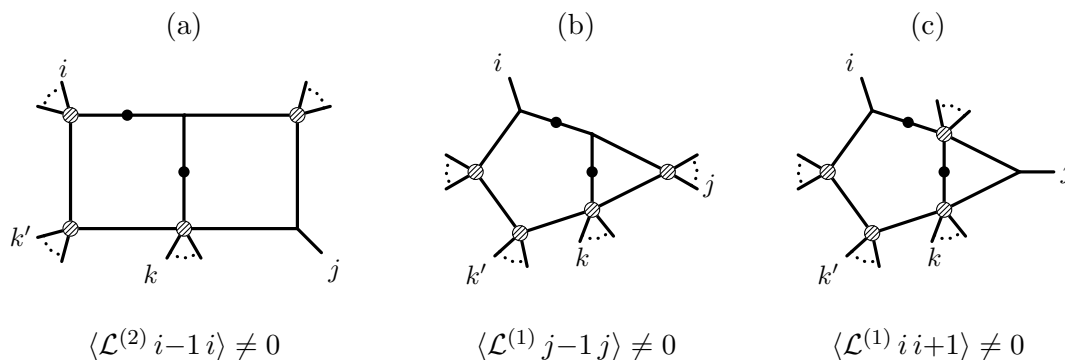


Figure 3. These are the unique single-relaxations of table 2(a) that result in NMHV Landau diagrams. The computation of the associated Landau singularities is discussed in the text.

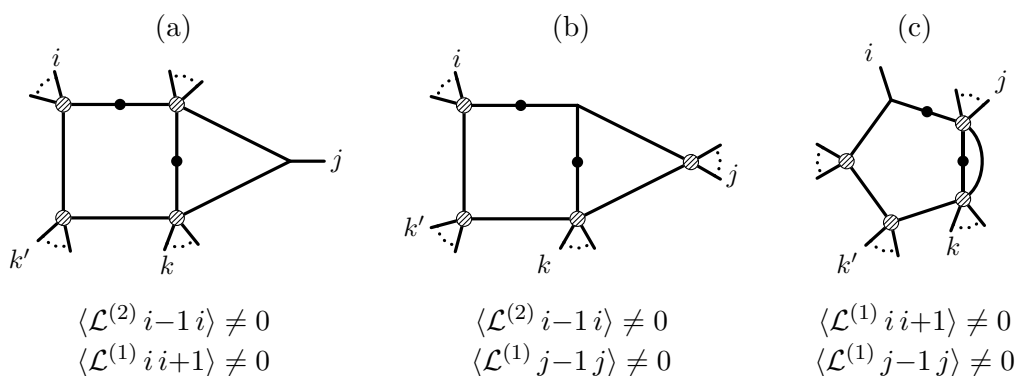


Figure 4. These are the unique minimally NMHV relaxations of the diagrams figure 3. As such, these are also double-relaxations of table 2(a). Computing the associated singularities is discussed in the text. Any further relaxations of triangles yield bubble subdiagrams. In (c), relaxing either of $\langle \mathcal{L}^{(2)} i i \pm 1 \rangle = 0$ yields the four-mass bubble-box of figure 2.

The same Landau singularities are obtained by following the codimension-two branches for the triangle.

Following the codimension-three branch for the triangle leads to the constraint

$$\langle j (i i+1) (k k+1) (k' k'+1) \rangle = 0. \tag{5.15}$$

Relaxing both $\langle \mathcal{L}^{(2)} i-1 i \rangle = \langle \mathcal{L}^{(1)} j-1 j \rangle = 0$: leads to a box-triangle Landau diagram, figure 4(b). All branches of the triangle subdiagram result in bubble-type singularities, $\langle a a+1 b b+1 \rangle$, or higher codimension constraints.

Relaxing both $\langle \mathcal{L}^{(1)} i i+1 \rangle = \langle \mathcal{L}^{(1)} j-1 j \rangle = 0$: leads to a pentagon-bubble Landau diagram, figure 4(c), as discussed above and displayed in figure 2, with a singularity on the locus

$$\langle i (j j+1) (k k+1) (k' k'+1) \rangle = 0. \tag{5.16}$$

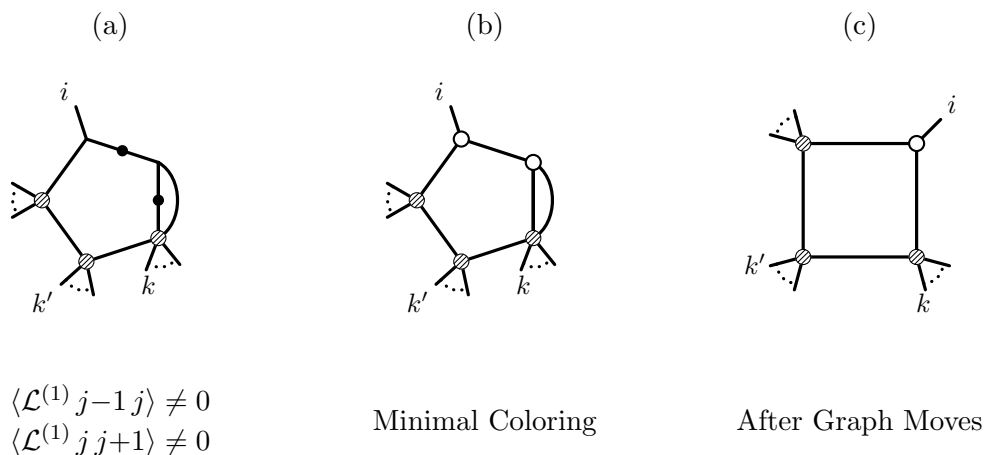


Figure 5. The Landau diagram (a) appears to have a minimally MHV coloring (b). Yet the corresponding on-shell function is related by the on-shell diagram moves of [24] to one in the NMHV helicity sector (c).

Relaxing both $\langle \mathcal{L}^{(1)} j-1 j \rangle = \langle \mathcal{L}^{(1)} j j+1 \rangle = 0$: is displayed in figure 5. This case is interesting because it emphasizes the interplay between on-shell diagrams and the amplituhedron.

From the on-shell diagram perspective, this diagram naively has a minimally MHV coloring, figure 5(b). However the graph moves that preserve on-shell functions (particularly the “collapse and re-expand” and “bubble deletion” of section 2.6 of [24]) permit redrawing the coloring as a three-mass box on-shell diagram figure 5(c), colored in its minimal helicity manner, $k \geq 1$. Since the graph moves preserve the on-shell function, the original on-shell diagram must also be minimally NMHV.

It is straightforward to check that the momentum twistor solution corresponding to this minimal coloring figure 5(a) is in fact a boundary of an NMHV amplituhedron, not an MHV one, and so the on-shell diagram and amplituhedron perspectives align.

For the two-loop amplitude, this diagram does not contribute new possible branch points, but this phenomenon is something to keep in mind for future studies.

There are no new NMHV triple relaxations, but we revisit a case discussed earlier to show how it naturally arises in this organizational scheme.

Relaxing all of $\langle \mathcal{L}^{(2)} i-1 i \rangle = \langle \mathcal{L}^{(1)} i i+1 \rangle = \langle \mathcal{L}^{(1)} j-1 j \rangle = 0$: leads to the bubble-box Landau diagram discussed above and displayed in figure 2. As mentioned above, this does not contribute a new two-loop singularity but it does indicate that two-loop NMHV amplitudes inherit the four-mass box singularity that appears at one loop only starting at $k = 2$. Our analysis indicates this is a fairly common phenomenon: Landau diagrams for an L -loop N^k MHV amplitude that contain bubble or triangle subdiagrams will often contain singularities that also contribute to $(L - 1)$ -loop N^{k+1} MHV amplitudes.

5.3 Two-loop NMHV symbol alphabets

The full set of loci in the external kinematic space $\text{Conf}_n(\mathbb{P}^3)$ where two-loop NMHV amplitudes have Landau singularities is obtained by carrying out the analysis of the previous

section for all Landau diagrams appearing in tables 1 and 2, together with all of their (still NMHV) relaxations. Among the set of singularities generated in this way are the two-loop MHV singularities that arise from the configuration shown in table 1, which live on the loci

$$\begin{aligned} \langle a a+1 b c \rangle &= 0, \\ \langle a a+1 \bar{b} \cap \bar{c} \rangle &= 0, \end{aligned} \tag{5.17}$$

for arbitrary indices a, b, c . The set of brackets appearing on the left-hand sides of eq. (5.17) correspond exactly to the set of symbol letters of two-loop MHV amplitudes originally found in [26].

For the NMHV configurations shown in table 2 we find additional singularities that live on loci of the form⁵

$$\begin{aligned} \langle i (i \pm 1 \ell) (j j+1) (k k+1) \rangle &= 0, \\ \langle j (j-1 j+1) (j' j'+1) (i \ell) \rangle &= 0, \\ \langle i (j j+1) (k k+1) (\ell \ell+1) \rangle &= 0, \\ \langle i i+1 \bar{j} \cap (k k' k'+1) \rangle &= 0, \\ \langle \bar{i} \cap (i i' i'+1) \cap \bar{j} \cap (j j' j'+1) \rangle &= 0, \\ \langle\langle (i i+1) \cap \bar{j}; (i j) (k k+1) (\ell \ell+1) \rangle\rangle &= 0, \end{aligned} \tag{5.18}$$

using notation explained in appendix A. The indices are restricted (as a consequence of planarity) to have the cyclic ordering $\ell \leq \{i, i'\} \leq \{j, j'\} \leq \{k, k'\} \leq \ell$ (or the reflection of this, with all \leq 's replaced by \geq 's) where the curly bracket notation means that the relative ordering of an index with its primed partner is not fixed (tracing back to the ambiguity discussed in section 3.3).

In addition to singularities of the type listed in eq. (5.18), two-loop NMHV amplitudes also have four-mass box singularities as discussed in the beginning of section 5 and illustrated in figure 2. Although guessing symbol letters from knowledge of singularity loci is in general nontrivial (see section 7 of [3]), we conjecture that the quantities appearing on the left-hand sides of eqs. (5.17) and (5.18), together with appropriate symbol letters of four-mass box type (see the example in the following section), constitute the symbol alphabet of two-loop NMHV amplitudes in SYM theory. It is to be understood that all degenerations of the indicated forms are meant to be included as well, for example such as taking $j = j' - 1$ in the first line. For certain values of some indices the expressions can degenerate into symbol letters (or products of symbol letters) that already appear in eq. (5.17), or elsewhere in eq. (5.18), but other degenerate cases are valid, new NMHV letters.

It is interesting to note that for arbitrary n the conjectural set of symbol letters in eq. (5.18) is not closed under parity, unlike the two in eq. (5.17) which are parity conjugates of each other.⁶ We know of no a priori reason why the symbol alphabet for

⁵Out of caution we have included on the first line the singularities of the type shown in eq. (5.2); but we remind the reader of the discussion in the subsequent paragraph; for $n = 8$ it happens that the first line is necessarily a particular case of the second and/or fourth so there is no controversy.

⁶More precisely, the parity conjugate of the first quantity in eq. (5.17) is $\langle a-1 a a+1 a+2 \rangle$ times the second; they become exactly parity conjugate in a gauge where the momentum twistors are scaled so that all four-brackets of four adjacent indices are set to 1.

a given amplitude in SYM theory should be closed under parity; in principle, the parity symmetry of the theory requires only that the symbol alphabet of N^k MHV amplitudes must be the parity conjugate of the symbol alphabet of N^{n-k-4} MHV amplitudes.

The absence of parity symmetry is a simple consequence of the fact that different branches of solutions to the Landau equations give non-zero support to amplitudes in different helicity sectors (or, equivalently, overlap boundaries of amplituhedra in different helicity sectors). From this point of view it appears to be an accident that the two-loop MHV symbol alphabet is closed under parity; we guess that this will continue to hold at arbitrary loop order. It is also an interesting consistency check that for $n < 8$ the symbol letters in eq. (5.18) necessarily degenerate into letters of the type already present at MHV order. This is consistent with all results available to date from the hexagon and heptagon amplitude bootstrap programs, which are based on the hypothesis that the symbol alphabet for all amplitudes with $n < 8$ is given by eq. (5.17) to all loop order. Genuinely new NMHV letters begin to appear only starting at $n = 8$, to which we now turn our attention.

5.4 Eight-point example

For the sake of illustration let us conclude by explicitly enumerating our conjecture for the two-loop NMHV symbol alphabet for the case $n = 8$. First let us recall that the corresponding MHV symbol alphabet [26] is comprised of 116 letters:

- 68 four-brackets of the form $\langle a a+1 b c \rangle$ (there are altogether of $\binom{8}{4} = 70$ four-brackets of the more general form $\langle a b c d \rangle$, but at $n = 8$ both $\langle 1 3 5 7 \rangle$ and $\langle 2 4 6 8 \rangle$ are excluded by the requirement that at least one pair of indices must be adjacent),
- 8 cyclic images of $\langle 1 2 \bar{4} \cap \bar{6} \rangle$,
- and 40 degenerate cases of $\langle a a+1 \bar{b} \cap \bar{c} \rangle$ consisting of 8 cyclic images each of $\langle 1 (23)(45)(78) \rangle$, $\langle 1 (23)(56)(78) \rangle$, $\langle 1 (28)(34)(56) \rangle$, $\langle 1 (28)(34)(67) \rangle$, as well as $\langle 1 (28)(45)(67) \rangle$.

Referring the reader again to appendix A for details on our notation, we conjecture that an additional 88 letters appear in the symbol alphabet of the two-loop $n = 8$ NMHV amplitude⁷

- 48 degenerate cases consisting of 16 dihedral images each of $\langle 1 (23)(45)(67) \rangle$, $\langle 1 (23)(45)(68) \rangle$, as well as $\langle 1 (28)(34)(57) \rangle$,
- 8 cyclic images of $\langle \bar{2} \cap (245) \cap \bar{8} \cap (856) \rangle$ (this set is closed under reflections, so adding all dihedral images would be overcounting),
- the 8 distinct dihedral images of $\langle \bar{2} \cap (245) \cap \bar{6} \cap (681) \rangle$ (which is distinct from its reflection but comes back to itself after cycling the indices by four),

⁷The $116+88 = 204$ symbol letters of this amplitude can be assembled into $204-8 = 196$ dual conformally invariant cross-ratios in many different ways. We cannot *a priori* rule out the possibility that the symbol of this amplitude might be expressible in terms of an even smaller set of carefully chosen multiplicatively independent cross-ratios, though this type of reduction is not possible in any known six- or seven-point examples.

- 16 dihedral images of $\langle\langle(12) \cap \bar{4}; (14)(56)(78)\rangle\rangle$,
- and finally 8 four-mass box-type letters.

The last of these were displayed in eq. (7.1) of [3] and take the form

$$f_{i\ell}f_{jk} \pm (f_{ik}f_{j\ell} - f_{ij}f_{k\ell}) \pm \sqrt{(f_{ij}f_{k\ell} - f_{ik}f_{j\ell} + f_{i\ell}f_{jk})^2 - 4f_{ij}f_{jk}f_{k\ell}f_{i\ell}}, \quad (5.19)$$

where $f_{ij} \equiv \langle ii+1 jj+1 \rangle$ and the signs may be chosen independently. For $n = 8$ there are two inequivalent choices $\{i, j, k, \ell\} = \{1, 3, 5, 7\}$ or $\{2, 4, 6, 8\}$, for a total of eight possible symbol letters of this type.

6 Conclusion

The symbol alphabets for all two-loop MHV amplitudes in SYM theory were first found in [26]. In [9, 27] it was found that two-loop NMHV amplitudes have the same symbol alphabets as the corresponding MHV amplitudes for $n = 6, 7$, which is now believed to be true to all loop order. However, the question of whether two-loop NMHV amplitudes for $n > 7$ have the same symbol alphabets as their MHV cousins has remained open. In this paper we find that the former have branch points (of the type shown in eq. (5.18)) not shared by the latter, answering this question in the negative.

Our conjectures for the two-loop NMHV symbol alphabets are formulated in terms of quantities analogous to the cluster \mathcal{A} -coordinates of [28], although it is simple to confirm that at least some of them are not cluster coordinates of the $\text{Gr}(4, n)$ cluster algebra (it is possible that none of them are, but some of them are more difficult to check). For the purpose of carrying out the amplitude bootstrap, it is however more convenient to assemble these letters into dual conformally invariant cross-ratios. In the literature considerable effort (see for example [29–33]) has gone into divining deep mathematical structure of amplitudes hidden in the particular kinds of cross-ratios that might appear, especially when they can be taken to cluster \mathcal{X} -coordinates (or Fock-Goncharov coordinates) of the type reviewed in [28]. However, we see no hint in the Landau analysis or inherent to the twistor or on-shell diagrams employed in this paper that suggests any preferred way of building such cross-ratios.

It is inherent in the approach taken here following [2, 3] (as well as in the amplitude bootstrap program itself) that we eschew knowledge of or interest in explicit representations of amplitudes in terms of local Feynman integrals. However, as mentioned in the conclusion of [3], the procedure of identifying relevant boundaries of amplituhedra and then solving the Landau equations associated to each one as if it literally represented some Feynman integral is suggestive that this approach might be thought of as naturally generating integrand expansions around the highest codimension amplituhedron boundaries.⁸ This approach might lead to a resolution of the controversy regarding the status of Landau singularities of the type eq. (5.2) obtained from maximal codimension boundaries. This analysis is, however, beyond the scope of our paper and we remain agnostic about the status of this

⁸We are grateful to N. Arkani-Hamed for extensive discussions on this point.

branch point in anticipation of empirical data. If this singularity is shown to be spurious, this would be an interesting result not easily explainable using on-shell diagram techniques, and it would signal that boundaries of amplituhedra contain more information waiting to be explored.

These observations highlight a point that we have emphasized several times in this paper and the prequel [3]. Namely, several threads in this tapestry, including the connection to on-shell diagrams reviewed in section 4 and the simple relation between twistor diagrams and Landau diagrams in appendix B, do not inherently rely on planarity. This hints at the tantalizing possibility that some of our toolbox may be useful for studying non-planar amplitudes about which much less is known (see [34–36]).

One of the stronger hints — the relationship between on-shell diagrams and Landau diagrams — also aids in corroborating results. A vanishing on-shell diagram indicates a location where the analytic structure of an amplitude is trivial; that is exactly the same information encoded by the boundaries of the amplituhedron. The simple connection between the results tabulated in section 3 and those obtained via the on-shell diagram approach provides an important cross-check supporting the validity of our analysis, as well as giving additional corroboration to the definition of amplituhedra.

Acknowledgments

We have benefited greatly from very stimulating discussions with N. Arkani-Hamed, L. Dixon and J. Bourjaily, and from collaboration with A. Volovich in the early stages of this work. This work was supported in part by: the US Department of Energy under contract DE-SC0010010 Task A, Simons Investigator Award #376208 of A. Volovich (JS), the Simons Fellowship Program in Theoretical Physics (MS), the National Science Foundation under Grant No. NSF PHY-1125915 (JS), and the Munich Institute for Astro- and Particle Physics (MIAPP) of the DFG cluster of excellence “Origin and Structure of the Universe” (JS). MS is also grateful to the CERN theory group for hospitality and support during the course of this work.

A Notation

Here we recall some standard momentum twistor notation and define some new notation used in section 5. The momentum twistors Z_a^I are n homogeneous coordinates on $\text{Conf}_n(\mathbb{P}^3)$ (so $I \in \{1, \dots, 4\}$ and $a \in \{1, \dots, n\}$) in terms of which we have the natural four-brackets

$$\langle a b c d \rangle \equiv \epsilon_{IJKL} Z_a^I Z_b^J Z_c^K Z_d^L. \tag{A.1}$$

We use (see for example eq. (2.38) of [25])

$$\langle x y (a b c) \cap (d e f) \rangle \equiv \langle x a b c \rangle \langle y d e f \rangle - \langle y a b c \rangle \langle x d e f \rangle \tag{A.2}$$

and in the special case when the two planes $(a b c)$, $(d e f)$ share a common point, say $f = c$, we use the shorthand

$$\langle c (x y) (a b) (d e) \rangle \equiv \langle x y (a b c) \cap (d e c) \rangle \tag{A.3}$$

to emphasize the otherwise non-manifest fact that this quantity is fully antisymmetric under the exchange of any two of the three lines (xy) , (ab) , and (de) . In section 5 we introduce a bracket for the intersection of four planes which is related by the obvious duality to an intersection of four points. Specifically, if we represent a plane (abc) by its dual point

$$(abc)_I \equiv \epsilon_{IJLK} Z_a^J Z_b^K Z_c^L \tag{A.4}$$

then we define

$$\begin{aligned} &\langle (a_1 a_2 a_3) \cap (b_1 b_2 b_3) \cap (c_1 c_2 c_3) \cap (d_1 d_2 d_3) \rangle \\ &\equiv \epsilon^{JKLM} (a_1 a_2 a_3)_I (b_1 b_2 b_3)_J (c_1 c_2 c_3)_K (d_1 d_2 d_3)_L. \end{aligned} \tag{A.5}$$

Our final new definition

$$\langle\langle (aa+1) \cap \bar{b}; (ab)(cd)(ef) \rangle\rangle \equiv \frac{\langle\langle (aa+1) \cap \bar{b} \rangle (ab)(cd)(ef) \rangle}{\langle a\bar{b} \rangle} \tag{A.6}$$

requires a little bit of explanation. The first quantity in the numerator recalls that the intersection of a line (ab) and a plane (cde) can be represented by the point (see for example p. 33 of [25])

$$(ab) \cap (cde) \equiv Z_a \langle bcde \rangle + Z_b \langle cdea \rangle. \tag{A.7}$$

Using this definition, the $(aa+1) \cap \bar{b}$ in the numerator of eq. (A.6) defines a point that feeds into “ c ” in the definition (A.3). By following the trail of definitions it is easy to check that the resulting bracket in the numerator of eq. (A.6) always has an overall factor of $\langle a\bar{b} \rangle$, which we divide out in order to make $\langle\langle . \rangle\rangle$ irreducible (for general arguments).

B Twistor diagrams to Landau diagrams

In this appendix, we explain how twistor diagrams and Landau diagrams are partial edge-to-node duals of each other. This map straightforwardly generalizes to any number of loops, and is easily inverted to map a Landau diagram into a twistor diagram.

We first note that the edges in a twistor diagram associated with the external labels are redundant, since the “empty” or “filled” property of the node already tracks the same information. So we can drop such edges. Then the following steps map a twistor diagram, τ , to a Landau diagram, λ :

1. For each loop line $\mathcal{L}^{(i)}$ in τ , identify one endpoint of $\mathcal{L}^{(i)}$ with the other endpoint of $\mathcal{L}^{(i)}$. Since τ are graphs, this identification preserves the order of the nodes along all $\mathcal{L}^{(i)}$.
2. Map each empty τ -node into a λ -edge. Identify the two λ -nodes defining the λ -edge as massive corners of λ .

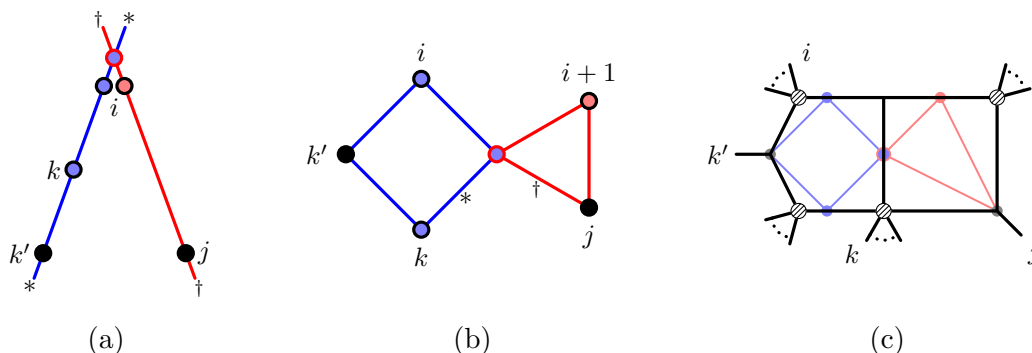


Figure 6. Figure (a) is momentum twistor diagram (with the superfluous edges associated with the external labels dropped), with the endpoints of $\mathcal{L}^{(1)}$ (denoted with \dagger) identified, and with the endpoints of $\mathcal{L}^{(2)}$ (denoted with $*$) identified. The resulting graph (b) comes from preserving the ordering of nodes along the line. Note we have used the ambiguity in ordering between k and k' to consider the case $k < k' < i$. Mapping any empty node to an edge between massive corners and mapping any filled node to a massless corner with two edges between massive corners, results in the Landau diagram (c). There would be a massive corner along the top of the Landau diagram, but the indices fix that corner to be zero.

3. Map each filled τ -node into two λ -edges sharing one common λ -node. Identify the common λ -node as a massless corner of λ , and the other two λ -nodes as massive corners of λ .
4. The external labels map from τ to λ such that:
 - the label of an empty τ -node maps to one of the two massless corners defining the new λ -edge, and
 - the label of a filled τ -node maps into a massless corner of λ .

This is a partial edge-to-node map because only the empty τ -nodes obey a proper edge-to-node exchange as they map to a λ -edge, while the filled τ -nodes are effectively unchanged as they map to λ -nodes. It is always possible to consistently assign the labels of τ to λ , though so doing may cause a massive corner of λ to completely vanish, as happens in the following concrete example.

We turn now to detailing how the two-loop twistor diagram, figure 6(a), (also the first column of table 2(b)) maps into one of its corresponding Landau diagrams, figure 6(c) (the second column of table 2(b)).

The first step is to identify the two nodes corresponding to the end-points of each $\mathcal{L}^{(i)}$, $i = 1, 2$. This closes the two lines into loops, and we formally think of the diagram as a graph, specified by its edges, nodes, and decorations of its nodes. The result is figure 6(b), with identified endpoints marked by $*$ and \dagger .

In this instance, there is an ambiguity in choosing $k' < k$ or $k < k'$. We demonstrate the latter case here to highlight that k' and k can be swapped with respect to how they appear on the loop line. The $k' < k$ differs from what we detail here by swapping ordering

of the two nodes along the loop. Then the filled k' node would be on the bottom of the box in figure 6(b), while the empty k node would be on the left of the box.

In the $k < k'$ case we are considering, the resulting graph becomes the Landau diagram, figure 6(c) under the partial edge-to-node dual map, as described in the steps above. Note in figure 6(c) that the empty nodes of the original twistor diagram are identified with edges of the resulting Landau diagram. In contrast, the filled nodes are identified with massless corners, which are themselves nodes. So this is only a partial edge-to-node map.

Open Access. This article is distributed under the terms of the Creative Commons Attribution License ([CC-BY 4.0](https://creativecommons.org/licenses/by/4.0/)), which permits any use, distribution and reproduction in any medium, provided the original author(s) and source are credited.

References

- [1] T. Dennen, M. Spradlin and A. Volovich, *Landau singularities and symbology: one- and two-loop MHV amplitudes in SYM theory*, *JHEP* **03** (2016) 069 [[arXiv:1512.07909](https://arxiv.org/abs/1512.07909)] [[INSPIRE](#)].
- [2] T. Dennen, I. Prlina, M. Spradlin, S. Stanojevic and A. Volovich, *Landau singularities from the amplituhedron*, *JHEP* **06** (2017) 152 [[arXiv:1612.02708](https://arxiv.org/abs/1612.02708)] [[INSPIRE](#)].
- [3] I. Prlina, M. Spradlin, J. Stankowicz, S. Stanojevic and A. Volovich, *All-helicity symbol alphabets from unwound amplituhedra*, [arXiv:1711.11507](https://arxiv.org/abs/1711.11507) [[INSPIRE](#)].
- [4] A.B. Goncharov, M. Spradlin, C. Vergu and A. Volovich, *Classical polylogarithms for amplitudes and Wilson loops*, *Phys. Rev. Lett.* **105** (2010) 151605 [[arXiv:1006.5703](https://arxiv.org/abs/1006.5703)] [[INSPIRE](#)].
- [5] J. Maldacena, D. Simmons-Duffin and A. Zhiboedov, *Looking for a bulk point*, *JHEP* **01** (2017) 013 [[arXiv:1509.03612](https://arxiv.org/abs/1509.03612)] [[INSPIRE](#)].
- [6] L.D. Landau, *On analytic properties of vertex parts in quantum field theory*, *Nucl. Phys.* **13** (1959) 181 [[INSPIRE](#)].
- [7] R.J. Eden, P.V. Landshoff, D.I. Olive and J.C. Polkinghorne, *The analytic S-matrix*, Cambridge University Press, Cambridge U.K. (1966).
- [8] L.J. Dixon, J.M. Drummond and J.M. Henn, *Bootstrapping the three-loop hexagon*, *JHEP* **11** (2011) 023 [[arXiv:1108.4461](https://arxiv.org/abs/1108.4461)] [[INSPIRE](#)].
- [9] L.J. Dixon, J.M. Drummond and J.M. Henn, *Analytic result for the two-loop six-point NMHV amplitude in $N = 4$ super Yang-Mills theory*, *JHEP* **01** (2012) 024 [[arXiv:1111.1704](https://arxiv.org/abs/1111.1704)] [[INSPIRE](#)].
- [10] L.J. Dixon, J.M. Drummond, M. von Hippel and J. Pennington, *Hexagon functions and the three-loop remainder function*, *JHEP* **12** (2013) 049 [[arXiv:1308.2276](https://arxiv.org/abs/1308.2276)] [[INSPIRE](#)].
- [11] L.J. Dixon, M. von Hippel and A.J. McLeod, *The four-loop six-gluon NMHV ratio function*, *JHEP* **01** (2016) 053 [[arXiv:1509.08127](https://arxiv.org/abs/1509.08127)] [[INSPIRE](#)].
- [12] S. Caron-Huot, L.J. Dixon, A. McLeod and M. von Hippel, *Bootstrapping a five-loop amplitude using Steinmann relations*, *Phys. Rev. Lett.* **117** (2016) 241601 [[arXiv:1609.00669](https://arxiv.org/abs/1609.00669)] [[INSPIRE](#)].

- [13] J.M. Drummond, G. Papathanasiou and M. Spradlin, *A symbol of uniqueness: the cluster bootstrap for the 3-loop MHV heptagon*, *JHEP* **03** (2015) 072 [[arXiv:1412.3763](#)] [[INSPIRE](#)].
- [14] L.J. Dixon et al., *Heptagons from the Steinmann cluster bootstrap*, *JHEP* **02** (2017) 137 [[arXiv:1612.08976](#)] [[INSPIRE](#)].
- [15] J.L. Bourjaily et al., *The elliptic double-box integral: massless amplitudes beyond polylogarithms*, *Phys. Rev. Lett.* **120** (2018) 121603 [[arXiv:1712.02785](#)] [[INSPIRE](#)].
- [16] D. Nandan, M.F. Paulos, M. Spradlin and A. Volovich, *Star integrals, convolutions and simplices*, *JHEP* **05** (2013) 105 [[arXiv:1301.2500](#)] [[INSPIRE](#)].
- [17] S. Caron-Huot and K.J. Larsen, *Uniqueness of two-loop master contours*, *JHEP* **10** (2012) 026 [[arXiv:1205.0801](#)] [[INSPIRE](#)].
- [18] N. Arkani-Hamed and J. Trnka, *The amplituhedron*, *JHEP* **10** (2014) 030 [[arXiv:1312.2007](#)] [[INSPIRE](#)].
- [19] N. Arkani-Hamed, H. Thomas and J. Trnka, *Unwinding the amplituhedron in binary*, *JHEP* **01** (2018) 016 [[arXiv:1704.05069](#)] [[INSPIRE](#)].
- [20] N. Arkani-Hamed and J. Trnka, *Into the amplituhedron*, *JHEP* **12** (2014) 182 [[arXiv:1312.7878](#)] [[INSPIRE](#)].
- [21] J.M. Drummond, J. Henn, V.A. Smirnov and E. Sokatchev, *Magic identities for conformal four-point integrals*, *JHEP* **01** (2007) 064 [[hep-th/0607160](#)] [[INSPIRE](#)].
- [22] L.F. Alday and J.M. Maldacena, *Gluon scattering amplitudes at strong coupling*, *JHEP* **06** (2007) 064 [[arXiv:0705.0303](#)] [[INSPIRE](#)].
- [23] J.M. Drummond, J. Henn, G.P. Korchemsky and E. Sokatchev, *Dual superconformal symmetry of scattering amplitudes in $N = 4$ super-Yang-Mills theory*, *Nucl. Phys. B* **828** (2010) 317 [[arXiv:0807.1095](#)] [[INSPIRE](#)].
- [24] N. Arkani-Hamed et al., *Grassmannian geometry of scattering amplitudes*, Cambridge University Press, Cambridge U.K. (2016), [[arXiv:1212.5605](#)] [[INSPIRE](#)].
- [25] N. Arkani-Hamed, J.L. Bourjaily, F. Cachazo and J. Trnka, *Local integrals for planar scattering amplitudes*, *JHEP* **06** (2012) 125 [[arXiv:1012.6032](#)] [[INSPIRE](#)].
- [26] S. Caron-Huot, *Superconformal symmetry and two-loop amplitudes in planar $N = 4$ super Yang-Mills*, *JHEP* **12** (2011) 066 [[arXiv:1105.5606](#)] [[INSPIRE](#)].
- [27] S. Caron-Huot and S. He, *Jumpstarting the all-loop S -matrix of planar $N = 4$ super Yang-Mills*, *JHEP* **07** (2012) 174 [[arXiv:1112.1060](#)] [[INSPIRE](#)].
- [28] J. Golden, A.B. Goncharov, M. Spradlin, C. Vergu and A. Volovich, *Motivic amplitudes and cluster coordinates*, *JHEP* **01** (2014) 091 [[arXiv:1305.1617](#)] [[INSPIRE](#)].
- [29] J. Golden and M. Spradlin, *A cluster bootstrap for two-loop MHV amplitudes*, *JHEP* **02** (2015) 002 [[arXiv:1411.3289](#)] [[INSPIRE](#)].
- [30] J. Drummond, J. Foster and O. Gürdoğan, *Cluster adjacency properties of scattering amplitudes*, [[arXiv:1710.10953](#)] [[INSPIRE](#)].
- [31] J. Golden, M.F. Paulos, M. Spradlin and A. Volovich, *Cluster polylogarithms for scattering amplitudes*, *J. Phys. A* **47** (2014) 474005 [[arXiv:1401.6446](#)] [[INSPIRE](#)].
- [32] T. Harrington and M. Spradlin, *Cluster functions and scattering amplitudes for six and seven points*, *JHEP* **07** (2017) 016 [[arXiv:1512.07910](#)] [[INSPIRE](#)].

- [33] J. Golden and M. Spradlin, *The differential of all two-loop MHV amplitudes in $\mathcal{N} = 4$ Yang-Mills theory*, *JHEP* **09** (2013) 111 [[arXiv:1306.1833](#)] [[INSPIRE](#)].
- [34] N. Arkani-Hamed, J.L. Bourjaily, F. Cachazo and J. Trnka, *Singularity structure of maximally supersymmetric scattering amplitudes*, *Phys. Rev. Lett.* **113** (2014) 261603 [[arXiv:1410.0354](#)] [[INSPIRE](#)].
- [35] Z. Bern, E. Herrmann, S. Litsey, J. Stankowicz and J. Trnka, *Logarithmic singularities and maximally supersymmetric amplitudes*, *JHEP* **06** (2015) 202 [[arXiv:1412.8584](#)] [[INSPIRE](#)].
- [36] Z. Bern, E. Herrmann, S. Litsey, J. Stankowicz and J. Trnka, *Evidence for a nonplanar amplituhedron*, *JHEP* **06** (2016) 098 [[arXiv:1512.08591](#)] [[INSPIRE](#)].

All-helicity symbol alphabets from unwound amplituhedra

I. Prlina,^a M. Spradlin,^{a,b} J. Stankowicz,^{a,c} S. Stanojevic^a and A. Volovich^{a,b}

^a*Department of Physics, Brown University,
Providence RI 02912, U.S.A.*

^b*School of Natural Sciences, Institute for Advanced Study,
Princeton NJ 08540, U.S.A.*

^c*Kavli Institute for Theoretical Physics, University of California,
Santa Barbara CA 93106, U.S.A.*

E-mail: igor_prlina@brown.edu, marcus_spradlin@brown.edu,
james_stankowicz@brown.edu, stefan_stanojevic@brown.edu,
anastasia_volovich@brown.edu

ABSTRACT: We review an algorithm for determining the branch points of general amplitudes in planar $\mathcal{N} = 4$ super-Yang-Mills theory from amplituhedra. We demonstrate how to use the recent reformulation of amplituhedra in terms of ‘sign flips’ in order to streamline the application of this algorithm to amplitudes of any helicity. In this way we recover the known branch points of all one-loop amplitudes, and we find an ‘emergent positivity’ on boundaries of amplituhedra.

KEYWORDS: Scattering Amplitudes, Supersymmetric Gauge Theory

ARXIV EPRINT: [1711.11507](https://arxiv.org/abs/1711.11507)

Contents

1	Introduction	1
2	Review	3
2.1	The kinematic domain	3
2.2	Amplituhedra...	4
2.3	...and their boundaries	5
2.4	The Landau equations	6
2.5	Summary: the algorithm	8
3	One-loop branches	8
4	One-loop boundaries	12
4.1	A criterion for establishing absent branches	12
4.2	MHV lower bounds	13
4.3	NMHV lower bounds	14
4.4	N ² MHV lower bounds	16
4.5	Emergent positivity	17
4.6	Parity and upper bounds	17
4.7	Increasing helicity	17
5	The hierarchy of one-loop boundaries	19
5.1	A graphical notation for low-helicity boundaries	20
5.2	A graphical recursion for generating low-helicity boundaries	21
6	Solving Landau equations in momentum twistor space	25
7	Singularities and symbology	27
8	Conclusion	29

1 Introduction

Physical principles impose strong constraints on the scattering amplitudes of elementary particles. For example, when working at finite order in perturbation theory, unitarity and locality appear to constrain amplitudes to be holomorphic functions with poles and branch points at precisely specified locations in the space of complexified kinematic data describing the configuration of particles. Indeed, it has been a long-standing goal to understand how to use the tightly prescribed analytic structure of scattering amplitudes to determine them directly, without relying on traditional (and, often computationally complex) Feynman diagram techniques.

The connection between the physical and mathematical structure of scattering amplitudes has been especially well studied in planar $\mathcal{N} = 4$ super-Yang-Mills [1] SYM¹ theory in

¹We use “SYM” to mean the planar limit, unless otherwise specified.

four spacetime dimensions, where the analytic structure of amplitudes is especially tame. The overall aim of this paper, its predecessors [2, 3], and its descendant(s), is to ask a question that might be hopeless in another, less beautiful quantum field theory: can we understand the branch cut structure of general scattering amplitudes in SYM theory?

The motivation for asking this question is two-fold. The first is the expectation that the rich mathematical structure that underlies the integrands of SYM theory (the rational $4L$ -forms that arise from summing L -loop Feynman diagrams, prior to integrating over loop momenta) is reflected in the corresponding scattering amplitudes. For example, it has been observed that both integrands [4] and amplitudes [5–7] are deeply connected to the mathematics of cluster algebras.

Second, on a more practical level, knowledge of the branch cut structure of amplitudes is the key ingredient in the amplitude bootstrap program, which represents the current state of the art for high loop order amplitude calculations in SYM theory. In particular the hexagon bootstrap (see for example [8]), which has succeeded in computing all six-particle amplitudes through five loops [9], is predicated on the hypothesis that at any loop order, these amplitudes can have branch points only on 9 specific loci in the space of external data. Similarly the heptagon bootstrap [10], which has revealed the symbols of the seven-particle four-loop MHV and three-loop NMHV amplitudes [11], assumes 42 particular branch points. One result we hope follows from understanding the branch cut structure of general amplitudes in SYM theory is a proof of this counting to all loop order for six- and seven-particle amplitudes.

It is a general property of quantum field theory (see for example [12, 13]) that the locations of singularities of an amplitude can be determined from knowledge of the poles of its integrand by solving the Landau equations [14]. Constructing explicit representations for integrands can be a challenging problem in general, but in SYM theory this can be side-stepped by using various on-shell methods [15–18] to efficiently determine the locations of integrand poles. This problem is beautifully geometrized by amplituhedra [19], which are spaces encoding representations of integrands in such a way that the boundaries of an amplituhedron correspond precisely to the poles of the corresponding integrand. Therefore, as pointed out in [3] (which we now take as our conceptual framework), the Landau equations can be interpreted as defining a map that associates to any boundary of an amplituhedron the locus in the space of external data where the corresponding amplitude has a singularity.

Only MHV amplitudes were considered in [3]. In this paper we show how to extend the analysis to amplitudes of arbitrary helicity. This is greatly aided by a recent combinatorial reformulation of amplituhedra in terms of “sign flips” [20]. As a specific application of our algorithm we classify the branch points of all one-loop amplitudes in SYM theory. Although the singularity structure of these amplitudes is of course well-understood (see for example [21–29]), this exercise serves a useful purpose in preparing a powerful toolbox for the sequel [30] to this paper where we will see that boundaries of one-loop amplituhedra are the basic building blocks at all loop order. In particular we find a surprising ‘emergent positivity’ on boundaries of one-loop amplituhedra that allows boundaries to be efficiently mapped between different helicity sectors, and recycled to higher loop levels.

The rest of this paper is organized as follows. In section 2 we review relevant definitions and background material and summarize the general procedure for finding singularities of amplitudes. In sections 3 and 4 we classify the relevant boundaries of all one-loop amplituhedra. Section 5 outlines a simple graphical notation for certain boundaries and shows that the one-loop boundaries all assemble into a simple graphical hierarchy which will prove useful for organizing higher-loop computations. In section 6 we show how to formulate and efficiently solve the Landau equations directly in momentum twistor space, thereby completing the identification of all branch points of one-loop amplitudes. The connection between these results and symbol alphabets is discussed in section 7.

2 Review

This section provides a thorough introduction to the problem our work aims to solve. The concepts and techniques reviewed here will be illuminated in subsequent sections via several concrete examples.

2.1 The kinematic domain

Scattering amplitudes are (in general multivalued) functions of the kinematic data (the energies and momenta) describing some number of particles participating in some scattering process. Specifically, amplitudes are functions only of the kinematic information about the particles entering and exiting the process, called *external data* in order to distinguish it from information about virtual particles which may be created and destroyed during the scattering process itself. A general scattering amplitude in SYM theory is labeled by three integers: the number of particles n , the helicity sector $0 \leq k \leq n - 4$, and the loop order $L \geq 0$, with $L = 0$ called *tree level* and $L > 0$ called *L-loop level*. Amplitudes with $k = 0$ are called maximally helicity violating (MHV) while those with $k > 0$ are called (next-to-) k maximally helicity violating (N^k MHV).

The kinematic configuration space of SYM theory admits a particularly simple characterization: n -particle scattering amplitudes² are multivalued functions on $\text{Conf}_n(\mathbb{P}^3)$, the space of configurations of n points in \mathbb{P}^3 [5]. A generic point in $\text{Conf}_n(\mathbb{P}^3)$ may be represented by a collection of n homogeneous coordinates Z_a^I on \mathbb{P}^3 (here $I \in \{1, \dots, 4\}$ and $a \in \{1, \dots, n\}$) called *momentum twistors* [31], with two such collections considered equivalent if the corresponding $4 \times n$ matrices $Z \equiv (Z_1 \cdots Z_n)$ differ by left-multiplication by an element of $\text{GL}(4)$. We use the standard notation

$$\langle a b c d \rangle = \epsilon_{IJKL} Z_a^I Z_b^J Z_c^K Z_d^L \tag{2.1}$$

for the natural $\text{SL}(4)$ -invariant four-bracket on momentum twistors and use the shorthand $\langle \cdots \bar{a} \cdots \rangle = \langle \cdots a-1 a a+1 \cdots \rangle$, with the understanding that all particle labels are always

²Here and in all that follows, we mean components of superamplitudes suitably normalized by dividing out the tree-level Parke-Taylor-Nair superamplitude [32, 33]. We expect our results to apply equally well to BDS- [34] and BDS-like [35] regulated MHV and non-MHV amplitudes. The set of branch points of a non-MHV ratio function [36] should be a subset of those of the corresponding non-MHV amplitude, but our analysis cannot exclude the possibility that it may be a proper subset due to cancellations.

taken mod n . We write (ab) to denote the line in \mathbb{P}^3 containing Z_a and Z_b , (abc) to denote the plane containing Z_a, Z_b and Z_c , and so \bar{a} denotes the plane $(a-1 a a+1)$. The bar notation is motivated by *parity*, which is a \mathbb{Z}_2 symmetry of SYM theory that maps N^k MHV amplitudes to N^{n-k-4} MHV amplitudes while mapping the momentum twistors according to $\{Z_a\} \mapsto \{W_a = *(a-1 a a+1)\}$.

When discussing N^k MHV amplitudes it is conventional to consider an enlarged kinematic space where the momentum twistors are promoted to homogeneous coordinates \mathcal{Z}_a , bosonized momentum twistors [19] on \mathbb{P}^{k+3} which assemble into an $n \times (k+4)$ matrix $\mathcal{Z} \equiv (\mathcal{Z}_1 \cdots \mathcal{Z}_n)$. The analog of eq. (2.1) is then the $SL(k+4)$ -invariant bracket which we denote by $[\cdot]$ instead of $\langle \cdot \rangle$. Given some \mathcal{Z} and an element of the Grassmannian $Gr(k, k+4)$ represented by a $k \times (k+4)$ matrix Y , one can obtain an element of $Conf_n(\mathbb{P}^3)$ by projecting onto the complement of Y . The four-brackets of the *projected external data* obtained in this way are given by

$$\langle abcd \rangle \equiv [Y \mathcal{Z}_a \mathcal{Z}_b \mathcal{Z}_c \mathcal{Z}_d]. \tag{2.2}$$

Tree-level amplitudes are rational functions of the brackets while loop-level amplitudes have both poles and branch cuts, and are properly defined on an infinitely-sheeted cover of $Conf_n(\mathbb{P}^3)$. For each k there exists an open set $\mathcal{D}_{n,k} \subset Conf_n(\mathbb{P}^3)$ called the *principal domain* on which amplitudes are known to be holomorphic and non-singular. Amplitudes are initially defined only on $\mathcal{D}_{n,k}$ and then extended to all of (the appropriate cover of) $Conf_n(\mathbb{P}^3)$ by analytic continuation.

A simple characterization of the principal domain for n -particle N^k MHV amplitudes was given in [20]: $\mathcal{D}_{n,k}$ may be defined as the set of points in $Conf_n(\mathbb{P}^3)$ that can be represented by a Z -matrix with the properties

1. $\langle aa+1 bb+1 \rangle > 0$ for all a and $b \notin \{a-1, a, a+1\}$,³ and
2. the sequence $\langle 123\bullet \rangle$ has precisely k sign flips,

where we use the notation $\bullet \in \{1, 2, \dots, n\}$ so that

$$\langle 123\bullet \rangle \equiv \{0, 0, 0, \langle 1234 \rangle, \langle 1235 \rangle, \dots, \langle 123n \rangle\}. \tag{2.3}$$

It was also shown that an alternate but equivalent condition is to say that the sequence $\langle aa+1 b\bullet \rangle$ has precisely k sign flips for all a, b (omitting trivial zeros, and taking appropriate account of the twisted cyclic symmetry where necessary). The authors of [20] showed, and we review in section 2.2, that for Y 's inside an N^k MHV amplituhedron, the projected external data have the two properties above.

2.2 Amplituhedra...

A matrix is said to be *positive* or *non-negative* if all of its ordered maximal minors are positive or non-negative, respectively. In particular, we say that the external data are positive if the $n \times (k+4)$ matrix \mathcal{Z} described in the previous section is positive.

³As explained in [20], the cyclic symmetry on the n particle labels is “twisted”, which manifests itself here in the fact that if k is even, and if $a = n$ or $b = n$, then cycling around n back to 1 introduces an extra minus sign. The condition in these cases is therefore $(-1)^{k+1} \langle cc+1 n 1 \rangle > 0$ for all $c \notin \{1, n-1, n\}$.

A point in the n -particle N^k MHV L -loop *amplituhedron* $\mathcal{A}_{n,k,L}$ is a collection $(Y, \mathcal{L}^{(\ell)})$ consisting of a point $Y \in \text{Gr}(k, k+4)$ and L lines $\mathcal{L}^{(1)}, \dots, \mathcal{L}^{(L)}$ (called the *loop momenta*) in the four-dimensional complement of Y . We represent each $\mathcal{L}^{(\ell)}$ as a $2 \times (k+4)$ matrix with the understanding that these are representatives of equivalence classes under the equivalence relation that identifies any linear combination of the rows of Y with zero.

For given positive external data \mathcal{Z} , the amplituhedron $\mathcal{A}_{n,k,L}(\mathcal{Z})$ was defined in [19] for $n \geq 4$ as the set of $(Y, \mathcal{L}^{(\ell)})$ that can be represented as

$$Y = CZ, \tag{2.4}$$

$$\mathcal{L}^{(\ell)} = D^{(\ell)} \mathcal{Z}, \tag{2.5}$$

in terms of a $k \times n$ real matrix C and L $2 \times n$ real matrices $D^{(\ell)}$ satisfying the positivity property that for any $0 \leq m \leq L$, all $(2m+k) \times n$ matrices of the form

$$\begin{pmatrix} D^{(i_1)} \\ D^{(i_2)} \\ \vdots \\ D^{(i_m)} \\ C \end{pmatrix} \tag{2.6}$$

are positive. The D -matrices are understood as representatives of equivalence classes and are defined only up to translations by linear combinations of rows of the C -matrix.

One of the main results of [20] was that amplituhedra can be characterized directly by (projected) four-brackets, eq. (2.2), without any reference to C or $D^{(\ell)}$'s, by saying that for given positive \mathcal{Z} , a collection $(Y, \mathcal{L}^{(\ell)})$ lies inside $\mathcal{A}_{n,k,L}(\mathcal{Z})$ if and only if

1. the projected external data lie in the principal domain $\mathcal{D}_{n,k}$,
2. $\langle \mathcal{L}^{(\ell)} a a+1 \rangle > 0$ for all ℓ and a ,⁴
3. for each ℓ , the sequence $\langle \mathcal{L}^{(\ell)} 1 \bullet \rangle$ has precisely $k+2$ sign flips, and
4. $\langle \mathcal{L}^{(\ell_1)} \mathcal{L}^{(\ell_2)} \rangle > 0$ for all $\ell_1 \neq \ell_2$.

Here the notation $\langle \mathcal{L} a b \rangle$ means $\langle A B a b \rangle$ if the line \mathcal{L} is represented as $(A B)$ for two points A, B . It was also shown that items 2 and 3 above are equivalent to saying that the sequence $\langle \mathcal{L}^{(\ell)} a \bullet \rangle$ has precisely $k+2$ sign flips for any ℓ and a .

2.3 ... and their boundaries

The amplituhedron $\mathcal{A}_{n,k,L}$ is an open set with boundaries at loci where one or more of the inequalities in the above definitions become saturated. For example, there are boundaries where Y becomes such that one or more of the projected four-brackets $\langle a a+1 b b+1 \rangle$ become zero. Such projected external data lie on a boundary of the principal domain

⁴Again, the twisted cyclic symmetry implies that the correct condition for the case $a = n$ is $(-1)^{k+1} \langle \mathcal{L}^{(\ell)} n 1 \rangle > 0$.

$\mathcal{D}_{n,k}$. Boundaries of this type are already present in tree-level amplituhedra, which are well-understood and complementary to the focus of our work.

Instead, the boundaries relevant to our analysis occur when Y is such that the projected external data are generic, but the $\mathcal{L}^{(\ell)}$ satisfy one or more *on-shell conditions* of the form

$$\langle \mathcal{L}^{(\ell)} a a+1 \rangle = 0 \quad \text{and/or} \quad \langle \mathcal{L}^{(\ell_1)} \mathcal{L}^{(\ell_2)} \rangle = 0. \quad (2.7)$$

We refer to boundaries of this type as \mathcal{L} -boundaries.⁵ The collection of loop momenta satisfying a given set of on-shell conditions comprises a set whose connected components we call *branches*. Consider two sets of on-shell conditions S, S' , with $S' \subset S$ a proper subset, and $B (B')$ a branch of solutions to $S (S')$. Since $S' \subset S$, B' imposes fewer constraints on the degrees of freedom of the loop momenta than B does. In the case when $B \subset B'$, we say B' is a *relaxation* of B . We use $\overline{\mathcal{A}_{n,k,L}}$ to denote the closure of the amplituhedron, consisting of $\mathcal{A}_{n,k,L}$ together with all of its boundaries. We say that $\mathcal{A}_{n,k,L}$ has a *boundary of type B* if $B \cap \overline{\mathcal{A}_{n,k,L}} \neq \emptyset$ and $\dim(B \cap \overline{\mathcal{A}_{n,k,L}}) = \dim(B)$.

2.4 The Landau equations

In [3] it was argued, based on well-known and general properties of scattering amplitudes in quantum field theory (see in particular [12]), that all information about the locations of branch points of amplitudes in SYM theory can be extracted from knowledge of the \mathcal{L} -boundaries of amplituhedra via the Landau equations [13, 14]. In order to formulate the Landau equations we must parameterize the space of loop momenta in terms of $4L$ variables d_A . For example, we could take⁶ $\mathcal{L}^{(\ell)} = D^{(\ell)} \mathcal{Z}$ with

$$D^{(1)} = \begin{pmatrix} 1 & 0 & d_1 & d_2 \\ 0 & 1 & d_3 & d_4 \end{pmatrix}, \quad D^{(2)} = \begin{pmatrix} 1 & 0 & d_5 & d_6 \\ 0 & 1 & d_7 & d_8 \end{pmatrix}, \quad \text{etc.}, \quad (2.8)$$

but any other parameterization works just as well.

Consider now an \mathcal{L} -boundary of some $\mathcal{A}_{n,k,L}$ on which the L lines $\mathcal{L}^{(\ell)}$ satisfy d on-shell constraints

$$f_J = 0 \quad (J = 1, 2, \dots, d), \quad (2.9)$$

each of which is of the form of one of the brackets shown in eq. (2.7). The *Landau equations* for this set of on-shell constraints comprise eq. (2.9) together with a set of equations on d auxiliary variables α_J known as *Feynman parameters*:

$$\sum_{J=1}^d \alpha_J \frac{\partial f_J}{\partial d_A} = 0 \quad (A = 1, \dots, 4L). \quad (2.10)$$

The latter set of equations are sometimes referred to as the *Kirchhoff conditions*.

⁵In the sequel [30] we will strengthen this definition to require that $\langle \mathcal{L}^{(1)} \mathcal{L}^{(2)} \rangle = 0$ at two loops.

⁶By writing each \mathcal{L} as a 2×4 matrix, instead of $2 \times (k+4)$, we mean to imply that we are effectively working in a gauge where the last four columns of Y are zero and so the first k columns of each \mathcal{L} are irrelevant and do not need to be displayed.

We are never interested in the values of the Feynman parameters, we only want to know under what conditions nontrivial solutions to Landau equations exist. Here, “nontrivial” means that the α_J must not all vanish.⁷ Altogether we have $d + 4L$ equations in $d + 4L$ variables (the d α_J ’s and the $4L$ d_A ’s). However, the Kirchhoff conditions are clearly invariant under a projective transformation that multiplies all of the α_J simultaneously by a common nonzero number, so the effective number of free parameters is only $d + 4L - 1$. Therefore, we might expect that nontrivial solutions to the Landau equations do not generically exist, but that they may exist on codimension-one loci in $\text{Conf}_n(\mathbb{P}^3)$ — these are the loci on which the associated scattering amplitude may have a singularity according to [13, 14].

However the structure of solutions is rather richer than this naive expectation suggests because the equations are typically polynomial rather than linear, and they may not always be algebraically independent. As we will see in the examples considered in section 6, it is common for nontrivial solutions to exist for generic projected external data,⁸ and it can happen that there are branches of solutions that exist only on loci of codimension higher than one. We will not keep track of solutions of either of these types since they do not correspond to branch points in the space of generic projected external data.

There are two important points about our procedure which were encountered in [3] and deserve to be emphasized. The first is a subtlety that arises from the fact that the on-shell conditions satisfied on a given boundary of some amplituhedron are not always independent. For example, the end of section 3 of [3] discusses a boundary of $\mathcal{A}_{n,0,2}$ described by nine on-shell conditions with the property that the ninth is implied by the other eight. This situation arises generically for $L > 1$, and a procedure — called *resolution* — for dealing with these cases was proposed in [3]. We postpone further discussion of this point to the sequel as this paper focuses only on one-loop examples.

Second, there is a fundamental asymmetry between the two types of Landau equations, (2.9) and (2.10), in two respects. When solving the on-shell conditions we are only interested in branches of solutions that (A1) exist for generic projected external data, and that (A2) have nonempty intersection with $\overline{\mathcal{A}_{n,k,L}}$ with correct dimension. In contrast, when further imposing the Kirchhoff constraints on these branches, we are interested in solutions that (B1) exist on codimension-one loci in $\text{Conf}_n(\mathbb{P}^3)$, and (B2) need not remain within $\overline{\mathcal{A}_{n,k,L}}$. The origin of this asymmetry was discussed in [3]. In brief, it arises from Cutkoskian intuition whereby singularities of an amplitude may arise from configurations of loop momenta that are outside the physical domain of integration (by virtue of being complex; or, in the current context, being outside the closure of the amplituhedron), and are

⁷Solutions for which some of the Feynman parameters vanish are often called “subleading” Landau singularities in the literature, in contrast to a “leading” Landau singularity for which all α ’s are nonzero. We will make no use of this terminology and pay no attention to the values of the α ’s other than ensuring they do not all vanish.

⁸Solutions of this type were associated with infrared singularities in [2]. We do not keep track of these solutions since the infrared structure of amplitudes in massless gauge theory is understood to all loop order based on exponentiation [34, 37]. However, if some set of Landau equations has an “IR solution” at some particular $\mathcal{L}^{(\ell)}$, there may be other solutions, at different values of $\mathcal{L}^{(\ell)}$, that exist only on loci of codimension one. In such cases we do need to keep track of the latter.

only accessible after analytic continuation to some higher sheet; whereas the monodromy of an amplitude around a singularity is computed by an integral over the physical domain with the cut propagators replaced by delta functions. The resulting monodromy will be zero, i.e. the branch point doesn't really exist, if there is no overlap between the physical domain and the locus where the cuts are satisfied, motivating (A2) above. In summary, it is important to “solve the on-shell conditions first” and then impose the Kirchhoff conditions on the appropriate branches of solutions only afterwards.

2.5 Summary: the algorithm

The Landau equations may be interpreted as defining a map which associates to each boundary of the amplituhedron $\mathcal{A}_{n,k,L}$ a locus in $\text{Conf}_n(\mathbb{P}^3)$ on which the corresponding n -point $N^k\text{MHV}$ L -loop amplitude has a singularity. The Landau equations themselves have no way to indicate whether a singularity is a pole or branch point. However, it is expected that all poles in SYM theory arise from boundaries that are present already in the tree-level amplituhedra [19]. These occur when some $\langle a a+1 b b+1 \rangle$ go to zero as discussed at the beginning of section 2.3. The aim of our work is to understand the loci where amplitudes have branch points, so we confine our attention to the \mathcal{L} -boundaries defined in that section.

The algorithm for finding all branch points of the n -particle $N^k\text{MHV}$ L -loop amplitude is therefore simple in principle:

1. Enumerate all \mathcal{L} -boundaries of $\mathcal{A}_{n,k,L}$ for generic projected external data.
2. For each \mathcal{L} -boundary, identify the codimension-one loci (if there are any) in $\text{Conf}_n(\mathbb{P}^3)$ on which the corresponding Landau equations admit nontrivial solutions.

However, it remains a difficult and important outstanding problem to fully characterize the boundaries of general amplituhedra. In the remainder of this paper we focus on the special case $L = 1$, since all \mathcal{L} -boundaries of $\mathcal{A}_{n,k,1}$ (which have been discussed extensively in [38]) may be enumerated directly for any given n :

- 1(a). Start with a list of all possible sets of on-shell conditions of the form $\langle \mathcal{L} a a+1 \rangle = 0$.
- 1(b). For each such set, identify all branches of solutions that exist for generic projected external data.
- 1(c). For each such branch B , determine the values of k for which $\mathcal{A}_{n,k,1}$ has a boundary of type B .

It would be enormously inefficient to carry out this simple-minded algorithm beyond one loop. Fortunately, we will see in the sequel that the one-loop results of this paper can be exploited very effectively to generate \mathcal{L} -boundaries of $L > 1$ amplituhedra.

3 One-loop branches

In this section we carry out steps 1(a) and 1(b) listed at the end of section 2.5. To that end we first introduce a graphical notation for representing sets of on-shell conditions via

Landau diagrams. Landau diagrams take the form of ordinary Feynman diagrams, with external lines labeled $1, \dots, n$ in cyclic order and one internal line (called a *propagator*) corresponding to each on-shell condition. Landau diagrams relevant to amplituhedra are always planar. Each internal face of an L -loop Landau diagram is labeled by a distinct $\ell \in \{1, \dots, L\}$, and each external face may be labeled by the pair $(a a+1)$ of external lines bounding that face.

The set of on-shell conditions encoded in a given Landau diagram is read off as follows:

- To each propagator bounding an internal face ℓ and an external face $(a a+1)$ we associate the on-shell condition $\langle \mathcal{L}^{(\ell)} a a+1 \rangle = 0$.
- To each propagator bounding two internal faces ℓ_1, ℓ_2 we associate the on-shell condition $\langle \mathcal{L}^{(\ell_1)} \mathcal{L}^{(\ell_2)} \rangle = 0$.

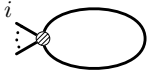


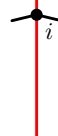


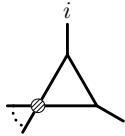
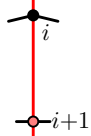
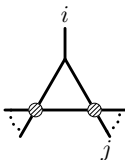

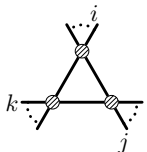
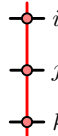
At one loop we only have on-shell conditions of the first type. Moreover, since \mathcal{L} only has four degrees of freedom (the dimension of $\text{Gr}(2, 4)$ is four), solutions to a set of on-shell conditions will exist for generic projected external data only if the number of conditions is $d \leq 4$. Diagrams with $d = 1, 2, 3, 4$ are respectively named tadpoles, bubbles, triangles and boxes. The structure of solutions to a set of on-shell conditions can change significantly depending on how many pairs of conditions involve adjacent indices. Out of abundance of caution it is therefore necessary to consider separately the eleven distinct types of Landau diagrams shown in the second column of table 1. For $d > 1$ their names are qualified by indicating the number of nodes with valence greater than three, called *masses*. These rules suffice to uniquely name each distinct type of diagram except the two two-mass boxes shown in table 1 which are conventionally called “easy” and “hard”. This satisfies step 1(a) of the algorithm.

Proceeding now to step 1(b), we display in the third column of table 1 all branches of solutions (as always, for generic projected external data) to the on-shell conditions associated to each Landau diagram. These expressions are easily checked by inspection or by a short calculation. More details and further discussion of the geometry of these problems can be found for example in [39]. The three-mass triangle solution involves the quantities

$$\begin{aligned} \rho(\alpha) &= -\alpha \langle i j+1 k k+1 \rangle - (1 - \alpha) \langle i+1 j+1 k k+1 \rangle, \\ \sigma(\alpha) &= \alpha \langle i j k k+1 \rangle + (1 - \alpha) \langle i+1 j k k+1 \rangle, \end{aligned} \tag{3.1}$$

and the four-mass box solution is sufficiently messy that we have chosen not to write it out explicitly.

Altogether there are nineteen distinct types of branches, which we have numbered (1) through (19) in table 1 for ease of reference. The set of solutions to any set of on-shell conditions of the form $\langle \mathcal{L} a a+1 \rangle$ must be closed under parity, since each line $(a a+1)$ maps to itself. Most sets of on-shell conditions have two branches of solutions related to each other by parity. Only the tadpole, two-mass bubble, and three-mass triangle (branches (1), (4), and (9) respectively) have single branches of solutions that are closed under parity.

Name	Landau Diagram	Branches	k-Validity	Low-k Twistor Diagram	Singularity Locus/Loci
tadpole ($n \geq 4$)		(1) $\mathcal{L} = (\alpha Z_i + (1-\alpha)Z_{i+1}, A)$	$0 \leq k \leq n-4$		0
one-mass bubble ($n \geq 4$)		(2) $\mathcal{L} = (Z_i, A)$ (3) $\mathcal{L} = \bar{i} \cap P$	$0 \leq k \leq n-4$ $n-4 \geq k \geq 0$		0
two-mass bubble ($n \geq 4$)		(4) $\mathcal{L} = (\alpha Z_i + (1-\alpha)Z_{i+1}, \beta Z_j + (1-\beta)Z_{j+1})$	$0 \leq k \leq n-4$		$\langle ii+1 jj+1 \rangle$
one-mass triangle ($n \geq 4$)		(5) $\mathcal{L} = (Z_i, \alpha Z_{i+1} + (1-\alpha)Z_{i+2})$ (6) $\mathcal{L} = (Z_{i+1}, \alpha Z_{i-1} + (1-\alpha)Z_i)$	$0 \leq k \leq n-4$ $n-4 \geq k \geq 0$		0
two-mass triangle ($n \geq 5$)		(7) $\mathcal{L} = (Z_i, \alpha Z_j + (1-\alpha)Z_{j+1})$ (8) $\mathcal{L} = \bar{i} \cap (jj+1A)$	$0 \leq k \leq n-5$ $n-4 \geq k \geq 1$		0
three-mass triangle ($n \geq 6$)		(9) $\mathcal{L} = (\alpha Z_i + (1-\alpha)Z_{i+1}, \rho(\alpha)Z_j + \sigma(\alpha)Z_{j+1})$	$1 \leq k \leq n-5$		$f_{ij}f_{jk}f_{ki}$

Name	Landau Diagram	Branches	k-Validity	Low-k Twistor Diagram	Singularity Locus/Loci
one-mass box ($n \geq 5$)		(10) $\mathcal{L} = (ii+2)$ (11) $\mathcal{L} = \bar{i}\bar{i}+2$	$0 \leq k \leq n-5$ $n-4 \geq k \geq 1$		$\langle i\bar{i}+2 \rangle \langle \bar{i}i+2 \rangle$
two-mass easy box ($n \geq 6$)		(12) $\mathcal{L} = (ij)$ (13) $\mathcal{L} = \bar{i}\bar{i}j$	$0 \leq k \leq n-6$ $n-4 \geq k \geq 2$		$\langle i\bar{j} \rangle \langle \bar{i}j \rangle$
two-mass hard box ($n \geq 6$)		(14) $\mathcal{L} = \bar{i}+1\bar{i}\cap(ijj+1)$ (15) $\mathcal{L} = \bar{i}\cap(i+1jj+1)$	$1 \leq k \leq n-5$ $n-5 \geq k \geq 1$		$\langle \bar{i}i+2 \rangle \langle ii+1jj+1 \rangle$
three-mass box ($n \geq 7$)		(16) $\mathcal{L} = (ijj+1)\cap(ikk+1)$ (17) $\mathcal{L} = (\bar{i}\cap(jj+1), \bar{i}\cap(kk+1))$	$1 \leq k \leq n-6$ $n-5 \geq k \geq 2$		$\langle i(i-1i+1)(jj+1)(kk+1) \rangle$
four-mass box ($n \geq 8$)		(18) $\mathcal{L} =$ (19) $\mathcal{L} =$ } see table 2 of [40]	$2 \leq k \leq n-6$ $n-6 \geq k \geq 2$		$(f_{ij}f_{kl} - f_{ik}f_{jl} + f_{il}f_{jk})^2 - 4f_{ij}f_{jk}f_{kl}f_{il} \equiv \Delta_{ijkl}$

Table 1. This table shows: the eleven Landau diagrams corresponding to sets of one-loop on-shell conditions that can be satisfied for generic projected external data; the nineteen branches of solutions to these on-shell conditions; the range of k for which N^k MHV amplituhedra have boundaries of each type; the twistor diagram depicting the low- k solution (or one low- k solution for the one-mass triangle and two-mass hard box); the loci in $\text{Conf}_n(\mathbb{P}^3)$ where the Landau equations for each branch admit nontrivial solutions (where the quantity in the last column vanishes). At one loop it happens that the loci are the same for each branch of solutions to a given set of on-shell conditions. Here α, β are arbitrary numbers, A is an arbitrary point in \mathbb{P}^3 , P is an arbitrary plane in \mathbb{P}^3 , $\rho(\alpha), \sigma(\alpha)$ are defined in eq. (3.1), $f_{ab} \equiv \langle a a+1 b b+1 \rangle$, and $\langle i(i-1i+1)(jj+1)(kk+1) \rangle \equiv \langle i-1ijj+1 \rangle \langle ii+1kk+1 \rangle - (j \leftrightarrow k)$.

4 One-loop boundaries

We now turn to the last step 1(c) from the end of section 2.5: for each of the nineteen branches B listed in table 1, we must determine the values of k for which $\mathcal{A}_{n,k,1}$ has a boundary of type B (defined in section 2.3). The results of this analysis are listed in the fourth column of the table 1. Our strategy for obtaining these results is two-fold.

In order to prove that an amplituhedron has a boundary of type B , it suffices to write down a pair of matrices C, D such that definitions (2.4) and (2.5) hold, C and $\begin{pmatrix} D \\ C \end{pmatrix}$ are both non-negative, and the external data projected through $Y = CZ$ are generic for generic positive Z . We call such a pair C, D a *valid configuration* for B . In the sections below we present explicit valid configurations for each of the nineteen branches. Initially we consider for each branch only the lowest value of k for which a valid configuration exists; in section 4.7 we explain how to grow these to larger values of k and establish the upper bounds on k shown in table 1.

However, in order to prove that an amplituhedron does not have a boundary of type B , it does not suffice to find a configuration that is not valid; one must show that no valid configuration exists. We address this problem in the next section.

4.1 A criterion for establishing absent branches

Fortunately, for \mathcal{L} -boundaries of the type under consideration there is a simple criterion for establishing when no valid configuration can exist. The crucial ingredient is that if $(Y, \mathcal{L}) \in \overline{\mathcal{A}_{n,k,1}}$ and $\langle \mathcal{L} a a+1 \rangle = 0$ for some a , then $\langle \mathcal{L} a a+2 \rangle$ must necessarily be non-positive;⁹ the proof of this assertion, which we omit here, parallels that of a closely related statement proven in section 6 of [20].

Consider now a line of the form $\mathcal{L} = (\alpha Z_a + \beta Z_{a+1}, A)$ for some point A and some parameters α, β which are not both vanishing. We will show that an \mathcal{L} of this form can lie in the closure of an amplituhedron only if $\mathcal{L} = (a a+1)$ or $\alpha\beta \geq 0$.

First, as just noted, since $\langle \mathcal{L} a a+1 \rangle = 0$ we must have

$$0 \geq \langle \mathcal{L} a a+2 \rangle = \beta \langle a+1 A a a+2 \rangle. \tag{4.1}$$

On the other hand, as mentioned at the end of section 2.2, we also have $\langle \mathcal{L} a a+1 \rangle \geq 0$ for all a . Applying this to $a + 1$ gives

$$0 \leq \langle \mathcal{L} a+1 a+2 \rangle = \alpha \langle a A a+1 a+2 \rangle. \tag{4.2}$$

If $\langle a a+1 a+2 A \rangle \neq 0$, then the two inequalities (4.1) and (4.2) imply that $\alpha\beta \geq 0$.

This is the conclusion we wanted, but it remains to address what happens if $\langle a a+1 a+2 A \rangle = 0$. In this case \mathcal{L} lies in the plane $(a a+1 a+2)$ so we can take

⁹ Unless $a \in \{n-1, n\}$, when one must take into account the twisted cyclic symmetry. In all that follows we will for simplicity always assume that indices are outside of this range, which lets us uniformly ignore all sign factors that might arise from the twisted cyclic symmetry; these signs necessarily always conspire to ensure that all statements about amplitudes are \mathbb{Z}_n cyclically invariant.

$\mathcal{L} = (\alpha Z_a + \beta Z_{a+1}, \gamma Z_{a+1} + \delta Z_{a+2})$. Then we have

$$\begin{aligned} 0 &\geq \langle \mathcal{L} a+1 a+3 \rangle = -\alpha \delta \langle a a+1 a+2 a+3 \rangle, \\ 0 &\leq \langle \mathcal{L} a-1 a \rangle = \beta \delta \langle a-1 a a+1 a+2 \rangle. \end{aligned} \quad (4.3)$$

Both of the four-brackets in these inequalities are positive (for generic projected external data) since they are of the form $\langle a a+1 b b+1 \rangle$, so we conclude that either $\delta = 0$, which means that $\mathcal{L} = (a a+1)$, or else we again have $\alpha\beta \geq 0$.

In conclusion, we have developed a robust test which establishes that

$$\mathcal{L} = (\alpha Z_a + \beta Z_{a+1}, A) \in \overline{\mathcal{A}_{n,k,1}} \text{ only if } \mathcal{L} = (a a+1) \text{ or } \alpha\beta \geq 0. \quad (4.4)$$

This statement is independent of k (and Y), but when applied to particular branches, we will generally encounter cases for which $\alpha\beta$ is negative unless certain sequences of four-brackets of the projected external data have a certain number of sign flips; this signals that the branch may intersect $\overline{\mathcal{A}_{n,k,1}}$ only for certain values of k .

4.2 MHV lower bounds

The fact that MHV amplituhedra only have boundaries of type (1)–(7), (10) and (12) (referring to the numbers given in the “Branches” column of table 1) follows implicitly from the results of [3] where all boundaries of one- (and two-) loop MHV amplituhedra were studied. It is nevertheless useful to still consider these cases since we will need the corresponding D -matrices below to establish that amplituhedra have boundaries of these types for all $0 \leq k \leq n-4$.

In this and the following two sections we always assume, without loss of generality, that indices i, j, k, ℓ are cyclically ordered and non-adjacent ($i+1 < j < j+1 < k < k+1 < \ell$), and moreover that $1 < i$ and $\ell < n$. In particular, this means that we ignore potential signs from the twisted cyclic symmetry (see footnote 9).

Branch (4) is a prototype for several other branches, so we begin with it instead of branch (1). The solution for \mathcal{L} shown in table 1 may be represented as $\mathcal{L} = DZ$ with

$$D = \begin{pmatrix} & i & i+1 & j & j+1 \\ \alpha & 1-\alpha & 0 & 0 & \\ 0 & 0 & \beta & 1-\beta & \end{pmatrix}, \quad (4.5)$$

where we display only the nonzero columns of the $2 \times n$ matrix in the indicated positions $i, i+1, j$ and $j+1$. This solves the two-mass bubble on-shell conditions for all values of the parameters α and β . This branch intersects $\overline{\mathcal{A}_{n,0,1}}$ when they lie in the range $0 \leq \alpha, \beta \leq 1$, where the matrix D is non-negative. Thus we conclude that MHV amplituhedra have boundaries of type (4).

Branches (5), (6), (7), (10), and (12) can all be represented by special cases of eq. (4.5) for α and/or β taking values 0 and/or 1, and/or with columns relabeled, so MHV amplituhedra also have boundaries of all of these types.

Branch (1) may be represented by

$$D = \begin{pmatrix} & i-1 & i & i+1 & i+2 & \\ \cdots & 0 & \alpha & 1-\alpha & 0 & \cdots \\ \cdots & \alpha_{i-1} & \alpha_i & \alpha_{i+1} & \alpha_{i+2} & \cdots \end{pmatrix}. \quad (4.6)$$

This provides a solution to the tadpole on-shell condition $\langle \mathcal{L} i i+1 \rangle = 0$ for all values of the parameters, and there clearly are ranges for which D is non-negative. Note that all but two of the parameters in the second row could be gauged away, but this fact is not relevant at the moment (see footnote 10). If $0 \leq \alpha \leq 1$, we could have either $\alpha_a = 0$ for $a < i + 1$ and $\alpha_a > 0$ for $a > i$, or $\alpha = 0$ for $a > i$ and $\alpha_a < 0$ for $a < i + 1$. We conclude that MHV amplituhedra also have boundaries of this type.

Branch (2) is the special case $\alpha = 1$ of branch (1).

Branch (3) may be represented by

$$D = \begin{pmatrix} & i-1 & i & i+1 & \\ & 1 & 0 & \alpha & \\ & 0 & 1 & \beta & \end{pmatrix} \quad (4.7)$$

for arbitrary α, β , which is non-negative for $\alpha \leq 0$ and $\beta \geq 0$, so MHV amplituhedra also have boundaries of this type.

4.3 NMHV lower bounds

Branch (8) of the two-mass triangle may be represented as

$$D = \begin{pmatrix} & i & i+1 & & j & j+1 & \\ \alpha & 1-\alpha & & 0 & 0 & & \\ 0 & 0 & & -\langle \bar{i} j+1 \rangle & \langle \bar{i} j \rangle & & \end{pmatrix} \quad (4.8)$$

for arbitrary α . For generic projected external data $\mathcal{L} \neq (j j+1)$, so criterion (4.4) shows that this configuration has a chance to lie on the boundary of an amplituhedron only if $-\langle \bar{i} j+1 \rangle \langle \bar{i} j \rangle \geq 0$. This is not possible for MHV external data, where the ordered four-brackets are always positive, so MHV amplituhedra do not have boundaries of this type. But note that the inequality can be satisfied if there is at least one sign flip in the sequence $\langle \bar{i} \bullet \rangle$, between $\bullet = j$ and $\bullet = j+1$. This motivates us to consider $k = 1$, so let us now check that with

$$C = \begin{pmatrix} & i-1 & i & i+1 & j & j+1 & \\ c_{i-1} & c_i & c_{i+1} & c_j & c_{j+1} & & \end{pmatrix}, \quad (4.9)$$

the pair C, D is a valid configuration. First of all, it is straightforward to check that $\mathcal{L} = D\mathcal{Z}$ still satisfies the two-mass triangle on-shell conditions. This statement is not completely trivial since these conditions now depend on $Y = C\mathcal{Z}$ because of the

projection (2.2). Second, in order for C to be non-negative we need all five of the indicated c_a 's to be non-negative. Moreover, in order to support generic projected external data, we need them all to be nonzero — if, say, c_i were equal to zero, then $\langle i-1 \ i+1 \ j \ j+1 \rangle$ would vanish, etc. Finally, for $\left(\frac{D}{C}\right)$ to be non-negative we need

$$0 \leq \alpha \leq \frac{c_i}{c_i + c_{i+1}}. \tag{4.10}$$

This branch intersects $\overline{\mathcal{A}_{n,1,1}}$ for α in this range, so we conclude that NMHV amplituhedra have boundaries of this type.

Branch (9) is the general solution of the three-mass triangle, and is already given in table 1 in D -matrix form as

$$D = \begin{pmatrix} & i & i+1 & j & j+1 \\ \alpha & 1-\alpha & 0 & 0 & \\ 0 & 0 & \rho(\alpha) & \sigma(\alpha) & \end{pmatrix}, \tag{4.11}$$

with $\rho(\alpha)$ and $\sigma(\alpha)$ defined in eq. (3.1). For generic projected external data this \mathcal{L} can never attain the value $\langle i \ i+1 \rangle$ or $\langle j \ j+1 \rangle$. Applying criterion (4.4) for both $a = i$ and $a = j$ shows that this configuration has a chance to lie on the boundary of an amplituhedron only if $\alpha(1-\alpha) \geq 0$ and $\rho(\alpha)\sigma(\alpha) \geq 0$. This is not possible for MHV external data, so we conclude that MHV amplituhedra do not have boundaries of this type. However, the $\rho(\alpha)\sigma(\alpha) \geq 0$ inequality can be satisfied if the sequences $\langle i \ k \ k+1 \bullet \rangle$ and $\langle i+1 \ k \ k+1 \bullet \rangle$ change sign between $\bullet = j$ and $\bullet = j+1$, as long as the sequences $\langle j \ k \ k+1 \bullet \rangle$ and $\langle j+1 \ k \ k+1 \bullet \rangle$ do not flip sign here. Consider for $k = 1$ the matrix

$$C = \begin{pmatrix} & i & i+1 & j & j+1 & k & k+1 \\ \alpha c_i & (1-\alpha)c_i & c_j & c_{j+1} & c_k & c_{k+1} & \end{pmatrix}. \tag{4.12}$$

Then C, D is a valid configuration because (1) $\mathcal{L} = D\mathcal{Z}$ satisfies the three-mass triangle on-shell conditions (for all values of α and the c 's), and, (2) for $0 \leq \alpha \leq 1$ and all c 's positive, the C -matrix is non-negative and supports generic positive external data (because it has at least $k+4 = 5$ nonzero columns), and (3) for this range of parameters $\left(\frac{D}{C}\right)$ is also non-negative. Since this branch intersects $\overline{\mathcal{A}_{n,1,1}}$ for a range of α , we conclude that NMHV amplituhedra have boundaries of this type.

Branch (16) is the special case $\alpha = 1$ of branch (9).

Branch (14) is the special case $j \rightarrow i + 1, k \rightarrow j$ of branch (16).

Branch (15) is equivalent to the mirror image of branch (14), after relabeling.

Branch (11) is the special case $j = i + 2$ of branch (15).

4.4 N²MHV lower bounds

Branch (17) may be represented by

$$D = \begin{pmatrix} & j & j+1 & k & k+1 \\ 0 & 0 & -\langle \bar{i} k+1 \rangle & \langle \bar{i} k \rangle \\ -\langle \bar{i} j+1 \rangle & \langle \bar{i} j \rangle & 0 & 0 \end{pmatrix}. \quad (4.13)$$

For generic projected external data the corresponding \mathcal{L} will never attain the value $(j j+1)$ or $(k k+1)$. We can apply criterion (4.4) for both $a = j$ and $a = k$, which reveals that this configuration has a chance to lie on a boundary of an amplituhedron only if both $-\langle \bar{i} j+1 \rangle \langle \bar{i} j \rangle \geq 0$ and $-\langle \bar{i} k+1 \rangle \langle \bar{i} k \rangle \geq 0$. This is impossible for MHV external data, and it is also impossible in the NMHV case, where some projected four-brackets may be negative but the sequence $\langle \bar{i} \bullet \rangle$ may only flip sign once, whereas we need it to flip sign twice, once between $\bullet = j$ and $\bullet = j+1$, and again between $\bullet = k$ and $\bullet = k+1$. We conclude that $k < 2$ amplituhedra do not have boundaries of this form. Consider now pairing (4.13) with the $k = 2$ matrix

$$C = \begin{pmatrix} i-1 & i & i+1 & j & j+1 & k & k+1 \\ c_{11} & c_{12} & c_{13} & c_{14} & c_{15} & 0 & 0 \\ c_{21} & c_{22} & c_{23} & 0 & 0 & c_{24} & c_{25} \end{pmatrix}. \quad (4.14)$$

It is straightforward to check that C, D is a valid configuration for a range of values of c 's, so we conclude that $k = 2$ amplituhedra have boundaries of this type.

Branch (13) may be represented by

$$D = \begin{pmatrix} i-1 & i & i+1 \\ \langle i \bar{j} \rangle & -\langle i-1 \bar{j} \rangle & 0 \\ 0 & -\langle i+1 \bar{j} \rangle & \langle i \bar{j} \rangle \end{pmatrix}, \quad (4.15)$$

which by (4.4) cannot lie on a boundary of an amplituhedron unless the sequence $\langle \bar{j} \bullet \rangle$ flips sign twice, first between $\bullet = i-1$ and i and again between $\bullet = i$ and $i+1$. Therefore, neither MHV nor NMHV amplituhedra have boundaries of this type. However it is straightforward to verify that with

$$C = \begin{pmatrix} i-1 & i & i+1 & j-1 & j & j+1 \\ c_{11} & c_{12} & 0 & c_{13} & c_{14} & c_{15} \\ 0 & c_{21} & c_{22} & c_{23} & c_{24} & c_{25} \end{pmatrix} \quad (4.16)$$

the pair C, D is a valid configuration for a range of values of c 's, so $k = 2$ amplituhedra do have boundaries of this type.

Branches (18) and (19) of the four-mass box may be represented as

$$D = \begin{pmatrix} i & i+1 & j & j+1 \\ \alpha & 1-\alpha & 0 & 0 \\ 0 & 0 & \beta & 1-\beta \end{pmatrix}, \quad (4.17)$$

where α and β are fixed by requiring that \mathcal{L} intersects the lines $(k, k+1)$ and $(\ell, \ell+1)$. The values of α and β on the two branches were written explicitly in [40]; however, the complexity of those expressions makes analytic positivity analysis difficult. We have therefore resorted to numerical testing: using the algorithm described in section 5.4 of [4], we generate a random positive $n \times (k + 4)$ \mathcal{Z} -matrix and a random positive $k \times n$ C -matrix. After projecting through $Y = CZ$, we obtain projected external data with the correct N^k MHV sign-flipping properties. We have checked numerically that both four-mass box branches lie on the boundary of N^k MHV amplituhedra only for $k \geq 2$, for many instances of randomly generated external data.

4.5 Emergent positivity

The analysis of sections 4.2, 4.3 and 4.4 concludes the proof of all of the lower bounds on k shown in the fourth column of table 1. We certainly do not claim to have written down the most general possible valid C, D configurations; the ones we display for $k > 0$ have been specifically chosen to demonstrate an interesting feature we call *emergent positivity*.

In each $k > 0$ case we encountered D -matrices that are only non-negative if certain sequences of projected four-brackets of the form $\langle a, a+1, b, \bullet \rangle$ change sign k times, at certain precisely specified locations. It is straightforward to check that within the range of validity of each C, D pair we have written down, the structure of the C matrix is such that it automatically puts the required sign flips in just the right places to make the D matrix, on its own, non-negative (provided, of course, that $\binom{D}{C}$ is non-negative). It is not a priori obvious that it had to be possible to find pairs C, D satisfying this kind of emergent positivity; indeed, it is easy to find valid pairs for which it does not hold.

4.6 Parity and upper bounds

Parity relates each branch to itself or to the other branch associated with the same Landau diagram. Since parity is a symmetry of the amplituhedron [20] which relates k to $n - k - 4$, the lower bounds on k that we have established for various branches imply upper bounds on k for their corresponding parity conjugates. These results are indicated in the fourth column of table 1, where the inequalities are aligned so as to highlight the parity symmetry.

Although these k upper bounds are required by parity symmetry, they may seem rather mysterious from the analysis carried out so far. We have seen that certain branches can be boundaries of an amplituhedron only if certain sequences of four-brackets have (at least) one or two sign flips. In the next section, we explain a mechanism which gives an upper bound to the number of sign flips, or equivalently which gives the upper bounds on k that are required by parity symmetry.

4.7 Increasing helicity

So far we have only established that N^k MHV amplituhedra have boundaries of certain types for specific low (or, by parity symmetry, high) values of k . It remains to show that all of the branches listed in table 1 lie on boundaries of amplituhedra for all of the intermediate helicities. To this end we describe now an algorithm for converting a valid

configuration C_0, D_0 at the initial, minimal value of k_0 (with C_0 being the empty matrix for those branches with $k_0 = 0$) into a configuration that is valid at some higher value of k .

We maintain the structure of $D \equiv D_0$ and append to C_0 a matrix C' of dimensions $(k - k_0) \times n$ in order to build a configuration for helicity k . Defining $C = \begin{pmatrix} C_0 \\ C' \end{pmatrix}$, we look for a C' such that following properties are satisfied:

1. The same on-shell conditions are satisfied.
2. In order for the configuration to support generic projected external data, the C -matrix must have $m \geq k + 4$ nonzero columns, and the rank of any $m - 4$ of those columns must be k .
3. Both C and $\begin{pmatrix} D \\ C \end{pmatrix}$ remain non-negative.

Since the C -matrix only has n columns in total, it is manifest from property (2) that everything shuts off for $k > n - 4$, as expected.

Let us attempt to preserve the emergent positivity of D . If $k_0 = 0$ then this is trivial; the D -matrices in section 4.2 do not depend on any brackets, so adding rows to the empty C_0 has no effect on D . For $k_0 > 0$, let A and B be two entries in D_0 that are responsible for imposing a sign flip requirement. The argument applies equally to all of the $k_0 > 0$ branches, but for the sake of definiteness consider from eq. (4.8) the two four-bracket dependent entries $A = -\langle \bar{i} j+1 \rangle$ and $B = \langle \bar{i} j \rangle$. Assuming that C_0 is given by eq. (4.9) so that both A and B are positive with respect to $Y_0 = C_0 \mathcal{Z}$, then $AB = -[Y_0 \bar{i} j+1][Y_0 \bar{i} j] > 0$. If we append a second row C' and define $Y' = C' \mathcal{Z}$ then we have

$$\begin{aligned} A &= -[Y_0 Y' \mathcal{Z}_{i-1} \mathcal{Z}_i \mathcal{Z}_{i+1} \mathcal{Z}_{j+1}] = -c_j [\mathcal{Z}_j Y' \mathcal{Z}_i \mathcal{Z}_{i+1} \mathcal{Z}_{j+1}], \\ B &= [Y_0 Y' \mathcal{Z}_{i-1} \mathcal{Z}_i \mathcal{Z}_{i+1} \mathcal{Z}_j] = c_{j+1} [\mathcal{Z}_{j+1} Y' \mathcal{Z}_i \mathcal{Z}_{i+1} \mathcal{Z}_j]. \end{aligned} \tag{4.18}$$

Since c_j and c_{j+1} are both positive, we see that A and B still satisfy $AB > 0$, regardless of the value of Y' . By the same argument, arbitrary rows can be added to a C -matrix without affecting the on-shell conditions, so property (1) also holds trivially (and also if $k_0 = 0$).

The structure of the initial D_0 of sections 4.2, 4.3 and 4.4 are similar in that the nonzero columns of this matrix are grouped into at most two *clusters*.¹⁰ For example, for branch (17) there are two clusters $\{j, j+1\}$ and $\{k, k+1\}$ while for branch (3) there is only a single cluster $\{i-1, i, i+1\}$. Property (3) can be preserved most easily if we add suitable columns only in a *gap* between clusters. Let us illustrate how this works in the case of branch (4) where C_0 is empty and we can start by taking either

$$\begin{pmatrix} D_0 \\ C \end{pmatrix} = \begin{pmatrix} & i-1 & i & i+1 & i+2 & \cdots & j-1 & j & j+1 & j+2 & \\ \cdots & 0 & \alpha & 1-\alpha & 0 & \cdots & 0 & 0 & 0 & 0 & \cdots \\ \cdots & 0 & 0 & 0 & 0 & \cdots & 0 & \beta & 1-\beta & 0 & \cdots \\ \cdots & 0 & 0 & \vec{c}_{i+1} & \vec{c}_{i+2} & \cdots & \vec{c}_{j-1} & \vec{c}_j & 0 & 0 & \cdots \end{pmatrix} \tag{4.19}$$

¹⁰Branch (1) appears to be an exception, but only because eq. (4.6) as written is unnecessarily general: it is sufficient for the second row to have only three nonzero entries, either in columns $\{i-3, i-2, i-1\}$ or in columns $\{i+1, i+2, i+3\}$.

to fill in the gap between clusters $\{i, i+1\}$ and $\{j, j+1\}$, or

$$\begin{pmatrix} D_0 \\ C \end{pmatrix} = \begin{pmatrix} & i-1 & i & i+1 & i+2 & \cdots & j-1 & j & j+1 & j+2 & \\ \cdots & 0 & \alpha & 1-\alpha & 0 & \cdots & 0 & 0 & 0 & 0 & \cdots \\ \cdots & 0 & 0 & 0 & 0 & \cdots & 0 & \beta & 1-\beta & 0 & \cdots \\ \cdots & \vec{c}_{i-1} & \vec{c}_i & 0 & 0 & \cdots & 0 & 0 & \vec{c}_{j+1} & \vec{c}_{j+2} & \cdots \end{pmatrix} \quad (4.20)$$

to fill in the gap between $\{j, j+1\}$ and $\{i, i+1\}$ that “wraps around” from n back to 1. In both (4.19) and (4.20) each \vec{c}_a is understood to be a k -component column vector, and in both cases $\begin{pmatrix} D_0 \\ C \end{pmatrix}$ can be made non-negative as long as C is chosen to be non-negative.¹¹ In this manner we can trivially increment the k -validity of a given configuration until the gaps become full. This cutoff depends on the precise positions of the gaps, and is most stringent when the two clusters are maximally separated from each other, since this forces the gaps to be relatively small. In this worst case we can fit only $\lceil \frac{n}{2} \rceil$ columns into a C -matrix of one of the above two types. Keeping in mind property (2) that the C -matrix should have at least $k+4$ nonzero columns, we see that this construction can reach values of $k \leq \lceil \frac{n}{2} \rceil - 4$. In order to proceed further, we can (for example) add additional columns c_i and c_{j+1} to eq. (4.19), or c_{i+1} and c_j to eq. (4.20). Choosing a non-negative C then no longer trivially guarantees that $\begin{pmatrix} D_0 \\ C \end{pmatrix}$ will also be non-negative, but there are ranges of C for which this is possible to arrange, which is sufficient for our argument.

It is possible to proceed even further by adding additional, specially crafted columns in both gaps, but the argument is intricate and depends delicately on the particular structure of each individual branch (as evident from the delicate structure of k upper bounds in table 1). In the interest of brevity we terminate our discussion of the algorithm here and note that it is straightforward to check that for all boundaries, even in the worst case the gaps are always big enough to allow the construction we have described to proceed up to and including the parity-symmetric midpoint $k = \lfloor \frac{n}{2} \rfloor - 2$; then we appeal again to parity symmetry in order to establish the existence of valid configurations for k between this midpoint and the upper bound.

This finally concludes the proof of the k -bounds shown in the fourth column of table 1, and thereby step 1(c) from section 2.5.

5 The hierarchy of one-loop boundaries

Step (1) of our analysis (section 2.5) is now complete at one loop. Before moving on to step (2) we demonstrate that the boundaries classified in section 4 can be generated by a few simple graph operations applied to the maximal codimension boundaries of MHV amplituhedra (table 1 type (12) or, as a special case, (10)). This arrangement will prove useful in the sequel since one-loop boundaries are the basic building blocks for constructing boundary configurations at arbitrary loop order.

We call boundaries of type (2), (5)–(7), (10), (12), and (14)–(16) *low- k* boundaries since they are valid for the smallest value of k for their respective Landau diagrams. The

¹¹If k is even this is automatic; if k is odd the two rows of D_0 should be exchanged.

branches (8), (11), (13) and (17) are *high-k* boundaries and are respectively the parity conjugates of (7), (10), (12) and (16). Branch (3), the parity conjugate of branch (2), is properly regarded as a high-k boundary since (2) is low-k, but it is accidentally valid for all k. Branches (1), (4), and (9) are self-conjugate under parity and are considered both low-k and high-k, as are the parity-conjugate pair (18), (19).

5.1 A graphical notation for low-helicity boundaries

We begin by devising a graphical notation in terms of which the operations between momentum twistor solutions are naturally phrased. These graphs are *twistor diagrams*¹² depicting various configurations of intersecting lines in \mathbb{P}^3 . The elements of a twistor diagram, an example of which is shown in panel (a) of figure 1, are:

- The red line depicts an \mathcal{L} solving some on-shell conditions, specifically:
- if \mathcal{L} and a single line segment labeled i intersect at an empty node, then $\langle \mathcal{L} i i+1 \rangle = 0$, and
- if \mathcal{L} and two line segments intersect at a filled node labeled i , then $\langle \mathcal{L} i-1 i \rangle = \langle \mathcal{L} i i+1 \rangle = 0$.

An “empty” node is colored red, indicating the line passing through it. A “filled” node is filled in solid black, obscuring the line passing through it.

In general a given \mathcal{L} can pass through as many as four labeled nodes (for generic projected external data, which we always assume). If there are four, then none of them can be filled. If there are three, then at most one of them can be filled, and we choose to always draw it as either the first or last node along \mathcal{L} . If there are more than two, then any nodes between the first and last are called *non-MHV intersections*, which are necessarily empty. This name is appropriate because branches satisfying such on-shell constraints are not valid boundaries of MHV amplituhedra, and each non-MHV intersection in a twistor diagram increases the minimum value of k by one.

Although no such diagrams appear in this paper, the extension to higher loops is obvious: each \mathcal{L} is represented by a line of a different color, and the presence of an on-shell condition of the form $\langle \mathcal{L}^{(\ell_1)} \mathcal{L}^{(\ell_2)} \rangle = 0$ is indicated by an empty node at the intersection of the lines $\mathcal{L}^{(\ell_1)}$ and $\mathcal{L}^{(\ell_2)}$.

To each twistor diagram it is simple to associate one or more Landau diagrams, as also shown in figure 1. If a twistor diagram has a filled node at i then an associated Landau diagram has two propagators $\langle \mathcal{L} i-1 i \rangle$ and $\langle \mathcal{L} i i+1 \rangle$ requiring a massless corner at i in the Landau diagram. If a twistor diagram has an empty node on the line segment marked i then an associated Landau diagram only has the single propagator $\langle \mathcal{L} i i+1 \rangle$, requiring a massive corner in the Landau diagram. Therefore, twistor diagrams should be thought of as graphical shorthand which both depict the low-k solution to the cut conditions and simultaneously represent one or more Landau diagrams, as explained in the caption of figure 1.

¹²Not to be confused with the twistor diagrams of [41].

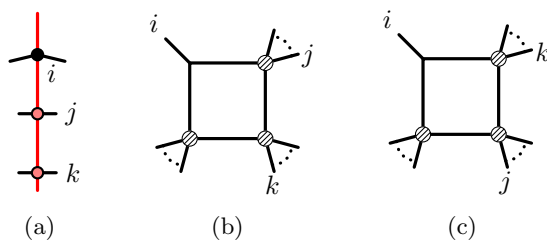


Figure 1. The twistor diagram shown in (a) depicts branch (16) of solutions to the three-mass box on-shell conditions $\langle \mathcal{L} i-1 i \rangle = \langle \mathcal{L} i i+1 \rangle = \langle \mathcal{L} j j+1 \rangle = \langle \mathcal{L} k k+1 \rangle = 0$, which is a valid boundary for $k \geq 1$. This branch passes through the point Z_i and intersects the lines $(j j+1)$ and $(k k+1)$. As drawn, the intersection at j is an example of a non-MHV intersection, but the figure is agnostic about the relative cyclic ordering of i, j, k and is intended to represent either possibility. Therefore, the corresponding Landau diagram can be either (b) or (c) depending on whether $i < j < k$ or $i < k < j$.

One useful feature of this graphical notation is that the nodes of a twistor diagram fully encode the total number of propagators, n_{props} , in the Landau diagram (and so also the total number of on-shell conditions): each filled node accounts for two propagators, and each empty node accounts for one propagator:

$$n_{\text{props}} = 2n_{\text{filled}} + n_{\text{empty}} . \tag{5.1}$$

This feature holds at higher loop order where this counting directly indicates how many propagators to associate with each loop.

Let us emphasize that a twistor diagram generally contains more information than its associated Landau diagram, as it indicates not only the set of on-shell conditions satisfied, but also specifies a particular branch of solutions thereto. The sole exception is the four-mass box, for which the above rules do not provide the twistor diagram with any way to distinguish the two branches (18), (19) of solutions. Moreover, the rules also do not provide any way to indicate that an \mathcal{L} lies in a particular plane, such as \bar{i} . Therefore we can only meaningfully represent the low- k boundaries defined at the beginning of section 5.

Given a twistor diagram depicting some branch, a twistor diagram corresponding to a relaxation of that branch may be obtained by deleting a non-MHV intersection of the type shown in (a) of figure 1, by replacing a filled node and its two line segments with an empty node and a single segment, or by deleting an empty node. In the associated Landau diagram, a relaxation corresponds to collapsing an internal edge of the graph. This is formalized in greater detail in section 5.2.

5.2 A graphical recursion for generating low-helicity boundaries

In figure 2 we organize twistor diagrams representing eight types of boundaries according to d and k ; these are respectively the number of on-shell conditions d satisfied on the boundary, and the minimum value of k for which the boundary is valid. It is evident from this data that there is a simple relation between d , k , and the number of filled (n_{filled})

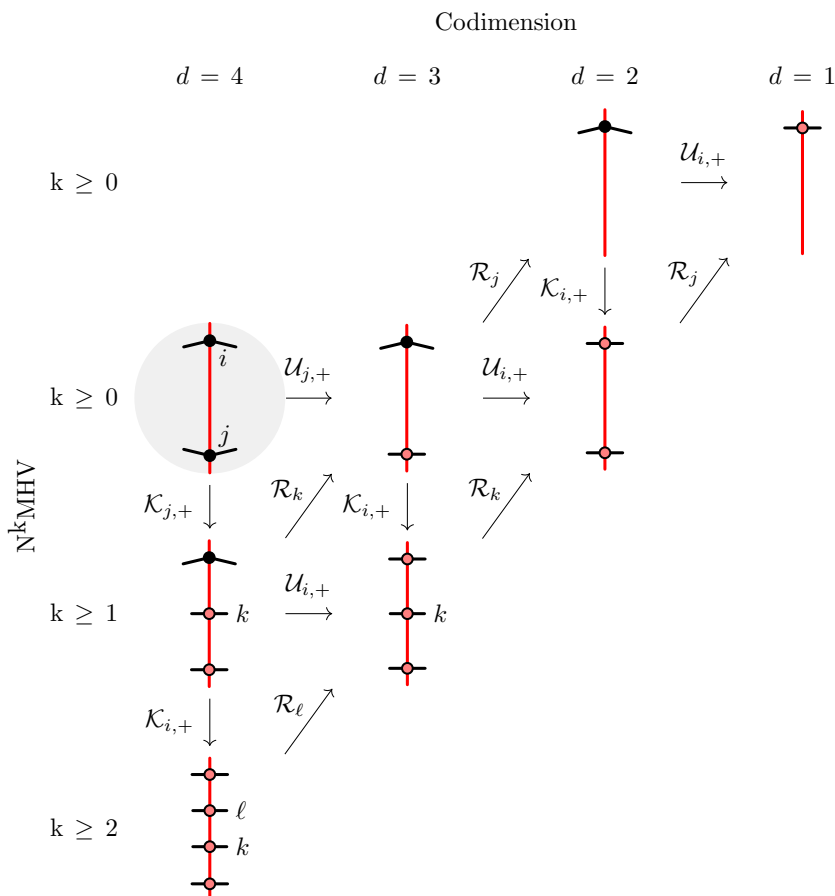


Figure 2. Twistor diagrams depicting eight types of low- k boundaries of $N^k\text{MHV}$ amplituhedra, organized according to the minimum value of k and the codimension d (equivalently, the number of on-shell conditions satisfied). These correspond respectively to branch types (2), (1), (12), (7), (4), (16), (9) and (18)/(19). The graph operators \mathcal{K} , \mathcal{R} , and \mathcal{U} are explained in the text and demonstrated in figures 3–5, respectively. Evidently all eight types of boundaries can be generated by acting with sequences of these operators on MHV maximal codimension boundaries of the type shown shaded in gray. There is an analogous parity-conjugated version of this hierarchy which relates all of the high- k branches to each other. The missing low- k boundary types (5), (6), (10), (11), (14) and (15) are degenerate cases which can be obtained by starting with $j = i + 1$ in the gray blob.

and empty (n_{empty}) nodes. Specifically, we see that an $N^k\text{MHV}$ amplituhedron can have boundaries of a type displayed in a given twistor diagram only if

$$k \geq 2n_{\text{empty}} + 3n_{\text{filled}} - d - 2 = n_{\text{empty}} + n_{\text{filled}} - 2, \tag{5.2}$$

where we have used eq. (5.1) with $n_{\text{props}} = d$. In the sequel we will describe a useful map from Landau diagrams to the on-shell diagrams of [4] which manifests the relation (5.2) and provides a powerful generalization thereof to higher loop order. The amplituhedron-based approach has some advantages over that of enumerating on-shell diagrams that will also be explored in the sequel. First of all, the minimal required helicity of a multi-loop configura-

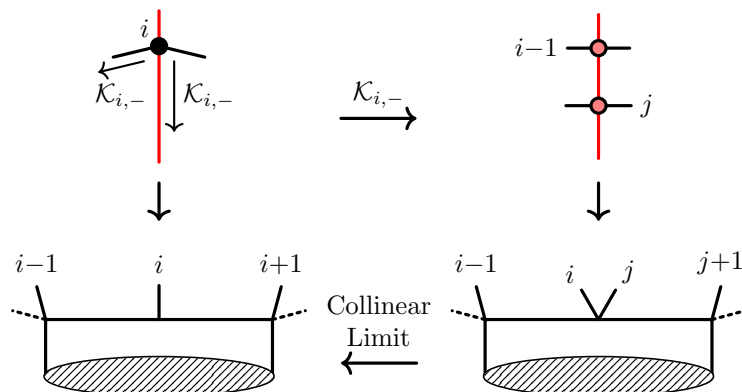


Figure 3. The graph operation \mathcal{K}_i maps an N^k MHV twistor diagram into an N^{k+1} MHV twistor diagram as shown in the top row. On Landau diagrams, this corresponds to replacing a massless corner by a massive corner; such an operation is effectively an inverse collinear limit. The shaded region in the figures represents an arbitrary planar sub-graph. A dashed external line on a Landau diagram may be either one massless external leg so the whole corner is massive, or completely removed so the whole corner is massless.

tion can be read off from each loop line separately. Second, we immediately know the relevant solution branches for a given helicity. And finally, compared to enumerating all relevant on-shell diagrams the amplituhedron-based method is significantly more compact since it can be used to produce a minimal subset of diagrams such that all allowed diagrams are relaxations thereof, including limits where massive external legs become massless or vanish.

From the data displayed in figure 2 we see that a natural organizational principle emerges: all N^k MHV one-loop twistor diagrams can be obtained from the unique maximal codimension MHV diagram (shown shaded in gray) via sequences of simple graph operations which we explain in turn.

The first graph operation \mathcal{K} increments the helicity of the diagram on which it operates. (The name \mathcal{K} is a reminder that it increases k .) Its operation is demonstrated in figure 3. Specifically, \mathcal{K}_i replaces a filled node at a point i along \mathcal{L} by two empty nodes, one at i and a second one on a new non-MHV intersection added to the diagram. Since n_{filled} decreases by one but n_{empty} increases by two under this operation, it is clear from eq. (5.2) that \mathcal{K}_i always increases by one the minimal value of k on which the branch indicated by the twistor diagram has support. From the point of view of Landau diagrams, this operation replaces a massless node with a massive one, as illustrated in the bottom row of figure 3, and hence it may be viewed as an “inverse” collinear limit.

The other two graph operations \mathcal{R} and \mathcal{U} both correspond to relaxations, as defined in section 2.3, since they each reduce the number of on-shell conditions by one, stepping thereby one column to the right in figure 2.

The operation \mathcal{R}_i simply removes (hence the name \mathcal{R}) an empty node i from a twistor diagram, as shown in figure 4. This corresponds to removing $\langle \mathcal{L} i i + 1 \rangle = 0$ from the set of on-shell conditions satisfied by \mathcal{L} .¹³

¹³Note that in line with the conventions adopted in section 5.1 we label \mathcal{R}_i only with the smaller label of a pair $(i i+1)$.

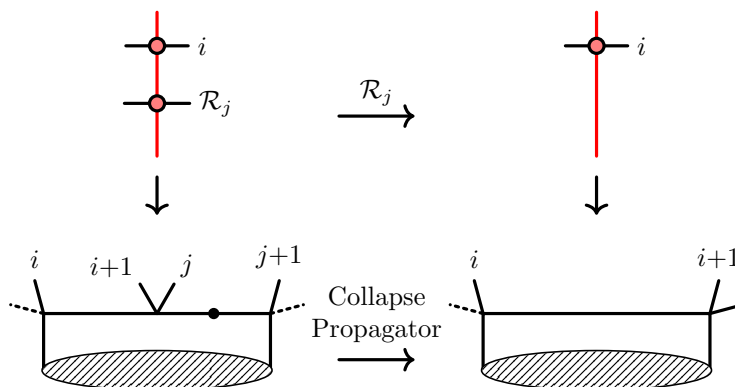


Figure 4. The graph operation \mathcal{R}_j relaxes \mathcal{L} by removing the condition that \mathcal{L} must pass through the line $(j\ j+1)$; this is equivalent to removing the on-shell condition $\langle \mathcal{L}\ j\ j+1 \rangle = 0$. On Landau diagrams, this corresponds to collapsing the propagator indicated by the filled dot in the bottom figure on the left. The shaded region in the figures represents an arbitrary planar sub-graph. A dashed external line on a Landau diagram may be either one massless external leg so the whole corner is massive, or completely removed so the whole corner is massless. It is to be understood that the graphical notation implies that $j \neq i + 2$ and $i \neq j + 2$; otherwise, the two empty nodes in the top left diagram would be represented by a single filled node on which the action of \mathcal{R} is undefined; the appropriate graph operation in this case would instead be \mathcal{U} .

The last operation, \mathcal{U} , corresponds to “un-pinning” a filled node (hence “ \mathcal{U} ”). Un-pinning means removing one constraint from a pair $\langle \mathcal{L}\ i-1\ i \rangle = \langle \mathcal{L}\ i\ i+1 \rangle = 0$. The line \mathcal{L} , which was pinned to the point i , is then free to slide along the line segment $(i-1\ i)$ or $(i\ i+1)$ (for $\mathcal{U}_{i,-}$ or $\mathcal{U}_{i,+}$, respectively). In the twistor diagram, this is depicted by replacing the filled node at the point i with a single empty node along the line segment $(i\ i\pm 1)$ (see figure 5). Only \mathcal{U}_+ appears in figure 2 because at one loop, all diagrams generated by any \mathcal{U}_- operation are equivalent, up to relabeling, to some diagram generated by a \mathcal{U}_+ . In general, however, it is necessary to track the subscript \pm since both choices are equally valid relaxations and can yield inequivalent twistor and Landau diagrams. From figure 2, we read off the following identity among the operators acting on any diagram g :

$$\mathcal{U}_{j,+}g = \mathcal{R}_k\mathcal{K}_{j,+}g. \tag{5.3}$$

There was no reason to expect the simple graphical pattern of figure 5 to emerge among the twistor diagrams. Indeed in section 3 we simply listed all possible sets of on-shell conditions without taking such an organizational principle into account. At higher loop order, however, the problem of enumerating all boundaries of N^k MHV amplituhedra benefits greatly from the fact that all valid configurations of each single loop can be iteratively generated via these simple rules, starting from the maximal codimension MHV boundaries. Stated somewhat more abstractly, these graph operations are instructions for naturally associating boundaries of different amplituhedra.

Before concluding this section it is worth noting (as is evident in figure 2) that relaxing a low- k boundary can never raise the minimum value of k for which that type of boundary is valid. In other words, we find that if $\mathcal{A}_{n,k,1}$ has a boundary of type B , and if B' is a

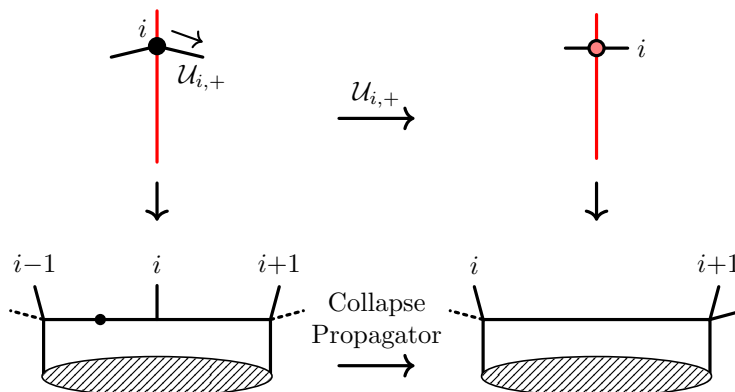


Figure 5. The graph operation $\mathcal{U}_{i,+}$ relaxes a line \mathcal{L} constrained to pass through the point i , shifting it to lie only along the line $(i\ i+1)$. This is equivalent to removing the on-shell constraint $\langle \mathcal{L}\ i-1\ i \rangle = 0$. (The equally valid relaxation $\mathcal{U}_{i,-}$, not pictured here, lets the intersection point slide onto $(i-1\ i)$.) On Landau diagrams, this corresponds to collapsing the propagator indicated by the filled dot in the bottom figure on the left. The shaded region in the figures represents an arbitrary planar sub-graph. A dashed external line on a Landau diagram may be either one massless external leg so the whole corner is massive, or completely removed so the whole corner is massless. As explained in the caption of figure 4, the \mathcal{U} operation can be thought of as a special case of the \mathcal{R} operation, and we distinguish the two because only the latter can change the helicity sector k .

relaxation of B , then $\mathcal{A}_{n,k,1}$ also has boundaries of type B' . This property does not hold in general beyond one loop; a counterexample involving two-loop MHV amplitudes appears in figure 4 of [3].

6 Solving Landau equations in momentum twistor space

As emphasized in section 2.5, the Landau equations naturally associate to each boundary of an amplituhedron a locus in $\text{Conf}_n(\mathbb{P}^3)$ on which the corresponding amplitude has a singularity. In this section we review the results of solving the Landau equations for each of the one-loop branches classified in section 3, thereby carrying out step 2 of the algorithm summarized in section 2.5. The results of this section were already tabulated in [2], but we revisit the analysis, choosing just two examples, in order to demonstrate the simplicity and efficiency of these calculations when carried out directly in momentum twistor space. The utility of this method is on better display in the higher-loop examples to be considered in the sequel.

As a first example, we consider the tadpole on-shell condition

$$f_1 \equiv \langle \mathcal{L}\ i\ i+1 \rangle = 0. \tag{6.1}$$

We choose any two other points Z_j, Z_k (which generically satisfy $\langle i\ i+1\ j\ k \rangle \neq 0$) in terms of which to parameterize

$$\mathcal{L} = (Z_i + d_1 Z_j + d_2 Z_k, Z_{i+1} + d_3 Z_j + d_4 Z_k). \tag{6.2}$$

Then the on-shell condition (6.1) admits solutions when

$$d_1 d_4 - d_2 d_3 = 0, \tag{6.3}$$

while the four Kirchhoff conditions (2.10) are

$$\alpha_1 d_4 = -\alpha_1 d_3 = -\alpha_1 d_2 = \alpha_1 d_1 = 0. \tag{6.4}$$

The only nontrivial solution (that means $\alpha_1 \neq 0$; see section 2.4) to the equations (6.3) and (6.4) is to set all four $d_A = 0$. Since this solution exists for all (generic) projected external data, it does not correspond to a branch point of an amplitude and is uninteresting to us. In other words, in this case the locus we associate to a boundary of this type is all of $\text{Conf}_n(\mathbb{P}^3)$.

As a second example, consider the two on-shell conditions corresponding to the two-mass bubble

$$f_1 \equiv \langle \mathcal{L} i i+1 \rangle = 0, \quad f_2 \equiv \langle \mathcal{L} j j+1 \rangle = 0. \tag{6.5}$$

In this case a convenient parameterization is

$$\mathcal{L} = (Z_i + d_1 Z_{i+1} + d_2 Z_k, Z_j + d_3 Z_{i+1} + d_4 Z_k). \tag{6.6}$$

Note that an asymmetry between i and j is necessarily introduced because we should not allow more than four distinct momentum twistors to appear in the parameterization, since they would necessarily be linearly dependent, and we assume of course that Z_k is generic (meaning, as before, that $\langle i i+1 j k \rangle \neq 0$). Then

$$\begin{aligned} f_1 &= -d_2 \langle i i+1 j k \rangle, \\ f_2 &= d_3 \langle i i+1 j j+1 \rangle + d_4 \langle i j j+1 k \rangle + (d_1 d_4 - d_2 d_3) \langle i+1 j j+1 k \rangle \end{aligned} \tag{6.7}$$

and the Kirchhoff conditions are

$$\begin{pmatrix} 0 & d_4 \langle i+1 j j+1 k \rangle \\ -\langle i i+1 j k \rangle & -d_3 \langle i+1 j j+1 k \rangle \\ 0 & \langle i i+1 j j+1 \rangle - d_2 \langle i+1 j j+1 k \rangle \\ 0 & \langle i j j+1 k \rangle + d_1 \langle i+1 j j+1 k \rangle \end{pmatrix} \begin{pmatrix} \alpha_1 \\ \alpha_2 \end{pmatrix} = 0. \tag{6.8}$$

Nontrivial solutions exist only if all 2×2 minors of the 4×2 coefficient matrix vanish. Three minors are trivially zero, and the one computed from the second and third rows evaluates simply to

$$-\langle i i+1 j k \rangle \langle i i+1 j j+1 \rangle = 0 \tag{6.9}$$

using the on-shell condition $f_1 = -d_2 \langle i i+1 j k \rangle = 0$. If this quantity vanishes, then the four remaining constraints (the two on-shell conditions $f_1 = f_2 = 0$ and the two remaining minors) can be solved for the four d_A , and then eq. (6.8) can be solved to find the two

α_j 's. Since $\langle i i+1 j k \rangle \neq 0$ by assumption, we conclude that the Landau equations admit nontrivial solutions only on the codimension-one locus in $\text{Conf}_n(\mathbb{P}^3)$ where

$$\langle i i+1 j j+1 \rangle = 0. \tag{6.10}$$

These two examples demonstrate that in some cases (e.g. the tadpole example) the Landau equations admit solutions for any (projected) external data, while in other cases (e.g. the bubble example) the Landau equations admit solutions only when there is a codimension-one constraint on the external data. A common feature of these examples is that some care must be taken in choosing how to parameterize \mathcal{L} . In particular, one must never express \mathcal{L} in terms of four momentum twistors (Z_i, Z_j , etc.) that appear in the specification of the on-shell conditions; otherwise, it can be impossible to disentangle the competing requirements that these satisfy some genericity (such as $\langle i i+1 j k \rangle \neq 0$ in the above examples) while simultaneously hoping to tease out the constraints they must satisfy in order to have a solution (such as eq. (6.10)). For example, although one might have been tempted to preserve the symmetry between i and j , it would have been a mistake to use the four twistors Z_i, Z_{i+1}, Z_j and Z_{j+1} in eq. (6.6).

Instead, it is safest to always pick four completely generic points Z_a, \dots, Z_d in terms of which to parameterize

$$\mathcal{L} = \begin{pmatrix} 1 & 0 & d_1 & d_2 \\ 0 & 1 & d_3 & d_4 \end{pmatrix} \begin{pmatrix} Z_a \\ Z_b \\ Z_c \\ Z_d \end{pmatrix}. \tag{6.11}$$

The disadvantage of being so careful is that intermediate steps in the calculation become much more lengthy, a problem we avoid in practice by using a computer algebra system such as Mathematica.

The results of this analysis for all one-loop branches are summarized in table 1. Naturally these are in accord with those of [14] (as tabulated in [2]). At one loop it happens that the singularity locus is the same for each branch of solutions to a given set of on-shell conditions, but this is not generally true at higher loop order.

7 Singularities and symbology

As suggested in the introduction (and explicit even in the title of this paper), one of the goals of our research program is to provide a priori derivations of the *symbol alphabets* of various amplitudes. We refer the reader to [42] for more details, pausing only to recall that the symbol alphabet of a generalized polylogarithm function F is a finite list of *symbol letters* $\{z_1, \dots, z_r\}$ such that F has *logarithmic* branch cuts (i.e., the cover has infinitely many sheets)¹⁴ between $z_i = 0$ and $z_i = \infty$ for each $i = 1, \dots, r$.

To date, symbol alphabets have been determined by explicit computation only for two-loop MHV amplitudes [43]; all other results on multi-loop SYM amplitudes in the literature

¹⁴These branch cuts usually do not all live on the same sheet; the symbol alphabet provides a list of all branch cuts that can be accessed after analytically continuing F to arbitrary sheets.

are based on a conjectured extrapolation of these results to higher loop order. Throughout the paper we have however been careful to phrase our results in terms of branch points, rather than symbol letters, for two reasons.

First of all, amplitudes in SYM theory are expected to be expressible as generalized polylogarithm functions, with symbol letters that have a familiar structure like those of the entries in the last column of table 1, only for sufficiently low (or, by parity conjugation, high) helicity. In contrast, the Landau equations are capable of detecting branch points of even more complicated amplitudes, such as those containing elliptic polylogarithms, which do not have traditional symbols.¹⁵

Second, even for amplitudes which do have symbols, determining the actual symbol alphabet from the singularity loci of the amplitude may require nontrivial extrapolation. Suppose that the Landau equations reveal that some amplitude has a branch point at $z = 0$ (where, for example, z may be one of the quantities in the last column of table 1). Then the symbol alphabet should contain a letter $f(z)$, where f in general could be an arbitrary function of z , with branch points arising in two possible ways. If $f(0) = 0$, then the amplitude will have a logarithmic branch point at $z = 0$ [44], but even if $f(0) \neq 0$, the amplitude can have an *algebraic* branch point (so the cover has finitely many sheets) at $z = 0$ if $f(z)$ has such a branch point there.

We can explore this second notion empirically since all one-loop amplitudes in SYM theory, and in particular their symbol alphabets, are well-known (following from one-loop integrated amplitudes in for example, [21–29]). According to our results from table 1, we find that one-loop amplitudes only have branch points on loci of the form

- $\langle i i+1 j j+1 \rangle = 0$ or $\langle i \bar{j} \rangle = 0$ for $0 \leq k \leq n - 4$,
- $\langle i(i-1 i+1)(j j+1)(k k+1) \rangle = 0$ for $1 \leq k \leq n - 5$, and
- $\Delta_{ijkl} = 0$ (defined in table 1) for $2 \leq k \leq n - 6$,

where i, j, k, ℓ can all range from 1 to n . Happily, the first two of these are in complete accord with the symbol letters of one-loop MHV and NMHV amplitudes, but the third reveals the foreshadowed algebraic branching since Δ_{ijkl} is not a symbol letter of the four-mass box integral contribution to $N^{2 \leq k \leq n-6}$ MHV amplitudes. Rather, the symbol alphabet of this amplitude consists of quantities of the form

$$f_{ij} \equiv \langle i i+1 j j+1 \rangle \quad \text{and} \quad f_{i\ell} f_{jk} \pm (f_{ik} f_{j\ell} - f_{ij} f_{k\ell}) \pm \sqrt{\Delta_{ijkl}}, \quad (7.1)$$

where the signs may be chosen independently. Since no symbol letter vanishes on the locus $\Delta_{ijkl} = 0$, amplitudes evidently do not have logarithmic branch points on this locus. Yet it is evident from the second expression of (7.1) that amplitudes with these letters have algebraic (in this instance, square-root- or double-sheet-type) branch points when $\Delta_{ijkl} = 0$.

Although we have only commented on the structure of various potential symbol entries and branch point loci here, let us emphasize that the methods of this paper can

¹⁵It would be interesting to understand how the “generalized symbols” of such amplitudes capture the singularity loci revealed by the Landau equations.

be used to determine precisely which symbol entries can appear in any given amplitude. For example, table 1 can be used to determine values of i , j and k for which the letter $\langle i(i-1\ i+1)(j\ j+1)(k\ k+1) \rangle$ can appear, as well as in which one-loop amplitudes, indexed by n and k , such letters will appear. An example of a fine detail along these lines evident already in table 1 is the fact that all NMHV amplitudes have branch points of two-mass easy type except for the special case $n = 6$, in accord with eq. (2.7) of [45].

We conclude this section by remarking that the problem of deriving symbol alphabets from the Landau singularity loci may remain complicated in general, but we hope that the simple, direct correspondence we have observed for certain one-loop amplitudes (and which was also observed for the two-loop MHV amplitudes studied in [3]) will continue to hold at arbitrary loop order for sufficiently simple singularities.

8 Conclusion

This paper presents first steps down the path of understanding the branch cut structure of SYM amplitudes for general helicity, following the lead of [3] and using the recent “unwound” formulation of the amplituhedron from [20]. Our algorithm is conceptually simple: we first enumerate the boundaries of an amplituhedron, and from there, without resorting to integral representations, we use the Landau equations directly to determine the locations of branch points of the corresponding amplitude.

One might worry that each of these steps grows rapidly in computational complexity at higher loop order. Classifying boundaries of amplituhedra is on its own a highly nontrivial problem, aspects of which have been explored in [38, 46–49]. In that light, the graphical tools presented in section 5.2, while already useful for organizing results as in figure 2, hint at the more enticing possibility of a method to enumerate twistor diagrams corresponding to all \mathcal{L} -boundaries of any given $\mathcal{A}_{n,k,L}$. Such an algorithm would start with the maximal codimension twistor diagrams at a given loop order, and apply the operators of section 5.2 in all ways until no further operations are possible. From these twistor diagrams come Landau diagrams, and from these come the branch points via the Landau equations. We saw in [3] and section 6 that analyzing the Landau equations can be made very simple in momentum twistor space.

Configurations of loop momenta in (the closure of) MHV amplituhedra are represented by non-negative D -matrices. In general, non-MHV configurations must be represented by indefinite D -matrices, but we observed in section 4.5 that even for non-MHV amplituhedra, D may always be chosen non-negative for all configurations on \mathcal{L} -boundaries. This ‘emergent positivity’ plays a crucial role by allowing the one-loop D -matrices presented in sections 4.2, 4.3 and 4.4 to be trivially recycled at higher values of helicity. One way to think about this is to say that going beyond MHV level introduces the C -matrix which “opens up” additional configuration space in which an otherwise indefinite D -matrix can become positive.

While the one-loop all-helicity results we obtain are interesting in their own right as first instances of all-helicity statements, this collection of information is valuable because it provides the building blocks for the two-loop analysis in the sequel. There we will argue

that the two-loop twistor diagrams with helicity k can be viewed as compositions of two one-loop diagrams with helicities k_1 and k_2 satisfying $k = k_1 + k_2$ or $k_1 + k_2 + 1$. We will also explore in detail the relation to on-shell diagrams, which are simply Landau diagrams with decorated nodes.

More speculatively, the ideas that higher-loop amplitudes can be constructed from lower-loop amplitudes, and that there is a close relation to on-shell diagrams, suggests the possibility that this toolbox may also be useful for finding symbols in the full, nonplanar SYM theory. For example, enumerating the on-shell conditions as we do here in the planar sector is similar in spirit to the nonplanar examples of [50] where certain integral representations were found such that individual integrals had support on only certain branches.¹⁶ There are of course far fewer known results in the nonplanar SYM theory, though there have been some preliminary studies [52–56].

Acknowledgments

We have benefited greatly from very stimulating discussions with N. Arkani-Hamed. This work was supported in part by: the US Department of Energy under contract DE-SC0010010 Task A, Simons Investigator Award #376208 (JS, AV), the Simons Fellowship Program in Theoretical Physics (MS), the IBM Einstein Fellowship (AV), the National Science Foundation under Grant No. NSF PHY-1125915 (JS), and the Munich Institute for Astro- and Particle Physics (MIAPP) of the DFG cluster of excellence “Origin and Structure of the Universe” (JS). MS and AV are also grateful to the CERN theory group for hospitality and support during the course of this work.

Open Access. This article is distributed under the terms of the Creative Commons Attribution License ([CC-BY 4.0](https://creativecommons.org/licenses/by/4.0/)), which permits any use, distribution and reproduction in any medium, provided the original author(s) and source are credited.

References

- [1] L. Brink, J.H. Schwarz and J. Scherk, *Supersymmetric Yang-Mills Theories*, *Nucl. Phys. B* **121** (1977) 77 [[INSPIRE](#)].
- [2] T. Dennen, M. Spradlin and A. Volovich, *Landau Singularities and Symbolology: One- and Two-loop MHV Amplitudes in SYM Theory*, *JHEP* **03** (2016) 069 [[arXiv:1512.07909](#)] [[INSPIRE](#)].
- [3] T. Dennen, I. Prlina, M. Spradlin, S. Stanojevic and A. Volovich, *Landau Singularities from the Amplituhedron*, *JHEP* **06** (2017) 152 [[arXiv:1612.02708](#)] [[INSPIRE](#)].
- [4] N. Arkani-Hamed, J.L. Bourjaily, F. Cachazo, A.B. Goncharov, A. Postnikov and J. Trnka, *Grassmannian Geometry of Scattering Amplitudes*, Cambridge University Press, (2016), [[arXiv:1212.5605](#)] [[INSPIRE](#)].

¹⁶Already in the planar case, one might interpret our algorithm as applying the Landau equations to integrands constructed in expansions around boundaries of amplituhedra, which is reminiscent of the prescriptive unitarity of [51].

- [5] J. Golden, A.B. Goncharov, M. Spradlin, C. Vergu and A. Volovich, *Motivic Amplitudes and Cluster Coordinates*, *JHEP* **01** (2014) 091 [[arXiv:1305.1617](#)] [[INSPIRE](#)].
- [6] J. Golden and M. Spradlin, *A Cluster Bootstrap for Two-Loop MHV Amplitudes*, *JHEP* **02** (2015) 002 [[arXiv:1411.3289](#)] [[INSPIRE](#)].
- [7] J. Drummond, J. Foster and O. Gürdoğan, *Cluster adjacency properties of scattering amplitudes*, *Phys. Rev. Lett.* **120** (2018) 161601 [[arXiv:1710.10953](#)] [[INSPIRE](#)].
- [8] L.J. Dixon, J.M. Drummond, C. Duhr, M. von Hippel and J. Pennington, *Bootstrapping six-gluon scattering in planar $N = 4$ super-Yang-Mills theory*, *PoS(LL2014)077* [[arXiv:1407.4724](#)] [[INSPIRE](#)].
- [9] S. Caron-Huot, L.J. Dixon, A. McLeod and M. von Hippel, *Bootstrapping a Five-Loop Amplitude Using Steinmann Relations*, *Phys. Rev. Lett.* **117** (2016) 241601 [[arXiv:1609.00669](#)] [[INSPIRE](#)].
- [10] J.M. Drummond, G. Papathanasiou and M. Spradlin, *A Symbol of Uniqueness: The Cluster Bootstrap for the 3-Loop MHV Heptagon*, *JHEP* **03** (2015) 072 [[arXiv:1412.3763](#)] [[INSPIRE](#)].
- [11] L.J. Dixon, J. Drummond, T. Harrington, A.J. McLeod, G. Papathanasiou and M. Spradlin, *Heptagons from the Steinmann Cluster Bootstrap*, *JHEP* **02** (2017) 137 [[arXiv:1612.08976](#)] [[INSPIRE](#)].
- [12] R.E. Cutkosky, *Singularities and discontinuities of Feynman amplitudes*, *J. Math. Phys.* **1** (1960) 429 [[INSPIRE](#)].
- [13] R.J. Eden, P.V. Landshoff, D.I. Olive and J.C. Polkinghorne, *The Analytic S-Matrix*, Cambridge University Press, (1966).
- [14] L.D. Landau, *On analytic properties of vertex parts in quantum field theory*, *Nucl. Phys.* **13** (1959) 181.
- [15] Z. Bern, L.J. Dixon, D.C. Dunbar and D.A. Kosower, *Fusing gauge theory tree amplitudes into loop amplitudes*, *Nucl. Phys.* **B 435** (1995) 59 [[hep-ph/9409265](#)] [[INSPIRE](#)].
- [16] F. Cachazo, P. Svrček and E. Witten, *MHV vertices and tree amplitudes in gauge theory*, *JHEP* **09** (2004) 006 [[hep-th/0403047](#)] [[INSPIRE](#)].
- [17] R. Britto, F. Cachazo, B. Feng and E. Witten, *Direct proof of tree-level recursion relation in Yang-Mills theory*, *Phys. Rev. Lett.* **94** (2005) 181602 [[hep-th/0501052](#)] [[INSPIRE](#)].
- [18] H. Elvang and Y.-t. Huang, *Scattering Amplitudes*, [arXiv:1308.1697](#) [[INSPIRE](#)].
- [19] N. Arkani-Hamed and J. Trnka, *The Amplituhedron*, *JHEP* **10** (2014) 030 [[arXiv:1312.2007](#)] [[INSPIRE](#)].
- [20] N. Arkani-Hamed, H. Thomas and J. Trnka, *Unwinding the Amplituhedron in Binary*, *JHEP* **01** (2018) 016 [[arXiv:1704.05069](#)] [[INSPIRE](#)].
- [21] G. 't Hooft and M.J.G. Veltman, *Scalar One Loop Integrals*, *Nucl. Phys.* **B 153** (1979) 365 [[INSPIRE](#)].
- [22] Z. Bern, L.J. Dixon and D.A. Kosower, *Dimensionally regulated pentagon integrals*, *Nucl. Phys.* **B 412** (1994) 751 [[hep-ph/9306240](#)] [[INSPIRE](#)].
- [23] Z. Bern, L.J. Dixon, D.C. Dunbar and D.A. Kosower, *One loop n point gauge theory amplitudes, unitarity and collinear limits*, *Nucl. Phys.* **B 425** (1994) 217 [[hep-ph/9403226](#)] [[INSPIRE](#)].

- [24] Z. Bern, L.J. Dixon, D.C. Dunbar and D.A. Kosower, *One loop gauge theory amplitudes with an arbitrary number of external legs*, in *Workshop on Continuous Advances in QCD Minneapolis, Minnesota, February 18–20, 1994*, pp. 3–21, [hep-ph/9405248](#) [[INSPIRE](#)].
- [25] A. Brandhuber, B.J. Spence and G. Travaglini, *One-loop gauge theory amplitudes in $N = 4$ super Yang-Mills from MHV vertices*, *Nucl. Phys. B* **706** (2005) 150 [[hep-th/0407214](#)] [[INSPIRE](#)].
- [26] Z. Bern, V. Del Duca, L.J. Dixon and D.A. Kosower, *All non-maximally-helicity-violating one-loop seven-gluon amplitudes in $N = 4$ super-Yang-Mills theory*, *Phys. Rev. D* **71** (2005) 045006 [[hep-th/0410224](#)] [[INSPIRE](#)].
- [27] R. Britto, F. Cachazo and B. Feng, *Generalized unitarity and one-loop amplitudes in $N = 4$ super-Yang-Mills*, *Nucl. Phys. B* **725** (2005) 275 [[hep-th/0412103](#)] [[INSPIRE](#)].
- [28] Z. Bern, L.J. Dixon and D.A. Kosower, *All Next-to-maximally-helicity-violating one-loop gluon amplitudes in $N = 4$ super-Yang-Mills theory*, *Phys. Rev. D* **72** (2005) 045014 [[hep-th/0412210](#)] [[INSPIRE](#)].
- [29] R.K. Ellis and G. Zanderighi, *Scalar one-loop integrals for QCD*, *JHEP* **02** (2008) 002 [[arXiv:0712.1851](#)] [[INSPIRE](#)].
- [30] I. Prlina, M. Spradlin, J. Stankowicz and S. Stanojevic, *Boundaries of Amplituhedra and NMHV Symbol Alphabets at Two Loops*, *JHEP* **04** (2018) 049 [[arXiv:1712.08049](#)] [[INSPIRE](#)].
- [31] A. Hodges, *Eliminating spurious poles from gauge-theoretic amplitudes*, *JHEP* **05** (2013) 135 [[arXiv:0905.1473](#)] [[INSPIRE](#)].
- [32] S.J. Parke and T.R. Taylor, *An Amplitude for n Gluon Scattering*, *Phys. Rev. Lett.* **56** (1986) 2459 [[INSPIRE](#)].
- [33] V.P. Nair, *A Current Algebra for Some Gauge Theory Amplitudes*, *Phys. Lett. B* **214** (1988) 215 [[INSPIRE](#)].
- [34] Z. Bern, L.J. Dixon and V.A. Smirnov, *Iteration of planar amplitudes in maximally supersymmetric Yang-Mills theory at three loops and beyond*, *Phys. Rev. D* **72** (2005) 085001 [[hep-th/0505205](#)] [[INSPIRE](#)].
- [35] L.F. Alday, D. Gaiotto and J. Maldacena, *Thermodynamic Bubble Ansatz*, *JHEP* **09** (2011) 032 [[arXiv:0911.4708](#)] [[INSPIRE](#)].
- [36] J.M. Drummond, J. Henn, G.P. Korchemsky and E. Sokatchev, *Dual superconformal symmetry of scattering amplitudes in $N = 4$ super-Yang-Mills theory*, *Nucl. Phys. B* **828** (2010) 317 [[arXiv:0807.1095](#)] [[INSPIRE](#)].
- [37] G.F. Sterman and M.E. Tejeda-Yeomans, *Multiloop amplitudes and resummation*, *Phys. Lett. B* **552** (2003) 48 [[hep-ph/0210130](#)] [[INSPIRE](#)].
- [38] Y. Bai, S. He and T. Lam, *The Amplituhedron and the One-loop Grassmannian Measure*, *JHEP* **01** (2016) 112 [[arXiv:1510.03553](#)] [[INSPIRE](#)].
- [39] N. Arkani-Hamed, J.L. Bourjaily, F. Cachazo and J. Trnka, *Local Integrals for Planar Scattering Amplitudes*, *JHEP* **06** (2012) 125 [[arXiv:1012.6032](#)] [[INSPIRE](#)].
- [40] J.L. Bourjaily, S. Caron-Huot and J. Trnka, *Dual-Conformal Regularization of Infrared Loop Divergences and the Chiral Box Expansion*, *JHEP* **01** (2015) 001 [[arXiv:1303.4734](#)] [[INSPIRE](#)].

- [41] A.P. Hodges, *Twistor diagram recursion for all gauge-theoretic tree amplitudes*, [hep-th/0503060](#) [INSPIRE].
- [42] A.B. Goncharov, M. Spradlin, C. Vergu and A. Volovich, *Classical Polylogarithms for Amplitudes and Wilson Loops*, *Phys. Rev. Lett.* **105** (2010) 151605 [[arXiv:1006.5703](#)] [INSPIRE].
- [43] S. Caron-Huot, *Superconformal symmetry and two-loop amplitudes in planar $N = 4$ super Yang-Mills*, *JHEP* **12** (2011) 066 [[arXiv:1105.5606](#)] [INSPIRE].
- [44] J. Maldacena, D. Simmons-Duffin and A. Zhiboedov, *Looking for a bulk point*, *JHEP* **01** (2017) 013 [[arXiv:1509.03612](#)] [INSPIRE].
- [45] D.A. Kosower, R. Roiban and C. Vergu, *The Six-Point NMHV amplitude in Maximally Supersymmetric Yang-Mills Theory*, *Phys. Rev. D* **83** (2011) 065018 [[arXiv:1009.1376](#)] [INSPIRE].
- [46] N. Arkani-Hamed and J. Trnka, *Into the Amplituhedron*, *JHEP* **12** (2014) 182 [[arXiv:1312.7878](#)] [INSPIRE].
- [47] S. Franco, D. Galloni, A. Mariotti and J. Trnka, *Anatomy of the Amplituhedron*, *JHEP* **03** (2015) 128 [[arXiv:1408.3410](#)] [INSPIRE].
- [48] D. Galloni, *Positivity Sectors and the Amplituhedron*, [arXiv:1601.02639](#) [INSPIRE].
- [49] S.N. Karp, L.K. Williams and Y.X. Zhang, *Decompositions of amplituhedra*, [arXiv:1708.09525](#) [INSPIRE].
- [50] Z. Bern, E. Herrmann, S. Litsey, J. Stankowicz and J. Trnka, *Evidence for a Nonplanar Amplituhedron*, *JHEP* **06** (2016) 098 [[arXiv:1512.08591](#)] [INSPIRE].
- [51] J.L. Bourjaily, E. Herrmann and J. Trnka, *Prescriptive Unitarity*, *JHEP* **06** (2017) 059 [[arXiv:1704.05460](#)] [INSPIRE].
- [52] Z. Bern, E. Herrmann, S. Litsey, J. Stankowicz and J. Trnka, *Logarithmic Singularities and Maximally Supersymmetric Amplitudes*, *JHEP* **06** (2015) 202 [[arXiv:1412.8584](#)] [INSPIRE].
- [53] N. Arkani-Hamed, J.L. Bourjaily, F. Cachazo and J. Trnka, *Singularity Structure of Maximally Supersymmetric Scattering Amplitudes*, *Phys. Rev. Lett.* **113** (2014) 261603 [[arXiv:1410.0354](#)] [INSPIRE].
- [54] Z. Bern, M. Enciso, H. Ita and M. Zeng, *Dual Conformal Symmetry, Integration-by-Parts Reduction, Differential Equations and the Nonplanar Sector*, *Phys. Rev. D* **96** (2017) 096017 [[arXiv:1709.06055](#)] [INSPIRE].
- [55] J.L. Bourjaily, S. Franco, D. Galloni and C. Wen, *Stratifying On-Shell Cluster Varieties: the Geometry of Non-Planar On-Shell Diagrams*, *JHEP* **10** (2016) 003 [[arXiv:1607.01781](#)] [INSPIRE].
- [56] S. Franco, D. Galloni, B. Penante and C. Wen, *Non-Planar On-Shell Diagrams*, *JHEP* **06** (2015) 199 [[arXiv:1502.02034](#)] [INSPIRE].

Landau singularities from the amplituhedron

T. Dennen,¹ I. Prlina, M. Spradlin, S. Stanojevic and A. Volovich

*Department of Physics, Brown University,
182 Hope Street, Providence RI 02912, U.S.A.*

E-mail: tristan.dennen@gmail.com, igor_prlina@brown.edu,
marcus_spradlin@brown.edu, stefan_stanojevic@brown.edu,
anastasia_volovich@brown.edu

ABSTRACT: We propose a simple geometric algorithm for determining the complete set of branch points of amplitudes in planar $\mathcal{N} = 4$ super-Yang-Mills theory directly from the amplituhedron, without resorting to any particular representation in terms of local Feynman integrals. This represents a step towards translating integrands directly into integrals. In particular, the algorithm provides information about the symbol alphabets of general amplitudes. We illustrate the algorithm applied to the one- and two-loop MHV amplitudes.

KEYWORDS: Extended Supersymmetry, Scattering Amplitudes

ARXIV EPRINT: [1612.02708](https://arxiv.org/abs/1612.02708)

¹Current address: Google Inc., Mountain View CA 94043, U.S.A.

Contents

1	Introduction	1
1.1	Momentum twistors	2
1.2	Positivity and the MHV amplituhedron	3
1.3	Landau singularities	4
2	Eliminating spurious singularities of MHV amplitudes	6
2.1	The spurious pentagon singularity	7
2.2	The spurious three-mass box singularity	8
2.3	A two-loop example	9
2.4	Summary	10
3	An amplituhedrony approach	11
3.1	One-loop MHV amplitudes	12
3.2	Two-loop MHV amplitudes: configurations of positive lines	13
3.3	Two-loop MHV amplitudes: Landau singularities	18
4	Discussion	22
A	Elimination of bubbles and triangles	24
A.1	Bubble sub-diagrams	24
A.2	Triangle sub-diagrams	25

1 Introduction

Ever since its conception, the Feynman diagram approach has been the standard paradigm for perturbative calculations in quantum field theory. While the method can, in principle, be used at any order in perturbation theory, the calculations get more and more demanding at each new loop order. Alternately one can seek hidden symmetries and new underlying principles which motivate new calculational approaches where the most basic features of Feynman diagrams, such as unitarity and locality, are emergent instead of manifest. Recent years have seen tremendous success in “reverse engineering” such new symmetries and principles from properties of scattering amplitudes. This approach has been particularly fruitful in simple quantum field theories such as the planar maximally supersymmetric $\mathcal{N} = 4$ super-Yang-Mills (SYM) theory [1].

In particular, it has been realized that the unitarity and locality of the integrands [2] of loop-level amplitudes in SYM theory can be seen to emerge from a very simple geometric principle of positivity [3]. Moreover, it has been proposed that all information about arbitrary integrands in this theory is encapsulated in objects called amplituhedra [4, 5] that

have received considerable recent attention; see for example [6–13]. Unfortunately, there remains a huge gap between our understanding of integrands and our understanding of the corresponding integrated amplitudes. Despite great advances in recent years we of course don’t have a magic wand that can be waved at a general integrand to “do the integrals”. Indeed, modern approaches to computing multi-loop amplitudes in SYM theory, such as the amplitude bootstrap [14, 15] even eschew knowledge of the integrand completely. It would be enormously valuable to close this gap between our understanding of integrands and amplitudes.

As a step in that direction, and motivated by [16], we began in [17] to systematically explore how integrands encode the singularities of integrated amplitudes, in particular their branch points. Scattering amplitudes in quantum field theory generally have very complicated discontinuity structure. The discontinuities across branch cuts are given by sums of unitarity cuts [18–23]. These discontinuities may appear on the physical sheet or after analytic continuation to other sheets; these higher discontinuities are captured by multiple unitarity cuts (see for example [24, 25]). A long-standing goal of the S-matrix program, in both its original and modern incarnations, has been to construct expressions for the scattering amplitudes of a quantum field theory based solely only on a few physical principles and a thorough knowledge of their analytic structure.

In [17] we studied the branch cut structure of one- and two-loop MHV amplitudes in SYM theory starting from certain representations of their integrands in terms of local Feynman integrals [26]. We recovered all of their known branch points, but we also encountered many other, spurious branch points that are artifacts of the particular representations used. Indeed, the analysis of [17] was completely insensitive to numerator factors in the integrand, but the numerators are really where all of the action is — in any standard quantum field theory the denominator of a loop integrand is a product of local propagators; the numerator is where all of the magic lies.

Our goal in this paper is to improve greatly on the analysis of [17]. We do this by presenting a method for asking the amplituhedron to directly provide a list of the physical branch points of a given amplitude. In the remainder of section 1 we briefly review the necessary background on momentum twistor notation, the MHV amplituhedron, and Landau singularities. In section 2 we demonstrate how to refine the analysis of [17] by scanning through the list of putative branch points found in that paper, and asking the amplituhedron to identify each one as physical or spurious. This is an ultimately inefficient approach, but armed with experience from that exercise we turn in section 3 to the development of a general, geometric algorithm for reading off the physical branch points of MHV amplitudes directly from the amplituhedron.

1.1 Momentum twistors

We begin by reviewing the basics of momentum twistor notation [27], which we use throughout our calculations. Momentum twistors are based on the correspondence between null rays in (complexified, compactified) Minkowski space and points in twistor space (\mathbb{P}^3), or equivalently, between complex lines in \mathbb{P}^3 and points in Minkowski space. We use Z_a, Z_b , etc. to denote points in \mathbb{P}^3 , which may be represented using four-component homogeneous

coordinates $Z_a^I = (Z_a^1, Z_a^2, Z_a^3, Z_a^4)$ subject to the identification $Z_a^I \sim tZ_a^I$ for any non-zero complex number t . We use (ab) as shorthand for the bitwistor $\epsilon_{IJKL}Z_a^KZ_b^L$. Geometrically, we can think of (ab) as the (oriented) line containing the points Z_a and Z_b . Similarly we use (abc) as shorthand for $\epsilon_{IJKL}Z_a^JZ_b^KZ_c^L$, which represents the (oriented) plane containing Z_a, Z_b and Z_c . Analogously, $(abc) \cap (def)$ stands for $\epsilon^{IJKL}(abc)_K(def)_L$, which represents the line where the two indicated planes intersect. In planar SYM theory we always focus on color-ordered partial amplitudes so an n -point amplitude is characterized by a set of n momentum twistors $Z_i^I, i \in \{1, \dots, n\}$ with a specified cyclic ordering. Thanks to this implicit cyclic ordering we can use \bar{i} as shorthand for the plane $(i-1\ i\ i+1)$, where indices are always understood to be mod n .

The natural $SL(4, \mathbb{C})$ invariant is the four-bracket denoted by

$$\langle abcd \rangle \equiv \epsilon_{IJKL}Z_a^IZ_b^JZ_c^KZ_d^L. \tag{1.1}$$

We will often be interested in a geometric understanding of the locus where such four-brackets might vanish, which can be pictured in several ways. For example, $\langle abcd \rangle = 0$ only if the two lines (ab) and (cd) intersect, or equivalently if the lines (ac) and (bd) intersect, or if the point a lies in the plane (bcd) , or if the point c lies on the plane (abd) , etc. Computations of four-brackets involving intersections may be simplified via the formula

$$\langle (abc) \cap (def) gh \rangle = \langle abcg \rangle \langle defh \rangle - \langle abch \rangle \langle defg \rangle. \tag{1.2}$$

In case the two planes are specified with one common point, say $f = c$, it is convenient to use the shorthand notation

$$\langle (abc) \cap (dec) gh \rangle \equiv \langle c(ab)(de)(gh) \rangle \tag{1.3}$$

which highlights the fact that this quantity is antisymmetric under exchange of any two of the three lines $(ab), (de),$ and (gh) .

1.2 Positivity and the MHV amplituhedron

In this paper we focus exclusively on MHV amplitudes. The integrand of an L -loop MHV amplitude is a rational function of the n momentum twistors Z_i specifying the kinematics of the n external particles, as well as of L loop momenta, each of which corresponds to some line $\mathcal{L}^{(\ell)}$ in $\mathbb{P}^3; \ell \in \{1, \dots, L\}$. The amplituhedron [4, 5] purports to provide a simple characterization of the integrand when the Z_i^I take values in a particular domain called the positive Grassmannian $G_+(4, n)$. In general $G_+(k, n)$ may be defined as the set of $k \times n$ matrices for which all ordered maximal minors are positive; that is, $\langle a_{i_1} \dots a_{i_k} \rangle > 0$ whenever $i_1 < \dots < i_k$.

Each line $\mathcal{L}^{(\ell)}$ may be characterized by specifying a pair of points $\mathcal{L}_1^{(\ell)}, \mathcal{L}_2^{(\ell)}$ that it passes through. We are always interested in $n \geq 4$, so the Z_i generically provide a basis for \mathbb{C}^4 . In the MHV amplituhedron a pair of points specifying each $\mathcal{L}^{(\ell)}$ may be expressed in the Z_i basis via an element of $G_+(2, n)$ called the D -matrix:

$$\mathcal{L}_\alpha^{(\ell)I} = \sum_{i=1}^n D_{\alpha i}^{(\ell)} Z_i^I, \quad \alpha = 1, 2. \tag{1.4}$$

For $n > 4$ the Z_i are generically overcomplete, so the map eq. (1.4) is many-to-one.

The L -loop n -point MHV amplituhedron is a $4L$ -dimensional subspace of the $2L(n-2)$ -dimensional space of L D -matrices. We will not need a precise characterization of that subspace, but only its grossest feature, which is that it is a subspace of the space of L mutually positive points in $G_+(2, n)$. This means that it lives in the subspace for which all ordered maximal minors of the matrices

$$\left(D^{(\ell)}\right), \quad \begin{pmatrix} D^{(\ell_1)} \\ D^{(\ell_2)} \end{pmatrix}, \quad \begin{pmatrix} D^{(\ell_1)} \\ D^{(\ell_2)} \\ D^{(\ell_3)} \end{pmatrix}, \quad \text{etc.}$$

are positive.

A key consequence of the positivity of the D -matrices is that, for positive external data $Z_i^I \in G_+(4, n)$, all loop variables $\mathcal{L}^{(\ell)}$ are oriented positively with respect to the external data and to each other: inside the amplituhedron,

$$\langle \mathcal{L}^{(\ell)} i i+1 \rangle > 0 \text{ for all } i \text{ and all } \ell, \text{ and} \tag{1.5}$$

$$\langle \mathcal{L}^{(\ell_1)} \mathcal{L}^{(\ell_2)} \rangle > 0 \text{ for all } \ell_1, \ell_2. \tag{1.6}$$

The boundaries of the amplituhedron coincide with the boundaries of the space of positive D -matrices, and occur for generic Z when one or more of these quantities approach zero.

It is worth noting that the above definition of positivity depends on the arbitrary choice of a special point Z_1 , since for example $\langle \mathcal{L} 1 2 \rangle > 0$ but the cyclically related quantity $\langle \mathcal{L} n 1 \rangle$ is negative. The choice of special point is essentially irrelevant: it just means that some special cases need to be checked. In calculations we can sidestep this subtlety by always choosing to analyze configurations involving points satisfying $1 \leq i < j < k < l \leq n$, which can be done without loss of generality. The geometric properties of figures 2–5 below are insensitive to the choice and always have full cyclic symmetry.

The integrand of an MHV amplitude is a canonical form $d\Omega$ defined by its having logarithmic singularities only on the boundary of the amplituhedron. The numerator of $d\Omega$ conspires to cancel all singularities that would occur outside this region (see [9] for some detailed examples). Our analysis will require no detailed knowledge of this form. Instead, we will appeal to “the amplituhedron” to tell us whether or not any given configuration of lines $\mathcal{L}^{(\ell)}$ overlaps the amplituhedron or its boundaries by checking whether eqs. (1.5) and (1.6) are satisfied (possibly with some $=$ instead of $>$).

1.3 Landau singularities

The goal of this paper is to understand the singularities of (integrated) amplitudes. For standard Feynman integrals, which are characterized by having only local propagators in the denominator, it is well-known that the locus in kinematic space where a Feynman integral can potentially develop a singularity is determined by solving the Landau equations [20, 28, 29] which we now briefly review.

After Feynman parameterization any L -loop scattering amplitude in D spacetime dimensions may be expressed as a linear combination of integrals of the form

$$\int \prod_{r=1}^L d^D l_r \int_{\alpha_i \geq 0} d^\nu \alpha \delta \left(1 - \sum_{i=1}^\nu \alpha_i \right) \frac{\mathcal{N}(l_r^\mu, p_i^\mu, \dots)}{\mathcal{D}^\nu} \tag{1.7}$$

where ν is the number of propagators in the diagram, each of which has an associated Feynman parameter α_i , \mathcal{N} is some numerator factor which may depend on the L loop momenta l_r^μ as well as the external momenta p_i^μ , and finally the denominator involves

$$\mathcal{D} = \sum_{i=1}^{\nu} \alpha_i (q_i^2 - m_i^2), \tag{1.8}$$

where q_i^μ is the momentum flowing along propagator i which carries mass m_i . The integral can be viewed as a multidimensional contour integral in the $LD + \nu$ integration variables (l_r^μ, α_i) , where the α_i contours begin at $\alpha_i = 0$ and the l_r^μ contours are considered closed by adding a point at infinity. Although the correct contour for a physical scattering process is dictated by an appropriate $i\epsilon$ prescription in the propagators, a complete understanding of the integral, including its analytic continuation off the physical sheet, requires arbitrary contours to be considered.

An integral of the above type can develop singularities when the denominator \mathcal{D} vanishes in such a way that the contour of integration cannot be deformed to avoid the singularity. This can happen in two distinct situations:

- (1) The surface $\mathcal{D} = 0$ can pinch the contour simultaneously in all integration variables (l_r^μ, α_i) . This is called the “leading Landau singularity”, though it is important to keep in mind that it is only a potential singularity. The integral may have a branch point instead of a singularity, or it may be a completely regular point, depending on the behavior of the numerator factor \mathcal{N} .
- (2) The denominator may vanish on the boundary when one or more of the $\alpha_i = 0$ and pinch the contour in the other integration variables. These are called subleading Landau singularities.

The Landau conditions encapsulating both possible situations are

$$\sum_{i \in \text{loop}} \alpha_i q_i^\mu = 0 \text{ for each loop, and} \tag{1.9}$$

$$\alpha_i (q_i^2 - m_i^2) = 0 \text{ for each } i. \tag{1.10}$$

For leading singularities eq. (1.10) is satisfied by $q_i^2 - m_i^2 = 0$ for each i , while subleading singularities have one or more i for which $q_i^2 - m_i^2 \neq 0$ but the corresponding $\alpha_i = 0$. We will always refer to equations of type $q_i^2 - m_i^2$ as “cut conditions” since they correspond to putting some internal propagators on-shell. It is important to emphasize that the Landau equations themselves have no knowledge of the numerator factor \mathcal{N} , which can alter the structure of a singularity or even cancel a singularity entirely.

Sometimes (i.e., for some diagram topologies), the Landau equations (1.9) and (1.10) may admit solutions for arbitrary external kinematics p_i^μ . This usually indicates an infrared divergence in the integral (we will not encounter ultraviolet divergences in SYM theory), which may or may not be visible by integration along the physical contour.

In other cases, solutions to the Landau equations might exist only when the p_i^μ lie on some subspace of the external kinematic space. MHV amplitudes in SYM theory are

expected to have only branch point type singularities (after properly normalizing them by dividing out a tree-level Parke-Taylor [30] factor), so for these amplitudes we are particularly interested in solutions which exist only on codimension-one slices of the external kinematic space. Even when the p_i^μ live on a slice where solutions of the Landau equations exist, the solutions generally occur for values of the integration variables α_i and l_r^μ that are off the physical contour (for example, the α_i could be complex). This indicates a branch point of the integral that is not present on the physical sheet but only becomes apparent after suitable analytic continuation away from the physical contour.

Finally let us note that we have ignored a class of branch points called “second-type singularities” [28, 31, 32] which arise from pinch singularities at infinite loop momentum. As argued in [17], these should be absent in planar SYM theory when one uses a regulator that preserves dual conformal symmetry.

2 Eliminating spurious singularities of MHV amplitudes

In principle one can write explicit formulas for any desired integrand in planar SYM theory by triangulating the interior of the amplituhedron and constructing the canonical form $d\Omega$ with logarithmic singularities on its boundary. However, general triangulations may produce arbitrarily complicated representations for $d\Omega$. In particular, these may have no semblance to standard Feynman integrals with only local propagators in the denominator (see [6] for some explicit examples). It is therefore not immediately clear that the Landau equations have any relevance to the amplituhedron. The connection will become clear in the following section; here we begin by revisiting the analysis of [17] with the amplituhedron as a guide.

In [17] we analyzed the potential Landau singularities of one- and two-loop MHV amplitudes by relying on the crutch of representations of these amplitudes in terms of one- and two-loop chiral pentagon and double-pentagon integrals [26]. The solutions to the various sets of Landau equations for these integral topologies represent *potential* singularities of the amplitudes, but this set of potential singularities is too large for two reasons. First of all, the chiral integrals are dressed with very particular numerator factors to which the Landau equations are completely insensitive. Scalar pentagon and double pentagon integrals certainly have singularities that are eliminated by the numerator factors of their chiral cousins. Second, some actual singularities of individual chiral integrals may be spurious in the full amplitude due to cancellations when all of the contributing chiral integrals are summed.

It is a priori highly non-trivial to see which singularities of individual integrals survive the summation to remain singularities of the full amplitude. However, the amplituhedron hypothesis provides a quick way to detect spurious singularities from simple considerations of positive geometry. In this section we refine our analysis of [17] to determine which *potential* singularities identified in that paper are *actual* singularities by appealing to the amplituhedron as an oracle to tell us which cuts of the amplitude have zero or non-zero support on the (boundary of the) amplituhedron.

Specifically, we propose a check that is motivated by the Cutkosky rules [21], which tell us that to compute the cut of an amplitude with respect to some set of cut conditions, one

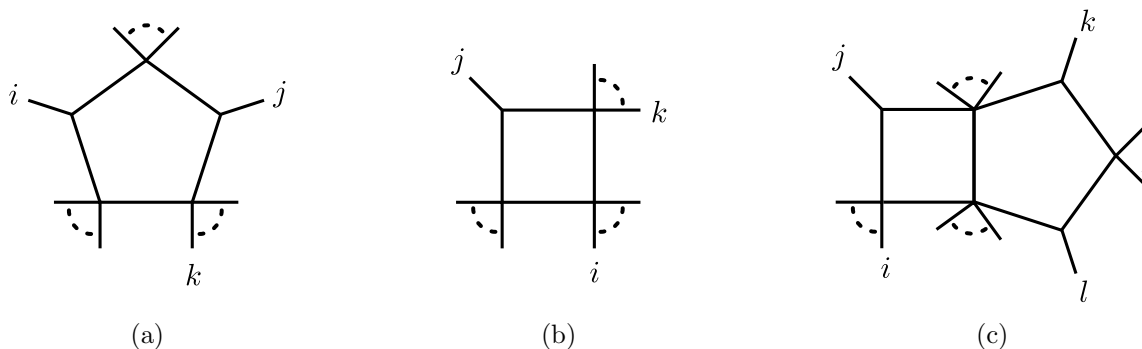


Figure 1. Three examples of cuts on which MHV amplitudes have no support; these appeared as spurious singularities in the Landau equation analysis of [17] since scalar pentagon and double pentagon integrals do have these cuts.

replaces the on-shell propagators in the integrand corresponding to those cut conditions by delta-functions, and integrates the resulting quantity over the loop momenta. The result of such a calculation has a chance to be non-zero only if the locus where the cut conditions are all satisfied has non-trivial overlap with the domain of integration of the loop momentum variables. In the present context, that domain is the space of mutually positive lines, i.e., the interior of the amplituhedron. This principle will lead to a fundamental asymmetry between the two types of Landau equations in our analysis. The full set of Landau equations including both eqs. (1.9) and (1.10) should be solvable only on a codimension-one locus in the space of external momenta in order to obtain a valid branch point. However, guided by Cutkosky, we claim that the cut conditions (1.10) must be solvable inside the positive domain for arbitrary (positive) external kinematics; otherwise the discontinuity around the putative branch point is zero and we should discard it as spurious.

In the remainder of this section we will demonstrate this hypothesis by means of the examples shown in figure 1. The leading Landau singularities of each of these diagrams were found to be singularities of the scalar pentagon and double-pentagon integrals analyzed in [17], but it is clear that MHV amplitudes have no support on these cut configurations. In the next three subsections we will see how to understand their spuriousness directly from the amplituhedron. This will motivate us to seek a better, more direct algorithm to be presented in the following section.

2.1 The spurious pentagon singularity

The first spurious singularity of MHV amplitudes arising from the integral representation used in [17] is the leading Landau singularity of the pentagon shown in figure 1a, which is located on the locus where

$$\langle i j k k+1 \rangle \langle \bar{i} \cap \bar{j} k k+1 \rangle = 0. \quad (2.1)$$

It was noted already in [21] that this solution of the Landau equations does not correspond to a branch point of the pentagon integral. It arises from cut conditions that put all five

propagators of the pentagon on-shell:

$$0 = \langle \mathcal{L} i-1 i \rangle = \langle \mathcal{L} i i+1 \rangle = \langle \mathcal{L} j-1 j \rangle = \langle \mathcal{L} j j+1 \rangle = \langle \mathcal{L} k k+1 \rangle, \quad (2.2)$$

where \mathcal{L} is the loop momentum. The first four of these cut conditions admit two discrete solutions [26]: either $\mathcal{L} = (i j)$ or $\mathcal{L} = \bar{i} \cap \bar{j}$. The second of these cannot avoid lying outside the amplituhedron. We see this by representing its D -matrix as

$$D = \begin{pmatrix} i-1 & i & i+1 \\ \langle i \bar{j} \rangle & -\langle i-1 \bar{j} \rangle & 0 \\ 0 & \langle i+1 \bar{j} \rangle & -\langle i \bar{j} \rangle \end{pmatrix}, \quad (2.3)$$

where we indicate only the nonzero columns of the $2 \times n$ matrix in positions $i-1$, i and $i+1$, per the labels above the matrix. The non-zero 2×2 minors of this matrix,

$$\langle i \bar{j} \rangle \langle i+1 \bar{j} \rangle, \quad \langle i-1 \bar{j} \rangle \langle i \bar{j} \rangle, \quad -\langle i \bar{j} \rangle^2 \quad (2.4)$$

have indefinite signs for general positive external kinematics, so this \mathcal{L} lies discretely outside the amplituhedron.

We proceed with the first solution $\mathcal{L} = (i j)$ which can be represented by the trivial D -matrix

$$D = \begin{pmatrix} i & j \\ 1 & 0 \\ 0 & 1 \end{pmatrix}. \quad (2.5)$$

Although this is trivially positive, upon substituting $\mathcal{L} = (i j)$ into eq. (2.2) we find that the fifth cut condition can only be satisfied for special kinematics satisfying

$$\langle i j k k+1 \rangle = 0. \quad (2.6)$$

Therefore, according to the Cutkosky-inspired rule discussed three paragraphs ago, the monodromy around this putative singularity vanishes for general kinematics and hence it is not a valid branch point at one loop. Indeed this conclusion is easily verified by looking at the explicit results of [33].

2.2 The spurious three-mass box singularity

The second spurious one-loop singularity encountered in [17] is a subleading singularity of the pentagon which lives on the locus

$$\langle j (j-1 j+1) (i i+1) (k k+1) \rangle = 0 \quad (2.7)$$

and arises from the cut conditions shown in figure 1b:

$$0 = \langle \mathcal{L} i i+1 \rangle = \langle \mathcal{L} j-1 j \rangle = \langle \mathcal{L} j j+1 \rangle = \langle \mathcal{L} k k+1 \rangle. \quad (2.8)$$

These are of three-mass box type and have the two solutions [4]

$$\mathcal{L} = (j i i+1) \cap (j k k+1) \text{ or } \mathcal{L} = (\bar{j} \cap (i i+1), \bar{j} \cap (k k+1)). \quad (2.9)$$

The two solutions may be represented respectively by the D -matrices

$$D = \begin{pmatrix} & i & i+1 & j \\ & 0 & 0 & 1 \\ \langle i+1 j k k+1 \rangle & -\langle i j k k+1 \rangle & & 0 \end{pmatrix} \quad (2.10)$$

and

$$D = \begin{pmatrix} & i & i+1 & k & k+1 \\ \langle i+1 \bar{j} \rangle & -\langle i \bar{j} \rangle & 0 & 0 & \\ 0 & 0 & -\langle \bar{j} k+1 \rangle & \langle \bar{j} k \rangle & \end{pmatrix}. \quad (2.11)$$

Neither matrix is non-negative definite when the Z 's are in the positive domain $G_+(4, n)$, so we again reach the (correct) conclusion that one-loop MHV amplitudes do not have singularities on the locus where eq. (2.7) is satisfied (for generic i, j and k).

2.3 A two-loop example

The two-loop scalar double-pentagon integral considered in [17] has a large number of Landau singularities that are spurious singularities of two-loop MHV amplitudes. It would be cumbersome to start with the full list and eliminate the spurious singularities one at a time using the amplituhedron. Here we will be content to consider one example in detail before abandoning this approach in favor of one more directly built on the amplituhedron.

We consider the Landau singularities shown in eq. (4.12) of [17] which live on the locus

$$\langle j(j-1 j+1)(i-1 i)(kl) \rangle \langle j(j-1 j+1)(i-1 i) \bar{k} \cap \bar{l} \rangle = 0. \quad (2.12)$$

We consider the generic case when the indices i, j, k, l are well-separated; certain degenerate cases do correspond to non-spurious singularities. This singularity is of pentagon-box type shown in figure 1c since it was found in [17] to arise from the eight cut conditions

$$\begin{aligned} \langle \mathcal{L}^{(1)} i-1 i \rangle &= \langle \mathcal{L}^{(1)} j-1 j \rangle = \langle \mathcal{L}^{(1)} j j+1 \rangle = \langle \mathcal{L}^{(1)} \mathcal{L}^{(2)} \rangle = 0, \\ \langle \mathcal{L}^{(2)} k-1 k \rangle &= \langle \mathcal{L}^{(2)} k k+1 \rangle = \langle \mathcal{L}^{(2)} l-1 l \rangle = \langle \mathcal{L}^{(2)} ll+1 \rangle = 0. \end{aligned} \quad (2.13)$$

The last four equations have two solutions $\mathcal{L}^{(2)} = (kl)$ or $\mathcal{L}^{(2)} = \bar{k} \cap \bar{l}$, but as in the previous subsection, only the first of these has a chance to avoid being outside the amplituhedron. Taking $\mathcal{L}^{(2)} = (kl)$, the two solutions to the first four cut conditions are then

$$\mathcal{L}^{(1)} = (j i-1 i) \cap (j k l) = (Z_j, Z_{i-1} \langle i j k l \rangle - Z_i \langle i-1 j k l \rangle) \text{ or} \quad (2.14)$$

$$\mathcal{L}^{(1)} = \left((i-1 i) \cap \bar{j}, (kl) \cap \bar{j} \right) = \left(Z_{i-1} \langle i \bar{j} \rangle - Z_i \langle i-1 \bar{j} \rangle, Z_k \langle l \bar{j} \rangle - Z_l \langle k \bar{j} \rangle \right). \quad (2.15)$$

The D -matrices corresponding to the first solution can be taken as

$$\begin{pmatrix} D^{(1)} \\ D^{(2)} \end{pmatrix} = \begin{pmatrix} & i-1 & i & j & k & l \\ & 0 & 0 & 1 & 0 & 0 \\ \langle i j k l \rangle & -\langle i-1 j k l \rangle & 0 & 0 & 0 & \\ 0 & 0 & 0 & 1 & 0 & \\ 0 & 0 & 0 & 0 & 0 & 1 \end{pmatrix}. \quad (2.16)$$

Evidently two of its 4×4 minors are $-\langle i j k l \rangle$ and $\langle i-1 j k l \rangle$, which have opposite signs for generic Z in the positive domain. D -matrices corresponding to the second solution can be written as

$$\begin{pmatrix} D^{(1)} \\ D^{(2)} \end{pmatrix} = \begin{pmatrix} i-1 & i & k & l \\ \langle i \bar{j} \rangle & -\langle i-1 \bar{j} \rangle & 0 & 0 \\ 0 & 0 & \langle l \bar{j} \rangle & -\langle k \bar{j} \rangle \\ 0 & 0 & 1 & 0 \\ 0 & 0 & 0 & 1 \end{pmatrix}, \quad (2.17)$$

which again has minors of opposite signs.

We conclude that the locus where the cut conditions (2.13) are satisfied lies strictly outside the amplituhedron, and therefore that there is no discontinuity around the putative branch point at (2.12). Indeed, this is manifested by the known fact [34] that two-loop MHV amplitudes do not have symbol entries which vanish on this locus. Actually, while correct, we were slightly too hasty in reaching this conclusion, since we only analyzed one set of cut conditions. Although it doesn't happen in this example, in general there may exist several different collections of cut conditions associated to the same Landau singularity, and the discontinuity around that singularity would receive additive contributions from each distinct set of associated cut contributions.

2.4 Summary

We have shown, via a slight refinement of the analysis carried out in [17], that the spurious branch points of one- and two-loop MHV amplitudes encountered in that paper can be eliminated simply on the basis of positivity constraints in the amplituhedron. It is simple to see that the cuts considered above have no support for MHV amplitudes so it may seem like overkill to use the fancy language of the amplituhedron. However we wanted to highlight the following approach:

- (1) First, consider a representation of an amplitude as a sum over a particular type of Feynman integrals. Find the Landau singularities of a generic term in the sum. These tell us the loci in Z -space where the amplitude *may* have a singularity.
- (2) For each *potential* singularity obtained in (1), check whether the corresponding on-shell conditions have a non-zero intersection with the (closure of) the amplituhedron. If the answer is no, for all possible sets of cut conditions associated with a given Landau singularity, then the singularity must be spurious.

This approach is conceptually straightforward but inefficient. One manifestation of this inefficiency is that although double pentagon integrals are characterized by four free indices i, j, k, l , we will see in the next section the vast majority of the resulting potential singularities are spurious. Specifically we will see that in order for the solution to a given set of cut conditions to have support inside the (closure of the) amplituhedron, the conditions must be relaxed in such a way that they involve only three free indices. In other words, most of the $\mathcal{O}(n^4)$ singularities of individual double pentagon integrals must necessarily cancel out when they are summed, leaving only $\mathcal{O}(n^3)$ physical singularities of the full two-loop MHV

amplitudes. (The fact that these amplitudes have only $\mathcal{O}(n^3)$ singularities is manifest in the result of [34].) This motivates us to seek a more “amplituhedrony” approach to finding singularities where we do not start by considering any particular representation of the amplitude, but instead start by thinking directly about positive configurations of loops $\mathcal{L}^{(\ell)}$.

3 An amplituhedrony approach

The most significant drawback of the approach taken in the previous section is that it relies on having explicit representations of an integrand in terms of local Feynman integrals. These have been constructed for all two-loop amplitudes in SYM theory [35], but at higher loop order even finding such representations becomes a huge computational challenge that we would like to be able to bypass. Also, as the loop order increases, the number of potential Landau singularities grows rapidly, and the vast majority of these potential singularities will fail the positivity analysis and hence turn out to be spurious. We would rather not have to sift through all of this chaff to find the wheat.

Let’s begin by taking a step back to appreciate that the only reason we needed the crutch of local Feynman integrals in the previous section is that each Feynman diagram topology provides a set of propagators for which we can solve the associated Landau equations (1.9) and (1.10) to find potential singularities. Then, for each set of cut conditions, we can determine whether the associated Landau singularity is physical or spurious by asking the amplituhedron whether or not the set of loops $\mathcal{L}^{(\ell)}$ satisfying the cut conditions has any overlap with the amplituhedron.

In this section we propose a more “amplituhedrony” approach that does not rely on detailed knowledge of integrands. We invert the logic of the previous section: instead of using Feynman diagrams to generate sets of cut conditions that we need to check one by one, we can ask the amplituhedron itself to directly identify all potentially “valid” sets of cut conditions that are possibly relevant to the singularities of an amplitude.

To phrase the problem more abstractly: for a planar n -particle amplitude at L -loop order, there are in general $nL + L(L-1)/2$ possible local cut conditions one can write down:

$$\langle \mathcal{L}^{(\ell)} i i+1 \rangle = 0 \text{ for all } \ell, i \text{ and } \langle \mathcal{L}^{(\ell_1)} \mathcal{L}^{(\ell_2)} \rangle = 0 \text{ for all } \ell_1 \neq \ell_2. \tag{3.1}$$

We simply need to characterize which subsets of these cut conditions can possibly be simultaneously satisfied for loop momenta $\mathcal{L}^{(\ell)}$ living in the closure of the amplituhedron. Each such set of cut conditions is a subset of one or more maximal subsets, and these maximal subsets are just the maximal codimension boundaries of the amplituhedron.

Fortunately, the maximal codimension boundaries of the MHV amplituhedron are particularly simple, as explained in [5]. Each loop momentum $\mathcal{L}^{(\ell)}$ must take the form $(i j)$ for some i and j (that can be different for different ℓ), and the condition of mutual positivity enforces an emergent planarity: if all of the lines $\mathcal{L}^{(\ell)}$ are drawn as chords on a disk between points on the boundary labeled $1, 2, \dots, n$, then positivity forbids any two lines to cross in the interior of the disk. In what follows we follow a somewhat low-brow analysis in which we systematically consider relaxations away from the maximum codimension boundaries,

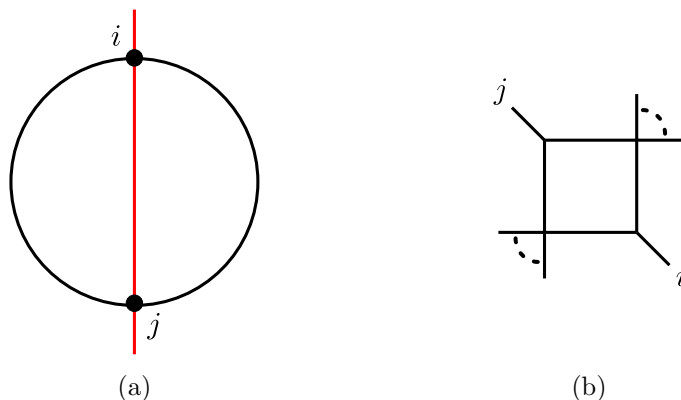


Figure 2. (a) A maximum codimension boundary of the one-loop MHV amplituhedron. The circle is a schematic depiction of the n line segments $(12), (23), \dots, (n1)$ connecting the n cyclically ordered external kinematic points $Z_i \in G_+(4, n)$ and the red line shows the loop momentum $\mathcal{L} = (ij)$. (b) The corresponding Landau diagram, which is a graphical depiction of the four cut conditions (3.3) that are satisfied on this boundary.

but the procedure can be streamlined by better harnessing this emergent planarity, which certainly pays off at higher loop order [36].

In the next few subsections we demonstrate this “amplituhedrony” approach explicitly at one and two loops before summarizing the main idea at the end of the section.

3.1 One-loop MHV amplitudes

The maximum codimension boundaries of the one-loop MHV amplituhedron occur when

$$\mathcal{L} = (ij), \tag{3.2}$$

as depicted in figure 2a. On this boundary four cut conditions of “two-mass easy” type [33] are manifestly satisfied:

$$\langle \mathcal{L} i-1 i \rangle = \langle \mathcal{L} i i+1 \rangle = \langle \mathcal{L} j-1 j \rangle = \langle \mathcal{L} j j+1 \rangle = 0, \tag{3.3}$$

as depicted in the Landau diagram shown in figure 2b. (For the moment we consider i and j to be well separated so there are no accidental degenerations.) The Landau analysis of eq. (3.3) has been performed long ago [20, 28] and reviewed in the language of momentum twistors in [17]. A leading solution to the Landau equations exists only if

$$\langle i \bar{j} \rangle \langle \bar{i} j \rangle = 0. \tag{3.4}$$

Subleading Landau equations are obtained by relaxing one of the four on-shell conditions. This leads to cuts of two-mass triangle type, which are uninteresting (they exist for generic kinematics, so don’t correspond to branch points of the amplitude). At sub-subleading order we reach cuts of bubble type. For example if we relax the second and fourth condition in eq. (3.3) then we encounter a Landau singularity which lives on the locus

$$\langle i-1 i j-1 j \rangle = 0. \tag{3.5}$$

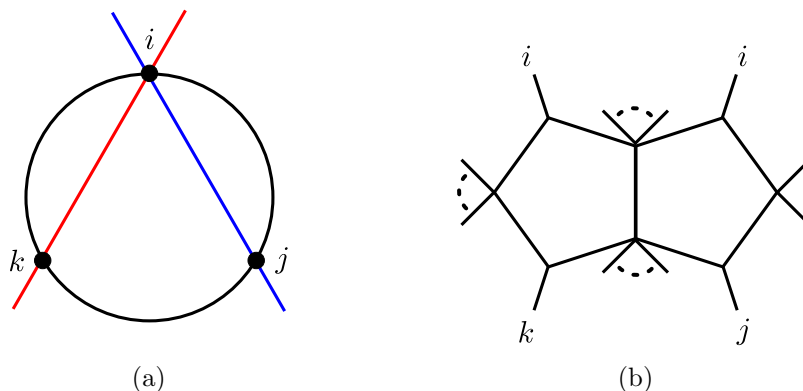


Figure 3. (a) A maximum codimension boundary of the two-loop MHV amplituhedron. (b) The corresponding Landau diagram (which, it should be noted, does not have the form of a standard Feynman integral) depicting the nine cut conditions (3.7)–(3.9) that are satisfied on this boundary.

Other relaxations either give no constraint on kinematics, or the same as eq. (3.5) with $i \rightarrow i+1$ and/or $j \rightarrow j+1$.

Altogether, we reach the conclusion that all physical branch points of one-loop MHV amplitudes occur on loci of the form

$$\langle a \bar{b} \rangle = 0 \text{ or } \langle a a+1 b b+1 \rangle = 0 \tag{3.6}$$

for various a, b . (Note that whenever we say there is a branch point at $x = 0$, we mean more specifically that there is a branch cut between $x = 0$ and $x = \infty$.) Indeed, these exhaust the branch points of the one-loop MHV amplitudes (first computed in [33]) except for branch points arising as a consequence of infrared regularization, which are captured by the BDS ansatz [37].

3.2 Two-loop MHV amplitudes: configurations of positive lines

We divide the two-loop analysis into two steps. First, in this subsection, we classify valid configurations of mutually non-negative lines. This provides a list of the sets of cut conditions on which two-loop MHV amplitudes have nonvanishing support. Then in the following subsection we solve the Landau equations for each set of cut conditions, to find the actual location of the corresponding branch point.

At two loops the MHV amplituhedron has two distinct kinds of maximum codimension boundaries [5]. The first type has $\mathcal{L}^{(1)} = (ij)$ and $\mathcal{L}^{(2)} = (kl)$ for distinct cyclically ordered i, j, k, l . Since $\langle \mathcal{L}^{(1)} \mathcal{L}^{(2)} \rangle$ is non-vanishing (inside the positive domain $G_+(4, n)$) in this case, this boundary can be thought of as corresponding to a cut of a product of one-loop Feynman integrals, with no common propagator $\langle \mathcal{L}^{(1)} \mathcal{L}^{(2)} \rangle$. Therefore we will not learn anything about two-loop singularities beyond what is already apparent at one loop.

The more interesting type of maximum codimension boundary has $\mathcal{L}^{(1)} = (ij)$ and $\mathcal{L}^{(2)} = (ik)$, as depicted in figure 3a. Without loss of generality $i < j < k$, and for now we will moreover assume that i, j and k are well-separated to avoid any potential degenerations. (These can be relaxed at the end of the analysis, in particular to see that

the degenerate case $j = k$ gives nothing interesting.) On this boundary the following nine cut conditions shown in the Landau diagram of figure 3b are simultaneously satisfied:

$$\langle \mathcal{L}^{(1)} i-1 i \rangle = \langle \mathcal{L}^{(1)} i i+1 \rangle = \langle \mathcal{L}^{(2)} i-1 i \rangle = \langle \mathcal{L}^{(2)} i i+1 \rangle = 0, \quad (3.7)$$

$$\langle \mathcal{L}^{(1)} j-1 j \rangle = \langle \mathcal{L}^{(1)} j j+1 \rangle = \langle \mathcal{L}^{(2)} k-1 k \rangle = \langle \mathcal{L}^{(2)} k k+1 \rangle = 0, \quad (3.8)$$

$$\langle \mathcal{L}^{(1)} \mathcal{L}^{(2)} \rangle = 0. \quad (3.9)$$

This is the maximal set of cuts that can be simultaneously satisfied while keeping the $\mathcal{L}^{(\ell)}$'s inside the closure of the amplituhedron for generic $Z \in G_+(4, n)$. We immediately note that since only three free indices i, j, k are involved, this set of cuts manifestly has size $\mathcal{O}(n^3)$, representing immediate savings compared to the larger $\mathcal{O}(n^4)$ set of double-pentagon cut conditions as discussed at the end of the previous section.

We can generate other, smaller sets of cut conditions by relaxing some of the nine shown in eqs. (3.7)–(3.9). This corresponds to looking at subleading singularities, in the language of the Landau equations. However, it is not interesting to consider relaxations that lead to $\langle \mathcal{L}^{(1)} \mathcal{L}^{(2)} \rangle \neq 0$ because, as mentioned above, it essentially factorizes the problem into a product of one-loop cuts. Therefore in what follows we only consider cuts on which $\langle \mathcal{L}^{(1)} \mathcal{L}^{(2)} \rangle = 0$.

By relaxing various subsets of the other 8 conditions we can generate 2^8 subsets of cut conditions. In principle each subset should be analyzed separately, but there is clearly a natural stratification of relaxations which we can exploit to approach the problem systematically. In fact, we will see that the four cut conditions in eq. (3.7) that involve the point i play a special role. Specifically, we will see that the four cut conditions in eq. (3.8) involving j and k can always be relaxed, or un-relaxed, “for free”, with no impact on positivity. Therefore, we see that whether a configuration of loops may be positive or not depends only on which subset of the four cut conditions (3.7) is relaxed.

In this subsection we will classify the subsets of eq. (3.7) that lead to valid configurations of positive lines $\mathcal{L}^{(\ell)}$, and in the next subsection we will find the locations of the corresponding Landau singularities.

Relaxing none of eq. (3.7) [figure 3a]. At maximum codimension we begin with the obviously valid pair of mutually non-negative lines represented trivially by

$$\begin{pmatrix} D^{(1)} \\ D^{(2)} \end{pmatrix} = \begin{pmatrix} i & j & k \\ 1 & 0 & 0 \\ 0 & 1 & 0 \\ 1 & 0 & 0 \\ 0 & 0 & 1 \end{pmatrix}. \quad (3.10)$$

Relaxing any one of eq. (3.7). The four cases are identical up to relabeling so we consider relaxing the condition $\langle \mathcal{L}^{(2)} i i+1 \rangle = 0$, shown in figure 4a. In this case the remaining seven cut conditions on the first two lines of eqs. (3.7) and (3.8) admit the one-parameter family of solutions

$$\mathcal{L}^{(1)} = (i j), \quad \mathcal{L}^{(2)} = (Z_k, \alpha Z_{i-1} + (1 - \alpha) Z_i). \quad (3.11)$$

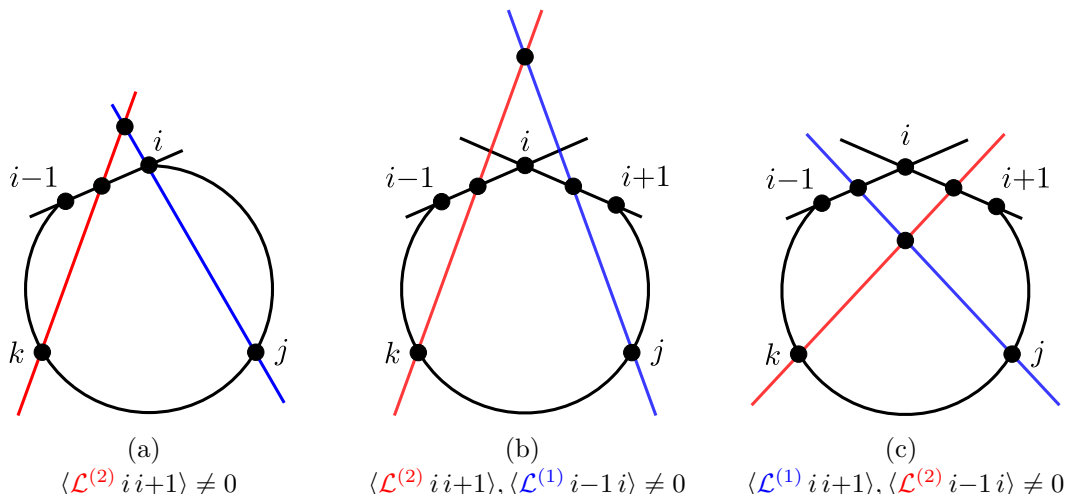


Figure 4. Three different invalid relaxations of the maximal codimension boundary shown in figure 3.

We recall that the parity conjugate solutions having $\mathcal{L}^{(1)} = \bar{i} \cap \bar{j}$ lie discretely outside the amplituhedron as seen in eq. (2.3). The corresponding D -matrices

$$\begin{pmatrix} D^{(1)} \\ D^{(2)} \end{pmatrix} = \begin{pmatrix} i-1 & i & j & k \\ 0 & 1 & 0 & 0 \\ 0 & 0 & 1 & 0 \\ \alpha & 1-\alpha & 0 & 0 \\ 0 & 0 & 0 & 1 \end{pmatrix} \tag{3.12}$$

are mutually non-negative for $0 \leq \alpha \leq 1$. It remains to impose the final cut condition that $\mathcal{L}^{(1)}$ and $\mathcal{L}^{(2)}$ intersect:

$$\langle \mathcal{L}^{(1)} \mathcal{L}^{(2)} \rangle = \alpha \langle i-1 i j k \rangle = 0. \tag{3.13}$$

For general positive external kinematics this will only be satisfied when $\alpha = 0$, which brings us back to the maximum codimension boundary. We conclude that the loop configurations of this type do not generate branch points.

Relaxing $\langle \mathcal{L}^{(1)} i-1 i \rangle = 0$ and $\langle \mathcal{L}^{(2)} i i+1 \rangle = 0$ [figure 4b]. In this case the six remaining cut conditions in eqs. (3.7) and (3.8) admit the two-parameter family of solutions

$$\mathcal{L}^{(1)} = (\alpha Z_i + (1-\alpha)Z_{i+1}, Z_j), \quad \mathcal{L}^{(2)} = (\beta Z_i + (1-\beta)Z_{i-1}, Z_k). \tag{3.14}$$

The corresponding D -matrices

$$\begin{pmatrix} D^{(1)} \\ D^{(2)} \end{pmatrix} = \begin{pmatrix} i-1 & i & i+1 & j & k \\ 0 & \alpha & 1-\alpha & 0 & 0 \\ 0 & 0 & 0 & 1 & 0 \\ 1-\beta & \beta & 0 & 0 & 0 \\ 0 & 0 & 0 & 0 & 1 \end{pmatrix} \tag{3.15}$$

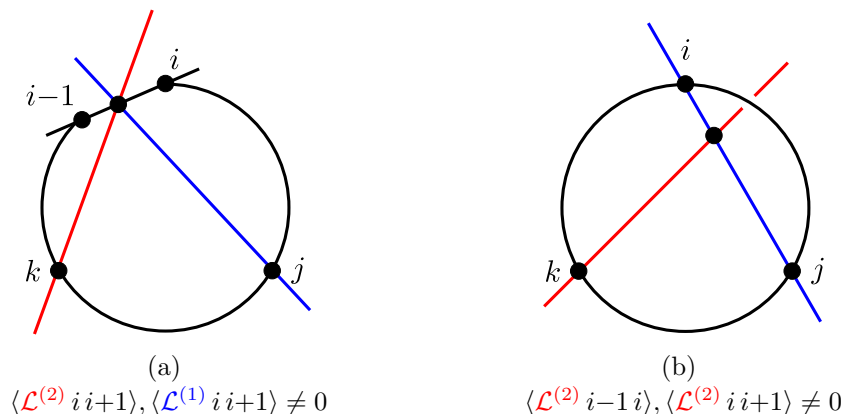


Figure 5. Two valid double relaxations of figure 3. The other two possibilities are obtained by taking $i \rightarrow i+1$ in (a) or $\mathcal{L}^{(2)} \rightarrow \mathcal{L}^{(1)}$ and $j \leftrightarrow k$ in (b).

are mutually non-negative if $0 \leq \alpha, \beta \leq 1$. Imposing that the two loops intersect gives the constraint

$$\langle \mathcal{L}^{(1)} \mathcal{L}^{(2)} \rangle = \alpha(1-\beta)\langle i-1ijk \rangle + (1-\alpha)\beta\langle ii+1jk \rangle + (1-\alpha)(1-\beta)\langle i-1i+1jk \rangle = 0, \quad (3.16)$$

which is not satisfied for general positive kinematics unless $\alpha = \beta = 1$, which again brings us back to the maximum codimension boundary.

Relaxing the two conditions $\langle \mathcal{L}^{(1)} ii+1 \rangle = \langle \mathcal{L}^{(2)} ii-1 \rangle = 0$, depicted in figure 4c, is easily seen to lead to the same conclusion.

Relaxing $\langle \mathcal{L}^{(1)} ii+1 \rangle = 0$ and $\langle \mathcal{L}^{(2)} ii+1 \rangle = 0$ [figure 5a]. In this case there is a one-parameter family of solutions satisfying all seven remaining cut conditions including $\langle \mathcal{L}^{(1)} \mathcal{L}^{(2)} \rangle = 0$:

$$\mathcal{L}^{(1)} = (\alpha Z_i + (1-\alpha)Z_{i+1}, Z_j), \quad \mathcal{L}^{(2)} = (\alpha Z_i + (1-\alpha)Z_{i+1}, Z_k). \quad (3.17)$$

The D -matrices can be represented as

$$\begin{pmatrix} D^{(1)} \\ D^{(2)} \end{pmatrix} = \begin{pmatrix} i & i+1 & j & k \\ \alpha & 1-\alpha & 0 & 0 \\ 0 & 0 & 1 & 0 \\ \alpha & 1-\alpha & 0 & 0 \\ 0 & 0 & 0 & 1 \end{pmatrix}, \quad (3.18)$$

which is a valid mutually non-negative configuration for $0 \leq \alpha \leq 1$. We conclude that these configurations represent physical branch points of two-loop MHV amplitudes by appealing to Cutkoskian intuition, according to which we would compute the discontinuity of the amplitude around this branch point by integrating over $0 \leq \alpha \leq 1$ (in figure 5a this corresponds to integrating the intersection point of the two \mathcal{L} 's over the line segment between Z_{i-1} and Z_i).

Relaxing the two conditions $\langle \mathcal{L}^{(1)} ii-1 \rangle = \langle \mathcal{L}^{(2)} ii-1 \rangle = 0$ is clearly equivalent up to relabeling.

Relaxing $\langle \mathcal{L}^{(2)} i-1 i \rangle = 0$ and $\langle \mathcal{L}^{(2)} i i+1 \rangle = 0$ [figure 5b]. The seven remaining cut conditions admit a one-parameter family of solutions

$$\mathcal{L}^{(1)} = (i j), \quad \mathcal{L}^{(2)} = (\alpha Z_i + (1 - \alpha) Z_j, Z_k), \quad (3.19)$$

which can be represented by

$$\begin{pmatrix} D^{(1)} \\ D^{(2)} \end{pmatrix} = \begin{pmatrix} i & j & k \\ 1 & 0 & 0 \\ 0 & 1 & 0 \\ \alpha & 1 - \alpha & 0 \\ 0 & 0 & 1 \end{pmatrix}. \quad (3.20)$$

This is a valid configuration of mutually non-negative lines for $0 \leq \alpha \leq 1$ so we expect it to correspond to a physical branch point. Clearly the same conclusion holds if we were to completely relax $\mathcal{L}^{(1)}$ at i instead of $\mathcal{L}^{(2)}$.

Higher relaxations of eq. (3.7). So far we have considered the relaxation of any one or any two of the conditions shown in eq. (3.7). We have found that single relaxations do not yield branch points of the amplitude, and that four of the six double relaxations are valid while the two double relaxations shown in figures 4b and 4c are invalid.

What about triple relaxations? These can be checked by explicit construction of the relevant D -matrices, but it is also easy to see graphically that any triple relaxation is valid because they can all be reached by relaxing one of the valid double relaxations. For example, the triple relaxation where we relax all of eq. (3.7) except $\langle \mathcal{L}^{(1)} i-1 i \rangle = 0$ can be realized by rotating $\mathcal{L}^{(2)}$ in figure 5a clockwise around the point k so that it continues to intersect $\mathcal{L}^{(1)}$. As a second example, the triple relaxation where we relax all but $\langle \mathcal{L}^{(2)} i-1 i \rangle = 0$ can be realized by rotating $\mathcal{L}^{(1)}$ in figure 5a counter-clockwise around the point j so that it continues to intersect $\mathcal{L}^{(2)}$.

Finally we turn to the case when all four cut conditions in eq. (3.7) are relaxed. These relaxed cut conditions admit two branches of solutions, represented by D -matrices of the form

$$\begin{pmatrix} D^{(1)} \\ D^{(2)} \end{pmatrix} = \begin{pmatrix} j & j+1 & \cdots & k-1 & k \\ 1 & 0 & \cdots & 0 & 0 \\ \alpha_j & \alpha_{j+1} & \cdots & \alpha_{k-1} & \alpha_k \\ \alpha_j & \alpha_{j+1} & \cdots & \alpha_{k-1} & \alpha_k \\ 0 & 0 & \cdots & 0 & 1 \end{pmatrix} \quad (3.21)$$

or a similar form with α parameters wrapping the other way around from k to j :

$$\begin{pmatrix} D^{(1)} \\ D^{(2)} \end{pmatrix} = \begin{pmatrix} \cdots & j-1 & j & k & k+1 & \cdots \\ \cdots & \alpha_{j-1} & \alpha_j & -\alpha_k & -\alpha_{k+1} & \cdots \\ \cdots & 0 & 1 & 0 & 0 & \cdots \\ \cdots & \alpha_{j-1} & \alpha_j & -\alpha_k & -\alpha_{k+1} & \cdots \\ \cdots & 0 & 0 & 1 & 0 & \cdots \end{pmatrix}. \quad (3.22)$$

Both of these parameterize valid configuration of mutually non-negative lines as long as all of the α 's are positive.

Relaxing $\mathcal{L}^{(1)}$ at j and/or $\mathcal{L}^{(2)}$ at k . All of the configurations we have considered so far keep the four propagators in eq. (3.8) on shell. However it is easy to see that none of these conditions have any bearing on positivity one way or the other. For example, there is no way to render the configuration shown in figure 4b positive by moving $\mathcal{L}^{(1)}$ away from the vertex j while maintaining all of the other cut conditions. On the other hand, there is no way to spoil the positivity of the configuration shown in figure 5b by moving $\mathcal{L}^{(2)}$ away from the vertex k while maintaining all other cut conditions.

Summary. We call a set of cut conditions “valid” if the $m \geq 0$ -dimensional locus in \mathcal{L} -space where the conditions are simultaneously satisfied has non-trivial m -dimensional overlap with the closure of the amplituhedron. (The examples shown in figures 5a and 5b both have $m = 1$, but further relaxations would have higher-dimensional solution spaces.) As mentioned above, this criterion is motivated by Cutkoskian intuition that the discontinuity of the amplitude would be computed by an integral over the intersection of this locus with the (closure of the) amplituhedron. If this intersection is empty (or lives on a subspace that is less than m -dimensional) then such an integral would vanish, signalling that the putative singularity is actually spurious.

The nine cut conditions shown in eqs. (3.7)–(3.9) are solved by the configuration of lines shown in figure 3a that is a zero-dimensional boundary of the amplituhedron. We have systematically investigated relaxing various subsets of these conditions (with the exception of eq. (3.9), to stay within the realm of genuine two-loop singularities) to determine which relaxations are “valid” in the sense just described.

Conclusion. The most general valid relaxation of the configuration shown in figure 3a is either an arbitrary relaxation at the points j and k , or an arbitrary relaxation of figure 5a (or the same with $i \mapsto i+1$), or an arbitrary relaxation of figure 5b (or the same with $j \leftrightarrow k$). The configurations shown in figure 4, and further relaxations thereof that are not relaxations of those shown in figure 5, are invalid.

3.3 Two-loop MHV amplitudes: Landau singularities

In the previous subsection we asked the amplituhedron directly to tell us which possible sets of cut conditions are valid for two-loop MHV amplitudes, rather than starting from some integral representation and using the amplituhedron to laboriously sift through the many spurious singularities. We can draw Landau diagrams for each valid relaxation to serve as a graphical indicator of the cut conditions that are satisfied. The Landau diagram with nine propagators corresponding to the nine cut conditions satisfied by figure 3a was already displayed in figure 3b. The configurations shown in figures 5a and 5b satisfy the seven cut conditions corresponding to the seven propagators in figures 6a and 6b, respectively. We are now ready to determine the locations of the branch points associated to these valid cut configurations (and their relaxations) by solving the Landau equations.

The following calculations follow very closely those done in [17]. Note that throughout this section, in solving cut conditions we will always ignore branches of solutions (for example those of the type $\mathcal{L} = \bar{i} \cap \bar{j}$) which cannot satisfy positivity.

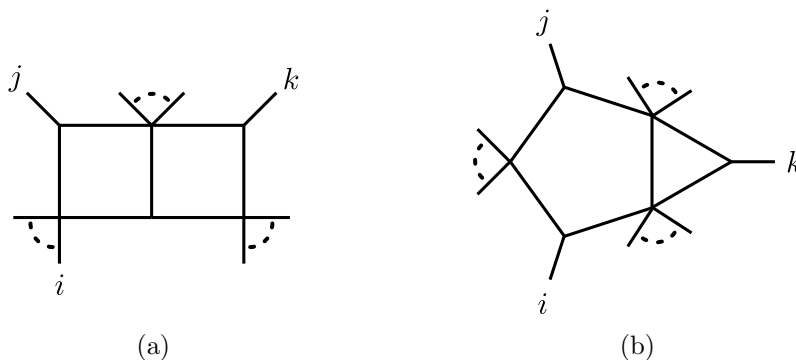


Figure 6. The Landau diagrams showing the seven cut conditions satisfied by figures 5a and 5b, respectively.

The double-box. For the double-box shown in figure 6a let us use $A \in \mathbb{P}^3$ to denote the point on the line $(i-1, i)$ where the two loop lines $\mathcal{L}^{(\ell)}$ intersect. These can then be parameterized as $\mathcal{L}^{(1)} = (A, Z_j)$ and $\mathcal{L}^{(2)} = (A, Z_k)$. The quickest way to find the location of the leading Landau singularity is to impose eq. (1.9) for each of the two loops. These are both of two-mass easy type, so we find that the Landau singularity lives on the locus (see [17])

$$\langle i-1 \ i \ j \ k \rangle \langle A \bar{j} \rangle = \langle i-1 \ i \ j \ k \rangle \langle A \bar{k} \rangle = 0. \tag{3.23}$$

These can be solved in two ways; either by

$$\langle i-1 \ i \ j \ k \rangle = 0 \tag{3.24}$$

or by solving the first condition for $A = \bar{j} \cap (i-1 \ i)$ and substituting this into the second condition to find

$$\langle i-1 \ i \ \bar{j} \cap \bar{k} \rangle = 0. \tag{3.25}$$

The astute reader may recall that in (2.6) we discarded a singularity of the same type as in eq. (3.24). This example highlights that it is crucial to appreciate the essential asymmetry between the roles of the two types of Landau equations. The on-shell conditions (1.9) by themselves only provide information about *discontinuities*. We discarded eq. (2.6) because the solution has support on a set of measure zero inside the closure of the amplituhedron, signalling that there is no discontinuity around the branch cut associated to the cut conditions shown in eq. (2.1). Therefore we never needed to inquire as to the actual location where the corresponding branch point might have been. To learn about the *location* of a branch point we have to solve also the second type of Landau equations (1.10). Indeed (3.24) does correspond to a branch point that lies outside the positive domain, but we don't discard it because the discontinuity of the amplitude around this branch point is nonzero. As mentioned above, according to the Cutkosky rules it would be computed by an integral over the line segment between Z_{i-1} and Z_i in figure 5a. When branch points lie outside $G_+(4, n)$, as in this case, it signals a discontinuity that does not exist on the physical sheet but on some other sheet; see the comments near the end of section 1.

Additional (sub^k-leading, for various k) Landau singularities are exposed by setting various sets of α 's to zero in the Landau equations and relaxing the associated cut conditions. Although these precise configurations were not analyzed in [17], the results of that paper, together with some very useful tricks reviewed in appendix A, are easily used to reveal branch points at the loci

$$\langle j(j-1, j+1)(k, k\pm 1)(i-1, i) \rangle = 0 \tag{3.26}$$

together with the same for $j \leftrightarrow k$, as well as $\langle a a+1 b b+1 \rangle = 0$ for a, b drawn from the set $\{i-1, j-1, j, k-1, k\}$.

The pentagon-triangle. With the help of appendix A and the results of [17] it is easily seen that the leading singularity of the pentagon-triangle shown in figure 6b is located on the locus where

$$\langle i\bar{j} \rangle \langle \bar{i}j \rangle = 0. \tag{3.27}$$

The computation of additional singularities essentially reduces to the same calculation for a three-mass pentagon, which was carried out in [17]. Altogether we find that branch points live on the loci

$$\begin{aligned} \langle i j k-1 k \rangle &= 0, \\ \langle i(i-1 i+1)(j-1 j)(k-1 k) \rangle &= 0, \\ \langle i(i-1 i+1)(j j+1)(k-1 k) \rangle &= 0, \\ \langle j(j-1 j+1)(i-1 i)(k-1 k) \rangle &= 0, \\ \langle j(j-1 j+1)(i i+1)(k-1 k) \rangle &= 0, \\ \langle i i\pm 1 j k \rangle &= 0, \\ \langle i j j\pm 1 k \rangle &= 0, \end{aligned} \tag{3.28}$$

together with the same collection with $(k-1 k) \rightarrow (k k+1)$, as well as all $\langle a a+1 b b+1 \rangle = 0$ for a, b drawn from the set $\{i-1, i, j-1, j, k-1, k\}$.

The maximum codimension boundaries. We left this case for last because it is somewhat more subtle. It is known that the final entries of the symbols of MHV amplitudes always have the form $\langle a \bar{b} \rangle$ [34]. We expect the leading Landau singularity of the maximum codimension boundary to expose branch points at the vanishing loci of these final entries.

However, if we naively solve the Landau equations for the diagram shown in 3b, we run into a puzzle. The first type of Landau equations (1.9) correspond to the nine cut conditions (3.7)–(3.9), which of course are satisfied by $\mathcal{L}^{(1)} = (i j)$ and $\mathcal{L}^{(2)} = (i k)$. The second type of Landau equations (1.10) does not impose any constraints for pentagons because it is always possible to find a vanishing linear combination of the five participating four-vectors. This naive Landau analysis therefore suggests that there is no leading branch point associated to the maximum codimension boundary.

This analysis is questionable because, as already noted above, the Landau diagram associated to the maximal codimension boundary, shown in figure 2b, does not have the form of a valid Feynman diagram. Therefore it makes little sense to trust the associated

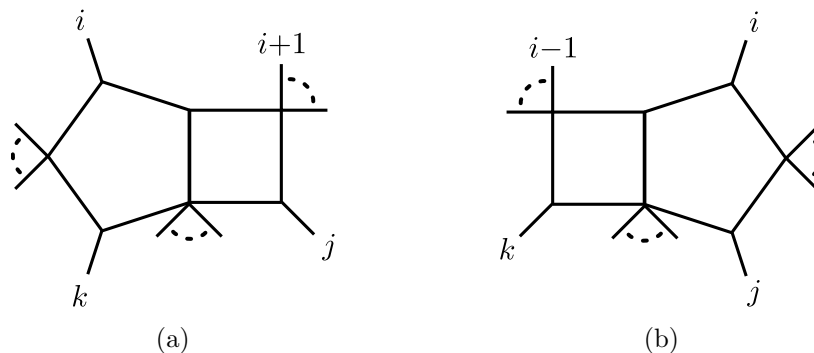


Figure 7. Landau diagrams corresponding to all of the cut conditions (3.7)–(3.9) except for (a) $\langle \mathcal{L}^{(1)} i-1 i \rangle = 0$, and (b) $\langle \mathcal{L}^{(2)} i i+1 \rangle = 0$. These are the only two cut conditions that are redundant (each is implied by the other eight, for generic kinematics) and, when omitted, lead to Landau diagrams that have the form of a standard Feynman integral. (In both figures $\mathcal{L}^{(1)}$ is the momentum in the right loop and $\mathcal{L}^{(2)}$ is the momentum in the left loop.)

Landau analysis. Instead let us note that the nine cut conditions (3.7)–(3.9) are not independent; indeed they cannot be as there are only eight degrees of freedom in the loop momenta.

We are therefore motivated to identify which of the nine cut conditions (1) is redundant, in the sense that it is implied by the other eight for generic external kinematics, and (2) has the property that when omitted, the Landau diagram for the remaining eight takes the form of a valid planar Feynman diagram. None of the conditions involving j and k shown in eq. (3.8) are redundant; all of them must be imposed to stay on the maximum codimension boundary. The remaining five conditions in eqs. (3.7) and (3.9) are redundant for general kinematics, but only two of them satisfy the second property. The corresponding Landau diagrams are shown in figure 7. Being valid planar Feynman diagrams, the integrand definitely receives contributions with these topologies (unlike figure 2b), and will exhibit the associated Landau singularities.

It remains to compute the location of the leading Landau singularities for these diagrams. For figure 7a the on-shell conditions for the pentagon set $\mathcal{L}^{(2)} = (i k)$ while the Kirkhoff condition for the box is

$$0 = \langle j (j-1 j+1) \mathcal{L}^{(2)}(i i+1) \rangle = \langle i \bar{j} \rangle \langle i i+1 j k \rangle. \tag{3.29}$$

The Landau equations associated to this topology therefore have solutions when $\langle i \bar{j} \rangle = 0$ or when $\langle i i+1 j k \rangle = 0$. However, on the locus $\langle i i+1 j k \rangle = 0$ it is no longer true that the eight on-shell conditions shown in figure 7a imply the ninth condition $\langle \mathcal{L}^{(1)} i-1 i \rangle = 0$. Therefore, this solution of the Landau equations is not relevant to the maximum codimension boundary.

We conclude that the leading Landau singularity of the maximum codimension boundary is located on the locus where $\langle i \bar{j} \rangle = 0$ or (from figure 7b) $\langle i \bar{k} \rangle = 0$. These results are in agreement with our expectation about the final symbol entries of MHV amplitudes [34]. Relaxations of figures 7a, 7b at j, k will not produce any symbol entries.

Conclusion. In conclusion, our analysis has revealed that two-loop MHV amplitudes have physical branch points on the loci of the form

$$\begin{aligned}
 \langle a \bar{b} \rangle &= 0, \\
 \langle a b c c+1 \rangle &= 0, \\
 \langle a a+1 \bar{b} \cap \bar{c} \rangle &= 0, \\
 \langle a (a-1 a+1) (b b+1) (c c+1) \rangle &= 0,
 \end{aligned}
 \tag{3.30}$$

for arbitrary indices a, b, c . Again let us note that when we say there is a branch point at $x = 0$, we mean a branch cut between $x = 0$ and $x = \infty$. Indeed, this result is in precise accord with the known symbol alphabet of two-loop MHV amplitudes in SYM theory [34].

4 Discussion

In this paper we have improved greatly on the analysis of [17] by asking the amplituhedron directly to tell us which branch points of an amplitude are physical. This analysis requires no detailed knowledge about how to write formulas for integrands by constructing the canonical “volume” form on the amplituhedron. We only used the amplituhedron’s grossest feature, which is that it is designed to guarantee that integrands have no poles outside the space of positive loop configurations. We have shown in several examples how to use this principle to completely classify the sets of cut conditions on which integrands can possibly have support. Let us emphasize that our proposal is a completely well-defined geometric algorithm:

- Input: a list of the maximal codimension boundaries of the amplituhedron; for MHV amplitudes these are known from [5].
- Step 1: for a given maximal codimension boundary, identify the list of all cut conditions satisfied on this boundary. For example, at the two-loop boundary shown in figure 3a, these would be the nine cut conditions satisfied by the Landau diagram in figure 3b, shown in eqs. (3.7)–(3.9). Consider all lower codimension boundaries that can be obtained by relaxing various subsets of these cut conditions, and eliminate those which do not overlap the closure of the amplituhedron, i.e. those which do not correspond to mutually non-negative configurations of lines $\mathcal{L}^{(\ell)}$.
- Step 2: for each valid set of cut conditions obtained in this manner, solve the corresponding Landau equations (1.9) and (1.10) to determine the location of the corresponding branch point of the amplitude.
- Output: a list of the loci in external kinematic space where the given amplitude has branch points.

As we have mentioned a few times in the text, this algorithm is motivated by intuition from the Cutkosky rules, according to which an amplitude’s discontinuity is computed by replacing some set of propagators with delta-functions. This localizes the integral onto the

intersection of the physical contour and the locus where the cut conditions are satisfied. Now is the time to confess that this intuitive motivation is not a proof of our algorithm, most notably because the positive kinematic domain lives in unphysical $(2, 2)$ signature and there is no understanding of how to make sense of the physical $i\epsilon$ contour in momentum twistor space (see however [38] for work in this direction). Nevertheless, the prescription works and it warrants serious further study, in part because it would be very useful to classify the possible branch points of more general amplitudes in SYM theory.

For amplitudes belonging to the class of generalized polylogarithm functions (which is believed to contain at least all MHV, NMHV and NNMHV amplitudes in SYM theory) the path from knowledge of branch points to amplitudes is fairly well-trodden. Such functions can be represented as iterated integrals [39] and analyzed using the technology of symbols and coproducts [40, 41]. It was emphasized in [16] that the analytic structure of an amplitude is directly imprinted on its symbol alphabet. In particular, the locus in external kinematic space where the letters of an amplitude's symbols vanish (or diverge) must exactly correspond to the locus where solutions of the Landau equations exist. The above algorithm therefore provides direct information about the zero locus of an amplitude's symbol alphabet. For example, the symbol alphabet of one-loop MHV amplitudes must vanish on the locus (3.6), and that of two-loop amplitudes must vanish on the locus (3.30). Strictly speaking this analysis does not allow one to actually determine symbol letters away from their vanishing locus, but it is encouraging that in both eqs. (3.6) and (3.30) the amplituhedron analysis naturally provides the correct symbol letters on the nose.

In general we expect that only letters of the type $\langle a a+1 b b+1 \rangle$ may appear in the first entry of the symbol of any amplitude [42]. At one loop, new letters of the type $\langle a \bar{b} \rangle$ begin to appear in the second entry. At two loops, additional new letters of the type $\langle a(a-1 a+1)(b b+1)(c c+1) \rangle$ also begin to appear in the second entry, and new letters of the type $\langle a b c c+1 \rangle$ and $\langle a a+1 \bar{b} \cap \bar{c} \rangle$ begin to appear in the third. As discussed at the end of section 3, the final entries of MHV amplitudes are always $\langle a \bar{b} \rangle$ [34]. In our paper we have given almost no thought to the question of where in the symbol a given type of letter may begin to appear. However, it seems clear that our geometric algorithm can be taken much further to expose this stratification of branch points, since the relationship between boundaries of the amplituhedron and Landau singularities is the same as the relationship between discontinuities and their branch points. For example it is clear that at any loop order, the lowest codimension boundaries of the amplituhedron that give rise to branch cuts are configurations where one of the lines \mathcal{L} intersects two lines $(i i+1)$ and $(j j+1)$, with all other lines lying in generic mutually positive position. These configurations give rise to the expected first symbol entries $\langle i i+1 j j+1 \rangle$. By systematically following the degeneration of configurations of lines onto boundaries of higher and higher codimension we expect there should be a way to derive the symbol alphabet of an amplitude entry by entry.

In many examples, mere knowledge of an amplitude's symbol alphabet, together with some other physical principles, has allowed explicit formulas for the amplitude to be constructed via a bootstrap approach. This approach has been particularly powerful for 6- [43–48], and 7-point [49] amplitudes, in which case the symbol alphabet is believed to be given, to all loop order, by the set of cluster coordinates on the kinematic configuration space [50].

It would be very interesting to use the algorithm outlined above to prove this conjecture, or to glean information about symbol alphabets for more general amplitudes, both MHV and non-MHV. One simple observation we can make in parting is to note that although maximum codimension boundaries of the L -loop MHV amplitude involve as many as $2L$ distinct points, the singularities that arise from genuinely L -loop configurations (rather than products of lower loop order) involve at most $L + 1$ points. Therefore we predict that the size of the symbol alphabet of L -loop MHV amplitudes should grow with n no faster than $\mathcal{O}(n^{L+1})$.

It would be very interesting to extend our results to non-MHV amplitudes. For the N^K amplitude, singularities should still be found only on the boundary of the N^K MHV amplituhedron, so the presented approach should still be applicable, albeit more complicated. An important difference would be the existence of poles, in addition to branch points, due to the presence of rational prefactors. We are not certain our approach would naturally distinguish these two types of singularities. However, the singularities of rational prefactors can be found using other means, for example by considering the boundaries of the tree-level amplituhedron.

Acknowledgments

We have benefitted from very stimulating discussions with N. Arkani-Hamed and are grateful to J. J. Stankowicz for collaboration on closely related questions and for detailed comments on the draft. MS and AV are grateful to NORDITA and to the CERN theory group for hospitality and support during the course of this work. This work was supported by the US Department of Energy under contract DE-SC0010010 Task A (MS, AV) and Early Career Award DE-FG02-11ER41742 (AV), as well as by Simons Investigator Award #376208 (AV).

A Elimination of bubbles and triangles

Here we collect a few comments on the elimination of bubble and triangle sub-diagrams in the Landau analysis. These tricks, together with the results of [17], can be used to easily obtain all of the Landau singularities reported in section 3.3.

A.1 Bubble sub-diagrams

The Landau equation for a bubble with propagators ℓ and $\ell + p$, which may be a sub-diagram of a larger diagram, are

$$\ell^2 = (\ell + p)^2 = 0, \tag{A.1}$$

$$\alpha_1 \ell^\mu + \alpha_2 (\ell + p)^\mu = 0, \tag{A.2}$$

where α_1 and α_2 are the Feynman parameters associated to the two propagators. The loop equation has solution

$$\ell^\mu = -\frac{\alpha_2}{\alpha_1 + \alpha_2} p^\mu \tag{A.3}$$

so that

$$\alpha_1 \ell^\mu = -\frac{\alpha_1 \alpha_2}{\alpha_1 + \alpha_2} p^\mu, \quad \alpha_2 (\ell + p)^\mu = \frac{\alpha_1 \alpha_2}{\alpha_1 + \alpha_2} p^\mu, \quad (\text{A.4})$$

while the on-shell conditions simply impose $p^2 = 0$. Therefore, we see that any Landau diagram containing this bubble sub-diagram is equivalent to the same diagram with the bubble replaced by a single on-shell line with momentum p^μ and modified Feynman parameter $\alpha' = \alpha_1 \alpha_2 / (\alpha_1 + \alpha_2)$. We do not need to keep track of the modified Feynman parameter; we simply move on to the rest of the diagram using the new Feynman parameter α' .

In conclusion, any bubble sub-diagram can be collapsed to a single edge, as far as the Landau analysis is concerned.

A.2 Triangle sub-diagrams

Similarly, we will now discuss the various branches associated to a triangle sub-diagram. The Landau equations for a triangle with edges carrying momenta $q_1 = \ell$, $q_2 = \ell + p_1 + p_2$ and $q_3 = \ell + p_2$, and with corresponding Feynman parameters α_1 , α_2 and α_3 , are

$$\ell^2 = (\ell + p_2)^2 = (\ell + p_1 + p_2)^2 = 0, \quad (\text{A.5})$$

$$\alpha_1 \ell^\mu + \alpha_2 (\ell + p_1 + p_2)^\mu + \alpha_3 (\ell + p_2)^\mu = 0. \quad (\text{A.6})$$

The solution to the loop equation is

$$\ell^\mu = -\frac{(\alpha_2 + \alpha_3)p_2^\mu + \alpha_2 p_1^\mu}{\alpha_1 + \alpha_2 + \alpha_3} \quad (\text{A.7})$$

while eqs. (A.5) impose the two conditions

$$0 = p_1^2 p_2^2 p_3^2, \quad (\text{A.8})$$

$$(\alpha_1 : \alpha_2 : \alpha_3) = (p_1^2(-p_1^2 + p_2^2 + p_3^2) : p_2^2(p_1^2 - p_2^2 + p_3^2) : p_3^2(p_1^2 + p_2^2 - p_3^2)) \quad (\text{A.9})$$

where $p_3 = -p_1 - p_2$. Suppose we follow the branch $p_1^2 = 0$. In this case α_1 is forced to vanish, effectively reducing the triangle to a bubble with edges

$$\alpha_2 q_2^\mu = \frac{\alpha_3 p_2^2}{p_2^2 - p_3^2} p_1^\mu, \quad \alpha_3 q_3^\mu = -\frac{\alpha_3 p_2^2}{p_2^2 - p_3^2} p_1^\mu. \quad (\text{A.10})$$

This is equivalent (by appendix A.1) to a single on-shell line carrying momentum p_1^μ . A similar conclusion clearly holds for the branches $p_2^2 = 0$ or $p_3^2 = 0$. If any two of p_1^2 , p_2^2 or p_3^2 simultaneously vanish, then the two corresponding Feynman parameters must vanish. Finally, if all three p_i^2 vanish, then the Landau equations are identically satisfied for any values of the three α_i . In conclusion, triangle sub-diagrams of a general Landau diagram can be analyzed by considering separately each of the seven branches outlined here.

Open Access. This article is distributed under the terms of the Creative Commons Attribution License ([CC-BY 4.0](https://creativecommons.org/licenses/by/4.0/)), which permits any use, distribution and reproduction in any medium, provided the original author(s) and source are credited.

References

- [1] L. Brink, J.H. Schwarz and J. Scherk, *Supersymmetric Yang-Mills theories*, *Nucl. Phys. B* **121** (1977) 77 [INSPIRE].
- [2] N. Arkani-Hamed, J.L. Bourjaily, F. Cachazo, S. Caron-Huot and J. Trnka, *The all-loop integrand for scattering amplitudes in planar $N = 4$ SYM*, *JHEP* **01** (2011) 041 [arXiv:1008.2958] [INSPIRE].
- [3] N. Arkani-Hamed et al., *Scattering amplitudes and the positive Grassmannian*, arXiv:1212.5605 [INSPIRE].
- [4] N. Arkani-Hamed and J. Trnka, *The amplituhedron*, *JHEP* **10** (2014) 030 [arXiv:1312.2007] [INSPIRE].
- [5] N. Arkani-Hamed and J. Trnka, *Into the amplituhedron*, *JHEP* **12** (2014) 182 [arXiv:1312.7878] [INSPIRE].
- [6] Y. Bai and S. He, *The amplituhedron from momentum twistor diagrams*, *JHEP* **02** (2015) 065 [arXiv:1408.2459] [INSPIRE].
- [7] S. Franco, D. Galloni, A. Mariotti and J. Trnka, *Anatomy of the amplituhedron*, *JHEP* **03** (2015) 128 [arXiv:1408.3410] [INSPIRE].
- [8] T. Lam, *Amplituhedron cells and Stanley symmetric functions*, *Commun. Math. Phys.* **343** (2016) 1025 [arXiv:1408.5531] [INSPIRE].
- [9] N. Arkani-Hamed, A. Hodges and J. Trnka, *Positive amplitudes in the amplituhedron*, *JHEP* **08** (2015) 030 [arXiv:1412.8478] [INSPIRE].
- [10] Y. Bai, S. He and T. Lam, *The amplituhedron and the one-loop Grassmannian measure*, *JHEP* **01** (2016) 112 [arXiv:1510.03553] [INSPIRE].
- [11] L. Ferro, T. Lukowski, A. Orta and M. Parisi, *Towards the amplituhedron volume*, *JHEP* **03** (2016) 014 [arXiv:1512.04954] [INSPIRE].
- [12] Z. Bern, E. Herrmann, S. Litsey, J. Stankowicz and J. Trnka, *Evidence for a nonplanar amplituhedron*, *JHEP* **06** (2016) 098 [arXiv:1512.08591] [INSPIRE].
- [13] D. Galloni, *Positivity sectors and the amplituhedron*, arXiv:1601.02639 [INSPIRE].
- [14] L.J. Dixon, J.M. Drummond, C. Duhr, M. von Hippel and J. Pennington, *Bootstrapping six-gluon scattering in planar $N = 4$ super-Yang-Mills theory*, *PoS(LL2014)077* [arXiv:1407.4724] [INSPIRE].
- [15] J. Golden and M. Spradlin, *A cluster bootstrap for two-loop MHV amplitudes*, *JHEP* **02** (2015) 002 [arXiv:1411.3289] [INSPIRE].
- [16] J. Maldacena, D. Simmons-Duffin and A. Zhiboedov, *Looking for a bulk point*, *JHEP* **01** (2017) 013 [arXiv:1509.03612] [INSPIRE].
- [17] T. Dennen, M. Spradlin and A. Volovich, *Landau singularities and symbology: one- and two-loop MHV amplitudes in SYM theory*, *JHEP* **03** (2016) 069 [arXiv:1512.07909] [INSPIRE].
- [18] S. Mandelstam, *Determination of the pion-nucleon scattering amplitude from dispersion relations and unitarity. General theory*, *Phys. Rev.* **112** (1958) 1344 [INSPIRE].
- [19] S. Mandelstam, *Analytic properties of transition amplitudes in perturbation theory*, *Phys. Rev.* **115** (1959) 1741 [INSPIRE].

- [20] L.D. Landau, *On analytic properties of vertex parts in quantum field theory*, *Nucl. Phys.* **13** (1959) 181 [INSPIRE].
- [21] R.E. Cutkosky, *Singularities and discontinuities of Feynman amplitudes*, *J. Math. Phys.* **1** (1960) 429 [INSPIRE].
- [22] Z. Bern, L.J. Dixon, D.C. Dunbar and D.A. Kosower, *Fusing gauge theory tree amplitudes into loop amplitudes*, *Nucl. Phys.* **B 435** (1995) 59 [hep-ph/9409265] [INSPIRE].
- [23] Z. Bern, L.J. Dixon and D.A. Kosower, *Progress in one loop QCD computations*, *Ann. Rev. Nucl. Part. Sci.* **46** (1996) 109 [hep-ph/9602280] [INSPIRE].
- [24] S. Abreu, R. Britto, C. Duhr and E. Gardi, *From multiple unitarity cuts to the coproduct of Feynman integrals*, *JHEP* **10** (2014) 125 [arXiv:1401.3546] [INSPIRE].
- [25] S. Abreu, R. Britto and H. Grönqvist, *Cuts and coproducts of massive triangle diagrams*, *JHEP* **07** (2015) 111 [arXiv:1504.00206] [INSPIRE].
- [26] N. Arkani-Hamed, J.L. Bourjaily, F. Cachazo and J. Trnka, *Local integrals for planar scattering amplitudes*, *JHEP* **06** (2012) 125 [arXiv:1012.6032] [INSPIRE].
- [27] A. Hodges, *Eliminating spurious poles from gauge-theoretic amplitudes*, *JHEP* **05** (2013) 135 [arXiv:0905.1473] [INSPIRE].
- [28] R.J. Eden, P.V. Landshoff, D.I. Olive and J.C. Polkinghorne, *The analytic S-matrix*, Cambridge University Press, Cambridge U.K., (1966) [INSPIRE].
- [29] S. Coleman and R.E. Norton, *Singularities in the physical region*, *Nuovo Cim.* **38** (1965) 438 [INSPIRE].
- [30] S.J. Parke and T.R. Taylor, *An amplitude for n gluon scattering*, *Phys. Rev. Lett.* **56** (1986) 2459 [INSPIRE].
- [31] D.B. Fairlie, P.V. Landshoff, J. Nuttall and J.C. Polkinghorne, *Singularities of the second type*, *J. Math. Phys.* **3** (1962) 594.
- [32] D.B. Fairlie, P.V. Landshoff, J. Nuttall and J.C. Polkinghorne, *Physical sheet properties of second type singularities*, *Phys. Lett.* **3** (1962) 55.
- [33] Z. Bern, L.J. Dixon, D.C. Dunbar and D.A. Kosower, *One loop n point gauge theory amplitudes, unitarity and collinear limits*, *Nucl. Phys.* **B 425** (1994) 217 [hep-ph/9403226] [INSPIRE].
- [34] S. Caron-Huot, *Superconformal symmetry and two-loop amplitudes in planar $N = 4$ super Yang-Mills*, *JHEP* **12** (2011) 066 [arXiv:1105.5606] [INSPIRE].
- [35] J.L. Bourjaily and J. Trnka, *Local integrand representations of all two-loop amplitudes in planar SYM*, *JHEP* **08** (2015) 119 [arXiv:1505.05886] [INSPIRE].
- [36] T. Dennen, *MHV Landau*, unpublished notes.
- [37] Z. Bern, L.J. Dixon and V.A. Smirnov, *Iteration of planar amplitudes in maximally supersymmetric Yang-Mills theory at three loops and beyond*, *Phys. Rev.* **D 72** (2005) 085001 [hep-th/0505205] [INSPIRE].
- [38] A.E. Lipstein and L. Mason, *From d logs to dilogs the super Yang-Mills MHV amplitude revisited*, *JHEP* **01** (2014) 169 [arXiv:1307.1443] [INSPIRE].
- [39] K.T. Chen, *Iterated path integrals*, *Bull. Amer. Math. Soc.* **83** (1977) 831 [INSPIRE].

- [40] A.B. Goncharov, *A simple construction of Grassmannian polylogarithms*, [arXiv:0908.2238](#) [[INSPIRE](#)].
- [41] A.B. Goncharov, M. Spradlin, C. Vergu and A. Volovich, *Classical polylogarithms for amplitudes and Wilson loops*, *Phys. Rev. Lett.* **105** (2010) 151605 [[arXiv:1006.5703](#)] [[INSPIRE](#)].
- [42] D. Gaiotto, J. Maldacena, A. Sever and P. Vieira, *Pulling the straps of polygons*, *JHEP* **12** (2011) 011 [[arXiv:1102.0062](#)] [[INSPIRE](#)].
- [43] L.J. Dixon, J.M. Drummond and J.M. Henn, *Bootstrapping the three-loop hexagon*, *JHEP* **11** (2011) 023 [[arXiv:1108.4461](#)] [[INSPIRE](#)].
- [44] L.J. Dixon, J.M. Drummond, M. von Hippel and J. Pennington, *Hexagon functions and the three-loop remainder function*, *JHEP* **12** (2013) 049 [[arXiv:1308.2276](#)] [[INSPIRE](#)].
- [45] L.J. Dixon, J.M. Drummond, C. Duhr and J. Pennington, *The four-loop remainder function and multi-Regge behavior at NNLLA in planar $N = 4$ super-Yang-Mills theory*, *JHEP* **06** (2014) 116 [[arXiv:1402.3300](#)] [[INSPIRE](#)].
- [46] L.J. Dixon and M. von Hippel, *Bootstrapping an NMHV amplitude through three loops*, *JHEP* **10** (2014) 065 [[arXiv:1408.1505](#)] [[INSPIRE](#)].
- [47] L.J. Dixon, M. von Hippel and A.J. McLeod, *The four-loop six-gluon NMHV ratio function*, *JHEP* **01** (2016) 053 [[arXiv:1509.08127](#)] [[INSPIRE](#)].
- [48] S. Caron-Huot, L.J. Dixon, A. McLeod and M. von Hippel, *Bootstrapping a five-loop amplitude using Steinmann relations*, *Phys. Rev. Lett.* **117** (2016) 241601 [[arXiv:1609.00669](#)] [[INSPIRE](#)].
- [49] J.M. Drummond, G. Papathanasiou and M. Spradlin, *A symbol of uniqueness: the cluster bootstrap for the 3-loop MHV heptagon*, *JHEP* **03** (2015) 072 [[arXiv:1412.3763](#)] [[INSPIRE](#)].
- [50] J. Golden, A.B. Goncharov, M. Spradlin, C. Vergu and A. Volovich, *Motivic amplitudes and cluster coordinates*, *JHEP* **01** (2014) 091 [[arXiv:1305.1617](#)] [[INSPIRE](#)].

Time-symmetrized description of nonunitary time asymmetric quantum evolution

This content has been downloaded from IOPscience. Please scroll down to see the full text.

2016 J. Phys. A: Math. Theor. 49 035301

(<http://iopscience.iop.org/1751-8121/49/3/035301>)

View [the table of contents for this issue](#), or go to the [journal homepage](#) for more

Download details:

IP Address: 128.6.218.72

This content was downloaded on 25/02/2016 at 06:00

Please note that [terms and conditions apply](#).

Time-symmetrized description of nonunitary time asymmetric quantum evolution

I P Prlina^{1,2} and N N Nedeljković²

¹Department of Physics, Brown University, Providence, RI 02912, USA

²University of Belgrade, Faculty of Physics, PO Box 368, Belgrade, Serbia

E-mail: igor_prlina@brown.edu and hekata@ff.bg.ac.rs

Received 3 August 2015, revised 25 November 2015

Accepted for publication 1 December 2015

Published 17 December 2015



CrossMark

Abstract

We discuss how systems which evolve manifestly asymmetrically in time can be described within the framework of the time-symmetrized quantum mechanics. An obvious case of asymmetry arises when a pure state evolves into a mixed state via effectively non-unitary evolution. A two-state method for finding the intermediate probability in postselected systems under such evolution is developed and the time-symmetry aspects of the method are explicitly considered. A specific feature is the existence of the so-called second scenario in which the state originating from the postselection measurement evolves under different evolution superoperator than the state from the preselection measurement. The evolution of the second scenario is explicitly defined. We illustrate the method with two characteristic examples: the spontaneous deexcitation of atoms and the systems approaching thermal equilibrium. We consider the systems with two energy levels and calculate the time-symmetrized probability of finding the system in excited state, under general preselection and postselection conditions. The consequences of the asymmetry of the time evolution on this probability are discussed. It is demonstrated that the arrow of time can be reconstructed in some special cases of postselected systems, while, for a general system, this is not the case.

Keywords: time-symmetrized, nonunitary, postselection, spontaneous deexcitation, thermalization, arrow of time, two-state method

1. Introduction

Within the framework of quantum mechanics, one standardly considers the systems which evolve unitarily. However, there are several important physical situations where the evolution

is effectively nonunitary, in a sense that a pure state evolves into a mixed state. Such situations arise when description of a subsystem is considered, under the influence of the environment. A typical case is the spontaneous radiative decay of atoms interacting with the field of emitted photons. A very general case is the interaction of the system with a thermal reservoir; in this case the pure state of the system evolves towards the mixed state of thermal equilibrium.

The fact that in quantum mechanics there is a nondeterministic reduction of state in the act of measurement, gives us the possibility to consider the so-called postselected (time-symmetrized, teleological) systems. Such systems are prepared in a given initial quantum state $|\Psi_{\text{in}}\rangle$ (preselection), but also in a final time the system must collapse into a given quantum state $|\Psi_{\text{fin}}\rangle$ due to the instantaneous and selective measurement. The quantum events considered within the framework of the postselected systems are related to the measurement in the instant of time $t = t^*$ between the initial time $t = t_{\text{in}}$ and the final time $t = t_{\text{fin}}$. It has been shown that the probability of a strong measurement in a case of unitary evolution in a postselected system can be expressed in a time symmetric way by the Aharonov–Bergmann–Lebowitz (ABL) formula [1]. That is, the probability is given in terms of two different states $|\Psi_1(t)\rangle$ and $|\Psi_2(t)\rangle$, where the first one is the result of evolution of the initial state $|\Psi_{\text{in}}\rangle$, while the second state is introduced in such a way that it would evolve into the given final state $|\Psi_{\text{fin}}\rangle$ [2–6]. The weak measurement on a postselected system leads to the so called weak value of the observable [7, 8].

An intriguing question arises whether the postselected systems which evolve non-unitarily (from pure state to mixed state) can be described within the framework of an ABL-like two-state method (TSM). That is, there are many nonunitarily evolving systems, which are time asymmetric in a sense that if we are to observe such systems, we would be able to reconstruct a direction of time. For example, spontaneous deexcitation of atoms is effectively nonunitary evolving system and a direction of time can be defined as the direction in which the survival probability of the excited state decreases. The use of the TSM means that we perform the time-symmetrization procedure, but the obtained theory is not necessarily time symmetric under the standard use of the term.

In the present paper we first consider the case of the non-unitary evolution of the pure state into a mixed state. The TSM closely follows the ABL procedure, but an important difference is that the states $|\Psi_1(t)\rangle$ and $|\Psi_2(t)\rangle$ evolve under different evolution operators \hat{U}_1 and \hat{U}_2 , respectively, such that $\hat{U}_1^\dagger \hat{U}_2 = \hat{I}$. The main result of this work is the development of the TSM description of postselected systems with non-unitary pure state \rightarrow mixed state evolution. A modification of the ABL procedure is necessary in this case due to the fact that the evolution can no longer be described by the evolution operator \hat{U} . That is, we have two mixed states $\hat{\rho}_1(t)$ and $\hat{\rho}_2(t)$ in the expression for the probability of strong measurement on postselected systems. These states evolve differently, governed by the superoperators \hat{U}_1 and \hat{U}_2 , and the explicit connection between these evolutions is found.

In order to illustrate the developed TSM for non-unitary evolutions, we consider two characteristic examples: the spontaneous deexcitation of atoms and a model of systems approaching thermal equilibrium. In the absence of postselection, these systems evolve asymmetrically in time, since in the first case the system always approaches the ground state, while in the second case the system approaches the state of thermal equilibrium. For both of the considered systems, we are able to operationally define the arrow of time, as a direction of time in which a given measurable test quantity decreases monotonously in time. When we introduce the postselection measurement, we have an extra state $\hat{\rho}_2(t)$, which describes the influence of the postselection on the system, in addition to the state $\hat{\rho}_1(t)$, which describes the

effect of the preselection. When the postselection condition is present, the same operational definition can be used to analyze the existence of the arrow of time. We demonstrate that when the TSM probability is used, the test quantity still decreases in time for the first system, while for the second one, monotonous behaviour exists only in special cases. Thus, some systems show time-asymmetry even after postselection, although in a general case the arrow of time does not necessarily exist within the framework of the TSM.

This article is organized as follows. In section 2 we present the general considerations of strong measurements on the teleological system with nonunitary time evolution. In section 3, we study the characteristic examples of the nonunitary pure state \rightarrow mixed state evolutions. Finally, in section 4, we conclude with some general considerations, and we present some possibilities for further research.

2. TSM for postselected systems with nonunitary evolution

2.1. Pure state \rightarrow pure state case

In the present paper we perform the time-symmetrization procedure, i.e. we develop an appropriate TSM for postselected quantum systems with effectively nonunitarily evolving states. The simplest situation is in the case when the initial pure state $|\Psi_{\text{in}}\rangle$ remains pure throughout the time evolution. In that case the state of the system $|\Psi_1(t)\rangle$ evolves towards the future according to the standard quantum-mechanical law

$$|\Psi_1(t)\rangle = \hat{U}_1(t_{\text{in}}, t)|\Psi_{\text{in}}\rangle, \quad (1)$$

but where $\hat{U}_1(t_{\text{in}}, t)$ is assumed to be a nonunitary operator, see the first scenario in figure 1. We analyze the probability of the measurement results for an observable $\hat{A} = \sum_k a_k \hat{\Pi}_k$ at the time $t^* > t_{\text{in}}$, under the condition that at the time $t = t_{\text{fin}} > t^*$ the system is postselected in the state $|\Psi_{\text{fin}}\rangle$. The quantities a_k are the eigenvalues of the measured observable, which can be degenerate, while $\hat{\Pi}_k$ are the corresponding eigenprojecting operators. We consider the quantum event, represented by the projecting operator $\hat{\Pi}_j$, i.e. we consider the probability of obtaining the eigenvalue a_j of the observable \hat{A} . The observable \hat{A} defines a unit operator decomposition $\hat{I} = \sum_k \hat{\Pi}_k$, where $\hat{\Pi}_k$ are the distinguishable quantum events of the given experimental setup.

For the corresponding conditional probability $\mathcal{P}_j(t^*) = \text{Prob}(|\Psi_1(t^*)\rangle/|\Psi_{\text{fin}}\rangle; \hat{A}, \hat{\Pi}_j)$ we have

$$\mathcal{P}_j(t^*) = \frac{\tilde{\mathcal{P}}_j(t^*)}{\mathcal{P}_0(t^*)}, \quad (2a)$$

where

$$\tilde{\mathcal{P}}_j(t^*) = \left\langle \Psi_1(t^*) \left| \hat{\Pi}_j \right| \Psi_1(t^*) \right\rangle \left| \langle \Psi_j(t_{\text{fin}}) | \Psi_{\text{fin}} \rangle \right|^2 \quad (2b)$$

and

$$\mathcal{P}_0(t^*) = \sum_k \tilde{\mathcal{P}}_k(t^*), \quad (2c)$$

where summation is over all projecting operators $\hat{\Pi}_k$ of the measured observable \hat{A} . In (2b), the first factor is the probability for obtaining the eigenvalue a_j at the time t^* , while the second factor is the probability for the system to collapse into $|\Psi_{\text{fin}}\rangle$ from the state $|\Psi_j(t_{\text{fin}})\rangle$ due to the postselection measurement at the time t_{fin} . We note that a specific feature of the

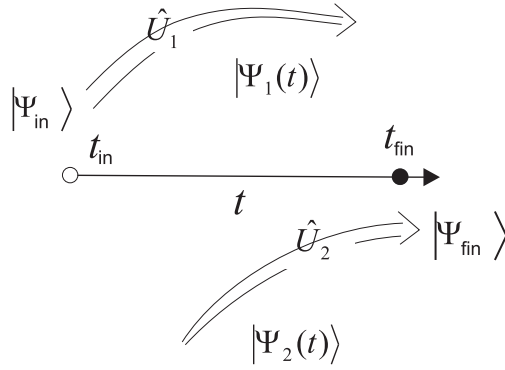


Figure 1. Schematic presentation of the two scenarios, with nonunitary evolutions of the states $|\Psi_1(t)\rangle$ and $|\Psi_2(t)\rangle$.

considered nonunitary evolution is the fact that the particle can leave the system, i.e. the norm of its quantum state does not have to be conserved in time. Therefore, in the expression for the probability we only assume that $\langle \Psi_{in} | \Psi_{in} \rangle = 1$ and $\langle \Psi_{fin} | \Psi_{fin} \rangle = 1$, but do not impose the conditions $\langle \Psi_1(t^*) | \Psi_1(t^*) \rangle = 1$ and $\langle \Psi_k(t_{fin}) | \Psi_k(t_{fin}) \rangle = 1$ for all k . The quantity $\mathcal{P}_0(t^*)$ represents the probability of formation of the postselected ensemble (under the nonselective intermediate measurement of the observable \hat{A} , corresponding to the assumed unit decomposition).

In (2b) and (2c), the vector $|\Psi_j(t_{fin})\rangle$ is the state of the system at the time t_{fin} . This state is a result of the (nonunitary) time evolution of the state of the system from the time $t = t^* + 0$ to the final time $t = t_{fin}$. The measurement of the observable \hat{A} at the time $t = t^*$ with a ‘result’ $\hat{\Pi}_j$ leads to the reduction $|\Psi_1(t)\rangle \rightarrow \hat{\Pi}_j |\Psi_1(t)\rangle / \sqrt{\langle \Psi_1(t) | \hat{\Pi}_j | \Psi_1(t) \rangle}$, which also represents a normalized pure state. Thus, the state of the system at the time t_{fin} is given by $|\Psi_j(t_{fin})\rangle = \hat{U}_1(t^*, t_{fin}) \hat{\Pi}_j |\Psi_1(t^*)\rangle / \sqrt{\langle \Psi_1(t^*) | \hat{\Pi}_j | \Psi_1(t^*) \rangle}$; therefore

$$\tilde{\mathcal{P}}_j(t^*) = \left| \langle \Psi_1(t^*) | \hat{\Pi}_j \hat{U}_1^\dagger(t^*, t_{fin}) | \Psi_{fin} \rangle \right|^2. \tag{3}$$

To follow the basic assumption of the TSM [1], it is necessary to express the probability in terms of the states depending exclusively on t^* . This can be achieved by introducing the second state $|\Psi_2(t)\rangle$ and an evolution operator \hat{U}_2 by the relation

$$|\Psi_{fin}\rangle = \hat{U}_2(t, t_{fin}) |\Psi_2(t)\rangle, \tag{4}$$

where \hat{U}_2 can be considered as a time evolution operator in the second scenario, see figure 1. With the introduced quantities $|\Psi_2\rangle$ and \hat{U}_2 of the second scenario, the expression for the probability can be ‘time symmetrized’ (expressed only via $|\Psi_1(t^*)\rangle$, $|\Psi_2(t^*)\rangle$ and $\hat{\Pi}_j$) under the following condition:

$$\hat{U}_1^\dagger(t, t_{fin}) \hat{U}_2(t, t_{fin}) = \hat{I}, \tag{5}$$

where \hat{I} is the unit operator. Under these assumptions the probability is given by the following expression:

$$\mathcal{P}_j(t^*) = \frac{\left| \langle \Psi_1(t^*) | \hat{\Pi}_j | \Psi_2(t^*) \rangle \right|^2}{\sum_k \left| \langle \Psi_1(t^*) | \hat{\Pi}_k | \Psi_2(t^*) \rangle \right|^2}. \quad (6)$$

The probability (6) is invariant to the transformations $|\Psi_1(t)\rangle \rightarrow f_1(t)|\Psi_1(t)\rangle$ and $|\Psi_2(t)\rangle \rightarrow f_2(t)|\Psi_2(t)\rangle$, for arbitrary complex functions $f_1(t)$ and $f_2(t)$, such that $f_1(t_{\text{in}}) = 1$ and $f_2(t_{\text{fin}}) = 1$. It is most natural to take $f_1(t) = 1, \forall t$, since this choice corresponds to the case of the evolution in the absence of postselection. However, there is no obvious choice of the function $f_2(t)$, because the second scenario has no interpretation outside the TSM. This ambiguity is closely related to the fact that we could have obtained the same result using the condition $\hat{U}_1^\dagger(t, t_{\text{fin}})\hat{U}_2(t, t_{\text{fin}}) = (1/f_2(t))\hat{I}$ instead of the condition (5). For the standard case of unitary evolution of the first scenario, $\hat{U}_1^\dagger = \hat{U}_1^{-1}$, the evolution operator of the second scenario is given by the relation $\hat{U}_2 = (1/f_2)\hat{U}_1$, which, for the choice of $f_2 = 1$, coincides with the evolution operator of the first scenario, as is usually implicitly presumed.

The probability (6) has the same form as the ABL probability [1], but the state $|\Psi_2(t^*)\rangle$ is differently defined. As in the ABL expression, all the eigenprojectors of the observable \hat{A} are present in (6). This reflects the well-known fact that the TSM probability of a considered quantum event depends on all distinguishable quantum events of the given experimental setup (corresponding to a given unit decomposition). This is different than in the absence of postselection, when the probability depends exclusively on the considered quantum event.

2.2. Pure state \rightarrow mixed state case

In the formerly considered pure state \rightarrow pure state case, the initial state can be expressed via statistical operator $\hat{\rho}_{\text{in}} = |\Psi_{\text{in}}\rangle\langle\Psi_{\text{in}}|$. This operator evolves into the pure state with (in general) nonunit norm, so that the state operator $\hat{\rho}_1(t) = \hat{U}_1(t_{\text{in}}, t)\hat{\rho}_{\text{in}}\hat{U}_1^\dagger(t_{\text{in}}, t) \equiv |\Psi_1(t)\rangle\langle\Psi_1(t)|$ is no longer a statistical operator ($\text{Tr} \hat{\rho}_1(t) \neq 1$), but it is still positive (self-adjoint) operator.

In the most general case, the initial pure state operator $\hat{\rho}_{\text{in}}$ could evolve into the mixed state operator $\hat{\rho}_1(t)$ at the time t , for example, when the considered system represents a subsystem of some closed quantum system. This fact cannot be expressed via evolution operator \hat{U}_1 in the form $\hat{\rho}_1(t) = \hat{U}_1(t_{\text{in}}, t)\hat{\rho}_{\text{in}}\hat{U}_1^\dagger(t_{\text{in}}, t)$. Instead, one can introduce a linear superoperator $\hat{U}_1(t_{\text{in}}, t): \hat{\rho}_{\text{in}} \rightarrow \hat{\rho}_1(t)$, which can be written as

$$\hat{\rho}_1(t) = \hat{U}_1(t_{\text{in}}, t)\hat{\rho}_{\text{in}}. \quad (7)$$

In order for the mixed state operator to describe the physical system it must remain positive (self-adjoint) operator at all times.

Again, we consider the measurement on the postselected quantum systems (time-symmetrized ensemble within the framework of nonunitary evolution) with given initial and final states $|\Psi_{\text{in}}\rangle$ and $|\Psi_{\text{fin}}\rangle$, respectively, i.e. $\hat{\rho}_{\text{in}} = |\Psi_{\text{in}}\rangle\langle\Psi_{\text{in}}|$ and $\hat{\rho}_{\text{fin}} = |\Psi_{\text{fin}}\rangle\langle\Psi_{\text{fin}}|$ ($\text{Tr} \hat{\rho}_{\text{in}} = 1$, $\text{Tr} \hat{\rho}_{\text{fin}} = 1$). The probability $\mathcal{P}_j(t^*) = \text{Prob}(\hat{\rho}_1(t^*)/|\Psi_{\text{fin}}\rangle; \hat{A}, \hat{\Pi}_j)$ is given by $\mathcal{P}_j(t^*) = \tilde{\mathcal{P}}_j(t^*)/\mathcal{P}_0(t^*)$. The quantity $\tilde{\mathcal{P}}_j(t^*)$ is expressed by

$$\tilde{\mathcal{P}}_j(t^*) = \text{Tr} \left[\hat{\rho}_1(t^*)\hat{\Pi}_j \right] \text{Tr} \left[\hat{\rho}_j(t_{\text{fin}})\hat{\Pi}_{\text{fin}} \right], \quad (8a)$$

where $\hat{\rho}_1(t^*) = \hat{U}_1(t_{\text{in}}, t^*)\hat{\rho}_{\text{in}}$ and $\hat{\rho}_j(t_{\text{fin}}) = \hat{U}_1(t^*, t_{\text{fin}})\hat{\rho}_j(t^*)$, while $\hat{\rho}_j(t^*) = \hat{\Pi}_j\hat{\rho}_1(t^*)\hat{\Pi}_j/\text{Tr}[\hat{\rho}_1(t^*)\hat{\Pi}_j]$ and $\hat{\Pi}_{\text{fin}} = \hat{\rho}_{\text{fin}}$. The probability \mathcal{P}_0 is the sum of all probabilities $\tilde{\mathcal{P}}_k(t^*)$ as in the pure state \rightarrow pure state case. Inserting the expression for $\hat{\rho}_j(t_{\text{fin}})$

in equation (8a), we get

$$\tilde{\mathcal{P}}_j(t^*) = \text{Tr} \left\{ \hat{\rho}_{\text{fin}} \left[\hat{U}_1(t^*, t_{\text{fin}}) \hat{\Pi}_j \hat{\rho}_1(t^*) \hat{\Pi}_j \right] \right\}. \quad (8b)$$

In the analogy to the TSM for pure state \rightarrow pure state case, we introduce the operator $\hat{\rho}_2(t)$ by the relation

$$\hat{\rho}_{\text{fin}} = \hat{U}_2(t, t_{\text{fin}}) \hat{\rho}_2(t), \quad (9)$$

where the superoperator $\hat{U}_2(t, t_{\text{fin}})$ governs the time evolution in the second scenario. In terms of the operator $\hat{\rho}_2(t)$ and superoperator $\hat{U}_2(t, t_{\text{fin}})$ we have

$$\tilde{\mathcal{P}}_j(t^*) = \text{Tr} \left\{ \left[\hat{U}_2(t^*, t_{\text{fin}}) \hat{\rho}_2(t^*) \right] \left[\hat{U}_1(t^*, t_{\text{fin}}) \hat{\Pi}_j \hat{\rho}_1(t^*) \hat{\Pi}_j \right] \right\}. \quad (10)$$

In order to complete the procedure, we need to define the adjoint operation for the superoperators. For the scalar product of hermitian operators \hat{A} and \hat{B} , needed for the definition of the adjoint operation, we take $\text{Tr}(\hat{A}\hat{B})$. The adjoint superoperator is defined by the relation $\text{Tr}[(\hat{U}^\dagger \hat{A})\hat{B}] = \text{Tr}[\hat{A}(\hat{U}\hat{B})]$, which has to be satisfied for all hermitian operators \hat{A} and \hat{B} . By applying this definition to expression (10), we obtain

$$\tilde{\mathcal{P}}_j(t^*) = \text{Tr} \left\{ \hat{\rho}_2(t^*) \hat{U}_2^\dagger(t^*, t_{\text{fin}}) \left[\hat{U}_1(t^*, t_{\text{fin}}) \hat{\Pi}_j \hat{\rho}_1(t^*) \hat{\Pi}_j \right] \right\}. \quad (11)$$

Under the composition condition $\hat{U}_2^\dagger(t^*, t_{\text{fin}}) \circ \hat{U}_1(t^*, t_{\text{fin}}) = \hat{I}$, equivalent to

$$\hat{U}_1^\dagger(t, t_{\text{fin}}) \circ \hat{U}_2(t, t_{\text{fin}}) = \hat{I}, \quad (12)$$

we get the expression

$$\tilde{\mathcal{P}}_j(t^*) = \text{Tr} \left[\hat{\rho}_2(t^*) \hat{\Pi}_j \hat{\rho}_1(t^*) \hat{\Pi}_j \right]. \quad (13)$$

The corresponding expression for the probability $\mathcal{P}_j(t^*)$ is given by:

$$\mathcal{P}_j(t^*) = \frac{\text{Tr} \left[\hat{\Pi}_j \hat{\rho}_1(t^*) \hat{\Pi}_j \hat{\rho}_2(t^*) \right]}{\sum_k \text{Tr} \left[\hat{\Pi}_k \hat{\rho}_1(t^*) \hat{\Pi}_k \hat{\rho}_2(t^*) \right]}. \quad (14)$$

Even though we have formally completed the time-symmetrization procedure, it is still difficult to operate directly with the evolution superoperators, and to find their adjoints, which are necessary for the calculations of mixed states $\hat{\rho}_1$ and $\hat{\rho}_2$. In order to computationally simplify the procedure, we represent the mixed state operators by vectors, or more concretely, by the appropriate vector columns, while the superoperators are represented by linear operators in this space. That is, in the vector representation, for a given finite-dimensional basis $\{|\alpha_1\rangle, |\alpha_2\rangle, \dots, |\alpha_N\rangle\}$, the selfadjoint operator \hat{A} is expressed by

$$\hat{A} \Leftrightarrow |\hat{A}\rangle = \begin{Bmatrix} A_{11} \\ A_{12} \\ \dots \\ A_{1N} \\ A_{21} \\ \dots \\ A_{NN} \end{Bmatrix}, \quad (15)$$

where $A_{ij} = \langle \alpha_i | \hat{A} | \alpha_j \rangle$ are the matrix elements of the operator \hat{A} . Within the introduced representation, for two self-adjoint operators \hat{A} and \hat{B} , the scalar product $\langle \hat{A} | \hat{B} \rangle = \sum_{i=1}^N \sum_{j=1}^N A_{ji}^* B_{ij}$. Taking into account that $A_{ji}^* = A_{ij}$, we see that the trace of the product of two self-adjoint operators \hat{A} and \hat{B} can be expressed via scalar product in the considered vector space:

$$\text{Tr}(\hat{A}\hat{B}) = \langle \hat{A} | \hat{B} \rangle. \quad (16)$$

Using the former relation, the probability $\tilde{\mathcal{P}}_j(t^*)$ given by (10) can be written as a scalar product:

$$\tilde{\mathcal{P}}_j(t^*) = \left\langle \hat{U}_2(t^*, t_{\text{fin}}) \hat{\rho}_2(t^*) \left| \hat{U}_1(t^*, t_{\text{fin}}) \hat{\Pi}_j \hat{\rho}_1(t^*) \hat{\Pi}_j \right. \right\rangle. \quad (17)$$

Within the proposed representation the operators $\hat{U}_2(t, t_{\text{fin}}) \hat{\rho}_2(t)$ and $\hat{U}_1(t, t_{\text{fin}}) \hat{\rho}_j(t)$, where $\hat{\rho}_j(t) \equiv \hat{\Pi}_j \hat{\rho}_1(t) \hat{\Pi}_j$, are represented by the vectors

$$\left| \hat{U}_2(t, t_{\text{fin}}) \hat{\rho}_2(t) \right\rangle = \hat{U}_2(t, t_{\text{fin}}) \left| \hat{\rho}_2(t) \right\rangle \quad (18a)$$

and

$$\left| \hat{U}_1(t, t_{\text{fin}}) \hat{\rho}_j(t) \right\rangle = \hat{U}_1(t, t_{\text{fin}}) \left| \hat{\rho}_j(t) \right\rangle, \quad (18b)$$

respectively. The operators \hat{U}_1 and \hat{U}_2 are the representations of the superoperators $\hat{\hat{U}}_1$ and $\hat{\hat{U}}_2$, respectively, in the considered vector space of mixed states. With the so defined evolution operators \hat{U}_1 and \hat{U}_2 , we have

$$\tilde{\mathcal{P}}_j(t^*) = \left\langle \hat{\rho}_2(t^*) \left| \hat{U}_2^\dagger(t^*, t_{\text{fin}}) \hat{U}_1(t^*, t_{\text{fin}}) \left| \hat{\Pi}_j \hat{\rho}_1(t^*) \hat{\Pi}_j \right. \right. \right\rangle. \quad (19)$$

According to (19), we see that the time symmetrized expression for the probability, i.e. the probability expressed only via $\hat{\rho}_1(t^*)$, $\hat{\rho}_2(t^*)$ and $\hat{\Pi}_j$, can be obtained if the operators \hat{U}_1 and \hat{U}_2 satisfy the relation

$$\hat{U}_1^\dagger(t, t_{\text{fin}}) \hat{U}_2(t, t_{\text{fin}}) = \hat{\mathcal{I}}, \quad (20)$$

which is of the same form as the condition (5) obtained in the pure state \rightarrow pure state case. Note that the condition (20) for the evolution operators is isomorphic to the condition (12) for the evolution superoperators. Under the requirement (20), the expression for the probability $\tilde{\mathcal{P}}_j(t^*)$ has the following form:

$$\tilde{\mathcal{P}}_j(t^*) = \left\langle \hat{\rho}_2(t^*) \left| \hat{\Pi}_j \hat{\rho}_1(t^*) \hat{\Pi}_j \right. \right\rangle. \quad (21)$$

In order to recover the expression (13), and thus the probability $\mathcal{P}_j(t^*)$ (14) (given via operators $\hat{\rho}_1(t)$ and $\hat{\rho}_2(t)$ instead via vectors $|\hat{\rho}_1(t)\rangle$ and $|\hat{\rho}_2(t)\rangle$), we use the relation (16).

The probability (14) reduces to the expression (6), for the pure state \rightarrow pure state evolution. In this case the action of a superoperator $\hat{\hat{U}}$ can be expressed via operator \hat{U} : $\hat{\hat{U}}(t_1, t_2) \hat{\rho} = \hat{U}(t_1, t_2) \hat{\rho} \hat{U}^\dagger(t_1, t_2)$. Similarly to the pure state \rightarrow pure state case, expression (14) is invariant to the transformations $\hat{\rho}_1(t) \rightarrow f_1(t) \hat{\rho}_1(t)$ and $\hat{\rho}_2(t) \rightarrow f_2(t) \hat{\rho}_2(t)$, under the condition $f_1(t_{\text{in}}) = f_2(t_{\text{fin}}) = 1$. If we want to have any interpretation of $\hat{\rho}_1$ and $\hat{\rho}_2$ as mixed state operators within their respective scenarios, the functions $f_1(t)$ and $f_2(t)$ must be real, positive functions. In the following examples, we will use the simplest choice, $f_1(t) = f_2(t) = 1$.

2.3. Time symmetry aspects of the TSM

Based on the expression (14) for the probability, we can answer the question in what sense is a postselected system with nonunitary evolution time-symmetric. That is, although we performed the time-symmetrization procedure by using the TSM, it is not clear whether the theory is time symmetric under the standard use of the term.

Any time-symmetric quantum theory must be invariant to the inversion of time. Both in the standard case of unitary evolution and in the considered case of non-unitary evolution, the inversion of time direction replaces the initial time with the final time ($t_{\text{in}} \leftrightarrow t_{\text{fin}}$), and the initial condition with the final condition ($\hat{\rho}_{\text{in}} \leftrightarrow \hat{\rho}_{\text{fin}}$). If we also include the exchange of the evolution operators of the first and second scenario $\hat{U}_1 \leftrightarrow \hat{U}_2$ to the definition of the time direction inversion operation, we have that $\hat{\rho}_1 \leftrightarrow \hat{\rho}_2$. This can be interpreted as the exchange of roles of the first and the second scenario under the reversal of time (see figure 1). The probability $\mathcal{P}_j(t^*)$ remains invariant under the so defined inversion of time, since this probability is obviously invariant to $\hat{\rho}_1 \leftrightarrow \hat{\rho}_2$.

To understand the physical implications of the introduced transformations, let us consider two separate systems: the first system is prepared in the state $\hat{\rho}_{\text{in}}$ at the time t_{in} and evolves towards the future under the superoperator \hat{U}_1 , while the second system is prepared in the state $\hat{\rho}_{\text{fin}}$ at the time t_{fin} and evolves under the superoperator \hat{U}_2 backwards in time (towards the past); the validity of the relation $\hat{U}_1^\dagger \circ \hat{U}_2 = \hat{I}$ is presumed. We can additionally postselect the two systems: the postselection in the first of the two considered systems is at the time $t = t_{\text{fin}}$ in the state $\hat{\rho}_{\text{fin}}$, while the postselection in the second one is at the time $t = t_{\text{in}}$ in the state $\hat{\rho}_{\text{in}}$. At the time $t = t^*$, within the framework of the first scenario of the first and the second system, we have the states $\hat{U}_1(t_{\text{in}}, t^*)\hat{\rho}_{\text{in}} = \hat{\rho}_1(t^*)$ and $\hat{U}_2(t_{\text{fin}}, t^*)\hat{\rho}_{\text{fin}} = \hat{\rho}_2(t^*)$, respectively.

The second scenario is standardly introduced, and its evolution superoperator is determined by the evolution in the first scenario, which is the same as the time evolution in the absence of postselection. In the first system the evolution in the absence of postselection is given by the superoperator \hat{U}_1 , while the second scenario superoperator $\hat{U}_2 = (\hat{U}_1^\dagger)^{-1}$ is introduced as ‘auxiliary’ operator to obtain time symmetrization. On the other hand, in the second system, the ‘real’ evolution is given by the superoperator \hat{U}_2 , and the superoperator $(\hat{U}_2^\dagger)^{-1} = \hat{U}_1$ is now auxiliary. Therefore, at the time $t = t^*$, in the second scenarios of the first and the second system we get the states $\hat{U}_2(t_{\text{fin}}, t^*)\hat{\rho}_{\text{fin}} = \hat{\rho}_2(t^*)$ and $\hat{U}_1(t_{\text{in}}, t^*)\hat{\rho}_{\text{in}} = \hat{\rho}_1(t^*)$.

The intermediate probability of the quantum event $\hat{\Pi}_j$ at the time $t = t^*$ is the same in both systems. In that sense, one can say that the theory for nonunitary evolution can be time-symmetrized, i.e. for every system and its direction of time there exists a different (dual) system with different direction of time, such that it is impossible to distinguish between them by measurements with postselection. However, the existence of two different evolutions \hat{U}_1 and \hat{U}_2 in the first scenarios of the considered two systems means that we are actually considering two different physical systems. For that reason, presented theory is not time-symmetrized in a standard way.

3. Examples

3.1. Spontaneous deexcitation of postselected atoms

Spontaneous radiative deexcitation of atomic systems is standardly considered as a consequence of the coupling of these systems to the field of photons. From the standpoint of the atomic subsystem this can be effectively described as a nonunitary evolution from pure state \rightarrow mixed state. The simplest case is when we consider only the ground state $|\alpha\rangle$ and the first excited atomic (electronic) energy eigenstate $|\beta\rangle$, corresponding to the energies E_α and $E_\beta > E_\alpha$, respectively. The characteristic quantity for this system (initially in the state $|\beta\rangle$) is the survival probability corresponding to the quantum event $\hat{\Pi}_\beta = |\beta\rangle\langle\beta|$.

From the time-dependent perturbative theory of radiative transitions, a pure state $|\Psi(t)\rangle$ describing the total system can be obtained. The effective description of the atomic subsystem is obtained by taking a partial trace of the state $|\Psi(t)\rangle\langle\Psi(t)|$ over the photon states. It follows that the excited atomic state $|\beta\rangle\langle\beta|$ exponentially decays into the mixture of the excited and the ground state:

$$\hat{U}_1(t_1, t_2)|\beta\rangle\langle\beta| = e^{-\Gamma_\beta\Delta_{12}} |\beta\rangle\langle\beta| + (1 - e^{-\Gamma_\beta\Delta_{12}})|\alpha\rangle\langle\alpha|, \quad (22a)$$

where $\Delta_{12} = t_2 - t_1$. The quantity Γ_β has the meaning of the transition rate; its reciprocal value, $\tau_\beta = 1/\Gamma_\beta$, is the lifetime of the level E_β . On the other hand, the ground state remains stationary, i.e.

$$\hat{U}_1(t_1, t_2)|\alpha\rangle\langle\alpha| = |\alpha\rangle\langle\alpha|. \quad (22b)$$

In order to fully define the evolution superoperator $\hat{U}_1(t_1, t_2)$ we need to define the action on $|\alpha\rangle\langle\beta|$ and $|\beta\rangle\langle\alpha|$, which directly gives its action on their Hermitian linear combinations. This action cannot be easily obtained from the mentioned theory. In the most general case we have the following linear combinations:

$$\hat{U}_1(t_1, t_2)|\alpha\rangle\langle\beta| = a_{12} |\alpha\rangle\langle\alpha| + b_{12} |\alpha\rangle\langle\beta| + c_{12} |\beta\rangle\langle\alpha| + d_{12} |\beta\rangle\langle\beta|, \quad (22c)$$

$$\hat{U}_1(t_1, t_2)|\beta\rangle\langle\alpha| = A_{12} |\alpha\rangle\langle\alpha| + B_{12} |\alpha\rangle\langle\beta| + C_{12} |\beta\rangle\langle\alpha| + D_{12} |\beta\rangle\langle\beta|, \quad (22d)$$

where $a_{12} = a(\Delta_{12})$, $b_{12} = b(\Delta_{12})$ etc. From the condition that the result of the action of the superoperator on a Hermitian operator is again a Hermitian operator, we get the relations: $a = A^*$, $d = D^*$, $B = c^*$ and $C = b^*$. It can be shown that the survival probability in presence of arbitrary postselection does not depend on the choice of these parameters. However, we will use the model which satisfies the physical composition condition: $\hat{U}_1(t_1, t_2) = \hat{U}_1(t', t_2) \circ \hat{U}_1(t_1, t')$. This is satisfied for the choice of parameters $a = c = d = 0$ ($A = B = D = 0$) and $b(t_2 - t_1) = b(t_2 - t')b(t' - t_1)$, i.e. $b_{12} = C_{12}^* = \exp(-\kappa\Delta_{12})$, where κ is an arbitrary complex constant.

In the vector-representation of the mixed states for the basis $\{|\alpha\rangle, |\beta\rangle\}$ we have

$$|\alpha\rangle\langle\alpha| \Leftrightarrow \begin{Bmatrix} 1 \\ 0 \\ 0 \\ 0 \end{Bmatrix}, \quad |\alpha\rangle\langle\beta| \Leftrightarrow \begin{Bmatrix} 0 \\ 1 \\ 0 \\ 0 \end{Bmatrix} \quad (23a)$$

and

$$|\beta\rangle\langle\alpha| \Leftrightarrow \begin{Bmatrix} 0 \\ 0 \\ 1 \\ 0 \end{Bmatrix}, \quad |\beta\rangle\langle\beta| \Leftrightarrow \begin{Bmatrix} 0 \\ 0 \\ 0 \\ 1 \end{Bmatrix}. \quad (23b)$$

Based on the expressions (22a)–(22d) we directly obtain the operator $\hat{U}_1(t_1, t_2)$ (representation of the superoperator $\hat{U}_1(t_1, t_2)$):

$$\hat{U}_1(t_1, t_2) = \begin{Bmatrix} 1 & 0 & 0 & 1 - e^{-\Gamma_\beta\Delta_{12}} \\ 0 & e^{-\kappa\Delta_{12}} & 0 & 0 \\ 0 & 0 & e^{-\kappa^*\Delta_{12}} & 0 \\ 0 & 0 & 0 & e^{-\Gamma_\beta\Delta_{12}} \end{Bmatrix}. \quad (24)$$

The operators $\hat{U}_1(t_{\text{in}}, t)$ and $\hat{U}_1(t, t_{\text{fin}})$ follow from (24) for $\Delta_{12} \rightarrow \Delta_i = t - t_{\text{in}}$ and $\Delta_{12} \rightarrow \Delta_f = t_{\text{fin}} - t$, respectively. By using the condition (20) we get

$$\hat{U}_2^{-1}(t, t_{\text{fin}}) = \hat{U}_1^\dagger(t, t_{\text{fin}}) = \begin{Bmatrix} 1 & 0 & 0 & 0 \\ 0 & e^{-\kappa^*\Delta_f} & 0 & 0 \\ 0 & 0 & e^{-\kappa\Delta_f} & 0 \\ 1 - e^{-\Gamma_\beta\Delta_f} & 0 & 0 & e^{-\Gamma_\beta\Delta_f} \end{Bmatrix}. \quad (25)$$

We consider the spontaneous deexcitation for which at the initial time t_{in} the atomic electronic state $|\beta\rangle$ is occupied; the corresponding statistical operator is $\hat{\rho}_{\text{in}} = |\beta\rangle\langle\beta|$. The mixed state $\hat{\rho}_1(t)$ of the system is given by

$$\hat{\rho}_1(t) = \hat{U}_1(t_{\text{in}}, t)(|\beta\rangle\langle\beta|). \quad (26)$$

Using (23b) and (24), we get the expression for the vector $|\hat{\rho}_1(t)\rangle$. According to (15), the corresponding operator is given by:

$$\hat{\rho}_1(t) = \begin{Bmatrix} 1 - e^{-\Gamma_\beta\Delta_i} & 0 \\ 0 & e^{-\Gamma_\beta\Delta_i} \end{Bmatrix}; \quad (27)$$

in the considered case the operator $\hat{\rho}_1(t)$ satisfies the condition $\text{Tr} \hat{\rho}_1(t) = 1$. In the absence of postselection, the survival probability for the atomic system in the mixed state $\hat{\rho}_1(t)$ at the time t is given by $\mathcal{P}_S^{(1)}(t) = \text{Tr} [\hat{\rho}_1(t)\hat{\Pi}_\beta] = \exp(-\Gamma_\beta\Delta_i)$, i.e. we get the well known exponential decay law. Since this probability monotonously decreases in time, it allows us to operationally define the arrow of time as such direction in which the survival probability decreases. In that sense, for this system, we can consider the evolution to be asymmetrical in time. The mean energy in the absence of postselection, $\langle E(t) \rangle = \mathcal{P}_S^{(1)}(t)E_\beta + [1 - \mathcal{P}_S^{(1)}(t)]E_\alpha$, behaves in the same manner. The simple exponential form of the survival probability will not be preserved in the case of postselected atomic systems.

The introduction of a postselection condition requires that the state $\hat{\rho}_{\text{fin}} = |\Psi_{\text{fin}}\rangle\langle\Psi_{\text{fin}}|$ is obtained by a measurement performed on the atomic system at the final time $t = t_{\text{fin}}$. By the choice of the particular postselection, we can control the time-symmetrized survival probability. We consider the most general postselection:

$$|\Psi_{\text{fin}}\rangle = \delta\sqrt{1-q} |\alpha\rangle + \sqrt{q} |\beta\rangle, \quad (28a)$$

where $\delta = \exp(i\varphi)$ is a phase factor. The state $|\Psi_{\text{fin}}\rangle$ ‘contains’ the state $|\alpha\rangle$ with probability $1 - q$ and the state $|\beta\rangle$ with probability q . The final mixed state operator is given by

$$\hat{\rho}_{\text{fin}} = (1 - q)|\alpha\rangle\langle\alpha| + \delta\sqrt{q(1 - q)}|\alpha\rangle\langle\beta| + \delta^*\sqrt{q(1 - q)}|\beta\rangle\langle\alpha| + q|\beta\rangle\langle\beta|; \quad (28b)$$

the corresponding vector-representation is

$$|\hat{\rho}_{\text{fin}}\rangle = \begin{Bmatrix} 1 - q \\ \delta\sqrt{q(1 - q)} \\ \delta^*\sqrt{q(1 - q)} \\ q \end{Bmatrix}. \quad (28c)$$

For a given postselection, it remains to calculate the mixed state operator $\hat{\rho}_2(t)$. In the vector representation $|\hat{\rho}_2(t)\rangle = \hat{U}_2^{-1}(t, t_{\text{fin}})|\hat{\rho}_{\text{fin}}(t)\rangle$, where $\hat{U}_2^{-1}(t, t_{\text{fin}})$ is given by expression (25) and $|\hat{\rho}_{\text{fin}}(t)\rangle$ by (28c). We get the vector $|\hat{\rho}_2(t)\rangle$ and the corresponding operator

$$\hat{\rho}_2(t) = \begin{Bmatrix} 1 - q & D \\ D^* & (1 - p)(1 - q) + pq \end{Bmatrix}, \quad (29)$$

where $p = \exp(-\Gamma_\beta\Delta_f)$ and $D = \delta\sqrt{q(1 - q)}\exp(-\kappa^*\Delta_f)$.

The survival probability $\mathcal{P}_S(t^*)$ at the time $t = t^*$ for the considered time-symmetrized system is expressed by (14), where $\hat{\Pi}_j = |\beta\rangle\langle\beta|$, the distinguishable quantum events are $\hat{\Pi}_\alpha = |\alpha\rangle\langle\alpha|$ and $\hat{\Pi}_\beta = |\beta\rangle\langle\beta|$, and the states $\hat{\rho}_1(t)$ and $\hat{\rho}_2(t)$ are given by (27) and (29), respectively. We get

$$\mathcal{P}_S(t^*) = \frac{1 + |\epsilon|^2(e^{\Gamma_\beta\Delta_f} - 1)}{1 + |\epsilon|^2(e^{\Gamma_\beta\Delta} - 1)}, \quad (30)$$

where $\Delta = t_{\text{fin}} - t_{\text{in}}$ and $|\epsilon|^2 = (1 - q)/q$. We note that the probability $\mathcal{P}_S(t^*)$ is independent on the quantity D , which means that the action of the superoperator \hat{U}_1 on $|\alpha\rangle\langle\beta|$ and $|\beta\rangle\langle\alpha|$ can be taken in somewhat arbitrary form. The obtained survival probability $\mathcal{P}_S(t)$ decreases in time in a similar manner as the probability $\mathcal{P}_S^{(1)}(t) = \exp(-\Gamma_\beta\Delta_i)$, for all postselection conditions. The fact that the survival probability monotonously decreases in time even in the presence of arbitrary postselection means that, by using the same criterion for establishing the direction of time as in the absence of postselection, we are able to reconstruct the arrow of time in the considered system. We note that this conclusion also remains valid for arbitrary preselection, as will be demonstrated as a special case of the TSM treatment of thermalization.

A specific postselection of the atomic system is what we will call the ‘natural’ postselection. It is expressed by the relation $|\epsilon|^2 = 1$, which corresponds to $q = 1/2$. In this case we obtain

$$\mathcal{P}_S(t) = e^{-\Gamma_\beta\Delta_i} = \mathcal{P}_S^{(1)}(t), \quad (31)$$

i.e. the survival probability of the postselected system coincides with the survival probability in the absence of postselection (the postselection has no effect). We note that the value $q = 1/2$, which corresponds to the natural postselection, is exactly the critical value for which the diagonal elements of the operator $\hat{\rho}_2$ are independent of time.

3.2. Thermalization within the TSM

As a second example we consider the quantum system in contact with a reservoir at a temperature T . We assume that, at the time $t = t_{\text{in}}$, the quantum system is in a pure state, given by a statistical operator $\hat{\rho}_{\text{in}}$. At the time t , the considered system is in the mixed state

described by the operator $\hat{\rho}_1(t)$, such that at the time $t \rightarrow \infty$ the system reaches the thermal equilibrium.

According to the general theory of pure state \rightarrow mixed state evolution, the (mixed) state operator at the time t is given by

$$\hat{\rho}_1(t) = \hat{U}_1(t_{\text{in}}, t)\hat{\rho}_{\text{in}}, \quad (32)$$

where \hat{U}_1 is the evolution superoperator. Equilibrium statistical physics cannot be used to determine this operator; we only have information for the time $t \rightarrow \infty$. That is, considering the system as a canonic ensemble, we have that

$$\hat{\rho}_1(t) \rightarrow \hat{\rho}_{\infty} = \frac{e^{-\hat{H}/kT}}{\text{Tr}(e^{-\hat{H}/kT})}, \quad t \rightarrow \infty, \quad (33)$$

where \hat{H} is the Hamiltonian of the system and k is the Boltzmann constant. We study the quantum system with two orthonormal energy eigenstates $|\alpha\rangle$ and $|\beta\rangle$, corresponding to the energies E_{α} and $E_{\beta} > E_{\alpha}$. In the considered case $\hat{H} = E_{\alpha}|\alpha\rangle\langle\alpha| + E_{\beta}|\beta\rangle\langle\beta|$, so that

$$\hat{\rho}_{\infty} = A|\alpha\rangle\langle\alpha| + B|\beta\rangle\langle\beta|, \quad (34a)$$

where

$$A \equiv \mathcal{P}_{\alpha}^{(\infty)} = \frac{e^{-E_{\alpha}/kT}}{e^{-E_{\alpha}/kT} + e^{-E_{\beta}/kT}} \quad (34b)$$

and

$$B \equiv \mathcal{P}_{\beta}^{(\infty)} = \frac{e^{-E_{\beta}/kT}}{e^{-E_{\alpha}/kT} + e^{-E_{\beta}/kT}} \quad (34c)$$

are the probabilities of finding the system in the states $|\alpha\rangle$ and $|\beta\rangle$, respectively, for $t \rightarrow \infty$. Obviously, A and B are real positive constants satisfying the relation $A + B = 1$, and also $B < A$.

The aim of the example is not to analyze the details of the process of thermalization; we only want to demonstrate that, in principle, the thermal evolution of postselected systems can be considered within the framework of the TSM. For that purpose, we construct a ‘toy-model’ linear superoperator $\hat{U}_1(t_{\text{in}}, t)$, such that

$$\hat{U}_1(t_{\text{in}}, t)\hat{\rho}_{\text{in}} \rightarrow \hat{\rho}_{\infty}, \quad t \rightarrow \infty, \quad (35a)$$

for any $\hat{\rho}_{\text{in}}$, where $\hat{\rho}_{\infty}$ is given by (34a). Another condition that we use in modelling the considered superoperator is

$$\text{Tr} \left[\hat{U}_1(t_{\text{in}}, t)\hat{\rho}_{\text{in}} \right] = 1, \quad t > t_{\text{in}}, \quad (35b)$$

which has to be satisfied for all $\hat{\rho}_{\text{in}}$. Obviously, we must also have:

$$\hat{U}_1(t_{\text{in}}, t) = \hat{I}, \quad t = t_{\text{in}}. \quad (35c)$$

The effective construction will be performed in the vector representation of the mixed state operators. We take that

$$|\hat{\rho}_{\text{in}}\rangle = \begin{Bmatrix} a \\ b \\ c \\ d \end{Bmatrix} \tag{36}$$

describes an initial state; from the relations $\hat{\rho}_{\text{in}}^\dagger = \hat{\rho}_{\text{in}}$ and $\text{Tr } \hat{\rho}_{\text{in}} = 1$ we get that a and d are real quantities, $c = b^*$ and $a + d = 1$. In the same representation, the condition (35a) reads as follows:

$$\hat{U}_1(t_{\text{in}}, \infty) \begin{Bmatrix} a \\ b \\ c \\ d \end{Bmatrix} = \begin{Bmatrix} A \\ 0 \\ 0 \\ B \end{Bmatrix}, \tag{37}$$

which has to be satisfied for all a, b, c and d satisfying the former relations. As the appropriate 4×4 matrix we take the matrix of the following form at $t \rightarrow \infty$:

$$\lim_{t \rightarrow \infty} \hat{U}_1(t_{\text{in}}, t) = \begin{Bmatrix} A & 0 & 0 & A \\ 0 & 0 & 0 & 0 \\ 0 & 0 & 0 & 0 \\ B & 0 & 0 & B \end{Bmatrix}. \tag{38}$$

This condition, as well as the condition $\lim_{t \rightarrow t_{\text{in}}} \hat{U}_1(t_{\text{in}}, t) = \hat{I}$, which is a direct consequence of (35c), is satisfied for the following operator:

$$\hat{U}_1(t_{\text{in}}, t) = \begin{Bmatrix} p_i + (1 - p_i)A & 0 & 0 & (1 - p_i)A \\ 0 & p_i & 0 & 0 \\ 0 & 0 & p_i & 0 \\ (1 - p_i)B & 0 & 0 & p_i + (1 - p_i)B \end{Bmatrix}, \tag{39}$$

where $p_i = p(\Delta_i)$ is an arbitrary continuous function of the time interval $\Delta_i = t - t_{\text{in}}$, satisfying the conditions $p(0) = 1$ and $p(\infty) = 0$. The composition law $\hat{U}_1(t_{\text{in}}, t) = \hat{U}_1(t', t)\hat{U}_1(t_{\text{in}}, t')$ can be used to obtain the operator $\hat{U}_1(t', t)$ for two arbitrary instants of time t' and t . The simplest solution of the problem is to generalize the expression (39) to arbitrary instants of time; namely, we take that $\hat{U}_1(t', t)$ is given by expression (39) in which $p_i = p(\Delta_i) \rightarrow p' = p(\Delta')$, where $\Delta' = t - t'$. This is possible providing that $p(t - t') = \exp(-\Gamma\Delta)$, where Γ is an arbitrary constant, with a positive real part. We take that Γ is real, so that any (Hermitian) state operator remains Hermitian during the time evolution. In that case, the operators $\hat{U}_1(t_{\text{in}}, t)$ and $\hat{U}_1(t, t_{\text{fin}})$ are given by the expression (39) for $p_i = \exp(-\Gamma\Delta_i)$ and for $p_i \rightarrow p_f = \exp(-\Gamma\Delta_f)$, where $\Delta_f = t_{\text{fin}} - t$, respectively.

We assume the most general preselection in a pure state

$$|\Psi_{\text{in}}\rangle = \delta_i \sqrt{1 - q_i} |\alpha\rangle + \sqrt{q_i} |\beta\rangle, \tag{40a}$$

where $\delta_i = \exp(i\varphi_i)$ is a phase factor. The corresponding initial mixed state operator is given by

$$\hat{\rho}_{\text{in}} = (1 - q_i)|\alpha\rangle\langle\alpha| + \delta_i \sqrt{q_i(1 - q_i)} |\alpha\rangle\langle\beta| + \delta_i^* \sqrt{q_i(1 - q_i)} |\beta\rangle\langle\alpha| + q_i |\beta\rangle\langle\beta|. \tag{40b}$$

Comparing (40b) with the expression (36) we get the values: $a = 1 - q_i$, $b = \delta_i \sqrt{q_i(1 - q_i)}$, $c = b^*$ and $d = q_i$. At the time t we have $|\hat{\rho}_1(t)\rangle = \hat{U}_1(t_{\text{in}}, t)|\hat{\rho}_{\text{in}}\rangle$, where $\hat{U}_1(t_{\text{in}}, t)$ is explicitly given by (39); finally, we obtain the mixed state operator $\hat{\rho}_1(t)$ in the following form:

$$\hat{\rho}_1(t) = \begin{Bmatrix} A_{\text{in}} & D_{\text{in}} \\ D_{\text{in}}^* & B_{\text{in}} \end{Bmatrix}, \quad (41)$$

where $A_{\text{in}} = (1 - q_i)p_i + A(1 - p_i)$, $B_{\text{in}} = q_i p_i + B(1 - p_i)$ and $D_{\text{in}} = \delta_i \sqrt{q_i(1 - q_i)} p_i$. The obtained operator describes the approach of the system towards the thermal equilibrium. By construction, for $t \rightarrow \infty$, $p_i \rightarrow 0$, so that $\hat{\rho}_1(t) \rightarrow \hat{\rho}_\infty$, where $\hat{\rho}_\infty$ is given by (34a). In the absence of postselection, the probability for the system to be found in the state $|\alpha\rangle$, $\mathcal{P}_\alpha^{(1)}(t) = \text{Tr}[\hat{\rho}_1(t)\hat{\Pi}_\alpha]$, is equal to A_{in} ; for the state $|\beta\rangle$, $\mathcal{P}_\beta^{(1)}(t) = \text{Tr}[\hat{\rho}_1(t)\hat{\Pi}_\beta] = B_{\text{in}}$. The eigenprojectors present in these probabilities are $\hat{\Pi}_\alpha = |\alpha\rangle\langle\alpha|$ and $\hat{\Pi}_\beta = |\beta\rangle\langle\beta|$. Obviously, $\lim_{t \rightarrow \infty} \mathcal{P}_\beta^{(1)}(t) = B \equiv \mathcal{P}_\beta^{(\infty)}$, where B is given by (34c). The evolution of the state $\hat{\rho}_1$ is asymmetric in time; namely, a simple criterion for the determination of direction of time is to find whether the probability $\mathcal{P}_\beta^{(1)}(t)$ reaches $\mathcal{P}_\beta^{(\infty)}$ at distant future (forward orientation of time) or at distant past (backward orientation of time). However, this criterion cannot be applied in the presence of postselection, since we are limited to the measurements between the initial and final time. A suitable test that can be easily generalized to the case with postselection, is the time behaviour of the function $|\mathcal{P}_\beta^{(1)}(t) - \mathcal{P}_\beta^{(\infty)}|$. We can say that the time ‘flows’ in the direction in which this function monotonously decreases. Since $\mathcal{P}_\beta^{(1)}(t) = B_{\text{in}}$ does indeed monotonously approach $\mathcal{P}_\beta^{(\infty)} = B$, within the first scenario one can recognize, under both criteria, the ‘thermodynamical’ arrow of time from the past towards the future.

What happens with the arrow of time within the framework of the TSM for the post-selected quantum system in thermal contact with a reservoir represents an open and intriguing question. To resolve the problem, we again consider the most general postselection condition, i.e. we take that

$$|\Psi_{\text{fin}}\rangle = \delta_f \sqrt{1 - q_f} |\alpha\rangle + \sqrt{q_f} |\beta\rangle, \quad (42)$$

where $\delta_f = \exp(i\varphi_f)$ is another phase factor. The corresponding quantities $\hat{\rho}_{\text{fin}}$ and $|\hat{\rho}_{\text{fin}}\rangle$ are given by (28b) and (28c), respectively, for $q = q_f$. The time-symmetrization procedure is the same as in the first example. First, using the explicit expression for the operator $\hat{U}_1(t, t_{\text{fin}})$ and the condition (20), we obtain the operator $\hat{U}_2^{-1}(t, t_{\text{fin}}) = \hat{U}_1^\dagger(t, t_{\text{fin}})$ and the vector $|\hat{\rho}_2(t)\rangle = \hat{U}_2^{-1}(t, t_{\text{fin}})|\rho_{\text{fin}}\rangle$. Secondly, we get the mixed state operator $\hat{\rho}_2(t)$ in the following form:

$$\hat{\rho}_2(t) = \begin{Bmatrix} A_{\text{fin}} & D_{\text{fin}} \\ D_{\text{fin}}^* & B_{\text{fin}} \end{Bmatrix}, \quad (43)$$

where $A_{\text{fin}} = (1 - q_f)p_f + A(1 - p_f) - q_f(1 - p_f)(A - B)$, $B_{\text{fin}} = q_f p_f + A(1 - p_f) - q_f(1 - p_f)(A - B)$ and $D_{\text{fin}} = \delta_f \sqrt{q_f(1 - q_f)} p_f$.

Finally, we calculate the TSM probability for the quantum event of interest. Again, we analyze the probability $\mathcal{P}_\beta(t^*)$ at the time $t = t^*$, which is given by (14), where $\hat{\Pi}_j = \hat{\Pi}_\beta$, and $\hat{\rho}_1(t)$ and $\hat{\rho}_2(t)$ are given by (40b) and (43), respectively. The distinguishable quantum events are again $\hat{\Pi}_\alpha$ and $\hat{\Pi}_\beta$. In the expression for the probability only the reductions $\hat{\Pi}_j \hat{\rho}_1(t) \hat{\Pi}_j$ and $\hat{\Pi}_j \hat{\rho}_2(t) \hat{\Pi}_j$, $j = \alpha, \beta$ are present, so the calculation is direct. We get

$$\mathcal{P}_\beta(t^*) = \frac{B_{\text{in}} B_{\text{fin}}}{A_{\text{in}} A_{\text{fin}} + B_{\text{in}} B_{\text{fin}}}. \quad (44)$$

This expression allows us to analyze the status of the ‘arrow of time’ in the considered example. As we have previously defined, the direction of time exists if the quantity $|\mathcal{P}_\beta(t) - \mathcal{P}_\beta^{(\infty)}|$ is a monotonous function of time. The behaviour of this function can be easily

obtained numerically, for any values of the preselection and postselection parameters, $q_i \in [0, 1]$ and $q_f \in [0, 1]$, as well as arbitrary temperature $T \in (0, \infty)$, i.e. $B \equiv \mathcal{P}_\beta^{(\infty)} \in (0, 1/2)$, and the interval $\Delta = t_{\text{fin}} - t_{\text{in}}$. We have found that, for almost all of the analyzed cases, the considered function is not monotonous. Thus, in general, the arrow of time, as defined, cannot be reconstructed in a postselected system, with the given evolution. The monotonous behaviour has been observed only for the following special cases. The first such situation is the natural postselection, which is again obtained for $q_f = 1/2$, for any temperature. In this case we have $\mathcal{P}_\beta(t) = \mathcal{P}_\beta^{(1)}(t)$ for all times between the initial and the final instant of time. Obviously, in this case the arrow of time is the same as in the absence of the postselection. Note that this existence of the arrow of time is not a purely thermodynamical property, since it requires a special postselection condition.

The other special case is the choice $B \equiv \mathcal{P}_\beta^{(\infty)} = 0$ (and thus $A = 1$), which corresponds to the absolutely cold reservoir ($T \rightarrow 0$). Under this assumption, the evolution operator $\hat{U}_1(t_{\text{in}}, t)$ given by (39) is of the same form as the expression (24) for the evolution operator for the spontaneous deexcitation, considered in the previous example. The probability in this case is given by

$$\mathcal{P}_\beta(t^*) = \frac{q_i p_i (1 - q_f) + 2q_i p_\Delta (q_f - 1/2)}{1 - q_f + 2q_i p_\Delta (q_f - 1/2)}, \quad (45)$$

where $p_\Delta = \exp(-\Gamma\Delta)$, $\Delta = t_{\text{fin}} - t_{\text{in}}$. The time dependence of the probability (45) comes only from the factor $q_i p_i (1 - q_f)$, which depends both on the preselection and the postselection condition. The probability monotonously decreases in time, regardless of the preselection and the postselection condition, except for $q_i = 0$ or $q_f = 1$, for which the probability is constant. Therefore, the obtained monotonous decrease in time is a purely thermodynamical phenomenon. Since in this case $|\mathcal{P}_\beta(t) - \mathcal{P}_\beta^{(\infty)}| = \mathcal{P}_\beta(t)$, this fact can be used to operationally define the thermodynamical arrow of time in the considered system. That is, if the postselected system is in contact with the reservoir of the near zero absolute temperature, the thermodynamical arrow of time points to the direction in which the probability of finding the system in the higher energy state decreases. This direction is the same as in the absence of postselection.

4. Concluding remarks

The main result of the present paper is the derivation of a general TSM for obtaining the corresponding probabilities for postselected systems, in the case of nonunitary, pure state \rightarrow mixed state evolution. In order to achieve this aim, it is necessary to introduce two different scenarios. That is, the system must be described by two different (mixed) states $\hat{\rho}_1(t)$ and $\hat{\rho}_2(t)$, which evolve from the preselected and the postselected state, $\hat{\rho}_{\text{in}}$ and $\hat{\rho}_{\text{fin}}$, respectively, under the action of two different evolution superoperators, \hat{U}_1 and \hat{U}_2 . The superoperator \hat{U}_1 is identical to the evolution operator in the absence of postselection, while \hat{U}_2 can be obtained from the condition $\hat{U}_1^\dagger(t, t_{\text{fin}}) \circ \hat{U}_2(t, t_{\text{fin}}) = \hat{I}$. For computational simplicity, we have also used a representation in which the mixed states are given as vector columns, while the superoperators are represented as matrices. In the sense discussed in section 2.3, one can say that the presented theory is time-symmetrized; however, it is not time-symmetrized under the standard use of the term.

The formalism of the two scenarios can give us more insight into the interplay of the preselection and the postselection condition at the time of intermediate measurement. The

developed method allows us to consider many significant systems which evolve nonunitarily, from the standpoint of the TSM. An interesting property of many of such systems is that they show an explicit time-asymmetry in the absence of postselection, in a sense that an arrow of time can be defined. Even in the presence of postselection, we are able to discuss the status of the arrow of time, from the standpoint of measurable TSM probabilities.

Two important and characteristic examples of nonunitary pure state \rightarrow mixed state evolving systems are spontaneously emitting atoms and the systems approaching thermal equilibrium. Both of the considered systems are relevant in many different areas of physics. We have analyzed these two systems in the approximation of two nondegenerate energy levels. In the case of spontaneous deexcitation of atoms, the evolution superoperator \hat{U}_1 follows from the theory of radiative transitions, while in the case of thermalization process, a toy-model of this superoperator has been constructed on physical grounds. By using the vector representation of the mixed states, we have found the superoperator \hat{U}_2 and the states of the two scenarios, $\hat{\rho}_1(t)$ and $\hat{\rho}_2(t)$. We have calculated the TSM probability of finding the system in the excited state, with a most general preselection and postselection condition. For the atomic decaying system in the absence of postselection, the probability of finding the atom in the excited state decays exponentially to zero. Operationally, the arrow of time can be defined as the direction of time in which this probability monotonously decreases. In the presence of arbitrary postselection, the corresponding survival probability also monotonously decreases in time; thus, the existence of the arrow of time persists. For the thermalization process in the absence of postselection, the probability of finding the system in the higher energy state exponentially approaches a given equilibrium value. This allows us to operationally define the arrow of time as a monotonous approach of this probability to the equilibrium value. However, the corresponding TSM probability does not satisfy this condition, except for the special cases such as the zero temperature, and the so-called natural postselection. This means that, in general, the thermodynamical arrow of time does not exist (under the given definition) in the postselected theory.

In this paper we focused on the so-called strong measurements in postselected systems. In the act of such a measurement, the state of the system collapses due to a strong coupling to the measuring device. While the strong postselected measurements are actively researched [9, 10], the results are mostly theoretical. The framework of postselected systems and time-symmetrized quantum mechanics allows for another nontrivial type of measurement, the so-called weak measurement [7, 8]. The coupling with the measuring device is weak, and thus, there is no reduction of the quantum state; the result of the measurement procedure is the so-called weak value of the observable. Recently, the concept of weak values has not only been applied for theoretical considerations [11, 12], but has also enabled an entire new class of experiments. The weak measurements have been applied to significantly enhance the measured experimental signal [13], but also to probe quantities fundamentally inaccessible to the strong measurements [14, 15]. The generalization of the formalism of the weak measurements to the case of nonunitary pure state \rightarrow mixed state evolution, analogously to the presented method, is a natural continuation of this work.

There are many open theoretical problems related to the nonunitary evolution. For example, the process of thermalization itself is not completely understood; another example is the well-known black hole information paradox. The TSM presented in this work allows us to consider such problems from a standpoint of postselected systems. It might be possible to gain new insight into these phenomena, especially if we indeed generalize the method to the weak measurements.

Acknowledgments

This work was supported in part by the Ministry of Education, Science and Technological Development, Republic of Serbia (Project 171016).

References

- [1] Aharonov Y, Bergmann P G and Lebowitz J L 1964 *Phys. Rev.* **134** B1410
- [2] Aharonov Y and Vaidman L 1991 *J. Phys. A: Math. Gen.* **24** 2315
- [3] Reznik B and Aharonov Y 1995 *Phys. Rev. A* **52** 2538
- [4] Aharonov Y and Vaidman L 2008 The two-state vector formalism: an updated review *Time in Quantum Mechanics (Lecture Notes in Physics vol 734)* ed J G Muga *et al* (Berlin: Springer)
- [5] Nedeljković N N, Nedeljković Lj D, Janev R K and Mišković Z L 1991 *Nucl. Instrum. Methods Phys. Res. B* **58** 519
- [6] Nedeljković N N and Majkić M D 2007 *Phys. Rev. A* **76** 042902
- [7] Aharonov Y and Vaidman L 1990 *Phys. Rev. A* **41** 11
- [8] Ritchie N W M, Story J G and Hulet R G 1991 *Phys. Rev. Lett.* **66** 1107
- [9] Ravon T and Vaidman L 2007 *J. Phys. A: Math. Theor.* **40** 2873
- [10] Nedeljković N N, Majkić M D and Galijaš S M D 2012 *J. Phys. B: At. Mol. Opt. Phys.* **45** 21502
- [11] Aharonov Y, Nussinov S, Popescu S and Vaidman L 2013 *Phys. Rev. A* **87** 014105
- [12] Vaidman L 2013 *Phys. Rev. A* **87** 052104
- [13] Hosten O and Kwiat P 2008 *Science* **319** 787
- [14] Kocsis S, Braverman B, Ravets S, Stevens M J, Mirin R P, Shalm L K and Steinberg A M 2011 *Science* **332** 1170
- [15] Lundeen J S, Sutherland B, Patel A, Stewart C and Bamber C 2011 *Nature* **474** 188

EFFECTIVE LIFETIMES OF THE POSTSELECTED HYDROGEN ATOMS

I. P. Prlina and N. N. Nedeljković

University of Belgrade, Faculty of Physics, P.O.Box 368, Belgrade, Serbia

Abstract. The time symmetrized two-state vector model is adapted for postselected quantum systems with effectively non-unitary evolutions. We study the radiative decay $2p \rightarrow 1s$ of the postselected hydrogen atom. The effective lifetime $\tau_{\text{eff}}(t)$ is obtained for a model postselection, and acceleration or attenuation of the decay due to the postselection is briefly discussed, with emphases on the possible experimental applications.

1. INTRODUCTION

In recent times, some interesting systems and phenomena based on the time-symmetrized two-state vector model (TVM) [1, 2, 3, 4] have been considered theoretically; for example, the weak trace describing the past of a quantum particle [5]. The practical applications of the so called weak measurements on the postselected systems have also been demonstrated, based on their ability to enhance the measured experimental signal [6]. Some intriguing experiments based on the TVM, such as determining the "trajectories" of individual photons [8] and the wave function of the photon itself [7], have been recently performed. In the cited experiments, the weak measurements have been used, because in that case the reduction of quantum state can be avoided. The "strong" measurements, which could also produce a series of intriguing results, have not gained such attention.

In the present article we apply the TVM to the quantum decay of the postselected atomic systems. To concretize the problem, we analyze the (radiative) decay of the hydrogen atoms, considering the $2p \rightarrow 1s$ transitions. That is, we derive the time-symmetrized survival probability $\mathcal{P}_S(t)$. As a consequence of postselection, we obtain a modified "decay law" in comparison to the exponential decay $\mathcal{P}_S^{(0)}(t) = \exp(-t/\tau)$, where τ is the radiative lifetime in the absence of postselection. The survival probability $\mathcal{P}_S(t)$ decreases in time with the effective lifetime $\tau_{\text{eff}}(t)$ different than τ .

2. THEORETICAL MODEL

We assume that the atomic system is preselected at the time t_{in} in the state $\hat{\rho}_{\text{in}} = |\beta\rangle\langle\beta|$, where $|\beta\rangle$ is the first excited atomic electronic state of energy E_β ; the ground state will be denoted by $|\alpha\rangle$. For the postselection we choose the "measurement" $\hat{\Pi}_{\text{fin}} \equiv \hat{\rho}_{\text{fin}} = |\Psi_{\text{fin}}\rangle\langle\Psi_{\text{fin}}|$. We analyze the intermediate survival probability $\mathcal{P}_S(t^*)$ at the time $t = t^*$, on the postselected (teleological) ensemble.

The probability $\mathcal{P}_S(t^*)$ is given by

$$\mathcal{P}_S(t^*) = \frac{\text{Tr}(\hat{\rho}_1(t^*)\hat{\Pi}_\beta) \text{Tr}(\hat{\rho}_\beta(t_{\text{fin}})\hat{\Pi}_{\text{fin}})}{\text{Tr}(\hat{\rho}_0(t_{\text{fin}})\hat{\Pi}_{\text{fin}})}, \quad (1)$$

for $\hat{\Pi}_\beta = |\beta\rangle\langle\beta|$. In Eq. (1), $\hat{\rho}_1(t^*)$ is the result of the time evolution of the initial state $\hat{\rho}_{\text{in}}$ at the time of the intermediate measurement. By considering the radiative transitions in the atomic systems standardly as a consequence of the coupling of these systems to the field of photons, we get: $\hat{\rho}_1(t^*) = e^{-\Gamma_\beta\Delta_i}|\beta\rangle\langle\beta| + |a(\Delta_i)|^2|\alpha\rangle\langle\alpha|$, where $\Delta_i = t^* - t_{\text{in}}$ and $|a(\Delta_i)| = \sqrt{1 - e^{-\Gamma_\beta\Delta_i}}$. The quantity Γ_β has the meaning of the transition rate; the quantity $\tau = 1/\Gamma_\beta$ is the lifetime of the level E_β . For the explicit calculation of the survival probability we also need the expression $\hat{\rho}_\beta(t_{\text{fin}}) = \hat{\rho}_1(t^*)/\Delta_i \rightarrow \Delta_f$, where $\Delta_f = t_{\text{fin}} - t^*$. In general, the quantity $\hat{\rho}_0(t_{\text{fin}})$ in Eq. (1) depends on the particular experimental setup. In the considered case we have $\hat{\rho}_0(t_{\text{fin}}) = \exp(-\Gamma_\beta\Delta_i)\hat{\rho}_\beta(t_{\text{fin}}) + |a(\Delta_i)|^2|\alpha\rangle\langle\alpha|$.

The postselection condition requires that the state $|\Psi_{\text{fin}}\rangle$ is obtained by measurement performed on the atomic system at the final time $t = t_{\text{fin}}$. By the choice of the particular postselection, providing that the teleological ensemble could exist, we modify the dynamics of the radiative decay. We consider the following postselection:

$$|\Psi_{\text{fin}}\rangle = \frac{|\beta\rangle + \epsilon|\alpha\rangle}{\sqrt{1 + |\epsilon|^2}}, \quad (2)$$

where ϵ is a complex parameter. By this kind of postselection, via the parameter ϵ , we can choose the desired fraction (percentage) of survived excited atoms at the final time $t = t_{\text{fin}}$, and analyze their behavior in the time $t = t^* < t_{\text{fin}}$.

Finally, for the survival probability $\mathcal{P}_S(t^*)$ we have:

$$\mathcal{P}_S(t^*) = \frac{1 + |\epsilon|^2 (e^{\Gamma_\beta\Delta_f} - 1)}{1 + |\epsilon|^2 (e^{\Gamma_\beta\Delta} - 1)}, \quad (3)$$

where $\Delta = t_{\text{fin}} - t_{\text{in}}$. To simplify the presentation of our results, we express the parameter ϵ in terms of the final survival probability \mathcal{P}_{Sf} , namely we take that $\mathcal{P}_S(t_{\text{fin}}) = \mathcal{P}_{\text{Sf}}$; from this we get $|\epsilon| = \sqrt{(1/\mathcal{P}_{\text{Sf}} - 1) / (e^{\Gamma_\beta\Delta} - 1)}$.

3. EFFECTIVE LIFETIME

We define the effective decay rate $\Gamma_{\text{eff}}(t)$ by the following relation: $\Gamma_{\text{eff}}(t) = -[d\mathcal{P}_S(t)/dt]/\mathcal{P}_S(t)$; the effective lifetime can be introduced as $\tau_{\text{eff}}(t) = 1/\Gamma_{\text{eff}}(t)$. The quantity $\tau_{\text{eff}}(t)$ can be obtained in the analytic form; namely, for the survival probability given by Eq. (3), we get

$$\tau_{\text{eff}} = \tau \left[1 + e^{t/\tau} \frac{\mathcal{P}_{Sf} - \mathcal{P}_{Sf}^{(0)}}{1 - \mathcal{P}_{Sf}} \right]. \quad (4)$$

The effective lifetime can be easily controlled by choosing the \mathcal{P}_{Sf} by the appropriate postselection condition; also, the effective lifetime depends on the time of postselection t_{fin} via the probability $\mathcal{P}_{Sf}^{(0)} = \mathcal{P}_S^{(0)}(t_{\text{fin}})$.

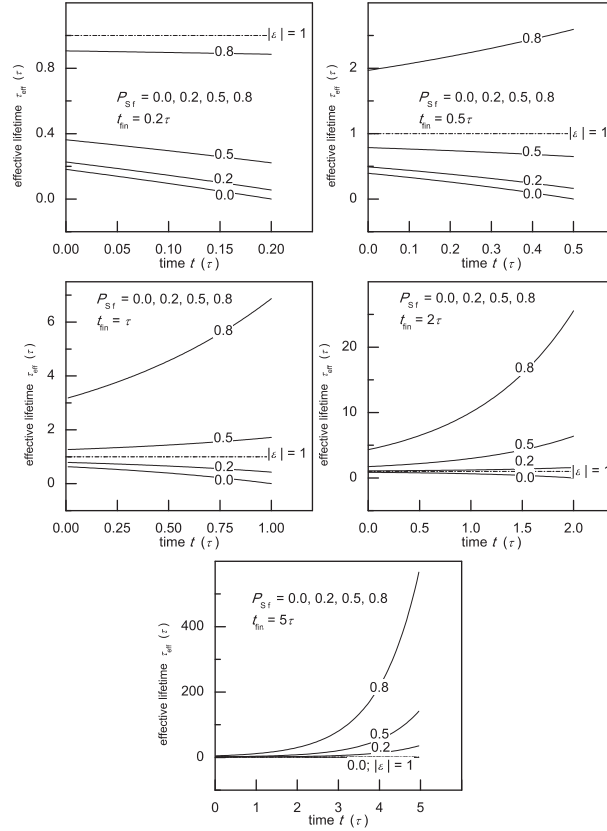


Figure 1. Effective lifetimes τ_{eff} .

In Fig. 1 we present the quantity $\tau_{\text{eff}}(t)$ obtained from Eq. (4) for the hydrogen atom postselected at different final times t_{fin} . For a given

final time, the effective lifetimes are considered for the atomic system post-selected for $\mathcal{P}_{\text{Sf}} = 0.2, 0.5$ and 0.8 , as well as for $\mathcal{P}_{\text{Sf}} = 0$, and for "natural postselection" $\mathcal{P}_{\text{Sf}} = \mathcal{P}_{\text{Sf}}^{(0)}$, i.e., for $|\epsilon| = 1$. For $\mathcal{P}_{\text{Sf}} = 1$, $\tau_{\text{eff}} = \infty$. For the natural postselection $\tau_{\text{eff}}(t) = \tau$; in other cases, the quantity $\tau_{\text{eff}}(t)$ could be less or greater than τ depending on the postselection and the final time. This circumstance can be interpreted as acceleration and attenuation of the decay, respectively, due to the postselection.

This conclusion could be of importance for the spectroscopy. That is, if the measurement of the spectral line is performed in the postselected atomic system such that $\tau_{\text{eff}} > \tau$, which is the case for $\mathcal{P}_{\text{Sf}} > \mathcal{P}_{\text{Sf}}^{(0)} = \exp(-t_{\text{fin}}/\tau)$, we could obtain more precise values of the atomic energies than in the absence of postselection, since the line width $\Gamma_{\text{eff}} < \Gamma_{\beta}$. Also, the same effect potentially allows to gain better monochromaticity of radiation, by collecting only those photons which originate from the postselected atoms. Detailed analysis of these applications requires an additional work.

Acknowledgements This work was supported in part by the Ministry of Education, Science and Technological Development, Republic of Serbia (Project 171016).

REFERENCES

- [1] Y. Aharonov, P. G Bergmann and J. L. Lebowitz, Phys. Rev. 134, B1410 (1964).
- [2] Y. Aharonov and L. Vaidman, J. Phys. A: Math. Gen. 24, 2315 (1991).
- [3] Y. Aharonov and L. Vaidman *The Two-State Vector Formalism: An Updated Review*, in: Time in Quantum Mechanics, Lect. Notes Phys. 734, edited by J.G. Muga, R. Sala Mayato and I.L. Egusquiza (Springer, Berlin Heidelberg, 2008).
- [4] N. N. Nedeljković and M. D. Majkić, Phys. Rev. A 76, 042902 (2007).
- [5] L. Vaidman, Phys. Rev A 87, 052104 (2013).
- [6] O. Hosten and P. Kwiat, Science 319, 787 (2008).
- [7] J. S. Lundeen, B. Sutherland, A. Patel, C. Stewart and C. Bamber, Nature 474, 188 (2011).
- [8] S. Kocsis, B. Braverman, S. Ravets, M. J. Stevens, R. P. Mirin, L. K. Shalm and A. M. Steinberg, Science 332, 1170 (2011)

POPULATION DYNAMICS OF THE SVI, CIVII AND ArVIII IONS IN THE GRAZING INCIDENCE ON SOLID SURFACE

M. D Majkić, S. M. D. Galijaš, I. P. Prlina and N. N. Nedeljković

University of Belgrade, Faculty of Physics, P.O.Box 368, Belgrade, Serbia

Abstract. We apply the two-state vector model recently adapted to the grazing incidence geometry to investigate the population dynamics of the SVI, CIVII and ArVIII ions interacting with solid surface. We calculate the corresponding intermediate population probabilities and rates, as well as the neutralization distances. The effect of the ionic core polarization is demonstrated: the magnitude of the population probability maxima increases and the neutralization distances decrease in respect to the point-like ionic core case. The population probabilities for the grazing incidence are shifted toward the smaller ion-surface distances compared to the escaping geometry.

1. INTRODUCTION

Recently, the population dynamics of the multiply charged ions ArVIII, KrVIII and XeVIII impinging the conducting solid surface in the grazing incidence geometry has been analyzed within the framework of the two-state vector model (TVM) [1, 2]. The effective modification of the Fermi-Dirac distribution of the electron momenta in solid due to the parallel ionic velocity v_{\parallel} has been taken into account. The results have been used to produce a complete quantum explanation of the classical trajectory of these ions during the cascade neutralization in the interaction with the solid surface. The ions ArVIII, KrVIII and XeVIII have the same ionic core charge $Z = 8$; their difference originated from different polarization of their cores.

In the present article we use the TVM to investigate the population of the Rydberg states of the SVI, CIVII and ArVIII ions under the grazing incidence. The intermediate population probabilities for these ions are known only for the ions escaping solid surfaces in the perpendicular direction [3], for small velocities $v = v_{\perp} \ll 1$ a.u. The ions SVI, CIVII and ArVIII have different core charges $Z = 6, 7$ and 8 , and different core polarizations. The effect of the parallel velocity, observed for the ions ArVIII, KrVIII and XeVIII is also expected for the ions SVI and CIVII.

2. POPULATION PROCESS IN THE SCATTERING GEOMETRY

The TVM is the time-symmetrized quantum model of the postselected systems: characteristic feature is the use of the two state vectors for describing the state of a single active electron. In the process of population of the Rydberg states of the considered ions, the first state vector evolves from the given initial state (electron in solid in the kinematically modified state μ'_M at the time $t = t_{in}$) toward the future. Simultaneously, the second state vector evolves toward the given final state (electron captured by the ion in a given ionic state $\nu_A = (n_A, l_A, m_A)$). The TVM population probabilities for the grazing geometry and for the ions escaping the surface perpendicularly are based on the same general expressions; however, the parallel velocity has a nontrivial effect [1, 2]. Within the framework of the TVM the intermediate population probability $P_{\nu_A}(t)$ is defined for the electron capture by the ion at the time t , when the ion is at the distance $R = R(t)$. The possibility that the captured electron can be recaptured by the solid is taken into account.

The basic physical quantity of our TVM is the so called mixed flux $I_{\mu'_M, \nu_A}$ [1, 4]. Using the mixed flux, we directly calculate the intermediate transition probability per unit energy parameter γ'_M at the time t

$$T_{\mu'_M, \nu_A}(t) = \left| \int_{t_{in}}^t I_{\mu'_M, \nu_A}(t') dt' \right|^2, \quad (1)$$

and the corresponding (velocity dependent) transition probability $T_{\nu_A}(t)$. We note that the energies $E'_M = -\gamma'^2_M/2$ are shifted due to the parallel velocity $v_{\parallel} \neq 0$. This shift can be calculated by applying the necessary Galilean transformations. Finally, we get the neutralization and population probabilities, which can be expressed as

$$P_{\nu_A}(t) = 1 - \exp[-T_{\nu_A}(t)]. \quad (2)$$

3. RESULTS

In Fig. 1 we present the population probabilities of the ions SVI, CIVII and ArVIII, for the polarized ionic cores and in the absence of core polarization (thick- and thin-solid curves, respectively). In the same figure we also present the corresponding rates $\Gamma_{\nu_A} = dP_{\nu_A}(t)/dt$. The population probabilities with polarized cores are positioned closer to the surface in comparison to the same quantities obtained in the point-like core approximation; the same effect has been observed in the case of normal escaping geometry in Ref. [3]. Population probabilities exhibit maxima at the distance $R = R_{max}$. The decrease of these probabilities closer to the surface is a consequence of the reionization process (electron recapture by the solid).

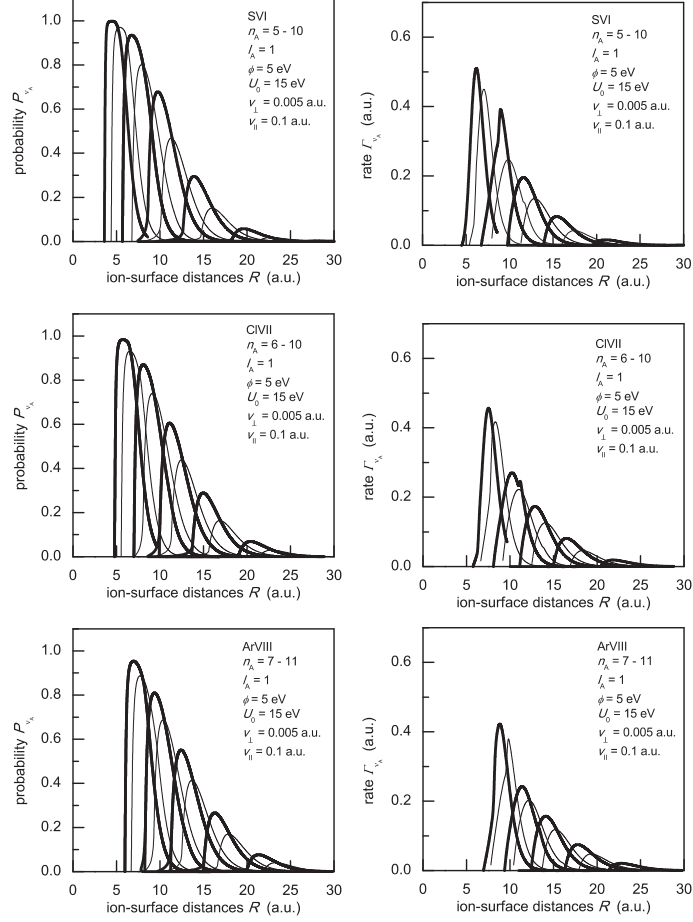


Figure 1. Population and neutralization probabilities and rates.

Neutralization distances R_c^N represent the position of maxima of the population rates Γ_{ν_A} ; these distances can be considered as distances at which the population process is mainly localized.

In Fig. 2 we present the neutralization distances R_c^N of the considered ions (obtained from the population rates) as a function of principal quantum number n_A (thick-solid curves), and compare the results with those obtained in Ref. [3] for the normal escaping geometry (dashed curves). The neutralization distances in the point-like case are presented by thin-solid curves. We see that the neutralization distances corresponding to the same ion and the same quantum state obtained in the present article in the case of grazing geometry are smaller in comparison to normal escaping geometry case. This means that the effect of the parallel velocity shifted the process

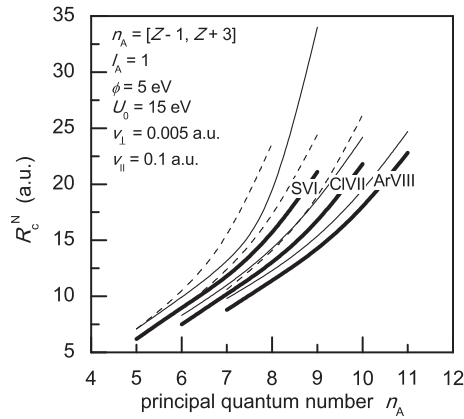


Figure 2. Neutralization distances R_c^N .

closer to the surface. This effect is more pronounced for greater quantum numbers.

From Fig. 2 we also recognize that the neutralization distances for polarized cores are smaller than in the case of point-like core approximation.

Acknowledgements This work was supported in part by the Ministry of Education, Science and Technological Development, Republic of Serbia (Project 171016).

REFERENCES

- [1] N. N. Nedeljković, M. D. Majkić and S. M. D. Galijaš, *J. Phys. B: At. Mol. Opt. Phys.* 45, 215202 (2012)
- [2] M. D. Majkić, N. N. Nedeljković and S. M. D. Galijaš, *J. Phys: Conf. Series* 399, 012009 (2012)
- [3] N. N. Nedeljković, M. D. Majkić, S. M. D. Galijaš and S. B. Mitrović, *App. Surf. Sci.* 254, 7000 (2008)
- [4] N. N. Nedeljković and M. D. Majkić, *Phys. Rev. A* 76, 042902 (2007).

POPULATION OF THE RYDBERG STATES OF THE ArVIII, KrVIII AND XeVIII IONS AT SOLID SURFACE FOR GRAZING INCIDENCE

S. M. D. Galijaš, N. N. Nedeljković, M. D. Majkić and I. P. Prlina

University of Belgrade, Faculty of Physics, P. O. Box 368, Belgrade, Serbia

Abstract. We consider the ArVIII, KrVIII and XeVIII ions interacting with solid surface in the grazing incidence geometry. We analyze the effect of the polarization of ionic core and the parallel velocity effect on the intermediate stages of the population process. Within the framework of the two-state vector model, it is demonstrated that the increase of the ionic polarization induces an increase of the population probability maxima and the population process is shifted to the smaller ion-surface distances. With increase of the projectile velocity, the population maxima increase and the region of the most effective population process becomes closer to the surface.

1. INTRODUCTION

Recently, we have analyzed the population of the Rydberg states of multiply charged ions ArVIII, KrVIII, and XeVIII, escaping solid surfaces in the normal direction, at low velocity [1] and for $v \approx 1$ a.u. [2]. For description of the process we developed the appropriate two-state vector model (TVM). The similar analysis can be performed for the scattering geometry, by taking into account the effective modification ($\vec{k} \rightarrow \vec{k}'$) of the angle averaged Fermi-Dirac distribution $\langle f \rangle_{\Omega_{\vec{k}}}$ of the electron momenta \vec{k} in the solid due to the ionic motion component parallel to the surface with velocity $v = v_{||}$ [3,4].

In the present article, we examine the multiply charged ions ArVIII, KrVIII and XeVIII in the scattering geometry under the grazing incidence within the framework of the TVM. The aim of the present analysis is to elucidate the role of the ionic core polarization on the intermediate stages of the population process in the considered geometry; namely, by taking into account the ionic core polarization, the ions with the same core charges will have different population histories. Within the framework of the TVM the process is defined under the teleological conditions, i.e., the state of a single active electron is described by two state vectors $|\Psi_1(t)\rangle$ and $|\Psi_2(t)\rangle$

evolving from the initial time toward the future and from the final time toward the past, respectively [1,2,4].

2. POPULATION DYNAMICS IN THE TVM

We consider the TVM electron exchange probabilities under the grazing geometrical conditions and for fixed initial and final electronic states. These states are determined by the parabolic quantum numbers $\mu_M = (\gamma_M, n_{1M}, m_M)$ and the spherical quantum numbers $\nu_A = (\gamma_A, n_{1A}, m_A)$, where γ_M and $\gamma_A(R)$ are the corresponding continuous and discrete energy parameters, respectively, of the electron in the solid and bounded to the ion at ion-surface distance R .

We calculate the intermediate transition probability density $T_{\mu'_M, \nu_A}(t)$ for kinematically shifted initial quantum numbers μ'_M , the velocity dependent intermediate transition probability

$$T_{\nu_A} = T_{\nu_A}^{(0)} \langle f \rangle_{\Omega_{\vec{k}}}, f_{\gamma}(\gamma'_M) \frac{v_{\perp} [\gamma'_M + \gamma_A(R)]^2}{\gamma'_M \tilde{\beta}} \left(1 + \frac{2\tilde{\alpha}}{\tilde{\beta}} \frac{1}{R} \right) R^{2\tilde{\alpha}} e^{-2\tilde{\beta}R}, \quad (1)$$

where $\gamma'_M = \gamma_A(R)$, and the corresponding population probability P_{ν_A} [4]. In (1) we have $\tilde{\alpha} = Z/\tilde{\gamma}_A - 1/2 + 1/4\gamma'_M$ and $\tilde{\beta} = \gamma'_M + (\tilde{\gamma}_A - \gamma'_M)g$, where $g = 1/2$ and $\tilde{\gamma}_A$ is the ionic energy parameter for the polarized core. The quantity $T_{\nu_A}^{(0)}$ is independent of γ'_M and R , and

$$f_{\gamma}(\gamma'_M) = 2^{\frac{1}{\gamma'_M}} \gamma'_M \frac{1}{\gamma'_M} + 1 (2e)^{\frac{1}{2\gamma'_M}} (3/4)^{\frac{2Zv^2}{\gamma'_M(\gamma'^2_M + v^2_{\perp})}}. \quad (2)$$

Polarization of the electron-cloud of the ionic core has been effectively taken into account by means of the Simons-Bloch potential [5].

3. RESULTS

The intermediate transition probability $T_{\nu_A}(t)$ given by (1), as well as the population probability $P_{\nu_A}(t)$, are peak-shaped, with maximum $P_{\nu_A}^{\max}$ at $R = R_{\max}$. The neutralization distances $R_c^N > R_{\max}$ (positions of maxima of the positive mode of the population rates $\Gamma_{\nu_A} = dP_{\nu_A}/dt$) can be considered as ion-surface distances at which the process is mainly localized.

In Figure 1 we present the population maxima $P_{\nu_A}^{\max}$ via parallel ionic velocity v_{\parallel} , for the ions ArVIII, KrVIII and XeVIII. An interesting rule can be recognized from the figure: population maxima for n_A , $n_A + 1$ and $n_A + 2$ of the ions ArVIII, KrVIII and XeVIII behave similarly. For a given n_A , with increase of the core polarization (ArVIII \rightarrow KrVIII \rightarrow XeVIII) population maxima increase; the quantities $P_{\nu_A}^{\max}$ for a given ion increase with increasing of the parallel projectile velocity v_{\parallel} .

In Figure 2 we present the neutralization distances via parallel ionic velocity for the population of the Rydberg states $n_A = 8 - 16$ of the ions

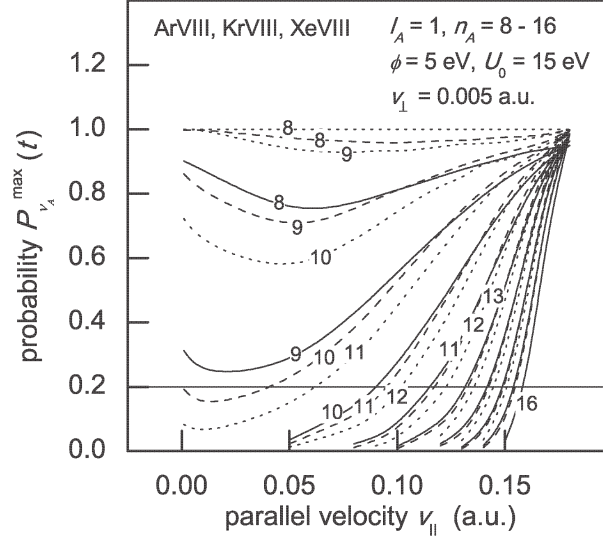


Figure 1. The population maxima $P_{\nu_A}^{\max}$ via parallel ionic velocity $v_{||}$, for the ions ArVIII, KrVIII and XeVIII, full, dashed and dotted curves, respectively.

ArVIII, KrVIII and XeVIII. With increase of the polarization of the ionic core and the increase of parallel ionic velocity we see a decrease of the neutralization distances R_c^N for population of the Rydberg state with a given n_A .

In Figure 2 we also present (by open circles) the minimal velocities necessary for population of the considered Rydberg state. For the parallel velocities smaller than this value the corresponding population probability is less than 0.2, see also Figure 1. Some of the Rydberg levels could be populated at each velocity; the neutralization distances for these states are independent of the projectile velocities. Polarization effect induces an increase of the probability maxima so that the minimal velocities decrease: for example, the Rydberg state $n_A = 10$ of the XeVIII can be populated at all velocities, the the population of the same Rydberg state of the ion KrVIII is possible only for $v_{||} > 0.04$ a.u., and for ArVIII only for $v_{||} > 0.09$ a.u.

The recognized influence of the core polarization (by which the ions Ar^{Z+} , Kr^{Z+} and Xe^{Z+} of the same Z are distinguished) on the position and magnitude of the population process, together with the parallel velocity effects on these intermediate characteristics of the process, introduces interesting new elements in the understanding of some ion-surface interactions phenomena. At present, these effects can be tested only indirectly, by comparing the measured kinetic energy gain due to the image acceleration of the ions with the corresponding quantity calculated using the TVM

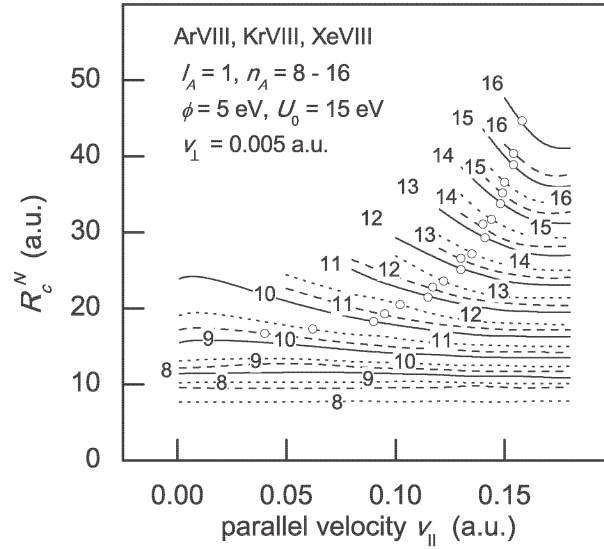


Figure 2. The neutralization distances R_c^N via parallel ionic velocity $v_{||}$, for the ions ArVIII, KrVIII and XeVIII, full, dashed and dotted curves, respectively.

results.

Acknowledgment This work was supported in part by the Ministry of Education and Science, Republic of Serbia (Project 171016).

REFERENCES

- [1] N. N. Nedeljković and M. D. Majkić, Phys. Rev. A 76, 042902 (2007).
- [2] S. M. D. Galijaš, N. N. Nedeljković and M. D. Majkić, Surf. Sci. 605, 723 (2011).
- [3] R. Zimny, Z. L. Mišković, N. N. Nedeljković and Lj. D. Nedeljković, Surf. Sci. 255, 135 (1991).
- [4] N. N. Nedeljković, M. D. Majkić, S. M. D. Galijaš and M. A. Mirković, this conference (2012).
- [5] G. Simons and A. N. Bloch, Phys. Rev. B 7, 2754 (1973).

BROWN UNIVERSITY

DOCTORAL THESIS

**Landau Singularities in Planar Massless
Theories**

Author:

Igor PRLINA

Supervisor:

Dr. Marcus SPRADLIN

*A thesis submitted in fulfillment of the requirements
for the degree of Doctor of Philosophy*

in the

High Energy Theory Group

Department of Physics

May 1, 2019

Declaration of Authorship

I, Igor PRLINA, declare that this thesis titled, “Landau Singularities in Planar Massless Theories” and the work presented in it are my own. I confirm that:

- This work was done wholly or mainly while in candidature for a research degree at this University.
- Where any part of this thesis has previously been submitted for a degree or any other qualification at this University or any other institution, this has been clearly stated.
- Where I have consulted the published work of others, this is always clearly attributed.
- Where I have quoted from the work of others, the source is always given. With the exception of such quotations, this thesis is entirely my own work.
- I have acknowledged all main sources of help.
- Where the thesis is based on work done by myself jointly with others, I have made clear exactly what was done by others and what I have contributed myself.

Signed:

Date:

BROWN UNIVERSITY

Abstract

Department of Physics

Doctor of Philosophy

Landau Singularities in Planar Massless Theories

by Igor PRLINA

In this work we present our contribution to the method of using Landau singularities for probing scattering amplitudes in planar massless quantum field theories. We start by proposing a simple geometric algorithm for determining the complete set of branch points of amplitudes in planar $\mathcal{N} = 4$ super-Yang-Mills theory directly from the amplituhedron, without resorting to any particular representation in terms of local Feynman integrals. This represents a step towards translating integrands directly into integrals. In particular, the algorithm provides information about the symbol alphabets of general amplitudes. First we illustrate the algorithm applied to the one- and two-loop MHV amplitudes. Then we demonstrate how to use the recent reformulation of amplituhedra in terms of ‘sign flips’ in order to streamline the application of this algorithm to amplitudes of any helicity. In this way we recover the known branch points of all one-loop amplitudes, and we find an ‘emergent positivity’ on boundaries of amplituhedra. Lastly, we look beyond planar $\mathcal{N} = 4$ super-Yang-Mills theory, and analyze Landau singularities of general massless planar theories. In massless quantum field theories the Landau equations are invariant under graph operations familiar from the theory of electrical circuits. Using a theorem on the Y - Δ reducibility of planar circuits we prove that the set of first-type Landau singularities of an n -particle scattering amplitude in any massless planar theory, in any spacetime dimension D , at any finite loop order in perturbation theory, is a subset of those of a certain n -particle $\lfloor (n-2)^2/4 \rfloor$ -loop “ziggurat” graph. We determine this singularity locus explicitly for $D = 4$ and $n = 6$ and find that it corresponds precisely to the vanishing of the symbol letters familiar from the hexagon bootstrap in SYM theory. Further implications for SYM theory are discussed.

Acknowledgements

I primarily want to thank my collaborators, Tristan Dennen, James Stankowicz, Stefan Stanojevic, Marcus Spradlin and Anastasia Volovich. I am also grateful to Nima Arkani-Hamed for helpful discussions as well as to my fellow graduate students in HET/Ph for useful conversations.

Contents

Declaration of Authorship	iii
Abstract	vi
Acknowledgements	vii
1 Introduction	1
2 Landau Singularities from the Amplituhedron	7
2.1 Introduction	7
2.1.1 Momentum Twistors	7
2.1.2 Positivity and the MHV Amplituhedron	8
2.1.3 Landau Singularities	10
2.2 Eliminating Spurious Singularities of MHV Amplitudes	12
2.2.1 The Spurious Pentagon Singularity	14
2.2.2 The Spurious Three-Mass Box Singularity	16
2.2.3 A Two-Loop Example	17
2.2.4 Summary	19
2.3 An Amplituhedrony Approach	20
2.3.1 One-Loop MHV Amplitudes	22
2.3.2 Two-Loop MHV Amplitudes: Configurations of Positive Lines	23
2.3.3 Two-Loop MHV Amplitudes: Landau Singularities	32
2.4 Discussion	37
2.5 Elimination of Bubbles and Triangles	41
2.5.1 Bubble sub-diagrams	41

2.5.2	Triangle sub-diagrams	42
3	All-Helicity Symbol Alphabets from Unwound Amplituhedra	43
3.1	Review	43
3.1.1	The Kinematic Domain	43
3.1.2	Amplituhedra ...	45
3.1.3	... and their Boundaries	47
3.1.4	The Landau Equations	47
3.1.5	Summary: The Algorithm	50
3.2	One-Loop Branches	51
3.3	One-Loop Boundaries	57
3.3.1	A Criterion for Establishing Absent Branches	57
3.3.2	MHV Lower Bounds	59
3.3.3	NMHV Lower Bounds	60
3.3.4	N ² MHV Lower Bounds	63
3.3.5	Emergent Positivity	65
3.3.6	Parity and Upper Bounds	65
3.3.7	Increasing Helicity	66
3.4	The Hierarchy of One-Loop Boundaries	69
3.4.1	A Graphical Notation for Low-helicity Boundaries	69
3.4.2	A Graphical Recursion for Generating Low-helicity Boundaries	71
3.5	Solving Landau Equations in Momentum Twistor Space	77
3.6	Singularities and Symbology	80
3.7	Conclusion	83
4	All-loop singularities of scattering amplitudes in massless planar theories	85
4.1	Landau Graphs and Singularities	85
4.2	Elementary Circuit Operations	87
4.3	Reduction of Planar Graphs	90
4.4	Landau Analysis of the Wheel	92

4.5	Second-Type Singularities	94
4.6	Planar SYM Theory	95
4.7	Symbol Alphabets	96
4.8	Conclusion	97
	Bibliography	99

List of Figures

2.1	Three examples of cuts on which MHV amplitudes have no support; these appeared as spurious singularities in the Landau equation analysis of [16] since scalar pentagon and double pentagon integrals do have these cuts.	14
2.2	(a) A maximum codimension boundary of the one-loop MHV amplitude-dron. The circle is a schematic depiction of the n line segments $(12), (23), \dots, (n1)$ connecting the n cyclically ordered external kinematic points $Z_i \in G_+(4, n)$ and the red line shows the loop momentum $\mathcal{L} = (ij)$. (b) The corresponding Landau diagram, which is a graphical depiction of the four cut conditions (2.30) that are satisfied on this boundary.	21
2.3	(a) A maximum codimension boundary of the two-loop MHV amplitude-dron. (b) The corresponding Landau diagram (which, it should be noted, does not have the form of a standard Feynman integral) depicting the nine cut conditions (2.34)–(2.36) that are satisfied on this boundary.	24
2.4	Three different invalid relaxations of the maximal codimension boundary shown in figure 2.3.	26
2.5	Two valid double relaxations of figure 2.3. The other two possibilities are obtained by taking $i \rightarrow i+1$ in (a) or $\mathcal{L}^{(2)} \rightarrow \mathcal{L}^{(1)}$ and $j \leftrightarrow k$ in (b).	28
2.6	The Landau diagrams showing the seven cut conditions satisfied by figures 2.5a and 2.5b, respectively.	33

2.7 Landau diagrams corresponding to all of the cut conditions (2.34)–(2.36) except for (a) $\langle \mathcal{L}^{(1)} i-1 i \rangle = 0$, and (b) $\langle \mathcal{L}^{(2)} i i+1 \rangle = 0$. These are the only two cut conditions that are redundant (each is implied by the other eight, for generic kinematics) and, when omitted, lead to Landau diagrams that have the form of a standard Feynman integral. (In both figures $\mathcal{L}^{(1)}$ is the momentum in the right loop and $\mathcal{L}^{(2)}$ is the momentum in the left loop.) . 36

3.1 Explicit twistor solution diagrams. 70

3.2 One-loop maximal codimension graph flow. 72

3.3 Graph operation on momentum twistor diagrams. 74

3.4 Removing graph operation on momentum twistor diagrams. 75

3.5 Un-pinning graph operation on momentum twistor diagrams. 76

4.1 Elementary circuit moves that preserve solution sets of the massless Landau equations: (a) series reduction, (b) parallel reduction, and (c) Y - Δ reduction. 88

4.2 The four-, six-, five- and seven-terminal ziggurat graphs. The open circles are terminals and the filled circles are vertices. The pattern continues in the obvious way, but note an essential difference between ziggurat graphs with an even or odd number of terminals in that only the latter have a terminal of degree three. 89

4.3 The six-terminal ziggurat graph can be reduced to a three loop graph by a sequence of three Y - Δ reductions and one FP assignment. In each case the vertex, edge, or face to be transformed is highlighted in gray. 89

4.4 The three-loop six-particle wheel graph. The leading first-type Landau singularities of this graph exhaust all possible first-type Landau singularities of six-particle amplitudes in any massless planar field theory, to any finite loop order. 93

List of Tables

3.1 One-loop Landau diagrams, branches, twistor diagrams, and loci.	56
---	----

The work before you is a culmination of decades of high-quality education I was blessed with. I dedicate this thesis to all my teachers who have selflessly worked on developing me intellectually. From my elementary school teacher, to my thesis advisor, I am indebted to them all. My greatest debt is to my parents, for teaching me both my first and most important lessons in life.

Chapter 1

Introduction

Ever since its conception, the Feynman diagram approach has been the standard paradigm for perturbative calculations in quantum field theory. While the method can, in principle, be used at any order in perturbation theory, the calculations get more and more demanding at each new loop order. Alternately one can seek hidden symmetries and new underlying principles which motivate new calculational approaches where the most basic features of Feynman diagrams, such as unitarity and locality, are emergent instead of manifest. Recent years have seen tremendous success in “reverse engineering” such new symmetries and principles from properties of scattering amplitudes. This approach has been particularly fruitful in simple quantum field theories such as the planar maximally supersymmetric $\mathcal{N} = 4$ super-Yang-Mills (SYM) theory [1].

In particular, it has been realized that the unitarity and locality of the integrands [2] of loop-level amplitudes in SYM theory can be seen to emerge from a very simple geometric principle of positivity [3]. Moreover, it has been proposed that all information about arbitrary integrands in this theory is encapsulated in objects called amplituhedra [4, 5] that have received considerable recent attention; see for example [6, 7, 8, 9, 10, 11, 12, 13]. Unfortunately, there remains a huge gap between our understanding of integrands and our understanding of the corresponding integrated amplitudes. Despite great advances in recent years we of course don’t have a magic wand that can be waved at a general integrand to “do the integrals”. Indeed, modern approaches to computing multi-loop amplitudes in SYM theory, such as the amplitude bootstrap [14, 15] even eschew knowledge of the integrand completely. It would be enormously valuable to close

this gap between our understanding of integrands and amplitudes.

Physical principles impose strong constraints on the scattering amplitudes of elementary particles. For example, when working at finite order in perturbation theory, unitarity and locality appear to constrain amplitudes to be holomorphic functions with poles and branch points at precisely specified locations in the space of complexified kinematic data describing the configuration of particles. Indeed, it has been a long-standing goal to understand how to use the tightly prescribed analytic structure of scattering amplitudes to determine them directly, without relying on traditional (and, often computationally complex) Feynman diagram techniques.

The connection between the physical and mathematical structure of scattering amplitudes has been especially well studied in planar $\mathcal{N} = 4$ super-Yang–Mills [1] SYM¹ theory in four spacetime dimensions, where the analytic structure of amplitudes is especially tame. One of the overall aims of this work, its predecessors [16, 17], and its descendant(s), is to ask a question that might be hopeless in another, less beautiful quantum field theory: can we understand the branch cut structure of general scattering amplitudes in SYM theory?

The motivation for asking this question is two-fold. The first is the expectation that the rich mathematical structure that underlies the integrands of SYM theory (the rational $4L$ -forms that arise from summing L -loop Feynman diagrams, prior to integrating over loop momenta) is reflected in the corresponding scattering amplitudes. For example, it has been observed that both integrands [3] and amplitudes [18, 15, 19] are deeply connected to the mathematics of cluster algebras.

Second, on a more practical level, knowledge of the branch cut structure of amplitudes is the key ingredient in the amplitude bootstrap program, which represents the current state of the art for high loop order amplitude calculations in SYM theory. In particular the hexagon bootstrap (see for example [14]), which has succeeded in computing all six-particle amplitudes through five loops [20], is predicated on the hypothesis that at any loop order, these amplitudes can have branch points only on 9 specific loci in the

¹We use “SYM” to mean the planar limit, unless otherwise specified.

space of external data. Similarly the heptagon bootstrap [21], which has revealed the symbols of the seven-particle four-loop MHV and three-loop NMHV amplitudes [22], assumes 42 particular branch points. One result we hope follows from understanding the branch cut structure of general amplitudes in SYM theory is a proof of this counting to all loop order for six- and seven-particle amplitudes.

As a step in that direction, and motivated by [23], a systematic exploration of how integrands encode the singularities of integrated amplitudes, in particular their branch points, has been performed in [16]. Scattering amplitudes in quantum field theory generally have very complicated discontinuity structure. The discontinuities across branch cuts are given by sums of unitarity cuts [24, 25, 26, 27, 28, 29]. These discontinuities may appear on the physical sheet or after analytic continuation to other sheets; these higher discontinuities are captured by multiple unitarity cuts (see for example [30, 31]). A long-standing goal of the S-matrix program, in both its original and modern incarnations, has been to construct expressions for the scattering amplitudes of a quantum field theory based solely only on a few physical principles and a thorough knowledge of their analytic structure. In [16] the branch cut structure of one- and two-loop MHV amplitudes in SYM theory starting from certain representations of their integrands in terms of local Feynman integrals [32] has been studied. In [16] all of their known branch points have been found, but many other, spurious branch points that are artifacts of the particular representations used, were also encountered. Indeed, the analysis of [16] was completely insensitive to numerator factors in the integrand, but the numerators are really where all of the action is—in any standard quantum field theory the denominator of a loop integrand is a product of local propagators; the numerator is where all of the magic lies.

One of the goals in this work is to improve greatly on the analysis of [16]. We do this by presenting a method for asking the amplituhedron to directly provide a list of the physical branch points of a given amplitude.

It is a general property of quantum field theory (see for example [27, 33]) that the locations of singularities of an amplitude can be determined from knowledge of the

poles of its integrand by solving the Landau equations [26]. Constructing explicit representations for integrands can be a challenging problem in general, but in SYM theory this can be side-stepped by using various on-shell methods [28, 34, 35, 36] to efficiently determine the locations of integrand poles. This problem is beautifully geometrized by amplituhedra [4], which are spaces encoding representations of integrands in such a way that the boundaries of an amplituhedron correspond precisely to the poles of the corresponding integrand. Therefore, as pointed out in [17], the Landau equations can be interpreted as defining a map that associates to any boundary of an amplituhedron the locus in the space of external data where the corresponding amplitude has a singularity.

Only MHV amplitudes were considered in [17]. In this paper we also show how to extend the analysis to amplitudes of arbitrary helicity. This is greatly aided by a recent combinatorial reformulation of amplituhedra in terms of “sign flips” [37]. As a specific application of our algorithm we classify the branch points of all one-loop amplitudes in SYM theory. Although the singularity structure of these amplitudes is of course well-understood (see for example [38, 39, 40, 41, 42, 43, 44, 45, 46]), this exercise serves a useful purpose in preparing a powerful toolbox for the sequel [47] to this paper where we will see that boundaries of one-loop amplituhedra are the basic building blocks at all loop order. In particular we find a surprising ‘emergent positivity’ on boundaries of one-loop amplituhedra that allows boundaries to be efficiently mapped between different helicity sectors, and recycled to higher loop levels.

While we have found an efficient method to obtain non-spurious singularities in planar $\mathcal{N} = 4$ super-Yang-Mills (SYM) theory, we have also analyzed the potential singularity structure of an arbitrary planar massless theory. For over half a century much has been learned from the study of singularities of scattering amplitudes in quantum field theory, an important class of which are encoded in the Landau equations [26]. This work combines two simple statements to arrive at a general result about such singularities. The first is based on the analogy between Feynman diagrams and electrical circuits, which also has been long appreciated and exploited; see for example [48, 49, 50] and chapter 18 of [51]. Here we use the fact that in *massless* field theories, the sets

of solutions to the Landau equations are invariant under the elementary graph operations familiar from circuit theory, including in particular the Y - Δ transformation which replaces a triangle subgraph with a tri-valent vertex, or vice versa. The second is a theorem of Gitler [52], who proved that any *planar* graph (of the type relevant to the analysis of Landau equations, specified below) can be Y - Δ reduced to a class we call *ziggurats*.

We conclude that the n -particle $\lfloor (n-2)^2/4 \rfloor$ -loop ziggurat graph encodes all possible first-type Landau singularities of any n -particle amplitude at any finite loop order in any massless planar theory. Although this result applies much more generally, our original motivation arose from related work [16, 17, 53, 47] on planar $\mathcal{N} = 4$ supersymmetric Yang-Mills (SYM) theory, for which our result has several interesting implications.

This work is organized as follows. In 2 we apply the Amplituhedron to directly obtain non-spurious singularities of MHV amplitudes, and we explicitly conduct the procedure at one and two loops [17]. In 3 we generalize the procedure to non MHV amplitudes and present the procedure at the one loop example [53]. Finally, in 4 we describe a method for finding all-loop singularities in general planar massless theories [54].

Chapter 2

Landau Singularities from the Amplituhedron

2.1 Introduction

2.1.1 Momentum Twistors

We begin by reviewing the basics of momentum twistor notation [55], which we use throughout our calculations. Momentum twistors are based on the correspondence between null rays in (complexified, compactified) Minkowski space and points in twistor space (\mathbb{P}^3), or equivalently, between complex lines in \mathbb{P}^3 and points in Minkowski space. We use Z_a, Z_b , etc. to denote points in \mathbb{P}^3 , which may be represented using four-component homogeneous coordinates $Z_a^I = (Z_a^1, Z_a^2, Z_a^3, Z_a^4)$ subject to the identification $Z_a^I \sim tZ_a^I$ for any non-zero complex number t . We use (ab) as shorthand for the bitwistor $\epsilon_{IJKL}Z_a^KZ_b^L$. Geometrically, we can think of (ab) as the (oriented) line containing the points Z_a and Z_b . Similarly we use (abc) as shorthand for $\epsilon_{IJKL}Z_a^IZ_b^KZ_c^L$, which represents the (oriented) plane containing Z_a, Z_b and Z_c . Analogously, $(abc) \cap (def)$ stands for $\epsilon^{IJKL}(abc)_K(def)_L$, which represents the line where the two indicated planes intersect. In planar SYM theory we always focus on color-ordered partial amplitudes so an n -point amplitude is characterized by a set of n momentum twistors $Z_i^I, i \in \{1, \dots, n\}$ with a specified cyclic ordering. Thanks to this implicit cyclic ordering we can use \bar{i} as shorthand for the plane $(i-1\ i\ i+1)$, where indices are always understood to be mod n .

The natural $SL(4, \mathbb{C})$ invariant is the four-bracket denoted by

$$\langle a b c d \rangle \equiv \epsilon_{IJKL} Z_a^I Z_b^J Z_c^K Z_d^L. \quad (2.1)$$

We will often be interested in a geometric understanding of the locus where such four-brackets might vanish, which can be pictured in several ways. For example, $\langle a b c d \rangle = 0$ only if the two lines (ab) and (cd) intersect, or equivalently if the lines (ac) and (bd) intersect, or if the point a lies in the plane (bcd) , or if the point c lies on the plane (abd) , etc. Computations of four-brackets involving intersections may be simplified via the formula

$$\langle (abc) \cap (def) gh \rangle = \langle abcg \rangle \langle defh \rangle - \langle abch \rangle \langle defg \rangle. \quad (2.2)$$

In case the two planes are specified with one common point, say $f = c$, it is convenient to use the shorthand notation

$$\langle (abc) \cap (dec) gh \rangle \equiv \langle c(ab)(de)(gh) \rangle \quad (2.3)$$

which highlights the fact that this quantity is antisymmetric under exchange of any two of the three lines (ab) , (de) , and (gh) .

2.1.2 Positivity and the MHV Amplituhedron

In this paper we focus exclusively on MHV amplitudes. The integrand of an L -loop MHV amplitude is a rational function of the n momentum twistors Z_i specifying the kinematics of the n external particles, as well as of L loop momenta, each of which corresponds to some line $\mathcal{L}^{(\ell)}$ in \mathbb{P}^3 ; $\ell \in \{1, \dots, L\}$. The amplituhedron [4, 5] purports to provide a simple characterization of the integrand when the Z_i^I take values in a particular domain called the positive Grassmannian $G_+(4, n)$. In general $G_+(k, n)$ may be defined as the set of $k \times n$ matrices for which all ordered maximal minors are positive; that is, $\langle a_{i_1} \cdots a_{i_k} \rangle > 0$ whenever $i_1 < \cdots < i_k$.

Each line $\mathcal{L}^{(\ell)}$ may be characterized by specifying a pair of points $\mathcal{L}_1^{(\ell)}$, $\mathcal{L}_2^{(\ell)}$ that it passes through. We are always interested in $n \geq 4$, so the Z_i generically provide a

basis for \mathbb{C}^4 . In the MHV amplituhedron a pair of points specifying each $\mathcal{L}^{(\ell)}$ may be expressed in the Z_i basis via an element of $G_+(2, n)$ called the D -matrix:

$$\mathcal{L}_\alpha^{(\ell)I} = \sum_{i=1}^n D_{\alpha i}^{(\ell)} Z_i^I, \quad \alpha = 1, 2. \quad (2.4)$$

For $n > 4$ the Z_i are generically overcomplete, so the map eq. (2.4) is many-to-one.

The L -loop n -point MHV amplituhedron is a $4L$ -dimensional subspace of the $2L(n - 2)$ -dimensional space of L D -matrices. We will not need a precise characterization of that subspace, but only its grossest feature, which is that it is a subspace of the space of L mutually positive points in $G_+(2, n)$. This means that it lives in the subspace for which all ordered maximal minors of the matrices

$$\begin{pmatrix} D^{(\ell)} \end{pmatrix}, \quad \begin{pmatrix} D^{(\ell_1)} \\ D^{(\ell_2)} \end{pmatrix}, \quad \begin{pmatrix} D^{(\ell_1)} \\ D^{(\ell_2)} \\ D^{(\ell_3)} \end{pmatrix}, \quad \text{etc.}$$

are positive.

A key consequence of the positivity of the D -matrices is that, for positive external data $Z_i^I \in G_+(4, n)$, all loop variables $\mathcal{L}^{(\ell)}$ are oriented positively with respect to the external data and to each other: inside the amplituhedron,

$$\langle \mathcal{L}^{(\ell)} i i+1 \rangle > 0 \text{ for all } i \text{ and all } \ell, \text{ and} \quad (2.5)$$

$$\langle \mathcal{L}^{(\ell_1)} \mathcal{L}^{(\ell_2)} \rangle > 0 \text{ for all } \ell_1, \ell_2. \quad (2.6)$$

The boundaries of the amplituhedron coincide with the boundaries of the space of positive D -matrices, and occur for generic Z when one or more of these quantities approach zero.

It is worth noting that the above definition of positivity depends on the arbitrary choice of a special point Z_1 , since for example $\langle \mathcal{L} 12 \rangle > 0$ but the cyclically related quantity $\langle \mathcal{L} n 1 \rangle$ is negative. The choice of special point is essentially irrelevant: it just means that some special cases need to be checked. In calculations we can sidestep this

subtlety by always choosing to analyze configurations involving points satisfying $1 \leq i < j < k < l \leq n$, which can be done without loss of generality. The geometric properties of figures 2.2–2.5 below are insensitive to the choice and always have full cyclic symmetry.

The integrand of an MHV amplitude is a canonical form $d\Omega$ defined by its having logarithmic singularities only on the boundary of the amplituhedron. The numerator of $d\Omega$ conspires to cancel all singularities that would occur outside this region (see [9] for some detailed examples). Our analysis will require no detailed knowledge of this form. Instead, we will appeal to “the amplituhedron” to tell us whether or not any given configuration of lines $\mathcal{L}^{(\ell)}$ overlaps the amplituhedron or its boundaries by checking whether eqs. (2.5) and (2.6) are satisfied (possibly with some $=$ instead of $>$).

2.1.3 Landau Singularities

The goal of this paper is to understand the singularities of (integrated) amplitudes. For standard Feynman integrals, which are characterized by having only local propagators in the denominator, it is well-known that the locus in kinematic space where a Feynman integral can potentially develop a singularity is determined by solving the Landau equations [26, 56, 33] which we now briefly review.

After Feynman parameterization any L -loop scattering amplitude in D spacetime dimensions may be expressed as a linear combination of integrals of the form

$$\int \prod_{r=1}^L d^D l_r \int_{\alpha_i \geq 0} d^v \alpha \delta \left(1 - \sum_{i=1}^v \alpha_i \right) \frac{\mathcal{N}(l_r^\mu, p_i^\mu, \dots)}{\mathcal{D}^v} \quad (2.7)$$

where v is the number of propagators in the diagram, each of which has an associated Feynman parameter α_i , \mathcal{N} is some numerator factor which may depend on the L loop momenta l_r^μ as well as the external momenta p_i^μ , and finally the denominator involves

$$\mathcal{D} = \sum_{i=1}^v \alpha_i (q_i^2 - m_i^2), \quad (2.8)$$

where q_i^μ is the momentum flowing along propagator i which carries mass m_i . The integral can be viewed as a multidimensional contour integral in the $LD + \nu$ integration variables (l_r^μ, α_i) , where the α_i contours begin at $\alpha_i = 0$ and the l_r^μ contours are considered closed by adding a point at infinity. Although the correct contour for a physical scattering process is dictated by an appropriate $i\epsilon$ prescription in the propagators, a complete understanding of the integral, including its analytic continuation off the physical sheet, requires arbitrary contours to be considered.

An integral of the above type can develop singularities when the denominator \mathcal{D} vanishes in such a way that the contour of integration cannot be deformed to avoid the singularity. This can happen in two distinct situations:

(1) The surface $\mathcal{D} = 0$ can pinch the contour simultaneously in all integration variables (l_r^μ, α_i) . This is called the “leading Landau singularity”, though it is important to keep in mind that it is only a potential singularity. The integral may have a branch point instead of a singularity, or it may be a completely regular point, depending on the behavior of the numerator factor \mathcal{N} .

(2) The denominator may vanish on the boundary when one or more of the $\alpha_i = 0$ and pinch the contour in the other integration variables. These are called subleading Landau singularities.

The Landau conditions encapsulating both possible situations are

$$\sum_{i \in \text{loop}} \alpha_i q_i^\mu = 0 \text{ for each loop, and} \quad (2.9)$$

$$\alpha_i (q_i^2 - m_i^2) = 0 \text{ for each } i. \quad (2.10)$$

For leading singularities eq. (2.10) is satisfied by $q_i^2 - m_i^2 = 0$ for each i , while subleading singularities have one or more i for which $q_i^2 - m_i^2 \neq 0$ but the corresponding $\alpha_i = 0$. We will always refer to equations of type $q_i^2 - m_i^2$ as “cut conditions” since they correspond to putting some internal propagators on-shell. It is important to emphasize that the Landau equations themselves have no knowledge of the numerator factor \mathcal{N} , which can alter the structure of a singularity or even cancel a singularity entirely.

Sometimes (i.e., for some diagram topologies), the Landau equations (2.9) and (2.10) may admit solutions for arbitrary external kinematics p_i^μ . This usually indicates an infrared divergence in the integral (we will not encounter ultraviolet divergences in SYM theory), which may or may not be visible by integration along the physical contour.

In other cases, solutions to the Landau equations might exist only when the p_i^μ lie on some subspace of the external kinematic space. MHV amplitudes in SYM theory are expected to have only branch point type singularities (after properly normalizing them by dividing out a tree-level Parke-Taylor [57] factor), so for these amplitudes we are particularly interested in solutions which exist only on codimension-one slices of the external kinematic space. Even when the p_i^μ live on a slice where solutions of the Landau equations exist, the solutions generally occur for values of the integration variables α_i and l_r^μ that are off the physical contour (for example, the α_i could be complex). This indicates a branch point of the integral that is not present on the physical sheet but only becomes apparent after suitable analytic continuation away from the physical contour.

Finally let us note that we have ignored a class of branch points called “second-type singularities” [58, 59, 33] which arise from pinch singularities at infinite loop momentum. As argued in [16], these should be absent in planar SYM theory when one uses a regulator that preserves dual conformal symmetry.

2.2 Eliminating Spurious Singularities of MHV Amplitudes

In principle one can write explicit formulas for any desired integrand in planar SYM theory by triangulating the interior of the amplituhedron and constructing the canonical form $d\Omega$ with logarithmic singularities on its boundary. However, general triangulations may produce arbitrarily complicated representations for $d\Omega$. In particular, these may have no semblance to standard Feynman integrals with only local propagators in the denominator (see [6] for some explicit examples). It is therefore not immediately clear that the Landau equations have any relevance to the amplituhedron. The connection will become clear in the following section; here we begin by revisiting the analysis of [16] with the amplituhedron as a guide.

In [16] we analyzed the potential Landau singularities of one- and two-loop MHV amplitudes by relying on the crutch of representations of these amplitudes in terms of one- and two-loop chiral pentagon and double-pentagon integrals [32]. The solutions to the various sets of Landau equations for these integral topologies represent *potential* singularities of the amplitudes, but this set of potential singularities is too large for two reasons. First of all, the chiral integrals are dressed with very particular numerator factors to which the Landau equations are completely insensitive. Scalar pentagon and double pentagon integrals certainly have singularities that are eliminated by the numerator factors of their chiral cousins. Second, some actual singularities of individual chiral integrals may be spurious in the full amplitude due to cancellations when all of the contributing chiral integrals are summed.

It is a priori highly non-trivial to see which singularities of individual integrals survive the summation to remain singularities of the full amplitude. However, the amplituhedron hypothesis provides a quick way to detect spurious singularities from simple considerations of positive geometry. In this section we refine our analysis of [16] to determine which *potential* singularities identified in that paper are *actual* singularities by appealing to the amplituhedron as an oracle to tell us which cuts of the amplitude have zero or non-zero support on the (boundary of the) amplituhedron.

Specifically, we propose a check that is motivated by the Cutkosky rules [27], which tell us that to compute the cut of an amplitude with respect to some set of cut conditions, one replaces the on-shell propagators in the integrand corresponding to those cut conditions by delta-functions, and integrates the resulting quantity over the loop momenta. The result of such a calculation has a chance to be non-zero only if the locus where the cut conditions are all satisfied has non-trivial overlap with the domain of integration of the loop momentum variables. In the present context, that domain is the space of mutually positive lines, i.e., the interior of the amplituhedron. This principle will lead to a fundamental asymmetry between the two types of Landau equations in our analysis. The full set of Landau equations including both eqs. (2.9) and (2.10) should be solvable only on a codimension-one locus in the space of external momenta in order

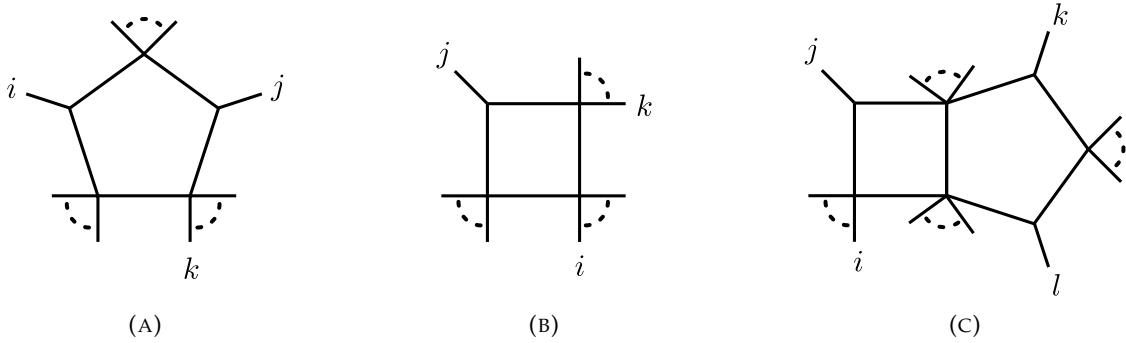


FIGURE 2.1: Three examples of cuts on which MHV amplitudes have no support; these appeared as spurious singularities in the Landau equation analysis of [16] since scalar pentagon and double pentagon integrals do have these cuts.

to obtain a valid branch point. However, guided by Cutkosky, we claim that the cut conditions (2.10) must be solvable inside the positive domain for arbitrary (positive) external kinematics; otherwise the discontinuity around the putative branch point is zero and we should discard it as spurious.

In the remainder of this section we will demonstrate this hypothesis by means of the examples shown in figure 2.1. The leading Landau singularities of each of these diagrams were found to be singularities of the scalar pentagon and double-pentagon integrals analyzed in [16], but it is clear that MHV amplitudes have no support on these cut configurations. In the next three subsections we will see how to understand their spuriousness directly from the amplituhedron. This will motivate us to seek a better, more direct algorithm to be presented in the following section.

2.2.1 The Spurious Pentagon Singularity

The first spurious singularity of MHV amplitudes arising from the integral representation used in [16] is the leading Landau singularity of the pentagon shown in figure 2.1a, which is located on the locus where

$$\langle ijkk+1 \rangle \langle \bar{i} \cap \bar{j} k k+1 \rangle = 0. \quad (2.11)$$

It was noted already in [27] that this solution of the Landau equations does not correspond to a branch point of the pentagon integral. It arises from cut conditions that put all five propagators of the pentagon on-shell:

$$0 = \langle \mathcal{L} i-1 i \rangle = \langle \mathcal{L} i i+1 \rangle = \langle \mathcal{L} j-1 j \rangle = \langle \mathcal{L} j j+1 \rangle = \langle \mathcal{L} k k+1 \rangle, \quad (2.12)$$

where \mathcal{L} is the loop momentum. The first four of these cut conditions admit two discrete solutions [32]: either $\mathcal{L} = (ij)$ or $\mathcal{L} = \bar{i} \cap \bar{j}$. The second of these cannot avoid lying outside the amplituhedron. We see this by representing its D -matrix as

$$D = \begin{pmatrix} i-1 & i & i+1 \\ \langle i \bar{j} \rangle & -\langle i-1 \bar{j} \rangle & 0 \\ 0 & \langle i+1 \bar{j} \rangle & -\langle i \bar{j} \rangle \end{pmatrix}, \quad (2.13)$$

where we indicate only the nonzero columns of the $2 \times n$ matrix in positions $i-1$, i and $i+1$, per the labels above the matrix. The non-zero 2×2 minors of this matrix,

$$\langle i \bar{j} \rangle \langle i+1 \bar{j} \rangle, \quad \langle i-1 \bar{j} \rangle \langle i \bar{j} \rangle, \quad -\langle i \bar{j} \rangle^2 \quad (2.14)$$

have indefinite signs for general positive external kinematics, so this \mathcal{L} lies discretely outside the amplituhedron.

We proceed with the first solution $\mathcal{L} = (ij)$ which can be represented by the trivial D -matrix

$$D = \begin{pmatrix} i & j \\ 1 & 0 \\ 0 & 1 \end{pmatrix}. \quad (2.15)$$

Although this is trivially positive, upon substituting $\mathcal{L} = (ij)$ into eq. (2.12) we find that the fifth cut condition can only be satisfied for special kinematics satisfying

$$\langle i j k k+1 \rangle = 0. \quad (2.16)$$

Therefore, according to the Cutkosky-inspired rule discussed three paragraphs ago, the monodromy around this putative singularity vanishes for general kinematics and hence it is not a valid branch point at one loop. Indeed this conclusion is easily verified by looking at the explicit results of [40].

2.2.2 The Spurious Three-Mass Box Singularity

The second spurious one-loop singularity encountered in [16] is a subleading singularity of the pentagon which lives on the locus

$$\langle j(j-1j+1)(ii+1)(kk+1) \rangle = 0 \quad (2.17)$$

and arises from the cut conditions shown in figure 2.1b:

$$0 = \langle \mathcal{L} ii+1 \rangle = \langle \mathcal{L} j-1j \rangle = \langle \mathcal{L} jj+1 \rangle = \langle \mathcal{L} kk+1 \rangle. \quad (2.18)$$

These are of three-mass box type and have the two solutions [4]

$$\mathcal{L} = (jii+1) \cap (jkk+1) \text{ or } \mathcal{L} = (\bar{j} \cap (ii+1), \bar{j} \cap (kk+1)). \quad (2.19)$$

The two solutions may be represented respectively by the D -matrices

$$D = \begin{pmatrix} i & i+1 & j \\ 0 & 0 & 1 \\ \langle i+1jkk+1 \rangle & -\langle ijkk+1 \rangle & 0 \end{pmatrix} \quad (2.20)$$

and

$$D = \begin{pmatrix} i & i+1 & k & k+1 \\ \langle i+1\bar{j} \rangle & -\langle i\bar{j} \rangle & 0 & 0 \\ 0 & 0 & -\langle \bar{j}k+1 \rangle & \langle \bar{j}k \rangle \end{pmatrix}. \quad (2.21)$$

Neither matrix is non-negative definite when the Z 's are in the positive domain $G_+(4, n)$, so we again reach the (correct) conclusion that one-loop MHV amplitudes do not have

singularities on the locus where eq. (2.17) is satisfied (for generic i, j and k).

2.2.3 A Two-Loop Example

The two-loop scalar double-pentagon integral considered in [16] has a large number of Landau singularities that are spurious singularities of two-loop MHV amplitudes. It would be cumbersome to start with the full list and eliminate the spurious singularities one at a time using the amplituhedron. Here we will be content to consider one example in detail before abandoning this approach in favor of one more directly built on the amplituhedron.

We consider the Landau singularities shown in eq. (4.12) of [16] which live on the locus

$$\langle j(j-1j+1)(i-1i)(kl) \rangle \langle j(j-1j+1)(i-1i)\bar{k} \cap \bar{l} \rangle = 0. \quad (2.22)$$

We consider the generic case when the indices i, j, k, l are well-separated; certain degenerate cases do correspond to non-spurious singularities. This singularity is of pentagon-box type shown in figure 2.1c since it was found in [16] to arise from the eight cut conditions

$$\begin{aligned} \langle \mathcal{L}^{(1)} i-1i \rangle &= \langle \mathcal{L}^{(1)} j-1j \rangle = \langle \mathcal{L}^{(1)} jj+1 \rangle = \langle \mathcal{L}^{(1)} \mathcal{L}^{(2)} \rangle = 0, \\ \langle \mathcal{L}^{(2)} k-1k \rangle &= \langle \mathcal{L}^{(2)} kk+1 \rangle = \langle \mathcal{L}^{(2)} l-1l \rangle = \langle \mathcal{L}^{(2)} ll+1 \rangle = 0. \end{aligned} \quad (2.23)$$

The last four equations have two solutions $\mathcal{L}^{(2)} = (kl)$ or $\mathcal{L}^{(2)} = \bar{k} \cap \bar{l}$, but as in the previous subsection, only the first of these has a chance to avoid being outside the amplituhedron. Taking $\mathcal{L}^{(2)} = (kl)$, the two solutions to the first four cut conditions are then

$$\mathcal{L}^{(1)} = (ji-1i) \cap (jkl) = (Z_j, Z_{i-1} \langle i j k l \rangle - Z_i \langle i-1 j k l \rangle) \text{ or} \quad (2.24)$$

$$\mathcal{L}^{(1)} = \left((i-1i) \cap \bar{j}, (kl) \cap \bar{j} \right) = \left(Z_{i-1} \langle i \bar{j} \rangle - Z_i \langle i-1 \bar{j} \rangle, Z_k \langle l \bar{j} \rangle - Z_l \langle k \bar{j} \rangle \right). \quad (2.25)$$

The D -matrices corresponding to the first solution can be taken as

$$\begin{pmatrix} D^{(1)} \\ D^{(2)} \end{pmatrix} = \begin{pmatrix} i-1 & i & j & k & l \\ 0 & 0 & 1 & 0 & 0 \\ \langle i j k l \rangle & -\langle i-1 j k l \rangle & 0 & 0 & 0 \\ 0 & 0 & 0 & 1 & 0 \\ 0 & 0 & 0 & 0 & 1 \end{pmatrix}. \quad (2.26)$$

Evidently two of its 4×4 minors are $-\langle i j k l \rangle$ and $\langle i-1 j k l \rangle$, which have opposite signs for generic Z in the positive domain. D -matrices corresponding to the second solution can be written as

$$\begin{pmatrix} D^{(1)} \\ D^{(2)} \end{pmatrix} = \begin{pmatrix} i-1 & i & k & l \\ \langle i \bar{j} \rangle & -\langle i-1 \bar{j} \rangle & 0 & 0 \\ 0 & 0 & \langle l \bar{j} \rangle & -\langle k \bar{j} \rangle \\ 0 & 0 & 1 & 0 \\ 0 & 0 & 0 & 1 \end{pmatrix}, \quad (2.27)$$

which again has minors of opposite signs.

We conclude that the locus where the cut conditions (2.23) are satisfied lies strictly outside the amplituhedron, and therefore that there is no discontinuity around the putative branch point at (2.22). Indeed, this is manifested by the known fact [60] that two-loop MHV amplitudes do not have symbol entries which vanish on this locus. Actually, while correct, we were slightly too hasty in reaching this conclusion, since we only analyzed one set of cut conditions. Although it doesn't happen in this example, in general there may exist several different collections of cut conditions associated to the same Landau singularity, and the discontinuity around that singularity would receive additive contributions from each distinct set of associated cut contributions.

2.2.4 Summary

We have shown, via a slight refinement of the analysis carried out in [16], that the spurious branch points of one- and two-loop MHV amplitudes encountered in that paper can be eliminated simply on the basis of positivity constraints in the amplituhedron. It is simple to see that the cuts considered above have no support for MHV amplitudes so it may seem like overkill to use the fancy language of the amplituhedron. However we wanted to highlight the following approach:

(1) First, consider a representation of an amplitude as a sum over a particular type of Feynman integrals. Find the Landau singularities of a generic term in the sum. These tell us the loci in Z -space where the amplitude *may* have a singularity.

(2) For each *potential* singularity obtained in (1), check whether the corresponding on-shell conditions have a non-zero intersection with the (closure of) the amplituhedron. If the answer is no, for all possible sets of cut conditions associated with a given Landau singularity, then the singularity must be spurious.

This approach is conceptually straightforward but inefficient. One manifestation of this inefficiency is that although double pentagon integrals are characterized by four free indices i, j, k, l , we will see in the next section the vast majority of the resulting potential singularities are spurious. Specifically we will see that in order for the solution to a given set of cut conditions to have support inside the (closure of the) amplituhedron, the conditions must be relaxed in such a way that they involve only three free indices. In other words, most of the $\mathcal{O}(n^4)$ singularities of individual double pentagon integrals must necessarily cancel out when they are summed, leaving only $\mathcal{O}(n^3)$ physical singularities of the full two-loop MHV amplitudes. (The fact that these amplitudes have only $\mathcal{O}(n^3)$ singularities is manifest in the result of [60].) This motivates us to seek a more “amplituhedrony” approach to finding singularities where we do not start by considering any particular representation of the amplitude, but instead start by thinking directly about positive configurations of loops $\mathcal{L}^{(\ell)}$.

2.3 An Amplituhedrony Approach

The most significant drawback of the approach taken in the previous section is that it relies on having explicit representations of an integrand in terms of local Feynman integrals. These have been constructed for all two-loop amplitudes in SYM theory [61], but at higher loop order even finding such representations becomes a huge computational challenge that we would like to be able to bypass. Also, as the loop order increases, the number of potential Landau singularities grows rapidly, and the vast majority of these potential singularities will fail the positivity analysis and hence turn out to be spurious. We would rather not have to sift through all of this chaff to find the wheat.

Let's begin by taking a step back to appreciate that the only reason we needed the crutch of local Feynman integrals in the previous section is that each Feynman diagram topology provides a set of propagators for which we can solve the associated Landau equations (2.9) and (2.10) to find potential singularities. Then, for each set of cut conditions, we can determine whether the associated Landau singularity is physical or spurious by asking the amplituhedron whether or not the set of loops $\mathcal{L}^{(\ell)}$ satisfying the cut conditions has any overlap with the amplituhedron.

In this section we propose a more “amplituhedrony” approach that does not rely on detailed knowledge of integrands. We invert the logic of the previous section: instead of using Feynman diagrams to generate sets of cut conditions that we need to check one by one, we can ask the amplituhedron itself to directly identify all potentially “valid” sets of cut conditions that are possibly relevant to the singularities of an amplitude.

To phrase the problem more abstractly: for a planar n -particle amplitude at L -loop order, there are in general $nL + L(L - 1)/2$ possible local cut conditions one can write down:

$$\langle \mathcal{L}^{(\ell)} i i+1 \rangle = 0 \text{ for all } \ell, i \text{ and } \langle \mathcal{L}^{(\ell_1)} \mathcal{L}^{(\ell_2)} \rangle = 0 \text{ for all } \ell_1 \neq \ell_2. \quad (2.28)$$

We simply need to characterize which subsets of these cut conditions can possibly be simultaneously satisfied for loop momenta $\mathcal{L}^{(\ell)}$ living in the closure of the amplituhedron. Each such set of cut conditions is a subset of one or more maximal subsets, and

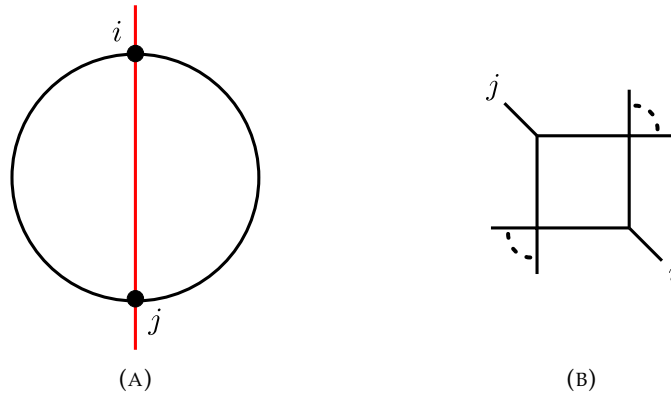


FIGURE 2.2: (a) A maximum codimension boundary of the one-loop MHV amplituhedron. The circle is a schematic depiction of the n line segments $(12), (23), \dots, (n1)$ connecting the n cyclically ordered external kinematic points $Z_i \in G_+(4, n)$ and the red line shows the loop momentum $\mathcal{L} = (ij)$. (b) The corresponding Landau diagram, which is a graphical depiction of the four cut conditions (2.30) that are satisfied on this boundary.

these maximal subsets are just the maximal codimension boundaries of the amplituhedron.

Fortunately, the maximal codimension boundaries of the MHV amplituhedron are particularly simple, as explained in [5]. Each loop momentum $\mathcal{L}^{(\ell)}$ must take the form (ij) for some i and j (that can be different for different ℓ), and the condition of mutual positivity enforces an emergent planarity: if all of the lines $\mathcal{L}^{(\ell)}$ are drawn as chords on a disk between points on the boundary labeled $1, 2, \dots, n$, then positivity forbids any two lines to cross in the interior of the disk. In what follows we follow a somewhat low-brow analysis in which we systematically consider relaxations away from the maximum codimension boundaries, but the procedure can be streamlined by better harnessing this emergent planarity, which certainly pays off at higher loop order [62].

In the next few subsections we demonstrate this “amplituhedrony” approach explicitly at one and two loops before summarizing the main idea at the end of the section.

2.3.1 One-Loop MHV Amplitudes

The maximum codimension boundaries of the one-loop MHV amplituhedron occur when

$$\mathcal{L} = (ij), \quad (2.29)$$

as depicted in figure 2.2a. On this boundary four cut conditions of “two-mass easy” type [40] are manifestly satisfied:

$$\langle \mathcal{L} i-1 i \rangle = \langle \mathcal{L} i i+1 \rangle = \langle \mathcal{L} j-1 j \rangle = \langle \mathcal{L} j j+1 \rangle = 0, \quad (2.30)$$

as depicted in the Landau diagram shown in figure 2.2b. (For the moment we consider i and j to be well separated so there are no accidental degenerations.) The Landau analysis of eq. (2.30) has been performed long ago [26, 33] and reviewed in the language of momentum twistors in [16]. A leading solution to the Landau equations exists only if

$$\langle i \bar{j} \rangle \langle \bar{i} j \rangle = 0. \quad (2.31)$$

Subleading Landau equations are obtained by relaxing one of the four on-shell conditions. This leads to cuts of two-mass triangle type, which are uninteresting (they exist for generic kinematics, so don’t correspond to branch points of the amplitude). At sub-subleading order we reach cuts of bubble type. For example if we relax the second and fourth condition in eq. (2.30) then we encounter a Landau singularity which lives on the locus

$$\langle i-1 i j-1 j \rangle = 0. \quad (2.32)$$

Other relaxations either give no constraint on kinematics, or the same as eq. (2.32) with $i \rightarrow i+1$ and/or $j \rightarrow j+1$.

Altogether, we reach the conclusion that all physical branch points of one-loop MHV amplitudes occur on loci of the form

$$\langle a \bar{b} \rangle = 0 \text{ or } \langle a a+1 b b+1 \rangle = 0 \quad (2.33)$$

for various a, b . (Note that whenever we say there is a branch point at $x = 0$, we mean more specifically that there is a branch cut between $x = 0$ and $x = \infty$.) Indeed, these exhaust the branch points of the one-loop MHV amplitudes (first computed in [40]) except for branch points arising as a consequence of infrared regularization, which are captured by the BDS ansatz [63].

2.3.2 Two-Loop MHV Amplitudes: Configurations of Positive Lines

We divide the two-loop analysis into two steps. First, in this subsection, we classify valid configurations of mutually non-negative lines. This provides a list of the sets of cut conditions on which two-loop MHV amplitudes have nonvanishing support. Then in the following subsection we solve the Landau equations for each set of cut conditions, to find the actual location of the corresponding branch point.

At two loops the MHV amplituhedron has two distinct kinds of maximum codimension boundaries [5]. The first type has $\mathcal{L}^{(1)} = (ij)$ and $\mathcal{L}^{(2)} = (kl)$ for distinct cyclically ordered i, j, k, l . Since $\langle \mathcal{L}^{(1)} \mathcal{L}^{(2)} \rangle$ is non-vanishing (inside the positive domain $G_+(4, n)$) in this case, this boundary can be thought of as corresponding to a cut of a product of one-loop Feynman integrals, with no common propagator $\langle \mathcal{L}^{(1)} \mathcal{L}^{(2)} \rangle$. Therefore we will not learn anything about two-loop singularities beyond what is already apparent at one loop.

The more interesting type of maximum codimension boundary has $\mathcal{L}^{(1)} = (ij)$ and $\mathcal{L}^{(2)} = (ik)$, as depicted in figure 2.3a. Without loss of generality $i < j < k$, and for now we will moreover assume that i, j and k are well-separated to avoid any potential degenerations. (These can be relaxed at the end of the analysis, in particular to see that the degenerate case $j = k$ gives nothing interesting.) On this boundary the following nine cut conditions shown in the Landau diagram of figure 2.3b are simultaneously

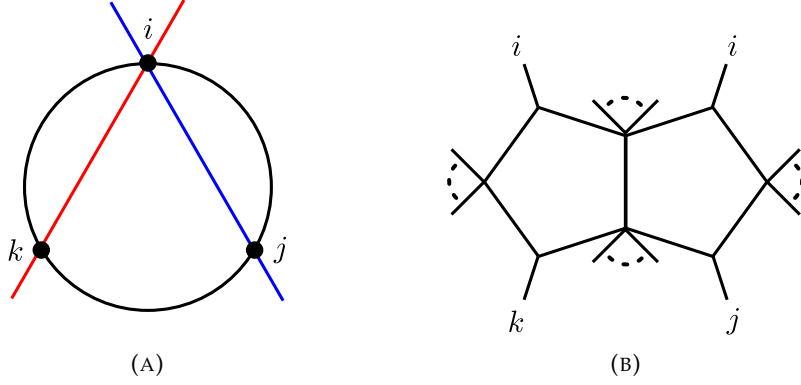


FIGURE 2.3: (a) A maximum codimension boundary of the two-loop MHV amplituhedron. (b) The corresponding Landau diagram (which, it should be noted, does not have the form of a standard Feynman integral) depicting the nine cut conditions (2.34)–(2.36) that are satisfied on this boundary.

satisfied:

$$\langle \mathcal{L}^{(1)} i-1 i \rangle = \langle \mathcal{L}^{(1)} i i+1 \rangle = \langle \mathcal{L}^{(2)} i-1 i \rangle = \langle \mathcal{L}^{(2)} i i+1 \rangle = 0, \quad (2.34)$$

$$\langle \mathcal{L}^{(1)} j-1 j \rangle = \langle \mathcal{L}^{(1)} j j+1 \rangle = \langle \mathcal{L}^{(2)} k-1 k \rangle = \langle \mathcal{L}^{(2)} k k+1 \rangle = 0, \quad (2.35)$$

$$\langle \mathcal{L}^{(1)} \mathcal{L}^{(2)} \rangle = 0. \quad (2.36)$$

This is the maximal set of cuts that can be simultaneously satisfied while keeping the $\mathcal{L}^{(\ell)}$'s inside the closure of the amplituhedron for generic $Z \in G_+(4, n)$. We immediately note that since only three free indices i, j, k are involved, this set of cuts manifestly has size $\mathcal{O}(n^3)$, representing immediate savings compared to the larger $\mathcal{O}(n^4)$ set of double-pentagon cut conditions as discussed at the end of the previous section.

We can generate other, smaller sets of cut conditions by relaxing some of the nine shown in eqs. (2.34)–(2.36). This corresponds to looking at subleading singularities, in the language of the Landau equations. However, it is not interesting to consider relaxations that lead to $\langle \mathcal{L}^{(1)} \mathcal{L}^{(2)} \rangle \neq 0$ because, as mentioned above, it essentially factorizes the problem into a product of one-loop cuts. Therefore in what follows we only consider cuts on which $\langle \mathcal{L}^{(1)} \mathcal{L}^{(2)} \rangle = 0$.

By relaxing various subsets of the other 8 conditions we can generate 2^8 subsets of cut conditions. In principle each subset should be analyzed separately, but there

is clearly a natural stratification of relaxations which we can exploit to approach the problem systematically. In fact, we will see that the four cut conditions in eq. (2.34) that involve the point i play a special role. Specifically, we will see that the four cut conditions in eq. (2.35) involving j and k can always be relaxed, or un-relaxed, “for free”, with no impact on positivity. Therefore, we see that whether a configuration of loops may be positive or not depends only on which subset of the four cut conditions (2.34) is relaxed.

In this subsection we will classify the subsets of eq. (2.34) that lead to valid configurations of positive lines $\mathcal{L}^{(\ell)}$, and in the next subsection we will find the locations of the corresponding Landau singularities.

Relaxing none of eq. (2.34) [figure 2.3a]. At maximum codimension we begin with the obviously valid pair of mutually non-negative lines represented trivially by

$$\begin{pmatrix} D^{(1)} \\ D^{(2)} \end{pmatrix} = \begin{matrix} & i & j & k \\ \begin{pmatrix} 1 & 0 & 0 \\ 0 & 1 & 0 \\ 1 & 0 & 0 \\ 0 & 0 & 1 \end{pmatrix} \end{matrix}. \quad (2.37)$$

Relaxing any one of eq. (2.34). The four cases are identical up to relabeling so we consider relaxing the condition $\langle \mathcal{L}^{(2)} ii+1 \rangle = 0$, shown in figure 2.4a. In this case the remaining seven cut conditions on the first two lines of eqs. (2.34) and (2.35) admit the one-parameter family of solutions

$$\mathcal{L}^{(1)} = (ij), \quad \mathcal{L}^{(2)} = (Z_k, \alpha Z_{i-1} + (1 - \alpha)Z_i). \quad (2.38)$$

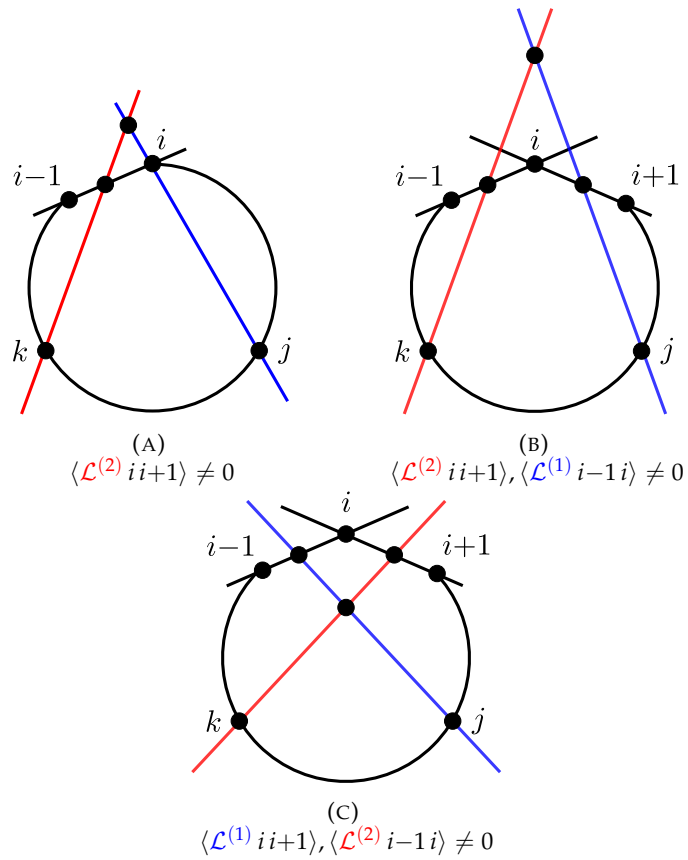


FIGURE 2.4: Three different invalid relaxations of the maximal codimension boundary shown in figure 2.3.

We recall that the parity conjugate solutions having $\mathcal{L}^{(1)} = \bar{i} \cap \bar{j}$ lie discretely outside the amplituhedron as seen in eq. (2.13). The corresponding D -matrices

$$\begin{pmatrix} D^{(1)} \\ D^{(2)} \end{pmatrix} = \begin{pmatrix} i-1 & i & j & k \\ 0 & 1 & 0 & 0 \\ 0 & 0 & 1 & 0 \\ \alpha & 1-\alpha & 0 & 0 \\ 0 & 0 & 0 & 1 \end{pmatrix} \quad (2.39)$$

are mutually non-negative for $0 \leq \alpha \leq 1$. It remains to impose the final cut condition that $\mathcal{L}^{(1)}$ and $\mathcal{L}^{(2)}$ intersect:

$$\langle \mathcal{L}^{(1)} \mathcal{L}^{(2)} \rangle = \alpha \langle i-1 i j k \rangle = 0. \quad (2.40)$$

For general positive external kinematics this will only be satisfied when $\alpha = 0$, which brings us back to the maximum codimension boundary. We conclude that the loop configurations of this type do not generate branch points.

Relaxing $\langle \mathcal{L}^{(1)} i-1 i \rangle = 0$ and $\langle \mathcal{L}^{(2)} i i+1 \rangle = 0$ [figure 2.4b]. In this case the six remaining cut conditions in eqs. (2.34) and (2.35) admit the two-parameter family of solutions

$$\mathcal{L}^{(1)} = (\alpha Z_i + (1-\alpha)Z_{i+1}, Z_j), \quad \mathcal{L}^{(2)} = (\beta Z_i + (1-\beta)Z_{i-1}, Z_k). \quad (2.41)$$

The corresponding D -matrices

$$\begin{pmatrix} D^{(1)} \\ D^{(2)} \end{pmatrix} = \begin{pmatrix} i-1 & i & i+1 & j & k \\ 0 & \alpha & 1-\alpha & 0 & 0 \\ 0 & 0 & 0 & 1 & 0 \\ 1-\beta & \beta & 0 & 0 & 0 \\ 0 & 0 & 0 & 0 & 1 \end{pmatrix} \quad (2.42)$$

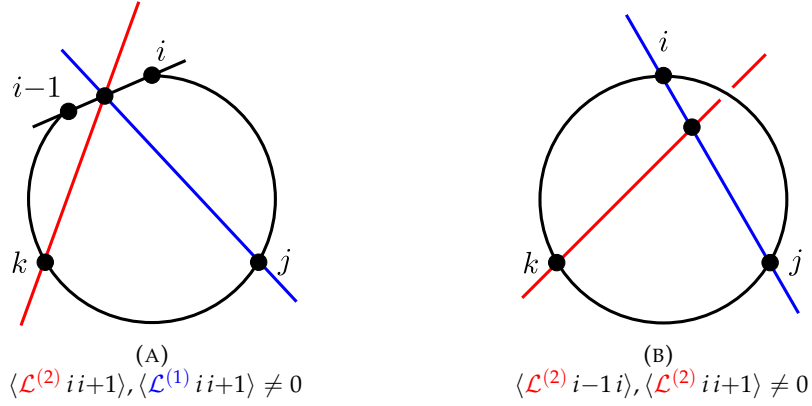


FIGURE 2.5: Two valid double relaxations of figure 2.3. The other two possibilities are obtained by taking $i \rightarrow i+1$ in (a) or $\mathcal{L}^{(2)} \rightarrow \mathcal{L}^{(1)}$ and $j \leftrightarrow k$ in (b).

are mutually non-negative if $0 \leq \alpha, \beta \leq 1$. Imposing that the two loops intersect gives the constraint

$$\langle \mathcal{L}^{(1)} \mathcal{L}^{(2)} \rangle = \alpha(1 - \beta) \langle i-1 i j k \rangle + (1 - \alpha)\beta \langle i i+1 j k \rangle + (1 - \alpha)(1 - \beta) \langle i-1 i+1 j k \rangle = 0, \quad (2.43)$$

which is not satisfied for general positive kinematics unless $\alpha = \beta = 1$, which again brings us back to the maximum codimension boundary.

Relaxing the two conditions $\langle \mathcal{L}^{(1)} ii+1 \rangle = \langle \mathcal{L}^{(2)} ii-1 \rangle = 0$, depicted in figure 2.4c, is easily seen to lead to the same conclusion.

Relaxing $\langle \mathcal{L}^{(1)} ii+1 \rangle = 0$ and $\langle \mathcal{L}^{(2)} ii+1 \rangle = 0$ [figure 2.5a]. In this case there is a one-parameter family of solutions satisfying all seven remaining cut conditions including $\langle \mathcal{L}^{(1)} \mathcal{L}^{(2)} \rangle = 0$:

$$\mathcal{L}^{(1)} = (\alpha Z_i + (1 - \alpha)Z_{i+1}, Z_j), \quad \mathcal{L}^{(2)} = (\alpha Z_i + (1 - \alpha)Z_{i+1}, Z_k). \quad (2.44)$$

The D -matrices can be represented as

$$\begin{pmatrix} D^{(1)} \\ D^{(2)} \end{pmatrix} = \begin{pmatrix} i & i+1 & j & k \\ \alpha & 1-\alpha & 0 & 0 \\ 0 & 0 & 1 & 0 \\ \alpha & 1-\alpha & 0 & 0 \\ 0 & 0 & 0 & 1 \end{pmatrix}, \quad (2.45)$$

which is a valid mutually non-negative configuration for $0 \leq \alpha \leq 1$. We conclude that these configurations represent physical branch points of two-loop MHV amplitudes by appealing to Cutkoskian intuition, according to which we would compute the discontinuity of the amplitude around this branch point by integrating over $0 \leq \alpha \leq 1$ (in figure 2.5a this corresponds to integrating the intersection point of the two \mathcal{L} 's over the line segment between Z_{i-1} and Z_i).

Relaxing the two conditions $\langle \mathcal{L}^{(1)} i i-1 \rangle = \langle \mathcal{L}^{(2)} i i-1 \rangle = 0$ is clearly equivalent up to relabeling.

Relaxing $\langle \mathcal{L}^{(2)} i-1 i \rangle = 0$ and $\langle \mathcal{L}^{(2)} i i+1 \rangle = 0$ [figure 2.5b]. The seven remaining cut conditions admit a one-parameter family of solutions

$$\mathcal{L}^{(1)} = (ij), \quad \mathcal{L}^{(2)} = (\alpha Z_i + (1-\alpha)Z_j, Z_k), \quad (2.46)$$

which can be represented by

$$\begin{pmatrix} D^{(1)} \\ D^{(2)} \end{pmatrix} = \begin{pmatrix} i & j & k \\ 1 & 0 & 0 \\ 0 & 1 & 0 \\ \alpha & 1-\alpha & 0 \\ 0 & 0 & 1 \end{pmatrix}. \quad (2.47)$$

This is a valid configuration of mutually non-negative lines for $0 \leq \alpha \leq 1$ so we expect it to correspond to a physical branch point. Clearly the same conclusion holds if we were to completely relax $\mathcal{L}^{(1)}$ at i instead of $\mathcal{L}^{(2)}$.

Higher relaxations of eq. (2.34). So far we have considered the relaxation of any one or any two of the conditions shown in eq. (2.34). We have found that single relaxations do not yield branch points of the amplitude, and that four of the six double relaxations are valid while the two double relaxations shown in figures 2.4b and 2.4c are invalid.

What about triple relaxations? These can be checked by explicit construction of the relevant D -matrices, but it is also easy to see graphically that any triple relaxation is valid because they can all be reached by relaxing one of the valid double relaxations. For example, the triple relaxation where we relax all of eq. (2.34) except $\langle \mathcal{L}^{(1)} i-1 i \rangle = 0$ can be realized by rotating $\mathcal{L}^{(2)}$ in figure 2.5a clockwise around the point k so that it continues to intersect $\mathcal{L}^{(1)}$. As a second example, the triple relaxation where we relax all but $\langle \mathcal{L}^{(2)} i-1 i \rangle = 0$ can be realized by rotating $\mathcal{L}^{(1)}$ in figure 2.5a counter-clockwise around the point j so that it continues to intersect $\mathcal{L}^{(2)}$.

Finally we turn to the case when all four cut conditions in eq. (2.34) are relaxed. These relaxed cut conditions admit two branches of solutions, represented by D -matrices of the form

$$\begin{pmatrix} D^{(1)} \\ D^{(2)} \end{pmatrix} = \begin{pmatrix} j & j+1 & \cdots & k-1 & k \\ 1 & 0 & \cdots & 0 & 0 \\ \alpha_j & \alpha_{j+1} & \cdots & \alpha_{k-1} & \alpha_k \\ \alpha_j & \alpha_{j+1} & \cdots & \alpha_{k-1} & \alpha_k \\ 0 & 0 & \cdots & 0 & 1 \end{pmatrix} \quad (2.48)$$

or a similar form with α parameters wrapping the other way around from k to j :

$$\begin{pmatrix} D^{(1)} \\ D^{(2)} \end{pmatrix} = \begin{pmatrix} \cdots & j-1 & j & k & k+1 & \cdots \\ \cdots & \alpha_{j-1} & \alpha_j & -\alpha_k & -\alpha_{k+1} & \cdots \\ \cdots & 0 & 1 & 0 & 0 & \cdots \\ \cdots & \alpha_{j-1} & \alpha_j & -\alpha_k & -\alpha_{k+1} & \cdots \\ \cdots & 0 & 0 & 1 & 0 & \cdots \end{pmatrix}. \quad (2.49)$$

Both of these parameterize valid configuration of mutually non-negative lines as long as all of the α 's are positive.

Relaxing $\mathcal{L}^{(1)}$ at j and/or $\mathcal{L}^{(2)}$ at k . All of the configurations we have considered so far keep the four propagators in eq. (2.35) on shell. However it is easy to see that none of these conditions have any bearing on positivity one way or the other. For example, there is no way to render the configuration shown in figure 2.4b positive by moving $\mathcal{L}^{(1)}$ away from the vertex j while maintaining all of the other cut conditions. On the other hand, there is no way to spoil the positivity of the configuration shown in figure 2.5b by moving $\mathcal{L}^{(2)}$ away from the vertex k while maintaining all other cut conditions.

Summary. We call a set of cut conditions “valid” if the $m \geq 0$ -dimensional locus in \mathcal{L} -space where the conditions are simultaneously satisfied has non-trivial m -dimensional overlap with the closure of the amplituhedron. (The examples shown in figures 2.5a and 2.5b both have $m = 1$, but further relaxations would have higher-dimensional solution spaces.) As mentioned above, this criterion is motivated by Cutkoskian intuition that the discontinuity of the amplitude would be computed by an integral over the intersection of this locus with the (closure of the) amplituhedron. If this intersection is empty (or lives on a subspace that is less than m -dimensional) then such an integral would vanish, signalling that the putative singularity is actually spurious.

The nine cut conditions shown in eqs. (2.34)–(2.36) are solved by the configuration of lines shown in figure 2.3a that is a zero-dimensional boundary of the amplituhedron. We have systematically investigated relaxing various subsets of these conditions (with

the exception of eq. (2.36), to stay within the realm of genuine two-loop singularities) to determine which relaxations are “valid” in the sense just described.

Conclusion: The most general valid relaxation of the configuration shown in figure 2.3a is either an arbitrary relaxation at the points j and k , or an arbitrary relaxation of figure 2.5a (or the same with $i \mapsto i+1$), or an arbitrary relaxation of figure 2.5b (or the same with $j \leftrightarrow k$). The configurations shown in figure 2.4, and further relaxations thereof that are not relaxations of those shown in figure 2.5, are invalid.

2.3.3 Two-Loop MHV Amplitudes: Landau Singularities

In the previous subsection we asked the amplituhedron directly to tell us which possible sets of cut conditions are valid for two-loop MHV amplitudes, rather than starting from some integral representation and using the amplituhedron to laboriously sift through the many spurious singularities. We can draw Landau diagrams for each valid relaxation to serve as a graphical indicator of the cut conditions that are satisfied. The Landau diagram with nine propagators corresponding to the nine cut conditions satisfied by figure 2.3a was already displayed in figure 2.3b. The configurations shown in figures 2.5a and 2.5b satisfy the seven cut conditions corresponding to the seven propagators in figures 2.6a and 2.6b, respectively. We are now ready to determine the locations of the branch points associated to these valid cut configurations (and their relaxations) by solving the Landau equations.

The following calculations follow very closely those done in [16]. Note that throughout this section, in solving cut conditions we will always ignore branches of solutions (for example those of the type $\mathcal{L} = \bar{i} \cap \bar{j}$) which cannot satisfy positivity.

The double-box. For the double-box shown in figure 2.6a let us use $A \in \mathbb{P}^3$ to denote the point on the line $(i-1, i)$ where the two loop lines $\mathcal{L}^{(\ell)}$ intersect. These can then be parameterized as $\mathcal{L}^{(1)} = (A, Z_j)$ and $\mathcal{L}^{(2)} = (A, Z_k)$. The quickest way to find the location of the leading Landau singularity is to impose eq. (2.9) for each of the two loops. These are both of two-mass easy type, so we find that the Landau singularity

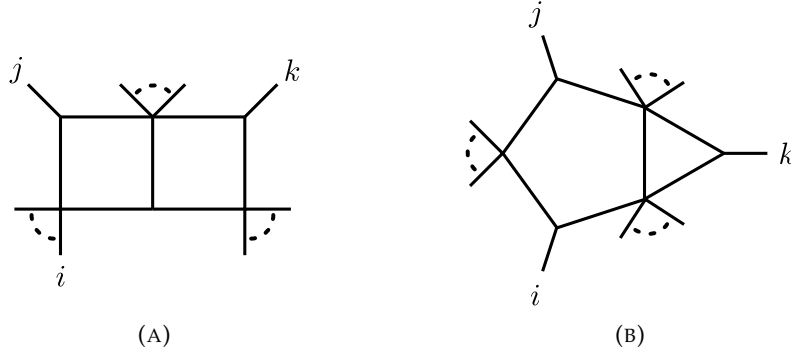


FIGURE 2.6: The Landau diagrams showing the seven cut conditions satisfied by figures 2.5a and 2.5b, respectively.

lives on the locus (see [16])

$$\langle i-1 j k \rangle \langle A \bar{j} \rangle = \langle i-1 j k \rangle \langle A \bar{k} \rangle = 0. \quad (2.50)$$

These can be solved in two ways; either by

$$\langle i-1 j k \rangle = 0 \quad (2.51)$$

or by solving the first condition for $A = \bar{j} \cap (i-1 i)$ and substituting this into the second condition to find

$$\langle i-1 i \bar{j} \cap \bar{k} \rangle = 0. \quad (2.52)$$

The astute reader may recall that in (2.16) we discarded a singularity of the same type as in eq. (2.51). This example highlights that it is crucial to appreciate the essential asymmetry between the roles of the two types of Landau equations. The on-shell conditions (2.9) by themselves only provide information about *discontinuities*. We discarded eq. (2.16) because the solution has support on a set of measure zero inside the closure of the amplituhedron, signalling that there is no discontinuity around the branch cut associated to the cut conditions shown in eq. (2.11). Therefore we never needed to inquire as to the actual location where the corresponding branch point might have been. To learn about the *location* of a branch point we have to solve also the second type of Landau equations (2.10). Indeed (2.51) does correspond to a branch point that lies outside

the positive domain, but we don't discard it because the discontinuity of the amplitude around this branch point is nonzero. As mentioned above, according to the Cutkosky rules it would be computed by an integral over the line segment between Z_{i-1} and Z_i in figure 2.5a. When branch points lie outside $G_+(4, n)$, as in this case, it signals a discontinuity that does not exist on the physical sheet but on some other sheet; see the comments near the end of section 1.

Additional (sub^k-leading, for various k) Landau singularities are exposed by setting various sets of α 's to zero in the Landau equations and relaxing the associated cut conditions. Although these precise configurations were not analyzed in [16], the results of that paper, together with some very useful tricks reviewed in appendix A, are easily used to reveal branch points at the loci

$$\langle j(j-1, j+1)(k, k\pm 1)(i-1, i) \rangle = 0 \quad (2.53)$$

together with the same for $j \leftrightarrow k$, as well as $\langle a a+1 b b+1 \rangle = 0$ for a, b drawn from the set $\{i-1, j-1, j, k-1, k\}$.

The pentagon-triangle. With the help of appendix A and the results of [16] it is easily seen that the leading singularity of the pentagon-triangle shown in figure 2.6b is located on the locus where

$$\langle i\bar{j} \rangle \langle \bar{i}j \rangle = 0. \quad (2.54)$$

The computation of additional singularities essentially reduces to the same calculation for a three-mass pentagon, which was carried out in [16]. Altogether we find that branch

points live on the loci

$$\begin{aligned}
\langle i j k-1 k \rangle &= 0, \\
\langle i(i-1 i+1)(j-1 j)(k-1 k) \rangle &= 0, \\
\langle i(i-1 i+1)(j j+1)(k-1 k) \rangle &= 0, \\
\langle j(j-1 j+1)(i-1 i)(k-1 k) \rangle &= 0, \\
\langle j(j-1 j+1)(i i+1)(k-1 k) \rangle &= 0, \\
\langle i i \pm 1 j k \rangle &= 0, \\
\langle i j j \pm 1 k \rangle &= 0,
\end{aligned} \tag{2.55}$$

together with the same collection with $(k-1 k) \rightarrow (k k+1)$, as well as all $\langle a a+1 b b+1 \rangle = 0$ for a, b drawn from the set $\{i-1, i, j-1, j, k-1, k\}$.

The maximum codimension boundaries. We left this case for last because it is somewhat more subtle. It is known that the final entries of the symbols of MHV amplitudes always have the form $\langle a \bar{b} \rangle$ [60]. We expect the leading Landau singularity of the maximum codimension boundary to expose branch points at the vanishing loci of these final entries.

However, if we naively solve the Landau equations for the diagram shown in 2.3b, we run into a puzzle. The first type of Landau equations (2.9) correspond to the nine cut conditions (2.34)–(2.36), which of course are satisfied by $\mathcal{L}^{(1)} = (ij)$ and $\mathcal{L}^{(2)} = (ik)$. The second type of Landau equations (2.10) does not impose any constraints for pentagons because it is always possible to find a vanishing linear combination of the five participating four-vectors. This naive Landau analysis therefore suggests that there is no leading branch point associated to the maximum codimension boundary.

This analysis is questionable because, as already noted above, the Landau diagram associated to the maximal codimension boundary, shown in figure (2.2b), does not have the form of a valid Feynman diagram. Therefore it makes little sense to trust the associated Landau analysis. Instead let us note that the nine cut conditions (2.34)–(2.36) are

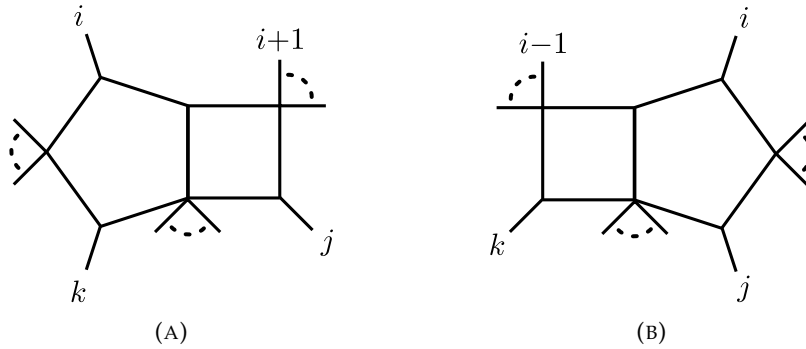


FIGURE 2.7: Landau diagrams corresponding to all of the cut conditions (2.34)–(2.36) except for (a) $\langle \mathcal{L}^{(1)} i-1 i \rangle = 0$, and (b) $\langle \mathcal{L}^{(2)} i i+1 \rangle = 0$. These are the only two cut conditions that are redundant (each is implied by the other eight, for generic kinematics) and, when omitted, lead to Landau diagrams that have the form of a standard Feynman integral. (In both figures $\mathcal{L}^{(1)}$ is the momentum in the right loop and $\mathcal{L}^{(2)}$ is the momentum in the left loop.)

not independent; indeed they cannot be as there are only eight degrees of freedom in the loop momenta.

We are therefore motivated to identify which of the nine cut conditions (1) is redundant, in the sense that it is implied by the other eight for generic external kinematics, and (2) has the property that when omitted, the Landau diagram for the remaining eight takes the form of a valid planar Feynman diagram. None of the conditions involving j and k shown in eq. (2.35) are redundant; all of them must be imposed to stay on the maximum codimension boundary. The remaining five conditions in eqs. (2.34) and (2.36) are redundant for general kinematics, but only two of them satisfy the second property. The corresponding Landau diagrams are shown in fig. 2.7. Being valid planar Feynman diagrams, the integrand definitely receives contributions with these topologies (unlike fig. 2.2b), and will exhibit the associated Landau singularities.

It remains to compute the location of the leading Landau singularities for these diagrams. For fig. 2.7a the on-shell conditions for the pentagon set $\mathcal{L}^{(2)} = (ik)$ while the Kirkhoff condition for the box is

$$0 = \langle j(j-1 j+1) \mathcal{L}^{(2)}(i i+1) \rangle = \langle i \bar{j} \rangle \langle i i+1 j k \rangle. \quad (2.56)$$

The Landau equations associated to this topology therefore have solutions when $\langle i \bar{j} \rangle =$

0 or when $\langle ii+1jk \rangle = 0$. However, on the locus $\langle ii+1jk \rangle = 0$ it is no longer true that the eight on-shell conditions shown in fig. 2.7a imply the ninth condition $\langle \mathcal{L}^{(1)} i-1i \rangle = 0$. Therefore, this solution of the Landau equations is not relevant to the maximum codimension boundary.

We conclude that the leading Landau singularity of the maximum codimension boundary is located on the locus where $\langle i\bar{j} \rangle = 0$ or (from fig. 2.7b) $\langle i\bar{k} \rangle = 0$. These results are in agreement with our expectation about the final symbol entries of MHV amplitudes [60]. Relaxations of Figures 7a, 7b at j, k will not produce any symbol entries.

Conclusion. In conclusion, our analysis has revealed that two-loop MHV amplitudes have physical branch points on the loci of the form

$$\begin{aligned}
 \langle a\bar{b} \rangle &= 0, \\
 \langle abc c+1 \rangle &= 0, \\
 \langle a a+1\bar{b} \cap \bar{c} \rangle &= 0, \\
 \langle a(a-1 a+1)(b b+1)(c c+1) \rangle &= 0,
 \end{aligned} \tag{2.57}$$

for arbitrary indices a, b, c . Again let us note that when we say there is a branch point at $x = 0$, we mean a branch cut between $x = 0$ and $x = \infty$. Indeed, this result is in precise accord with the known symbol alphabet of two-loop MHV amplitudes in SYM theory [60].

2.4 Discussion

In this paper we have improved greatly on the analysis of [16] by asking the amplituhedron directly to tell us which branch points of an amplitude are physical. This analysis requires no detailed knowledge about how to write formulas for integrands by constructing the canonical “volume” form on the amplituhedron. We only used the amplituhedron’s grossest feature, which is that it is designed to guarantee that integrands

have no poles outside the space of positive loop configurations. We have shown in several examples how to use this principle to completely classify the sets of cut conditions on which integrands can possibly have support. Let us emphasize that our proposal is a completely well-defined geometric algorithm:

- Input: a list of the maximal codimension boundaries of the amplituhedron; for MHV amplitudes these are known from [5].
- Step 1: For a given maximal codimension boundary, identify the list of all cut conditions satisfied on this boundary. For example, at the two-loop boundary shown in figure 2.3a, these would be the nine cut conditions satisfied by the Landau diagram in figure 2.3b, shown in eqs. (2.34)–(2.36). Consider all lower codimension boundaries that can be obtained by relaxing various subsets of these cut conditions, and eliminate those which do not overlap the closure of the amplituhedron, i.e. those which do not correspond to mutually non-negative configurations of lines $\mathcal{L}^{(\ell)}$.
- Step 2: For each valid set of cut conditions obtained in this manner, solve the corresponding Landau equations (2.9) and (2.10) to determine the location of the corresponding branch point of the amplitude.
- Output: a list of the loci in external kinematic space where the given amplitude has branch points.

As we have mentioned a few times in the text, this algorithm is motivated by intuition from the Cutkosky rules, according to which an amplitude’s discontinuity is computed by replacing some set of propagators with delta-functions. This localizes the integral onto the intersection of the physical contour and the locus where the cut conditions are satisfied. Now is the time to confess that this intuitive motivation is not a proof of our algorithm, most notably because the positive kinematic domain lives in unphysical $(2, 2)$ signature and there is no understanding of how to make sense of the physical $i\epsilon$ contour in momentum twistor space (see however [64] for work in this direction). Nevertheless, the prescription works and it warrants serious further study, in part

because it would be very useful to classify the possible branch points of more general amplitudes in SYM theory.

For amplitudes belonging to the class of generalized polylogarithm functions (which is believed to contain at least all MHV, NMHV and NNMHV amplitudes in SYM theory) the path from knowledge of branch points to amplitudes is fairly well-trodden. Such functions can be represented as iterated integrals [65] and analyzed using the technology of symbols and coproducts [66, 67]. It was emphasized in [23] that the analytic structure of an amplitude is directly imprinted on its symbol alphabet. In particular, the locus in external kinematic space where the letters of an amplitude's symbols vanish (or diverge) must exactly correspond to the locus where solutions of the Landau equations exist. The above algorithm therefore provides direct information about the zero locus of an amplitude's symbol alphabet. For example, the symbol alphabet of one-loop MHV amplitudes must vanish on the locus (2.33), and that of two-loop amplitudes must vanish on the locus (2.57). Strictly speaking this analysis does not allow one to actually determine symbol letters away from their vanishing locus, but it is encouraging that in both eqs. (2.33) and (2.57) the amplituhedron analysis naturally provides the correct symbol letters on the nose.

In general we expect that only letters of the type $\langle a a+1 b b+1 \rangle$ may appear in the first entry of the symbol of any amplitude [68]. At one loop, new letters of the type $\langle a \bar{b} \rangle$ begin to appear in the second entry. At two loops, additional new letters of the type $\langle a (a-1 a+1)(b b+1)(c c+1) \rangle$ also begin to appear in the second entry, and new letters of the type $\langle a b c c+1 \rangle$ and $\langle a a+1 \bar{b} \cap \bar{c} \rangle$ begin to appear in the third. As discussed at the end of section 3, the final entries of MHV amplitudes are always $\langle a \bar{b} \rangle$ [60]. In our paper we have given almost no thought to the question of where in the symbol a given type of letter may begin to appear. However, it seems clear that our geometric algorithm can be taken much further to expose this stratification of branch points, since the relationship between boundaries of the amplituhedron and Landau singularities is the same as the relationship between discontinuities and their branch points. For example it is clear that at any loop order, the lowest codimension boundaries of the

amplituhedron that give rise to branch cuts are configurations where one of the lines \mathcal{L} intersects two lines $(ii+1)$ and $(jj+1)$, with all other lines lying in generic mutually positive position. These configurations give rise to the expected first symbol entries $\langle ii+1 jj+1 \rangle$. By systematically following the degeneration of configurations of lines onto boundaries of higher and higher codimension we expect there should be a way to derive the symbol alphabet of an amplitude entry by entry.

In many examples, mere knowledge of an amplitude's symbol alphabet, together with some other physical principles, has allowed explicit formulas for the amplitude to be constructed via a bootstrap approach. This approach has been particularly powerful for 6- [69, 70, 71, 72, 73, 20], and 7-point [21] amplitudes, in which case the symbol alphabet is believed to be given, to all loop order, by the set of cluster coordinates on the kinematic configuration space [18]. It would be very interesting to use the algorithm outlined above to prove this conjecture, or to glean information about symbol alphabets for more general amplitudes, both MHV and non-MHV. One simple observation we can make in parting is to note that although maximum codimension boundaries of the L -loop MHV amplitude involve as many as $2L$ distinct points, the singularities that arise from genuinely L -loop configurations (rather than products of lower loop order) involve at most $L + 1$ points. Therefore we predict that the size of the symbol alphabet of L -loop MHV amplitudes should grow with n no faster than $\mathcal{O}(n^{L+1})$.

It would be very interesting to extend our results to non-MHV amplitudes. For the N^K amplitude, singularities should still be found only on the boundary of the N^K MHV amplituhedron, so the presented approach should still be applicable, albeit more complicated. An important difference would be the existence of poles, in addition to branch points, due to the presence of rational prefactors. We are not certain our approach would naturally distinguish these two types of singularities. However, the singularities of rational prefactors can be found using other means, for example by considering the boundaries of the tree-level amplituhedron.

2.5 Elimination of Bubbles and Triangles

Here we collect a few comments on the elimination of bubble and triangle sub-diagrams in the Landau analysis. These tricks, together with the results of [16], can be used to easily obtain all of the Landau singularities reported in section 2.3.3.

2.5.1 Bubble sub-diagrams

The Landau equation for a bubble with propagators ℓ and $\ell + p$, which may be a sub-diagram of a larger diagram, are

$$\ell^2 = (\ell + p)^2 = 0, \quad (2.58)$$

$$\alpha_1 \ell^\mu + \alpha_2 (\ell + p)^\mu = 0, \quad (2.59)$$

where α_1 and α_2 are the Feynman parameters associated to the two propagators. The loop equation has solution

$$\ell^\mu = -\frac{\alpha_2}{\alpha_1 + \alpha_2} p^\mu \quad (2.60)$$

so that

$$\alpha_1 \ell^\mu = -\frac{\alpha_1 \alpha_2}{\alpha_1 + \alpha_2} p^\mu, \quad \alpha_2 (\ell + p)^\mu = \frac{\alpha_1 \alpha_2}{\alpha_1 + \alpha_2} p^\mu, \quad (2.61)$$

while the on-shell conditions simply impose $p^2 = 0$. Therefore, we see that any Landau diagram containing this bubble sub-diagram is equivalent to the same diagram with the bubble replaced by a single on-shell line with momentum p^μ and modified Feynman parameter $\alpha' = \alpha_1 \alpha_2 / (\alpha_1 + \alpha_2)$. We do not need to keep track of the modified Feynman parameter; we simply move on to the rest of the diagram using the new Feynman parameter α' .

In conclusion, any bubble sub-diagram can be collapsed to a single edge, as far as the Landau analysis is concerned.

2.5.2 Triangle sub-diagrams

Similarly, we will now discuss the various branches associated to a triangle sub-diagram. The Landau equations for a triangle with edges carrying momenta $q_1 = \ell$, $q_2 = \ell + p_1 + p_2$ and $q_3 = \ell + p_2$, and with corresponding Feynman parameters α_1 , α_2 and α_3 , are

$$\ell^2 = (\ell + p_2)^2 = (\ell + p_1 + p_2)^2 = 0, \quad (2.62)$$

$$\alpha_1 \ell^\mu + \alpha_2 (\ell + p_1 + p_2)^\mu + \alpha_3 (\ell + p_2)^\mu = 0. \quad (2.63)$$

The solution to the loop equation is

$$\ell^\mu = -\frac{(\alpha_2 + \alpha_3)p_2^\mu + \alpha_2 p_1^\mu}{\alpha_1 + \alpha_2 + \alpha_3} \quad (2.64)$$

while eqs. (4.1) impose the two conditions

$$0 = p_1^2 p_2^2 p_3^2, \quad (2.65)$$

$$(\alpha_1 : \alpha_2 : \alpha_3) = (p_1^2(-p_1^2 + p_2^2 + p_3^2) : p_2^2(p_1^2 - p_2^2 + p_3^2) : p_3^2(p_1^2 + p_2^2 - p_3^2)) \quad (2.66)$$

where $p_3 = -p_1 - p_2$. Suppose we follow the branch $p_1^2 = 0$. In this case α_1 is forced to vanish, effectively reducing the triangle to a bubble with edges

$$\alpha_2 q_2^\mu = \frac{\alpha_3 p_2^2}{p_2^2 - p_3^2} p_1^\mu, \quad \alpha_3 q_3^\mu = -\frac{\alpha_3 p_2^2}{p_2^2 - p_3^2} p_1^\mu. \quad (2.67)$$

This is equivalent (by appendix A.1) to a single on-shell line carrying momentum p_1^μ . A similar conclusion clearly holds for the branches $p_2^2 = 0$ or $p_3^2 = 0$. If any two of p_1^2 , p_2^2 or p_3^2 simultaneously vanish, then the two corresponding Feynman parameters must vanish. Finally, if all three p_i^2 vanish, then the Landau equations are identically satisfied for any values of the three α_i . In conclusion, triangle sub-diagrams of a general Landau diagram can be analyzed by considering separately each of the seven branches outlined here.

Chapter 3

All-Helicity Symbol Alphabets from Unwound Amplituhedra

3.1 Review

This section provides a thorough introduction to the problem our work aims to solve. The concepts and techniques reviewed here will be illuminated in subsequent sections via several concrete examples.

3.1.1 The Kinematic Domain

Scattering amplitudes are (in general multivalued) functions of the kinematic data (the energies and momenta) describing some number of particles participating in some scattering process. Specifically, amplitudes are functions only of the kinematic information about the particles entering and exiting the process, called *external data* in order to distinguish it from information about virtual particles which may be created and destroyed during the scattering process itself. A general scattering amplitude in SYM theory is labeled by three integers: the number of particles n , the helicity sector $0 \leq k \leq n - 4$, and the loop order $L \geq 0$, with $L = 0$ called *tree level* and $L > 0$ called *L-loop level*. Amplitudes with $k = 0$ are called maximally helicity violating (MHV) while those with $k > 0$ are called (next-to-)^kmaximally helicity violating (N^k MHV).

The kinematic configuration space of SYM theory admits a particularly simple characterization: n -particle scattering amplitudes¹ are multivalued functions on $\text{Conf}_n(\mathbb{P}^3)$, the space of configurations of n points in \mathbb{P}^3 [18]. A generic point in $\text{Conf}_n(\mathbb{P}^3)$ may be represented by a collection of n homogeneous coordinates Z_a^I on \mathbb{P}^3 (here $I \in \{1, \dots, 4\}$ and $a \in \{1, \dots, n\}$) called *momentum twistors* [55], with two such collections considered equivalent if the corresponding $4 \times n$ matrices $Z \equiv (Z_1 \cdots Z_n)$ differ by left-multiplication by an element of $\text{GL}(4)$. We use the standard notation

$$\langle a b c d \rangle = \epsilon_{IJKL} Z_a^I Z_b^J Z_c^K Z_d^L \quad (3.1)$$

for the natural $\text{SL}(4)$ -invariant four-bracket on momentum twistors and use the shorthand $\langle \cdots \bar{a} \cdots \rangle = \langle \cdots a-1 a a+1 \cdots \rangle$, with the understanding that all particle labels are always taken mod n . We write (ab) to denote the line in \mathbb{P}^3 containing Z_a and Z_b , (abc) to denote the plane containing Z_a, Z_b and Z_c , and so \bar{a} denotes the plane $(a-1 a a+1)$. The bar notation is motivated by *parity*, which is a \mathbb{Z}_2 symmetry of SYM theory that maps $N^k\text{MHV}$ amplitudes to $N^{n-k-4}\text{MHV}$ amplitudes while mapping the momentum twistors according to $\{Z_a\} \mapsto \{W_a = *(a-1 a a+1)\}$.

When discussing $N^k\text{MHV}$ amplitudes it is conventional to consider an enlarged kinematic space where the momentum twistors are promoted to homogeneous coordinates \mathcal{Z}_a , bosonized momentum twistors [4] on \mathbb{P}^{k+3} which assemble into an $n \times (k+4)$ matrix $\mathcal{Z} \equiv (\mathcal{Z}_1 \cdots \mathcal{Z}_n)$. The analog of Eq. (3.1) is then the $\text{SL}(k+4)$ -invariant bracket which we denote by $[\cdot]$ instead of $\langle \cdot \rangle$. Given some \mathcal{Z} and an element of the Grassmannian $\text{Gr}(k, k+4)$ represented by a $k \times (k+4)$ matrix Y , one can obtain an element of $\text{Conf}_n(\mathbb{P}^3)$ by projecting onto the complement of Y . The four-brackets of the *projected external data* obtained in this way are given by

$$\langle a b c d \rangle \equiv [Y \mathcal{Z}_a \mathcal{Z}_b \mathcal{Z}_c \mathcal{Z}_d]. \quad (3.2)$$

¹Here and in all that follows, we mean components of superamplitudes suitably normalized by dividing out the tree-level Parke-Taylor-Nair superamplitude [57, 74]. We expect our results to apply equally well to BDS- [63] and BDS-like [75] regulated MHV and non-MHV amplitudes. The set of branch points of a non-MHV ratio function [76] should be a subset of those of the corresponding non-MHV amplitude, but our analysis cannot exclude the possibility that it may be a proper subset due to cancellations.

Tree-level amplitudes are rational functions of the brackets while loop-level amplitudes have both poles and branch cuts, and are properly defined on an infinitely-sheeted cover of $\text{Conf}_n(\mathbb{P}^3)$. For each k there exists an open set $\mathcal{D}_{n,k} \subset \text{Conf}_n(\mathbb{P}^3)$ called the *principal domain* on which amplitudes are known to be holomorphic and non-singular. Amplitudes are initially defined only on $\mathcal{D}_{n,k}$ and then extended to all of (the appropriate cover of) $\text{Conf}_n(\mathbb{P}^3)$ by analytic continuation.

A simple characterization of the principal domain for n -particle $N^k\text{MHV}$ amplitudes was given in [37]: $\mathcal{D}_{n,k}$ may be defined as the set of points in $\text{Conf}_n(\mathbb{P}^3)$ that can be represented by a Z -matrix with the properties

1. $\langle a a+1 b b+1 \rangle > 0$ for all a and $b \notin \{a-1, a, a+1\}$ ², and
2. the sequence $\langle 1 2 3 \bullet \rangle$ has precisely k sign flips,

where we use the notation $\bullet \in \{1, 2, \dots, n\}$ so that

$$\langle 1 2 3 \bullet \rangle \equiv \{0, 0, 0, \langle 1 2 3 4 \rangle, \langle 1 2 3 5 \rangle, \dots, \langle 1 2 3 n \rangle\}. \quad (3.3)$$

It was also shown that an alternate but equivalent condition is to say that the sequence $\langle a a+1 b \bullet \rangle$ has precisely k sign flips for all a, b (omitting trivial zeros, and taking appropriate account of the twisted cyclic symmetry where necessary). The authors of [37] showed, and we review in Sec. 3.1.2, that for Y 's inside an $N^k\text{MHV}$ amplituhedron, the projected external data have the two properties above.

3.1.2 Amplituhedra ...

A matrix is said to be *positive* or *non-negative* if all of its ordered maximal minors are positive or non-negative, respectively. In particular, we say that the external data are positive if the $n \times (k+4)$ matrix \mathcal{Z} described in the previous section is positive.

A point in the n -particle $N^k\text{MHV}$ L -loop *amplituhedron* $\mathcal{A}_{n,k,L}$ is a collection $(Y, \mathcal{L}^{(\ell)})$ consisting of a point $Y \in \text{Gr}(k, k+4)$ and L lines $\mathcal{L}^{(1)}, \dots, \mathcal{L}^{(L)}$ (called the *loop momenta*)

²As explained in [37], the cyclic symmetry on the n particle labels is “twisted”, which manifests itself here in the fact that if k is even, and if $a = n$ or $b = n$, then cycling around n back to 1 introduces an extra minus sign. The condition in these cases is therefore $(-1)^{k+1} \langle c c+1 n 1 \rangle > 0$ for all $c \notin \{1, n-1, n\}$.

in the four-dimensional complement of Y . We represent each $\mathcal{L}^{(\ell)}$ as a $2 \times (k+4)$ matrix with the understanding that these are representatives of equivalence classes under the equivalence relation that identifies any linear combination of the rows of Y with zero.

For given positive external data \mathcal{Z} , the amplituhedron $\mathcal{A}_{n,k,L}(\mathcal{Z})$ was defined in [4] for $n \geq 4$ as the set of $(Y, \mathcal{L}^{(\ell)})$ that can be represented as

$$Y = C\mathcal{Z}, \quad (3.4)$$

$$\mathcal{L}^{(\ell)} = D^{(\ell)}\mathcal{Z}, \quad (3.5)$$

in terms of a $k \times n$ real matrix C and L $2 \times n$ real matrices $D^{(\ell)}$ satisfying the positivity property that for any $0 \leq m \leq L$, all $(2m+k) \times n$ matrices of the form

$$\begin{pmatrix} D^{(i_1)} \\ D^{(i_2)} \\ \vdots \\ D^{(i_m)} \\ C \end{pmatrix} \quad (3.6)$$

are positive. The D -matrices are understood as representatives of equivalence classes and are defined only up to translations by linear combinations of rows of the C -matrix.

One of the main results of [37] was that amplituhedra can be characterized directly by (projected) four-brackets, Eq. (3.2), without any reference to C or $D^{(\ell)}$'s, by saying that for given positive \mathcal{Z} , a collection $(Y, \mathcal{L}^{(\ell)})$ lies inside $\mathcal{A}_{n,k,L}(\mathcal{Z})$ if and only if

1. the projected external data lie in the principal domain $\mathcal{D}_{n,k}$,
2. $\langle \mathcal{L}^{(\ell)} a a+1 \rangle > 0$ for all ℓ and a^3 ,
3. for each ℓ , the sequence $\langle \mathcal{L}^{(\ell)} 1 \bullet \rangle$ has precisely $k+2$ sign flips, and
4. $\langle \mathcal{L}^{(\ell_1)} \mathcal{L}^{(\ell_2)} \rangle > 0$ for all $\ell_1 \neq \ell_2$.

³Again, the twisted cyclic symmetry implies that the correct condition for the case $a = n$ is $(-1)^{k+1} \langle \mathcal{L}^{(\ell)} n 1 \rangle > 0$.

Here the notation $\langle \mathcal{L} a b \rangle$ means $\langle A B a b \rangle$ if the line \mathcal{L} is represented as $(A B)$ for two points A, B . It was also shown that items 2 and 3 above are equivalent to saying that the sequence $\langle \mathcal{L}^{(\ell)} a \bullet \rangle$ has precisely $k + 2$ sign flips for any ℓ and a .

3.1.3 ... and their Boundaries

The amplituhedron $\mathcal{A}_{n,k,L}$ is an open set with boundaries at loci where one or more of the inequalities in the above definitions become saturated. For example, there are boundaries where Y becomes such that one or more of the projected four-brackets $\langle a a+1 b b+1 \rangle$ become zero. Such projected external data lie on a boundary of the principal domain $\mathcal{D}_{n,k}$. Boundaries of this type are already present in tree-level amplituhedra, which are well-understood and complementary to the focus of our work.

Instead, the boundaries relevant to our analysis occur when Y is such that the projected external data are generic, but the $\mathcal{L}^{(\ell)}$ satisfy one or more *on-shell conditions* of the form

$$\langle \mathcal{L}^{(\ell)} a a+1 \rangle = 0 \quad \text{and/or} \quad \langle \mathcal{L}^{(\ell_1)} \mathcal{L}^{(\ell_2)} \rangle = 0. \quad (3.7)$$

We refer to boundaries of this type as \mathcal{L} -boundaries⁴. The collection of loop momenta satisfying a given set of on-shell conditions comprises a set whose connected components we call *branches*. Consider two sets of on-shell conditions S, S' , with $S' \subset S$ a proper subset, and $B (B')$ a branch of solutions to $S (S')$. Since $S' \subset S$, B' imposes fewer constraints on the degrees of freedom of the loop momenta than B does. In the case when $B \subset B'$, we say B' is a *relaxation* of B . We use $\overline{\mathcal{A}_{n,k,L}}$ to denote the closure of the amplituhedron, consisting of $\mathcal{A}_{n,k,L}$ together with all of its boundaries. We say that $\mathcal{A}_{n,k,L}$ has a *boundary of type B* if $B \cap \overline{\mathcal{A}_{n,k,L}} \neq \emptyset$ and $\dim(B \cap \overline{\mathcal{A}_{n,k,L}}) = \dim(B)$.

3.1.4 The Landau Equations

In [17] it was argued, based on well-known and general properties of scattering amplitudes in quantum field theory (see in particular [27]), that all information about the

⁴In the sequel [47] we will strengthen this definition to require that $\langle \mathcal{L}^{(1)} \mathcal{L}^{(2)} \rangle = 0$ at two loops.

locations of branch points of amplitudes in SYM theory can be extracted from knowledge of the \mathcal{L} -boundaries of amplituhedra via the Landau equations [26, 33]. In order to formulate the Landau equations we must parameterize the space of loop momenta in terms of $4L$ variables d_A . For example, we could take⁵ $\mathcal{L}^{(\ell)} = D^{(\ell)} \mathcal{Z}$ with

$$D^{(1)} = \begin{pmatrix} 1 & 0 & d_1 & d_2 \\ 0 & 1 & d_3 & d_4 \end{pmatrix}, \quad D^{(2)} = \begin{pmatrix} 1 & 0 & d_5 & d_6 \\ 0 & 1 & d_7 & d_8 \end{pmatrix}, \quad \text{etc.}, \quad (3.8)$$

but any other parameterization works just as well.

Consider now an \mathcal{L} -boundary of some $\mathcal{A}_{n,k,L}$ on which the L lines $\mathcal{L}^{(\ell)}$ satisfy d -on-shell constraints

$$f_J = 0 \quad (J = 1, 2, \dots, d), \quad (3.9)$$

each of which is of the form of one of the brackets shown in Eq. (3.7). The *Landau equations* for this set of on-shell constraints comprise Eq. (3.9) together with a set of equations on d auxiliary variables α_J known as *Feynman parameters*:

$$\sum_{J=1}^d \alpha_J \frac{\partial f_J}{\partial d_A} = 0 \quad (A = 1, \dots, 4L). \quad (3.10)$$

The latter set of equations are sometimes referred to as the *Kirchhoff conditions*.

We are never interested in the values of the Feynman parameters, we only want to know under what conditions nontrivial solutions to Landau equations exist. Here, “nontrivial” means that the α_J must not all vanish⁶. Altogether we have $d + 4L$ equations in $d + 4L$ variables (the d α_J ’s and the $4L$ d_A ’s). However, the Kirchhoff conditions are clearly invariant under a projective transformation that multiplies all of the α_J simultaneously by a common nonzero number, so the effective number of free parameters is

⁵By writing each \mathcal{L} as a 2×4 matrix, instead of $2 \times (k+4)$, we mean to imply that we are effectively working in a gauge where the last four columns of Y are zero and so the first k columns of each \mathcal{L} are irrelevant and do not need to be displayed.

⁶Solutions for which some of the Feynman parameters vanish are often called “subleading” Landau singularities in the literature, in contrast to a “leading” Landau singularity for which all α ’s are nonzero. We will make no use of this terminology and pay no attention to the values of the α ’s other than ensuring they do not all vanish.

only $d + 4L - 1$. Therefore, we might expect that nontrivial solutions to the Landau equations do not generically exist, but that they may exist on codimension-one loci in $\text{Conf}_n(\mathbb{P}^3)$ — these are the loci on which the associated scattering amplitude may have a singularity according to [26, 33].

However the structure of solutions is rather richer than this naive expectation suggests because the equations are typically polynomial rather than linear, and they may not always be algebraically independent. As we will see in the examples considered in Sec. 3.5, it is common for nontrivial solutions to exist for generic projected external data⁷, and it can happen that there are branches of solutions that exist only on loci of codimension higher than one. We will not keep track of solutions of either of these types since they do not correspond to branch points in the space of generic projected external data.

There are two important points about our procedure which were encountered in [17] and deserve to be emphasized. The first is a subtlety that arises from the fact that the on-shell conditions satisfied on a given boundary of some amplituhedron are not always independent. For example, the end of Sec. 3 of [17] discusses a boundary of $\mathcal{A}_{n,0,2}$ described by nine on-shell conditions with the property that the ninth is implied by the other eight. This situation arises generically for $L > 1$, and a procedure — called *resolution* — for dealing with these cases was proposed in [17]. We postpone further discussion of this point to the sequel as this paper focuses only on one-loop examples.

Second, there is a fundamental asymmetry between the two types of Landau equations, (3.9) and (3.10), in two respects. When solving the on-shell conditions we are only interested in branches of solutions that (A1) exist for generic projected external data, and that (A2) have nonempty intersection with $\overline{\mathcal{A}_{n,k,L}}$ with correct dimension. In contrast, when further imposing the Kirchhoff constraints on these branches, we are interested in solutions that (B1) exist on codimension-one loci in $\text{Conf}_n(\mathbb{P}^3)$, and (B2) need not

⁷Solutions of this type were associated with infrared singularities in [16]. We do not keep track of these solutions since the infrared structure of amplitudes in massless gauge theory is understood to all loop order based on exponentiation [77, 63]. However, if some set of Landau equations has an “IR solution” at some particular $\mathcal{L}^{(\ell)}$, there may be other solutions, at different values of $\mathcal{L}^{(\ell)}$, that exist only on loci of codimension one. In such cases we do need to keep track of the latter.

remain within $\overline{\mathcal{A}_{n,k,L}}$. The origin of this asymmetry was discussed in [17]. In brief, it arises from Cutkoskian intuition whereby singularities of an amplitude may arise from configurations of loop momenta that are outside the physical domain of integration (by virtue of being complex; or, in the current context, being outside the closure of the amplituhedron), and are only accessible after analytic continuation to some higher sheet; whereas the monodromy of an amplitude around a singularity is computed by an integral over the physical domain with the cut propagators replaced by delta functions. The resulting monodromy will be zero, i.e. the branch point doesn't really exist, if there is no overlap between the physical domain and the locus where the cuts are satisfied, motivating (A2) above. In summary, it is important to "solve the on-shell conditions first" and then impose the Kirchhoff conditions on the appropriate branches of solutions only afterwards.

3.1.5 Summary: The Algorithm

The Landau equations may be interpreted as defining a map which associates to each boundary of the amplituhedron $\mathcal{A}_{n,k,L}$ a locus in $\text{Conf}_n(\mathbb{P}^3)$ on which the corresponding n -point $N^k\text{MHV}$ L -loop amplitude has a singularity. The Landau equations themselves have no way to indicate whether a singularity is a pole or branch point. However, it is expected that all poles in SYM theory arise from boundaries that are present already in the tree-level amplituhedra [4]. These occur when some $\langle a+1 \ b+1 \rangle$ go to zero as discussed at the beginning of Sec. 3.1.3. The aim of our work is to understand the loci where amplitudes have branch points, so we confine our attention to the \mathcal{L} -boundaries defined in that section.

The algorithm for finding all branch points of the n -particle $N^k\text{MHV}$ L -loop amplitude is therefore simple in principle:

1. Enumerate all \mathcal{L} -boundaries of $\mathcal{A}_{n,k,L}$ for generic projected external data.
2. For each \mathcal{L} -boundary, identify the codimension-one loci (if there are any) in $\text{Conf}_n(\mathbb{P}^3)$ on which the corresponding Landau equations admit nontrivial solutions.

However, it remains a difficult and important outstanding problem to fully characterize the boundaries of general amplituhedra. In the remainder of this paper we focus on the special case $L = 1$, since all \mathcal{L} -boundaries of $\mathcal{A}_{n,k,1}$ (which have been discussed extensively in [10]) may be enumerated directly for any given n :

- 1(a). Start with a list of all possible sets of on-shell conditions of the form $\langle \mathcal{L} a a+1 \rangle = 0$.
- 1(b). For each such set, identify all branches of solutions that exist for generic projected external data.
- 1(c). For each such branch B , determine the values of k for which $\mathcal{A}_{n,k,1}$ has a boundary of type B .

It would be enormously inefficient to carry out this simple-minded algorithm beyond one loop. Fortunately, we will see in the sequel that the one-loop results of this paper can be exploited very effectively to generate \mathcal{L} -boundaries of $L > 1$ amplituhedra.

3.2 One-Loop Branches

In this section we carry out steps 1(a) and 1(b) listed at the end of Sec. 3.1.5. To that end we first introduce a graphical notation for representing sets of on-shell conditions via *Landau diagrams*. Landau diagrams take the form of ordinary Feynman diagrams, with external lines labeled $1, \dots, n$ in cyclic order and one internal line (called a *propagator*) corresponding to each on-shell condition. Landau diagrams relevant to amplituhedra are always planar. Each internal face of an L -loop Landau diagram is labeled by a distinct $\ell \in \{1, \dots, L\}$, and each external face may be labeled by the pair $(a a+1)$ of external lines bounding that face.

The set of on-shell conditions encoded in a given Landau diagram is read off as follows:

- To each propagator bounding an internal face ℓ and an external face $(a a+1)$ we associate the on-shell condition $\langle \mathcal{L}^{(\ell)} a a+1 \rangle = 0$.

- To each propagator bounding two internal faces ℓ_1, ℓ_2 we associate the on-shell condition $\langle \mathcal{L}^{(\ell_1)} \mathcal{L}^{(\ell_2)} \rangle = 0$.

At one loop we only have on-shell conditions of the first type. Moreover, since \mathcal{L} only has four degrees of freedom (the dimension of $\text{Gr}(2,4)$ is four), solutions to a set of on-shell conditions will exist for generic projected external data only if the number of conditions is $d \leq 4$. Diagrams with $d = 1, 2, 3, 4$ are respectively named tadpoles, bubbles, triangles and boxes. The structure of solutions to a set of on-shell conditions can change significantly depending on how many pairs of conditions involve adjacent indices. Out of abundance of caution it is therefore necessary to consider separately the eleven distinct types of Landau diagrams shown in the second column of Tab. 3.1. For $d > 1$ their names are qualified by indicating the number of nodes with valence greater than three, called *masses*. These rules suffice to uniquely name each distinct type of diagram except the two two-mass boxes shown in Tab. 3.1 which are conventionally called “easy” and “hard”. This satisfies step 1(a) of the algorithm.

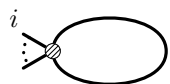


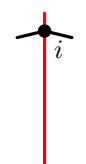
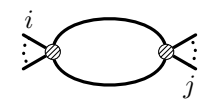

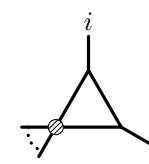
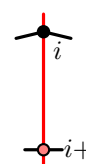
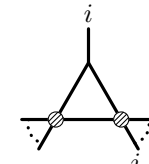
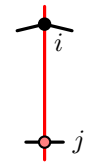
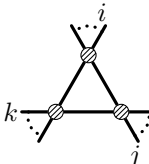
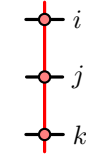
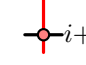
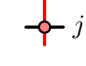
Proceeding now to step 1(b), we display in the third column of Tab. 3.1 all branches of solutions (as always, for generic projected external data) to the on-shell conditions associated to each Landau diagram. These expressions are easily checked by inspection or by a short calculation. More details and further discussion of the geometry of these problems can be found for example in [32]. The three-mass triangle solution involves the quantities

$$\begin{aligned} \rho(\alpha) &= -\alpha \langle i j+1 k k+1 \rangle - (1-\alpha) \langle i+1 j+1 k k+1 \rangle, \\ \sigma(\alpha) &= \alpha \langle i j k k+1 \rangle + (1-\alpha) \langle i+1 j k k+1 \rangle, \end{aligned} \tag{3.11}$$

and the four-mass box solution is sufficiently messy that we have chosen not to write it out explicitly.

Altogether there are nineteen distinct types of branches, which we have numbered (1) through (19) in Tab. 3.1 for ease of reference. The set of solutions to any set of on-shell conditions of the form $\langle \mathcal{L} a a+1 \rangle$ must be closed under parity, since each line $(a a+1)$ maps to itself. Most sets of on-shell conditions have two branches of solutions related

to each other by parity. Only the tadpole, two-mass bubble, and three-mass triangle (branches (1), (4), and (9) respectively) have single branches of solutions that are closed under parity.

tadpole ($n \geq 4$)		(1) $\mathcal{L} = (\alpha Z_i + (1-\alpha)Z_{i+1}, A)$	$0 \leq k \leq n-4$		0
one-mass bubble ($n \geq 4$)		(2) $\mathcal{L} = (Z_i, A)$	$0 \leq k \leq n-4$		0
two-mass bubble ($n \geq 4$)		(4) $\mathcal{L} = (\alpha Z_i + (1-\alpha)Z_{i+1},$ $\beta Z_j + (1-\beta)Z_{j+1})$	$0 \leq k \leq n-4$		$\langle ii+1 jj+1 \rangle$
one-mass triangle ($n \geq 4$)		(5) $\mathcal{L} = (Z_i, \alpha Z_{i+1} + (1-\alpha)Z_{i+2})$	$0 \leq k \leq n-4$		0
two-mass triangle ($n \geq 5$)		(7) $\mathcal{L} = (Z_i, \alpha Z_j + (1-\alpha)Z_{j+1})$	$0 \leq k \leq n-5$		0
three-mass triangle ($n \geq 6$)		(9) $\mathcal{L} = (\alpha Z_i + (1-\alpha)Z_{i+1},$ $\rho(\alpha)Z_j + \sigma(\alpha)Z_{j+1})$	$1 \leq k \leq n-5$		$f_{ij}f_{jk}f_{ki}$
		(6) $\mathcal{L} = (Z_{i+1}, \alpha Z_{i-1} + (1-\alpha)Z_i)$	$n-4 \geq k \geq 0$		
		(8) $\mathcal{L} = \bar{i} \cap (jj+1A)$	$n-4 \geq k \geq 1$		

Name	Landau Diagram	Branches	k-Validity	Low-k Twistor Diagram	Singularity Locus/Loci
one-mass box ($n \geq 5$)		(10) $\mathcal{L} = (ii+2)$ (11) $\mathcal{L} = \bar{i} \cap \bar{i+2}$	$0 \leq k \leq n-5$ $n-4 \geq k \geq 1$		$\langle \bar{i} \bar{i+2} \rangle \langle \bar{i} i+2 \rangle$
two-mass easy box ($n \geq 6$)		(12) $\mathcal{L} = (ij)$ (13) $\mathcal{L} = \bar{i} \cap \bar{j}$	$0 \leq k \leq n-6$ $n-4 \geq k \geq 2$		$\langle \bar{i} \bar{j} \rangle \langle \bar{i} j \rangle$
two-mass hard box ($n \geq 6$)		(14) $\mathcal{L} = \bar{i+1} \cap (ijj+1)$ (15) $\mathcal{L} = \bar{i} \cap (i+1jj+1)$	$1 \leq k \leq n-5$ $n-5 \geq k \geq 1$		$\langle \bar{i} i+2 \rangle \langle i i+1 jj+1 \rangle$
three-mass box ($n \geq 7$)		(16) $\mathcal{L} = (ijj+1) \cap (ikk+1)$ (17) $\mathcal{L} = (\bar{i} \cap (jj+1), \bar{i} \cap (kk+1))$	$1 \leq k \leq n-6$ $n-5 \geq k \geq 2$		$\langle i(i-1i+1)(jj+1)(kk+1) \rangle$
four-mass box ($n \geq 8$)		(18) $\mathcal{L} =$ (19) $\mathcal{L} =$ } see Tab. 2 of [78]	$2 \leq k \leq n-6$ $n-6 \geq k \geq 2$		$(f_{ij}f_{kl} - f_{ik}f_{jl} + f_{il}f_{jk})^2$ $-4f_{ij}f_{jk}f_{kl}f_{il} \equiv \Delta_{ijkl}$

which N⁺MHV amplituhedra have boundaries of each type; the twistor diagram depicting the low-k solution (or one low-k solution for the one-mass triangle and two-mass hard box); the loci in $\text{Conf}_n(\mathbb{P}^3)$ where the Landau equations for each branch admit nontrivial solutions (where the quantity in the last column vanishes). At one loop it happens that the loci are the same for each branch of solutions to a given set of on-shell conditions. Here α, β are arbitrary numbers, A is an arbitrary point in \mathbb{P}^3 , P is an arbitrary plane in \mathbb{P}^3 , $\rho(\alpha), \sigma(\alpha)$ are defined in Eq. (3.11), $f_{ab} \equiv \langle a a+1 b b+1 \rangle$, and $\langle i(i-1 i+1)(j j+1)(k k+1) \rangle \equiv \langle i-1 i j j+1 \rangle \langle i i+1 k k+1 \rangle - (j \leftrightarrow k)$.

3.3 One-Loop Boundaries

We now turn to the last step 1(c) from the end of Sec. 3.1.5: for each of the nineteen branches B listed in Tab. 3.1, we must determine the values of k for which $\mathcal{A}_{n,k,1}$ has a boundary of type B (defined in Sec. 3.1.3). The results of this analysis are listed in the fourth column of the Tab. 3.1. Our strategy for obtaining these results is two-fold.

In order to prove that an amplituhedron has a boundary of type B , it suffices to write down a pair of matrices C, D such that definitions (3.4) and (3.5) hold, C and $\begin{pmatrix} D \\ C \end{pmatrix}$ are both non-negative, and the external data projected through $Y = CZ$ are generic for generic positive Z . We call such a pair C, D a *valid configuration* for B . In the sections below we present explicit valid configurations for each of the nineteen branches. Initially we consider for each branch only the lowest value of k for which a valid configuration exists; in Sec. 3.3.7 we explain how to grow these to larger values of k and establish the upper bounds on k shown in Tab. 3.1.

However, in order to prove that an amplituhedron does not have a boundary of type B , it does not suffice to find a configuration that is not valid; one must show that no valid configuration exists. We address this problem in the next section.

3.3.1 A Criterion for Establishing Absent Branches

Fortunately, for \mathcal{L} -boundaries of the type under consideration there is a simple criterion for establishing when no valid configuration can exist. The crucial ingredient is that if $(Y, \mathcal{L}) \in \overline{\mathcal{A}_{n,k,1}}$ and $\langle \mathcal{L}^{a+1} \rangle = 0$ for some a , then $\langle \mathcal{L}^{a+2} \rangle$ must necessarily be non-positive⁸; the proof of this assertion, which we omit here, parallels that of a closely related statement proven in Sec. 6 of [37].

Consider now a line of the form $\mathcal{L} = (\alpha Z_a + \beta Z_{a+1}, A)$ for some point A and some parameters α, β which are not both vanishing. We will show that an \mathcal{L} of this form can lie in the closure of an amplituhedron only if $\mathcal{L} = (a+1)$ or $\alpha\beta \geq 0$.

⁸ Unless $a \in \{n-1, n\}$, when one must take into account the twisted cyclic symmetry. In all that follows we will for simplicity always assume that indices are outside of this range, which lets us uniformly ignore all sign factors that might arise from the twisted cyclic symmetry; these signs necessarily always conspire to ensure that all statements about amplitudes are \mathbb{Z}_n cyclically invariant.

First, as just noted, since $\langle \mathcal{L} a a+1 \rangle = 0$ we must have

$$0 \geq \langle \mathcal{L} a a+2 \rangle = \beta \langle a+1 A a a+2 \rangle. \quad (3.12)$$

On the other hand, as mentioned at the end of Sec. 3.1.2, we also have $\langle \mathcal{L} a a+1 \rangle \geq 0$ for all a . Applying this to $a+1$ gives

$$0 \leq \langle \mathcal{L} a+1 a+2 \rangle = \alpha \langle a A a+1 a+2 \rangle. \quad (3.13)$$

If $\langle a a+1 a+2 A \rangle \neq 0$, then the two inequalities (3.12) and (3.13) imply that $\alpha\beta \geq 0$.

This is the conclusion we wanted, but it remains to address what happens if $\langle a a+1 a+2 A \rangle = 0$. In this case \mathcal{L} lies in the plane $(a a+1 a+2)$ so we can take $\mathcal{L} = (\alpha Z_a + \beta Z_{a+1}, \gamma Z_{a+1} + \delta Z_{a+2})$. Then we have

$$\begin{aligned} 0 &\geq \langle \mathcal{L} a+1 a+3 \rangle = -\alpha\delta \langle a a+1 a+2 a+3 \rangle, \\ 0 &\leq \langle \mathcal{L} a-1 a \rangle = \beta\delta \langle a-1 a a+1 a+2 \rangle. \end{aligned} \quad (3.14)$$

Both of the four-brackets in these inequalities are positive (for generic projected external data) since they are of the form $\langle a a+1 b b+1 \rangle$, so we conclude that either $\delta = 0$, which means that $\mathcal{L} = (a a+1)$, or else we again have $\alpha\beta \geq 0$.

In conclusion, we have developed a robust test which establishes that

$$\mathcal{L} = (\alpha Z_a + \beta Z_{a+1}, A) \in \overline{\mathcal{A}_{n,k,1}} \text{ only if } \mathcal{L} = (a a+1) \text{ or } \alpha\beta \geq 0. \quad (3.15)$$

This statement is independent of k (and Y), but when applied to particular branches, we will generally encounter cases for which $\alpha\beta$ is negative unless certain sequences of four-brackets of the projected external data have a certain number of sign flips; this signals that the branch may intersect $\overline{\mathcal{A}_{n,k,1}}$ only for certain values of k .

3.3.2 MHV Lower Bounds

The fact that MHV amplituhedra only have boundaries of type (1)–(7), (10) and (12) (referring to the numbers given in the “Branches” column of Tab. 3.1) follows implicitly from the results of [17] where all boundaries of one- (and two-) loop MHV amplituhedra were studied. It is nevertheless useful to still consider these cases since we will need the corresponding D -matrices below to establish that amplituhedra have boundaries of these types for all $0 \leq k \leq n - 4$.

In this and the following two sections we always assume, without loss of generality, that indices i, j, k, ℓ are cyclically ordered and non-adjacent ($i+1 < j < j+1 < k < k+1 < \ell$), and moreover that $1 < i$ and $\ell < n$. In particular, this means that we ignore potential signs from the twisted cyclic symmetry (see footnote 8).

Branch (4) is a prototype for several other branches, so we begin with it instead of branch (1). The solution for \mathcal{L} shown in Tab. 3.1 may be represented as $\mathcal{L} = DZ$ with

$$D = \begin{matrix} & i & i+1 & j & j+1 \\ \begin{pmatrix} \alpha & 1-\alpha & 0 & 0 \\ 0 & 0 & \beta & 1-\beta \end{pmatrix}, & & & & \end{matrix} \quad (3.16)$$

where we display only the nonzero columns of the $2 \times n$ matrix in the indicated positions $i, i+1, j$ and $j+1$. This solves the two-mass bubble on-shell conditions for all values of the parameters α and β . This branch intersects $\overline{\mathcal{A}_{n,0,1}}$ when they lie in the range $0 \leq \alpha, \beta \leq 1$, where the matrix D is non-negative. Thus we conclude that MHV amplituhedra have boundaries of type (4).

Branches (5), (6), (7), (10), and (12) can all be represented by special cases of Eq. (3.16) for α and/or β taking values 0 and/or 1, and/or with columns relabeled, so MHV amplituhedra also have boundaries of all of these types.

Branch (1) may be represented by

$$D = \begin{pmatrix} & i-1 & i & i+1 & i+2 & \\ \cdots & 0 & \alpha & 1-\alpha & 0 & \cdots \\ \cdots & \alpha_{i-1} & \alpha_i & \alpha_{i+1} & \alpha_{i+2} & \cdots \end{pmatrix}. \quad (3.17)$$

This provides a solution to the tadpole on-shell condition $\langle \mathcal{L} i i+1 \rangle = 0$ for all values of the parameters, and there clearly are ranges for which D is non-negative. Note that all but two of the parameters in the second row could be gauged away, but this fact is not relevant at the moment (see footnote 9). If $0 \leq \alpha \leq 1$, we could have either $\alpha_a = 0$ for $a < i+1$ and $\alpha_a > 0$ for $a > i$, or $\alpha = 0$ for $a > i$ and $\alpha_a < 0$ for $a < i+1$. We conclude that MHV amplituhedra also have boundaries of this type.

Branch (2) is the special case $\alpha = 1$ of branch (1).

Branch (3) may be represented by

$$D = \begin{pmatrix} & i-1 & i & i+1 & \\ 1 & 0 & \alpha & & \\ 0 & 1 & \beta & & \end{pmatrix} \quad (3.18)$$

for arbitrary α, β , which is non-negative for $\alpha \leq 0$ and $\beta \geq 0$, so MHV amplituhedra also have boundaries of this type.

3.3.3 NMHV Lower Bounds

Branch (8) of the two-mass triangle may be represented as

$$D = \begin{pmatrix} & i & i+1 & & j & j+1 & \\ \alpha & 1-\alpha & & 0 & 0 & & \\ 0 & 0 & & -\langle \bar{i} j+1 \rangle & \langle \bar{i} j \rangle & & \end{pmatrix} \quad (3.19)$$

for arbitrary α . For generic projected external data $\mathcal{L} \neq (jj+1)$, so criterion (3.15) shows that this configuration has a chance to lie on the boundary of an amplituhedron only if $-\langle \bar{i}j+1 \rangle \langle \bar{i}j \rangle \geq 0$. This is not possible for MHV external data, where the ordered four-brackets are always positive, so MHV amplituhedra do not have boundaries of this type. But note that the inequality can be satisfied if there is at least one sign flip in the sequence $\langle \bar{i}\bullet \rangle$, between $\bullet = j$ and $\bullet = j+1$. This motivates us to consider $k = 1$, so let us now check that with

$$C = \begin{pmatrix} i-1 & i & i+1 & j & j+1 \\ c_{i-1} & c_i & c_{i+1} & c_j & c_{j+1} \end{pmatrix}, \quad (3.20)$$

the pair C, D is a valid configuration. First of all, it is straightforward to check that $\mathcal{L} = D\mathcal{Z}$ still satisfies the two-mass triangle on-shell conditions. This statement is not completely trivial since these conditions now depend on $Y = C\mathcal{Z}$ because of the projection (3.2). Second, in order for C to be non-negative we need all five of the indicated c_a 's to be non-negative. Moreover, in order to support generic projected external data, we need them all to be nonzero — if, say, c_i were equal to zero, then $\langle i-1 i+1 jj+1 \rangle$ would vanish, etc. Finally, for $\left(\frac{D}{C}\right)$ to be non-negative we need

$$0 \leq \alpha \leq \frac{c_i}{c_i + c_{i+1}}. \quad (3.21)$$

This branch intersects $\overline{\mathcal{A}_{n,1,1}}$ for α in this range, so we conclude that NMHV amplituhedra have boundaries of this type.

Branch (9) is the general solution of the three-mass triangle, and is already given in Tab. 3.1 in D -matrix form as

$$D = \begin{pmatrix} i & i+1 & j & j+1 \\ \alpha & 1-\alpha & 0 & 0 \\ 0 & 0 & \rho(\alpha) & \sigma(\alpha) \end{pmatrix}, \quad (3.22)$$

with $\rho(\alpha)$ and $\sigma(\alpha)$ defined in Eq. (3.11). For generic projected external data this \mathcal{L} can never attain the value $(i\ i+1)$ or $(j\ j+1)$. Applying criterion (3.15) for both $a = i$ and $a = j$ shows that this configuration has a chance to lie on the boundary of an amplituhedron only if $\alpha(1 - \alpha) \geq 0$ and $\rho(\alpha)\sigma(\alpha) \geq 0$. This is not possible for MHV external data, so we conclude that MHV amplituhedra do not have boundaries of this type. However, the $\rho(\alpha)\sigma(\alpha) \geq 0$ inequality can be satisfied if the sequences $\langle i\ k\ k+1\ \bullet \rangle$ and $\langle i+1\ k\ k+1\ \bullet \rangle$ change sign between $\bullet = j$ and $\bullet = j+1$, as long as the sequences $\langle j\ k\ k+1\ \bullet \rangle$ and $\langle j+1\ k\ k+1\ \bullet \rangle$ do not flip sign here. Consider for $k = 1$ the matrix

$$C = \begin{pmatrix} i & i+1 & j & j+1 & k & k+1 \\ \alpha c_i & (1-\alpha)c_i & c_j & c_{j+1} & c_k & c_{k+1} \end{pmatrix}. \quad (3.23)$$

Then C, D is a valid configuration because (1) $\mathcal{L} = DZ$ satisfies the three-mass triangle on-shell conditions (for all values of α and the c 's), and, (2) for $0 \leq \alpha \leq 1$ and all c 's positive, the C -matrix is non-negative and supports generic positive external data (because it has at least $k+4 = 5$ nonzero columns), and (3) for this range of parameters $\begin{pmatrix} D \\ C \end{pmatrix}$ is also non-negative. Since this branch intersects $\overline{\mathcal{A}_{n,1,1}}$ for a range of α , we conclude that NMHV amplituhedra have boundaries of this type.

Branch (16) is the special case $\alpha = 1$ of branch (9).

Branch (14) is the special case $j \rightarrow i + 1, k \rightarrow j$ of branch (16).

Branch (15) is equivalent to the mirror image of branch (14), after relabeling.

Branch (11) is the special case $j = i + 2$ of branch (15).

3.3.4 N^2 MHV Lower Bounds

Branch (17) may be represented by

$$D = \begin{pmatrix} & j & j+1 & k & k+1 \\ 0 & 0 & -\langle \bar{i} k+1 \rangle & \langle \bar{i} k \rangle \\ -\langle \bar{i} j+1 \rangle & \langle \bar{i} j \rangle & 0 & 0 \end{pmatrix}. \quad (3.24)$$

For generic projected external data the corresponding \mathcal{L} will never attain the value $(jj+1)$ or $(kk+1)$. We can apply criterion (3.15) for both $a = j$ and $a = k$, which reveals that this configuration has a chance to lie on a boundary of an amplituhedron only if both $-\langle \bar{i} j+1 \rangle \langle \bar{i} j \rangle \geq 0$ and $-\langle \bar{i} k+1 \rangle \langle \bar{i} k \rangle \geq 0$. This is impossible for MHV external data, and it is also impossible in the NMHV case, where some projected four-brackets may be negative but the sequence $\langle \bar{i} \bullet \rangle$ may only flip sign once, whereas we need it to flip sign twice, once between $\bullet = j$ and $\bullet = j+1$, and again between $\bullet = k$ and $\bullet = k+1$. We conclude that $k < 2$ amplituhedra do not have boundaries of this form. Consider now pairing (3.24) with the $k = 2$ matrix

$$C = \begin{pmatrix} i-1 & i & i+1 & j & j+1 & k & k+1 \\ c_{11} & c_{12} & c_{13} & c_{14} & c_{15} & 0 & 0 \\ c_{21} & c_{22} & c_{23} & 0 & 0 & c_{24} & c_{25} \end{pmatrix}. \quad (3.25)$$

It is straightforward to check that C, D is a valid configuration for a range of values of c 's, so we conclude that $k = 2$ amplituhedra have boundaries of this type.

Branch (13) may be represented by

$$D = \begin{pmatrix} i-1 & i & i+1 \\ \langle i \bar{j} \rangle & -\langle i-1 \bar{j} \rangle & 0 \\ 0 & -\langle i+1 \bar{j} \rangle & \langle i \bar{j} \rangle \end{pmatrix}, \quad (3.26)$$

which by (3.15) cannot lie on a boundary of an amplituhedron unless the sequence $\langle \bar{j} \bullet \rangle$ flips sign twice, first between $\bullet = i-1$ and i and again between $\bullet = i$ and $i+1$. Therefore, neither MHV nor NMHV amplituhedra have boundaries of this type. However it is straightforward to verify that with

$$C = \begin{matrix} & i-1 & i & i+1 & j-1 & j & j+1 \\ \begin{pmatrix} c_{11} & c_{12} & 0 & c_{13} & c_{14} & c_{15} \\ 0 & c_{21} & c_{22} & c_{23} & c_{24} & c_{25} \end{pmatrix} & & & & & & \end{matrix} \quad (3.27)$$

the pair C, D is a valid configuration for a range of values of c 's, so $k = 2$ amplituhedra do have boundaries of this type.

Branches (18) and (19) of the four-mass box may be represented as

$$D = \begin{matrix} & i & i+1 & j & j+1 \\ \begin{pmatrix} \alpha & 1-\alpha & 0 & 0 \\ 0 & 0 & \beta & 1-\beta \end{pmatrix}, & & & & \end{matrix} \quad (3.28)$$

where α and β are fixed by requiring that \mathcal{L} intersects the lines $(kk+1)$ and $(\ell\ell+1)$. The values of α and β on the two branches were written explicitly in [78]; however, the complexity of those expressions makes analytic positivity analysis difficult. We have therefore resorted to numerical testing: using the algorithm described in Sec. 5.4 of [3], we generate a random positive $n \times (k+4)$ \mathcal{Z} -matrix and a random positive $k \times n$ C -matrix. After projecting through $Y = C\mathcal{Z}$, we obtain projected external data with the correct N^k MHV sign-flipping properties. We have checked numerically that both four-mass box branches lie on the boundary of N^k MHV amplituhedra only for $k \geq 2$, for many instances of randomly generated external data.

3.3.5 Emergent Positivity

The analysis of Secs. 3.3.2, 3.3.3 and 3.3.4 concludes the proof of all of the lower bounds on k shown in the fourth column of Tab. 3.1. We certainly do not claim to have written down the most general possible valid C, D configurations; the ones we display for $k > 0$ have been specifically chosen to demonstrate an interesting feature we call *emergent positivity*.

In each $k > 0$ case we encountered D -matrices that are only non-negative if certain sequences of projected four-brackets of the form $\langle a \ a+1 \ b \ \bullet \rangle$ change sign k times, at certain precisely specified locations. It is straightforward to check that within the range of validity of each C, D pair we have written down, the structure of the C matrix is such that it automatically puts the required sign flips in just the right places to make the D matrix, on its own, non-negative (provided, of course, that $\binom{D}{C}$ is non-negative). It is not a priori obvious that it had to be possible to find pairs C, D satisfying this kind of emergent positivity; indeed, it is easy to find valid pairs for which it does not hold.

3.3.6 Parity and Upper Bounds

Parity relates each branch to itself or to the other branch associated with the same Landau diagram. Since parity is a symmetry of the amplituhedron [37] which relates k to $n - k - 4$, the lower bounds on k that we have established for various branches imply upper bounds on k for their corresponding parity conjugates. These results are indicated in the fourth column of Tab. 3.1, where the inequalities are aligned so as to highlight the parity symmetry.

Although these k upper bounds are required by parity symmetry, they may seem rather mysterious from the analysis carried out so far. We have seen that certain branches can be boundaries of an amplituhedron only if certain sequences of four-brackets have (at least) one or two sign flips. In the next section, we explain a mechanism which gives an upper bound to the number of sign flips, or equivalently which gives the upper bounds on k that are required by parity symmetry.

3.3.7 Increasing Helicity

So far we have only established that N^k MHV amplituhedra have boundaries of certain types for specific low (or, by parity symmetry, high) values of k . It remains to show that all of the branches listed in Tab. 3.1 lie on boundaries of amplituhedra for all of the intermediate helicities. To this end we describe now an algorithm for converting a valid configuration C_0, D_0 at the initial, minimal value of k_0 (with C_0 being the empty matrix for those branches with $k_0 = 0$) into a configuration that is valid at some higher value of k .

We maintain the structure of $D \equiv D_0$ and append to C_0 a matrix C' of dimensions $(k - k_0) \times n$ in order to build a configuration for helicity k . Defining $C = \begin{pmatrix} C_0 \\ C' \end{pmatrix}$, we look for a C' such that following properties are satisfied:

1. The same on-shell conditions are satisfied.
2. In order for the configuration to support generic projected external data, the C -matrix must have $m \geq k + 4$ nonzero columns, and the rank of any $m - 4$ of those columns must be k .
3. Both C and $\begin{pmatrix} D \\ C \end{pmatrix}$ remain non-negative.

Since the C -matrix only has n columns in total, it is manifest from property (2) that everything shuts off for $k > n - 4$, as expected.

Let us attempt to preserve the emergent positivity of D . If $k_0 = 0$ then this is trivial; the D -matrices in Sec. 3.3.2 do not depend on any brackets, so adding rows to the empty C_0 has no effect on D . For $k_0 > 0$, let A and B be two entries in D_0 that are responsible for imposing a sign flip requirement. The argument applies equally to all of the $k_0 > 0$ branches, but for the sake of definiteness consider from Eq. (3.19) the two four-bracket dependent entries $A = -\langle \bar{i} j+1 \rangle$ and $B = \langle \bar{i} j \rangle$. Assuming that C_0 is given by Eq. (3.20) so that both A and B are positive with respect to $Y_0 = C_0 \mathcal{Z}$, then $AB = -[Y_0 \bar{i} j+1][Y_0 \bar{i} j] >$

0. If we append a second row C' and define $Y' = C'Z$ then we have

$$\begin{aligned} A &= -[Y_0 Y' Z_{i-1} Z_i Z_{i+1} Z_{j+1}] = -c_j [Z_j Y' Z_i Z_{i+1} Z_{j+1}], \\ B &= [Y_0 Y' Z_{i-1} Z_i Z_{i+1} Z_j] = c_{j+1} [Z_{j+1} Y' Z_i Z_{i+1} Z_j]. \end{aligned} \quad (3.29)$$

Since c_j and c_{j+1} are both positive, we see that A and B still satisfy $AB > 0$, regardless of the value of Y' . By the same argument, arbitrary rows can be added to a C -matrix without affecting the on-shell conditions, so property (1) also holds trivially (and also if $k_0 = 0$).

The structure of the initial D_0 of Secs. 3.3.2, 3.3.3 and 3.3.4 are similar in that the nonzero columns of this matrix are grouped into at most two *clusters*⁹. For example, for branch (17) there are two clusters $\{j, j+1\}$ and $\{k, k+1\}$ while for branch (3) there is only a single cluster $\{i-1, i, i+1\}$. Property (3) can be preserved most easily if we add suitable columns only in a *gap* between clusters. Let us illustrate how this works in the case of branch (4) where C_0 is empty and we can start by taking either

$$\begin{pmatrix} D_0 \\ C \end{pmatrix} = \begin{pmatrix} & i-1 & i & i+1 & i+2 & \cdots & j-1 & j & j+1 & j+2 & \\ \cdots & 0 & \alpha & 1-\alpha & 0 & \cdots & 0 & 0 & 0 & 0 & \cdots \\ \cdots & 0 & 0 & 0 & 0 & \cdots & 0 & \beta & 1-\beta & 0 & \cdots \\ \cdots & 0 & 0 & \bar{c}_{i+1} & \bar{c}_{i+2} & \cdots & \bar{c}_{j-1} & \bar{c}_j & 0 & 0 & \cdots \end{pmatrix} \quad (3.30)$$

to fill in the gap between clusters $\{i, i+1\}$ and $\{j, j+1\}$, or

$$\begin{pmatrix} D_0 \\ C \end{pmatrix} = \begin{pmatrix} & i-1 & i & i+1 & i+2 & \cdots & j-1 & j & j+1 & j+2 & \\ \cdots & 0 & \alpha & 1-\alpha & 0 & \cdots & 0 & 0 & 0 & 0 & \cdots \\ \cdots & 0 & 0 & 0 & 0 & \cdots & 0 & \beta & 1-\beta & 0 & \cdots \\ \cdots & \bar{c}_{i-1} & \bar{c}_i & 0 & 0 & \cdots & 0 & 0 & \bar{c}_{j+1} & \bar{c}_{j+2} & \cdots \end{pmatrix} \quad (3.31)$$

to fill in the gap between $\{j, j+1\}$ and $\{i, i+1\}$ that “wraps around” from n back to 1. In

⁹Branch (1) appears to be an exception, but only because Eq. (3.17) as written is unnecessarily general: it is sufficient for the second row to have only three nonzero entries, either in columns $\{i-3, i-2, i-1\}$ or in columns $\{i+1, i+2, i+3\}$.

both (3.30) and (3.31) each \vec{c}_a is understood to be a k -component column vector, and in both cases $\binom{D_0}{C}$ can be made non-negative as long as C is chosen to be non-negative¹⁰. In this manner we can trivially increment the k -validity of a given configuration until the gaps become full. This cutoff depends on the precise positions of the gaps, and is most stringent when the two clusters are maximally separated from each other, since this forces the gaps to be relatively small. In this worst case we can fit only $\lceil \frac{n}{2} \rceil$ columns into a C -matrix of one of the above two types. Keeping in mind property (2) that the C -matrix should have at least $k + 4$ nonzero columns, we see that this construction can reach values of $k \leq \lceil \frac{n}{2} \rceil - 4$. In order to proceed further, we can (for example) add additional columns c_i and c_{j+1} to Eq. (3.30), or c_{i+1} and c_j to Eq. (3.31). Choosing a non-negative C then no longer trivially guarantees that $\binom{D_0}{C}$ will also be non-negative, but there are ranges of C for which this is possible to arrange, which is sufficient for our argument.

It is possible to proceed even further by adding additional, specially crafted columns in both gaps, but the argument is intricate and depends delicately on the particular structure of each individual branch (as evident from the delicate structure of k upper bounds in Tab. 3.1). In the interest of brevity we terminate our discussion of the algorithm here and note that it is straightforward to check that for all boundaries, even in the worst case the gaps are always big enough to allow the construction we have described to proceed up to and including the parity-symmetric midpoint $k = \lfloor \frac{n}{2} \rfloor - 2$; then we appeal again to parity symmetry in order to establish the existence of valid configurations for k between this midpoint and the upper bound.

This finally concludes the proof of the k -bounds shown in the fourth column of Tab. 3.1, and thereby step 1(c) from Sec. 3.1.5.

¹⁰If k is even this is automatic; if k is odd the two rows of D_0 should be exchanged.

3.4 The Hierarchy of One-Loop Boundaries

Step (1) of our analysis (Sec. 3.1.5) is now complete at one loop. Before moving on to step (2) we demonstrate that the boundaries classified in Sec. 3.3 can be generated by a few simple graph operations applied to the maximal codimension boundaries of MHV amplituhedra (Tab. 3.1 type (12) or, as a special case, (10)). This arrangement will prove useful in the sequel since one-loop boundaries are the basic building blocks for constructing boundary configurations at arbitrary loop order.

We call boundaries of type (2), (5)–(7), (10), (12), and (14)–(16) *low-k* boundaries since they are valid for the smallest value of k for their respective Landau diagrams. The branches (8), (11), (13) and (17) are *high-k* boundaries and are respectively the parity conjugates of (7), (10), (12) and (16). Branch (3), the parity conjugate of branch (2), is properly regarded as a high- k boundary since (2) is low- k , but it is accidentally valid for all k . Branches (1), (4), and (9) are self-conjugate under parity and are considered both low- k and high- k , as are the parity-conjugate pair (18), (19).

3.4.1 A Graphical Notation for Low-helicity Boundaries

We begin by devising a graphical notation in terms of which the operations between momentum twistor solutions are naturally phrased. These graphs are *twistor diagrams*¹¹ depicting various configurations of intersecting lines in \mathbb{P}^3 . The elements of a twistor diagram, an example of which is shown in panel (a) of Fig. 3.1, are:

- The red line depicts an \mathcal{L} solving some on-shell conditions, specifically:
- if \mathcal{L} and a single line segment labeled i intersect at an empty node, then $\langle \mathcal{L} i i+1 \rangle = 0$, and
- if \mathcal{L} and two line segments intersect at a filled node labeled i , then $\langle \mathcal{L} i-1 i \rangle = \langle \mathcal{L} i i+1 \rangle = 0$.

An “empty” node is colored red, indicating the line passing through it. A “filled” node is filled in solid black, obscuring the line passing through it.

¹¹Not to be confused with the twistor diagrams of [Hodges:2005bf].

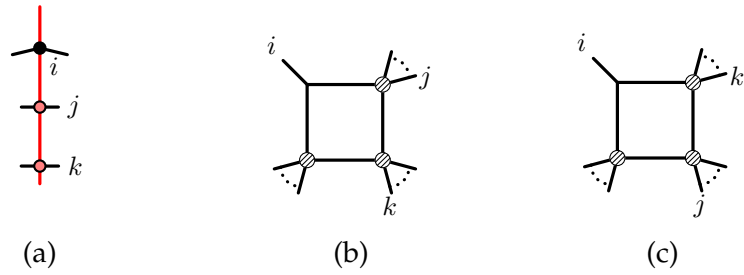


FIGURE 3.1: The twistor diagram shown in (a) depicts branch (16) of solutions to the three-mass box on-shell conditions $\langle \mathcal{L} i-1 i \rangle = \langle \mathcal{L} i i+1 \rangle = \langle \mathcal{L} j j+1 \rangle = \langle \mathcal{L} k k+1 \rangle = 0$, which is a valid boundary for $k \geq 1$. This branch passes through the point Z_i and intersects the lines $(j j+1)$ and $(k k+1)$. As drawn, the intersection at j is an example of a non-MHV intersection, but the figure is agnostic about the relative cyclic ordering of i, j, k and is intended to represent either possibility. Therefore, the corresponding Landau diagram can be either (b) or (c) depending on whether $i < j < k$ or $i < k < j$.

In general a given \mathcal{L} can pass through as many as four labeled nodes (for generic projected external data, which we always assume). If there are four, then none of them can be filled. If there are three, then at most one of them can be filled, and we choose to always draw it as either the first or last node along \mathcal{L} . If there are more than two, then any nodes between the first and last are called *non-MHV intersections*, which are necessarily empty. This name is appropriate because branches satisfying such on-shell constraints are not valid boundaries of MHV amplituhedra, and each non-MHV intersection in a twistor diagram increases the minimum value of k by one.

Although no such diagrams appear in this paper, the extension to higher loops is obvious: each \mathcal{L} is represented by a line of a different color, and the presence of an on-shell condition of the form $\langle \mathcal{L}^{(\ell_1)} \mathcal{L}^{(\ell_2)} \rangle = 0$ is indicated by an empty node at the intersection of the lines $\mathcal{L}^{(\ell_1)}$ and $\mathcal{L}^{(\ell_2)}$.

To each twistor diagram it is simple to associate one or more Landau diagrams, as also shown in Fig. 3.1. If a twistor diagram has a filled node at i then an associated Landau diagram has two propagators $\langle \mathcal{L} i-1 i \rangle$ and $\langle \mathcal{L} i i+1 \rangle$ requiring a massless corner at i in the Landau diagram. If a twistor diagram has an empty node on the line segment marked i then an associated Landau diagram only has the single propagator $\langle \mathcal{L} i i+1 \rangle$, requiring a massive corner in the Landau diagram. Therefore, twistor diagrams should

be thought of as graphical shorthand which both depict the low- k solution to the cut conditions and simultaneously represent one or more Landau diagrams, as explained in the caption of Fig. 3.1.

One useful feature of this graphical notation is that the nodes of a twistor diagram fully encode the total number of propagators, n_{props} , in the Landau diagram (and so also the total number of on-shell conditions): each filled node accounts for two propagators, and each empty node accounts for one propagator:

$$n_{\text{props}} = 2n_{\text{filled}} + n_{\text{empty}}. \quad (3.32)$$

This feature holds at higher loop order where this counting directly indicates how many propagators to associate with each loop.

Let us emphasize that a twistor diagram generally contains more information than its associated Landau diagram, as it indicates not only the set of on-shell conditions satisfied, but also specifies a particular branch of solutions thereto. The sole exception is the four-mass box, for which the above rules do not provide the twistor diagram with any way to distinguish the two branches (18), (19) of solutions. Moreover, the rules also do not provide any way to indicate that an \mathcal{L} lies in a particular plane, such as \bar{i} . Therefore we can only meaningfully represent the low- k boundaries defined at the beginning of Sec. 3.4.

Given a twistor diagram depicting some branch, a twistor diagram corresponding to a relaxation of that branch may be obtained by deleting a non-MHV intersection of the type shown in (a) of Fig. 3.1, by replacing a filled node and its two line segments with an empty node and a single segment, or by deleting an empty node. In the associated Landau diagram, a relaxation corresponds to collapsing an internal edge of the graph. This is formalized in greater detail in Sec. 3.4.2.

3.4.2 A Graphical Recursion for Generating Low-helicity Boundaries

In Fig. 3.2 we organize twistor diagrams representing eight types of boundaries according to d and k ; these are respectively the number of on-shell conditions d satisfied on

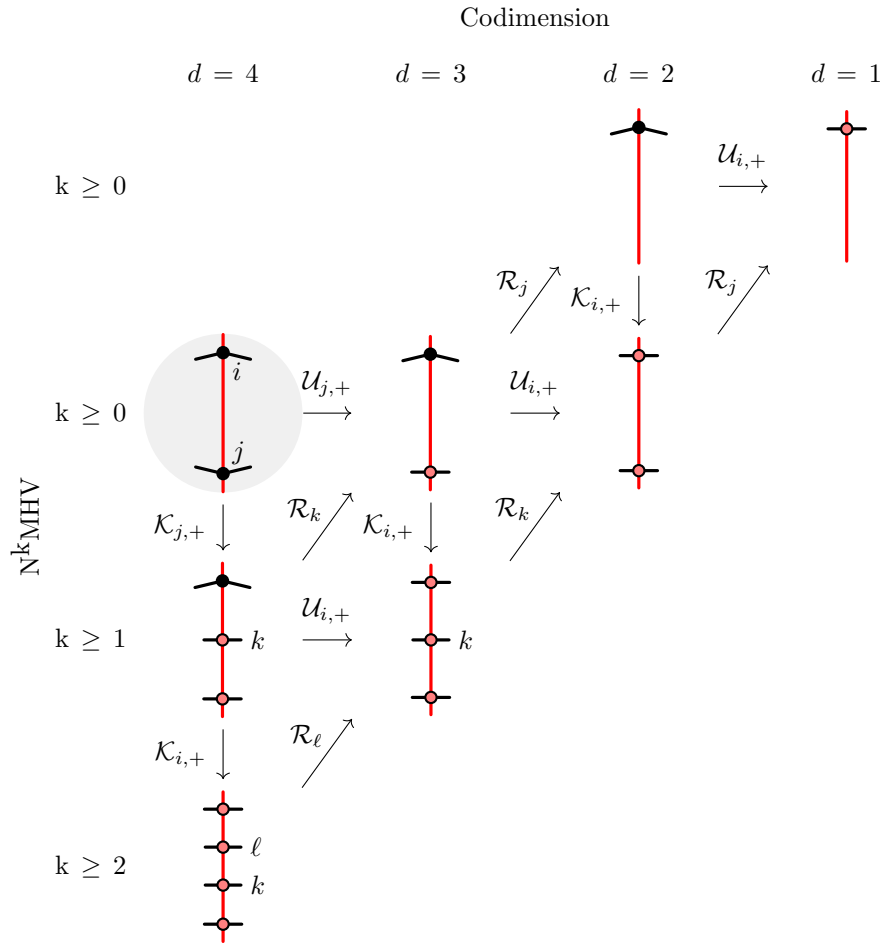


FIGURE 3.2: Twistor diagrams depicting eight types of low- k boundaries of $N^k \text{MHV}$ amplituhedra, organized according to the minimum value of k and the codimension d (equivalently, the number of on-shell conditions satisfied). These correspond respectively to branch types (2), (1), (12), (7), (4), (16), (9) and (18)/(19). The graph operators \mathcal{K} , \mathcal{R} , and \mathcal{U} are explained in the text and demonstrated in Figs. 3.3-3.5, respectively. Evidently all eight types of boundaries can be generated by acting with sequences of these operators on MHV maximal codimension boundaries of the type shown shaded in gray. There is an analogous parity-conjugated version of this hierarchy which relates all of the high- k branches to each other. The missing low- k boundary types (5), (6), (10), (11), (14) and (15) are degenerate cases which can be obtained by starting with $j = i + 1$ in the gray blob.

the boundary, and the minimum value of k for which the boundary is valid. It is evident from this data that there is a simple relation between d , k , and the number of filled (n_{filled}) and empty (n_{empty}) nodes. Specifically, we see that an $N^k\text{MHV}$ amplituhedron can have boundaries of a type displayed in a given twistor diagram only if

$$k \geq 2n_{\text{empty}} + 3n_{\text{filled}} - d - 2 = n_{\text{empty}} + n_{\text{filled}} - 2, \quad (3.33)$$

where we have used Eq. (3.32) with $n_{\text{props}} = d$. In the sequel we will describe a useful map from Landau diagrams to the on-shell diagrams of [3] which manifests the relation (3.33) and provides a powerful generalization thereof to higher loop order. The amplituhedron-based approach has some advantages over that of enumerating on-shell diagrams that will also be explored in the sequel. First of all, the minimal required helicity of a multi-loop configuration can be read off from each loop line separately. Second, we immediately know the relevant solution branches for a given helicity. And finally, compared to enumerating all relevant on-shell diagrams the amplituhedron-based method is significantly more compact since it can be used to produce a minimal subset of diagrams such that all allowed diagrams are relaxations thereof, including limits where massive external legs become massless or vanish.

From the data displayed in Fig. 3.2 we see that a natural organizational principle emerges: all $N^k\text{MHV}$ one-loop twistor diagrams can be obtained from the unique maximal codimension MHV diagram (shown shaded in gray) via sequences of simple graph operations which we explain in turn.

The first graph operation \mathcal{K} increments the helicity of the diagram on which it operates. (The name \mathcal{K} is a reminder that it increases k .) Its operation is demonstrated in Fig. 3.3. Specifically, \mathcal{K}_i replaces a filled node at a point i along \mathcal{L} by two empty nodes, one at i and a second one on a new non-MHV intersection added to the diagram. Since n_{filled} decreases by one but n_{empty} increases by two under this operation, it is clear from Eq. (3.33) that \mathcal{K}_i always increases by one the minimal value of k on which the branch indicated by the twistor diagram has support. From the point of view of Landau diagrams, this operation replaces a massless node with a massive one, as illustrated in

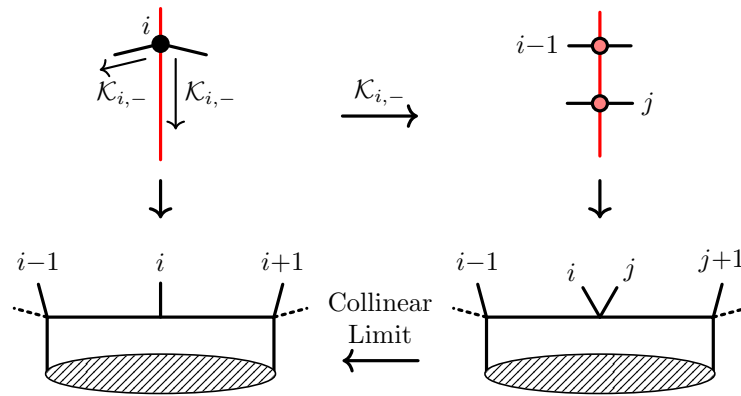


FIGURE 3.3: The graph operation \mathcal{K}_i maps an N^k MHV twistor diagram into an N^{k+1} MHV twistor diagram as shown in the top row. On Landau diagrams, this corresponds to replacing a massless corner by a massive corner; such an operation is effectively an inverse collinear limit. The shaded region in the figures represents an arbitrary planar sub-graph. A dashed external line on a Landau diagram may be either one massless external leg so the whole corner is massive, or completely removed so the whole corner is massless.

the bottom row of Fig. 3.3, and hence it may be viewed as an “inverse” collinear limit.

The other two graph operations \mathcal{R} and \mathcal{U} both correspond to relaxations, as defined in Sec. 3.1.3, since they each reduce the number of on-shell conditions by one, stepping thereby one column to the right in Fig. 3.2.

The operation \mathcal{R}_i simply removes (hence the name \mathcal{R}) an empty node i from a twistor diagram, as shown in Fig. 3.4. This corresponds to removing $\langle \mathcal{L} i i + 1 \rangle = 0$ from the set of on-shell conditions satisfied by \mathcal{L} ¹².

The last operation, \mathcal{U} , corresponds to “un-pinning” a filled node (hence “ \mathcal{U} ”). Un-pinning means removing one constraint from a pair $\langle \mathcal{L} i - 1 i \rangle = \langle \mathcal{L} i i + 1 \rangle = 0$. The line \mathcal{L} , which was pinned to the point i , is then free to slide along the line segment $(i - 1 i)$ or $(i i + 1)$ (for $\mathcal{U}_{i,-}$ or $\mathcal{U}_{i,+}$, respectively). In the twistor diagram, this is depicted by replacing the filled node at the point i with a single empty node along the line segment $(i i \pm 1)$ (see Fig. 3.5). Only \mathcal{U}_+ appears in Fig. 3.2 because at one loop, all diagrams generated by any \mathcal{U}_- operation are equivalent, up to relabeling, to some diagram generated by a \mathcal{U}_+ . In general, however, it is necessary to track the subscript \pm since both choices

¹²Note that in line with the conventions adopted in Sec. 3.4.1 we label \mathcal{R}_i only with the smaller label of a pair $(i i + 1)$.

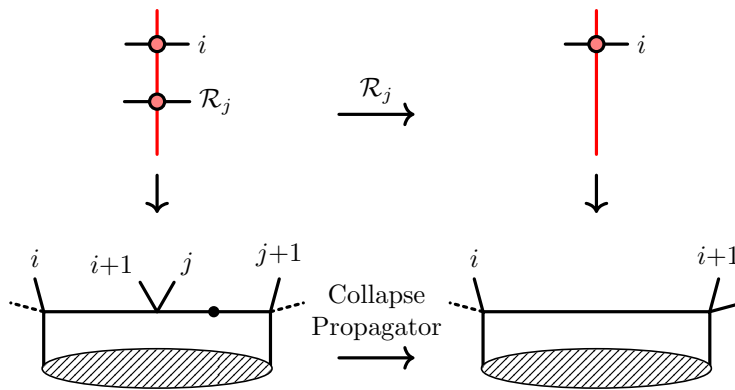


FIGURE 3.4: The graph operation \mathcal{R}_j relaxes \mathcal{L} by removing the condition that \mathcal{L} must pass through the line $(jj+1)$; this is equivalent to removing the on-shell condition $\langle \mathcal{L} jj+1 \rangle = 0$. On Landau diagrams, this corresponds to collapsing the propagator indicated by the filled dot in the bottom figure on the left. The shaded region in the figures represents an arbitrary planar sub-graph. A dashed external line on a Landau diagram may be either one massless external leg so the whole corner is massive, or completely removed so the whole corner is massless. It is to be understood that the graphical notation implies that $j \neq i+2$ and $i \neq j+2$; otherwise, the two empty nodes in the top left diagram would be represented by a single filled node on which the action of \mathcal{R} is undefined; the appropriate graph operation in this case would instead be \mathcal{U} .

are equally valid relaxations and can yield inequivalent twistor and Landau diagrams.

From Fig. 3.2, we read off the following identity among the operators acting on any diagram g :

$$\mathcal{U}_{j,+}g = \mathcal{R}_k\mathcal{K}_{j,+}g. \quad (3.34)$$

There was no reason to expect the simple graphical pattern of Fig. 3.5 to emerge among the twistor diagrams. Indeed in Sec. 3.2 we simply listed all possible sets of on-shell conditions without taking such an organizational principle into account. At higher loop order, however, the problem of enumerating all boundaries of $N^k\text{MHV}$ amplituhedra benefits greatly from the fact that all valid configurations of each single loop can be iteratively generated via these simple rules, starting from the maximal codimension MHV boundaries. Stated somewhat more abstractly, these graph operations are instructions for naturally associating boundaries of different amplituhedra.

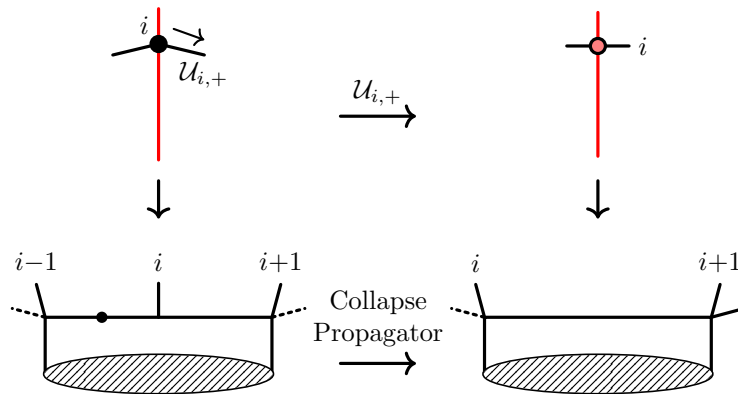


FIGURE 3.5: The graph operation $\mathcal{U}_{i,+}$ relaxes a line \mathcal{L} constrained to pass through the point i , shifting it to lie only along the line $(i\ i+1)$. This is equivalent to removing the on-shell constraint $\langle \mathcal{L}\ i-1\ i \rangle = 0$. (The equally valid relaxation $\mathcal{U}_{i,-}$, not pictured here, lets the intersection point slide onto $(i-1\ i)$.) On Landau diagrams, this corresponds to collapsing the propagator indicated by the filled dot in the bottom figure on the left. The shaded region in the figures represents an arbitrary planar sub-graph. A dashed external line on a Landau diagram may be either one massless external leg so the whole corner is massive, or completely removed so the whole corner is massless. As explained in the caption of Fig. 3.4, the \mathcal{U} operation can be thought of as a special case of the \mathcal{R} operation, and we distinguish the two because only the latter can change the helicity sector k .

Before concluding this section it is worth noting (as is evident in Fig. 3.2) that relaxing a low- k boundary can never raise the minimum value of k for which that type of boundary is valid. In other words, we find that if $\mathcal{A}_{n,k,1}$ has a boundary of type B , and if B' is a relaxation of B , then $\mathcal{A}_{n,k,1}$ also has boundaries of type B' . This property does not hold in general beyond one loop; a counterexample involving two-loop MHV amplitudes appears in Fig. 4 of [17].

3.5 Solving Landau Equations in Momentum Twistor Space

As emphasized in Sec. 3.1.5, the Landau equations naturally associate to each boundary of an amplituhedron a locus in $\text{Conf}_n(\mathbb{P}^3)$ on which the corresponding amplitude has a singularity. In this section we review the results of solving the Landau equations for each of the one-loop branches classified in Sec. 3.2, thereby carrying out step 2 of the algorithm summarized in Sec. 3.1.5. The results of this section were already tabulated in [16], but we revisit the analysis, choosing just two examples, in order to demonstrate the simplicity and efficiency of these calculations when carried out directly in momentum twistor space. The utility of this method is on better display in the higher-loop examples to be considered in the sequel.

As a first example, we consider the tadpole on-shell condition

$$f_1 \equiv \langle \mathcal{L} i i+1 \rangle = 0. \quad (3.35)$$

We choose any two other points Z_j, Z_k (which generically satisfy $\langle i i+1 j k \rangle \neq 0$) in terms of which to parameterize

$$\mathcal{L} = (Z_i + d_1 Z_j + d_2 Z_k, Z_{i+1} + d_3 Z_j + d_4 Z_k). \quad (3.36)$$

Then the on-shell condition (3.35) admits solutions when

$$d_1 d_4 - d_2 d_3 = 0, \quad (3.37)$$

while the four Kirchhoff conditions (3.10) are

$$\alpha_1 d_4 = -\alpha_1 d_3 = -\alpha_1 d_2 = \alpha_1 d_1 = 0. \quad (3.38)$$

The only nontrivial solution (that means $\alpha_1 \neq 0$; see Sec. 3.1.4) to the equations (3.37) and (3.38) is to set all four $d_A = 0$. Since this solution exists for all (generic) projected external data, it does not correspond to a branch point of an amplitude and is uninteresting to us. In other words, in this case the locus we associate to a boundary of this type is all of $\text{Conf}_n(\mathbb{P}^3)$.

As a second example, consider the two on-shell conditions corresponding to the two-mass bubble

$$f_1 \equiv \langle \mathcal{L} i i+1 \rangle = 0, \quad f_2 \equiv \langle \mathcal{L} j j+1 \rangle = 0. \quad (3.39)$$

In this case a convenient parameterization is

$$\mathcal{L} = (Z_i + d_1 Z_{i+1} + d_2 Z_k, Z_j + d_3 Z_{i+1} + d_4 Z_k). \quad (3.40)$$

Note that an asymmetry between i and j is necessarily introduced because we should not allow more than four distinct momentum twistors to appear in the parameterization, since they would necessarily be linearly dependent, and we assume of course that Z_k is generic (meaning, as before, that $\langle i i+1 j k \rangle \neq 0$). Then

$$\begin{aligned} f_1 &= -d_2 \langle i i+1 j k \rangle, \\ f_2 &= d_3 \langle i i+1 j j+1 \rangle + d_4 \langle i j j+1 k \rangle + (d_1 d_4 - d_2 d_3) \langle i+1 j j+1 k \rangle \end{aligned} \quad (3.41)$$

and the Kirchhoff conditions are

$$\begin{pmatrix} 0 & d_4 \langle i+1 jj+1 k \rangle \\ -\langle ii+1 jk \rangle & -d_3 \langle i+1 jj+1 k \rangle \\ 0 & \langle ii+1 jj+1 \rangle - d_2 \langle i+1 jj+1 k \rangle \\ 0 & \langle ijj+1 k \rangle + d_1 \langle i+1 jj+1 k \rangle \end{pmatrix} \begin{pmatrix} \alpha_1 \\ \alpha_2 \end{pmatrix} = 0. \quad (3.42)$$

Nontrivial solutions exist only if all 2×2 minors of the 4×2 coefficient matrix vanish. Three minors are trivially zero, and the one computed from the second and third rows evaluates simply to

$$-\langle ii+1 jk \rangle \langle ii+1 jj+1 \rangle = 0 \quad (3.43)$$

using the on-shell condition $f_1 = -d_2 \langle ii+1 jk \rangle = 0$. If this quantity vanishes, then the four remaining constraints (the two on-shell conditions $f_1 = f_2 = 0$ and the two remaining minors) can be solved for the four d_A , and then Eq. (3.42) can be solved to find the two α_J 's. Since $\langle ii+1 jk \rangle \neq 0$ by assumption, we conclude that the Landau equations admit nontrivial solutions only on the codimension-one locus in $\text{Conf}_n(\mathbb{P}^3)$ where

$$\langle ii+1 jj+1 \rangle = 0. \quad (3.44)$$

These two examples demonstrate that in some cases (e.g. the tadpole example) the Landau equations admit solutions for any (projected) external data, while in other cases (e.g. the bubble example) the Landau equations admit solutions only when there is a codimension-one constraint on the external data. A common feature of these examples is that some care must be taken in choosing how to parameterize \mathcal{L} . In particular, one must never express \mathcal{L} in terms of four momentum twistors (Z_i, Z_j , etc.) that appear in the specification of the on-shell conditions; otherwise, it can be impossible to disentangle the competing requirements that these satisfy some genericity (such as $\langle ii+1 jk \rangle \neq 0$ in the above examples) while simultaneously hoping to tease out the constraints they

must satisfy in order to have a solution (such as Eq. (3.44)). For example, although one might have been tempted to preserve the symmetry between i and j , it would have been a mistake to use the four twistors Z_i, Z_{i+1}, Z_j and Z_{j+1} in Eq. (3.40).

Instead, it is safest to always pick four completely generic points Z_a, \dots, Z_d in terms of which to parameterize

$$\mathcal{L} = \begin{pmatrix} 1 & 0 & d_1 & d_2 \\ 0 & 1 & d_3 & d_4 \end{pmatrix} \begin{pmatrix} Z_a \\ Z_b \\ Z_c \\ Z_d \end{pmatrix}. \quad (3.45)$$

The disadvantage of being so careful is that intermediate steps in the calculation become much more lengthy, a problem we avoid in practice by using a computer algebra system such as Mathematica.

The results of this analysis for all one-loop branches are summarized in Tab. 3.1. Naturally these are in accord with those of [26] (as tabulated in [16]). At one loop it happens that the singularity locus is the same for each branch of solutions to a given set of on-shell conditions, but this is not generally true at higher loop order.

3.6 Singularities and Symbology

As suggested in the introduction (and explicit even in the title of this paper), one of the goals of our research program is to provide a priori derivations of the *symbol alphabets* of various amplitudes. We refer the reader to [67] for more details, pausing only to recall that the symbol alphabet of a generalized polylogarithm function F is a finite list of *symbol letters* $\{z_1, \dots, z_r\}$ such that F has *logarithmic* branch cuts (i.e., the cover has infinitely many sheets)¹³ between $z_i = 0$ and $z_i = \infty$ for each $i = 1, \dots, r$.

To date, symbol alphabets have been determined by explicit computation only for two-loop MHV amplitudes [60]; all other results on multi-loop SYM amplitudes in the

¹³These branch cuts usually do not all live on the same sheet; the symbol alphabet provides a list of all branch cuts that can be accessed after analytically continuing F to arbitrary sheets.

literature are based on a conjectured extrapolation of these results to higher loop order. Throughout the paper we have however been careful to phrase our results in terms of branch points, rather than symbol letters, for two reasons.

First of all, amplitudes in SYM theory are expected to be expressible as generalized polylogarithm functions, with symbol letters that have a familiar structure like those of the entries in the last column of Tab. 3.1, only for sufficiently low (or, by parity conjugation, high) helicity. In contrast, the Landau equations are capable of detecting branch points of even more complicated amplitudes, such as those containing elliptic polylogarithms, which do not have traditional symbols¹⁴.

Second, even for amplitudes which do have symbols, determining the actual symbol alphabet from the singularity loci of the amplitude may require nontrivial extrapolation. Suppose that the Landau equations reveal that some amplitude has a branch point at $z = 0$ (where, for example, z may be one of the quantities in the last column of Tab. 3.1). Then the symbol alphabet should contain a letter $f(z)$, where f in general could be an arbitrary function of z , with branch points arising in two possible ways. If $f(0) = 0$, then the amplitude will have a logarithmic branch point at $z = 0$ [23], but even if $f(0) \neq 0$, the amplitude can have an *algebraic* branch point (so the cover has finitely many sheets) at $z = 0$ if $f(z)$ has such a branch point there.

We can explore this second notion empirically since all one-loop amplitudes in SYM theory, and in particular their symbol alphabets, are well-known (following from one-loop integrated amplitudes in for example, [38, 39, 40, 41, 42, 43, 44, 45, 46]). According to our results from Tab. 3.1, we find that one-loop amplitudes only have branch points on loci of the form

- $\langle i i+1 j j+1 \rangle = 0$ or $\langle i \bar{j} \rangle = 0$ for $0 \leq k \leq n - 4$,
- $\langle i(i-1 i+1)(j j+1)(k k+1) \rangle = 0$ for $1 \leq k \leq n - 5$, and
- $\Delta_{ijkl} = 0$ (defined in Tab. 3.1) for $2 \leq k \leq n - 6$,

¹⁴It would be interesting to understand how the “generalized symbols” of such amplitudes capture the singularity loci revealed by the Landau equations.

where i, j, k, ℓ can all range from 1 to n . Happily, the first two of these are in complete accord with the symbol letters of one-loop MHV and NMHV amplitudes, but the third reveals the foreshadowed algebraic branching since Δ_{ijkl} is not a symbol letter of the four-mass box integral contribution to $N^{2 \leq k \leq n-6}$ MHV amplitudes. Rather, the symbol alphabet of this amplitude consists of quantities of the form

$$f_{ij} \equiv \langle i \ i+1 \ j \ j+1 \rangle \quad \text{and} \quad f_{i\ell} f_{jk} \pm (f_{ik} f_{j\ell} - f_{ij} f_{k\ell}) \pm \sqrt{\Delta_{ijkl}}, \quad (3.46)$$

where the signs may be chosen independently. Since no symbol letter vanishes on the locus $\Delta_{ijkl} = 0$, amplitudes evidently do not have logarithmic branch points on this locus. Yet it is evident from the second expression of (3.46) that amplitudes with these letters have algebraic (in this instance, square-root- or double-sheet-type) branch points when $\Delta_{ijkl} = 0$.

Although we have only commented on the structure of various potential symbol entries and branch point loci here, let us emphasize that the methods of this paper can be used to determine precisely which symbol entries can appear in any given amplitude. For example, Tab. 3.1 can be used to determine values of i, j and k for which the letter $\langle i(i-1 \ i+1)(j \ j+1)(k \ k+1) \rangle$ can appear, as well as in which one-loop amplitudes, indexed by n and k , such letters will appear. An example of a fine detail along these lines evident already in Tab. 3.1 is the fact that all NMHV amplitudes have branch points of two-mass easy type except for the special case $n = 6$, in accord with Eq. (2.7) of [79].

We conclude this section by remarking that the problem of deriving symbol alphabets from the Landau singularity loci may remain complicated in general, but we hope that the simple, direct correspondence we have observed for certain one-loop amplitudes (and which was also observed for the two-loop MHV amplitudes studied in [17]) will continue to hold at arbitrary loop order for sufficiently simple singularities.

3.7 Conclusion

This paper presents first steps down the path of understanding the branch cut structure of SYM amplitudes for general helicity, following the lead of [17] and using the recent “unwound” formulation of the amplituhedron from [37]. Our algorithm is conceptually simple: we first enumerate the boundaries of an amplituhedron, and from there, without resorting to integral representations, we use the Landau equations directly to determine the locations of branch points of the corresponding amplitude.

One might worry that each of these steps grows rapidly in computational complexity at higher loop order. Classifying boundaries of amplituhedra is on its own a highly nontrivial problem, aspects of which have been explored in [5, 7, 10, 13, 80]. In that light, the graphical tools presented in Sec. 3.4.2, while already useful for organizing results as in Fig. 3.2, hint at the more enticing possibility of a method to enumerate twistor diagrams corresponding to all \mathcal{L} -boundaries of any given $\mathcal{A}_{n,k,L}$. Such an algorithm would start with the maximal codimension twistor diagrams at a given loop order, and apply the operators of Sec. 3.4.2 in all ways until no further operations are possible. From these twistor diagrams come Landau diagrams, and from these come the branch points via the Landau equations. We saw in [17] and Sec. 3.5 that analyzing the Landau equations can be made very simple in momentum twistor space.

Configurations of loop momenta in (the closure of) MHV amplituhedra are represented by non-negative D -matrices. In general, non-MHV configurations must be represented by indefinite D -matrices, but we observed in Sec. 3.3.5 that even for non-MHV amplituhedra, D may always be chosen non-negative for all configurations on \mathcal{L} -boundaries. This ‘emergent positivity’ plays a crucial role by allowing the one-loop D -matrices presented in Secs. 3.3.2, 3.3.3 and 3.3.4 to be trivially recycled at higher values of helicity. One way to think about this is to say that going beyond MHV level introduces the C -matrix which “opens up” additional configuration space in which an otherwise indefinite D -matrix can become positive.

While the one-loop all-helicity results we obtain are interesting in their own right

as first instances of all-helicity statements, this collection of information is valuable because it provides the building blocks for the two-loop analysis in the sequel. There we will argue that the two-loop twistor diagrams with helicity k can be viewed as compositions of two one-loop diagrams with helicities k_1 and k_2 satisfying $k = k_1 + k_2$ or $k_1 + k_2 + 1$. We will also explore in detail the relation to on-shell diagrams, which are simply Landau diagrams with decorated nodes.

More speculatively, the ideas that higher-loop amplitudes can be constructed from lower-loop amplitudes, and that there is a close relation to on-shell diagrams, suggests the possibility that this toolbox may also be useful for finding symbols in the full, non-planar SYM theory. For example, enumerating the on-shell conditions as we do here in the planar sector is similar in spirit to the nonplanar examples of [12] where certain integral representations were found such that individual integrals had support on only certain branches¹⁵. There are of course far fewer known results in the nonplanar SYM theory, though there have been some preliminary studies [82, 83, 84, 85, 86].

¹⁵Already in the planar case, one might interpret our algorithm as applying the Landau equations to integrands constructed in expansions around boundaries of amplituhedra, which is reminiscent of the prescriptive unitarity of [81].

Chapter 4

All-loop singularities of scattering amplitudes in massless planar theories

4.1 Landau Graphs and Singularities

We begin by reviewing the Landau equations, which encode the constraint of locality on the singularity structure of scattering amplitudes in perturbation theory via Landau graphs. We aim to connect the standard vocabulary used in relativistic field theory to that of network theory in order to streamline the rest of our discussion.

In *planar* quantum field theories, which will be the exclusive focus of this paper, we can restrict our attention to plane Landau graphs. An L -loop m -point plane Landau graph is a plane graph with $L+1$ faces and m distinguished vertices called *terminals* that must lie on a common face called the *unbounded face*. Henceforth we use the word “vertex” only for those that are not terminals, and the word “face” only for the L faces that are not the unbounded face.

Each edge j is assigned an arbitrary orientation and a four-component (or, more generally, a D -component) (energy-)momentum vector q_j , the analog of electric current. Reversing the orientation of an edge changes the sign of the associated q_j . At each vertex the vector sum of incoming momenta must equal the vector sum of outgoing momenta

(current conservation). This constraint is not applied at terminals, which are the locations where a circuit can be probed by connecting external sources or sinks of current. In field theory these correspond to the momenta carried by incoming or outgoing particles. If we label the terminals by $a = 1, \dots, m$ (in cyclic order around the unbounded face) and let P_a denote the D -momentum flowing into the graph at terminal a , then energy-momentum conservation requires that $\sum_a P_a = 0$ and implies that precisely L of the q_j 's are linearly independent.

Scattering amplitudes are (in general multivalued) functions of the P_a 's which can be expressed as a sum over all Landau graphs, followed by a DL -dimensional integral over all components of the linearly independent q_j 's. Amplitudes in different quantum field theories differ in how the various graphs are weighed (by P_a - and q_j -dependent factors) in that linear combination. These differences are indicated graphically by decorating each Landau graph (usually in many possible ways) with various embellishments, in which case they are called *Feynman diagrams*. We return to this important point later, but for now we keep our discussion as general as possible.

Our interest lies in understanding the loci in P_a -space on which amplitudes may have singularities, which are highly constrained by general physical principles. A Landau graph is said to have *Landau singularities of the first type* at values of P_a for which the *Landau equations* [26]

$$\alpha_j q_j^2 = 0 \text{ for each edge } j, \text{ and} \quad (4.1)$$

$$\sum_{\text{edges } j \in \mathcal{F}} \alpha_j q_j = 0 \text{ for each face } \mathcal{F} \quad (4.2)$$

admit nontrivial solutions for the *Feynman parameters* α_j (that means, omitting the trivial solution where all $\alpha_j = 0$). In the first line we have indicated our exclusive focus on *massless* field theories by omitting a term proportional to m_j^2 which would normally be present.

The Landau equations generally admit several branches of solutions. The *leading* Landau singularities of a graph \mathcal{G} are those associated to branches having $q_j^2 = 0$ for all j (regardless of whether any of the α_j 's are zero). This differs slightly from the more

conventional usage of the term “leading”, which requires all of the α_j 's to be nonzero. However, we feel that our usage is more natural in massless theories, where it is typical to have branches of solutions on which q_j^2 and α_j are *both* zero for certain edges j . Landau singularities associated to branches on which one or more of the q_j^2 are not zero (in which case the corresponding α_j 's must necessarily vanish) can be interpreted as leading singularities of a *relaxed* Landau graph obtained from \mathcal{G} by contracting the edges associated to the vanishing α_j 's.

A graph is called *c-connected* if it remains connected after removal of any $c-1$ vertices. It is easy to see that the set of Landau singularities for a 1-connected graph (sometimes called a “kissing graph” in field theory) is the union of Landau singularities associated to each 2-connected component since the Landau equations completely decouple. Therefore, without loss of generality we can confine our attention to 2-connected Landau graphs.

4.2 Elementary Circuit Operations

We refer to Eq. (4.2) as the *Kirchhoff conditions* in recognition of their circuit analog where the α_j 's play the role of resistances. The analog of the *on-shell conditions* (4.1) on the other hand is rather mysterious, but a very remarkable feature of massless theories is that:

The graph moves familiar from elementary electrical circuit theory preserve the solution sets of Eqs. (4.1) and (4.2), and hence, the sets of first-type Landau singularities in any massless field theory.

Let us now demonstrate this feature, beginning with the three elementary circuit moves shown in Fig. 4.1.

Series reduction (Fig. 4.1(a)) allows one to remove any vertex of degree two. Since $q_2 = q_1$ by momentum conservation, the structure of the Landau equations is trivially preserved if the two edges with Feynman parameters α_1, α_2 are replaced by a single edge carrying momentum $q' = q_1 = q_2$ and Feynman parameter $\alpha' = \alpha_1 + \alpha_2$.

Parallel reduction (Fig. 4.1(b)) allows one to collapse any bubble subgraph. It is easy to verify (see for example Appendix A.1 of [17]) that the structure of the Landau

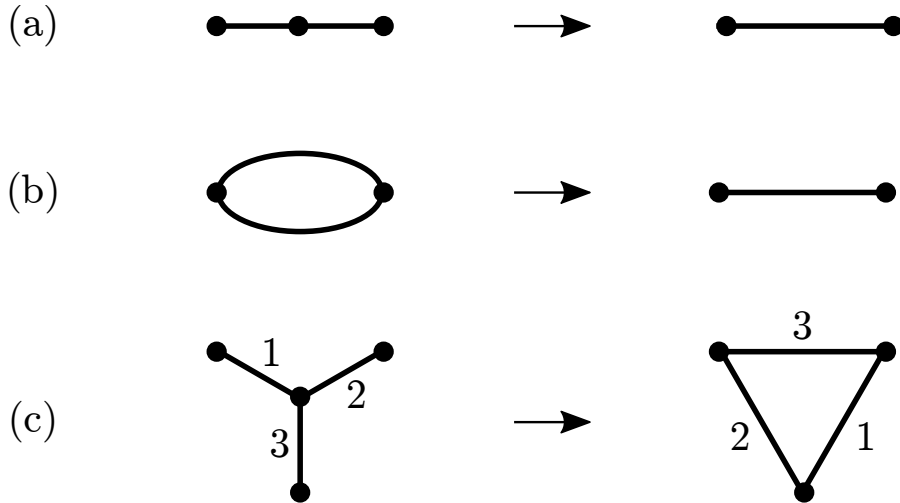


FIGURE 4.1: Elementary circuit moves that preserve solution sets of the massless Landau equations: (a) series reduction, (b) parallel reduction, and (c) Y - Δ reduction.

equations is preserved if the two edges of the bubble are replaced by a single edge carrying momentum $q' = q_1 + q_2$ and Feynman parameter $\alpha' = \alpha_1\alpha_2/(\alpha_1 + \alpha_2)$.

The Y - Δ reduction (Fig. 4.1(c)) replaces a vertex of degree three (a “ Y ”) with a triangle subgraph (a “ Δ ”), or vice versa. Generically the Feynman parameters α_i of the Δ are related to those of the Y , which we call β_i , by

$$\beta_1 = \frac{\alpha_2\alpha_3}{\alpha_1 + \alpha_2 + \alpha_3}, \quad \text{and cyclic.} \quad (4.3)$$

On branches where one or more of the parameters vanish, this relation must be suitably modified. For example, if a branch of solutions for a graph containing a Y has $\beta_1 = \beta_2 = 0$ but β_3 nonzero, then the corresponding branch for the reduced graph has $\alpha_3 = 0$ but α_1, α_2 nonzero.

The invariance of the Kirchhoff conditions (4.2) under Y - Δ reduction follows straightforwardly from these Feynman parameter assignments. The invariance of the on-shell conditions (4.1) is nontrivial, and follows from the analysis in Appendix A.2 of [17] by checking that the on-shell conditions before and after the reduction are equivalent for each branch of solutions to the Landau equations. Actually [17] mentions only seven of

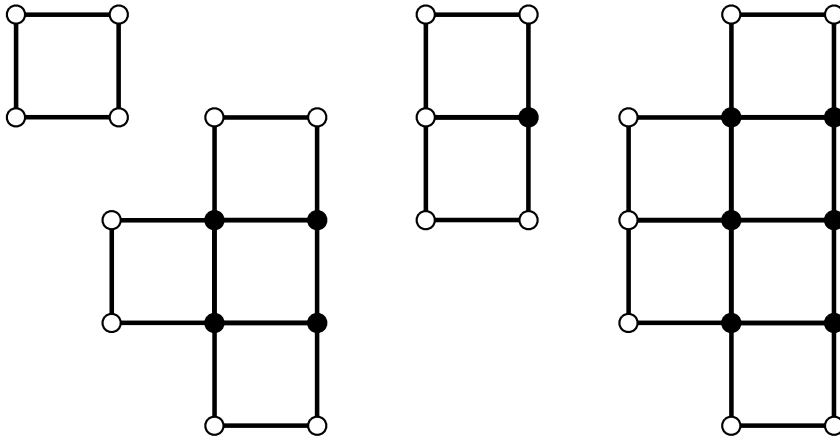


FIGURE 4.2: The four-, six-, five- and seven-terminal zigurat graphs. The open circles are terminals and the filled circles are vertices. The pattern continues in the obvious way, but note an essential difference between zigurat graphs with an even or odd number of terminals in that only the latter have a terminal of degree three.

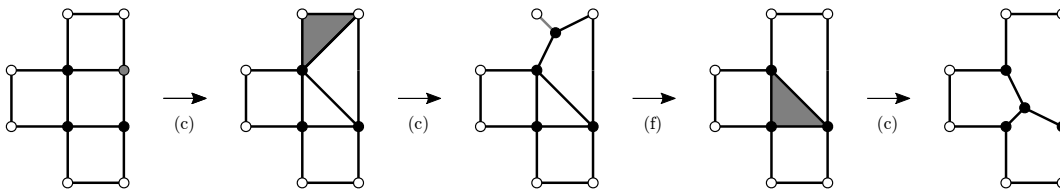


FIGURE 4.3: The six-terminal zigurat graph can be reduced to a three loop graph by a sequence of three $Y-\Delta$ reductions and one FP assignment. In each case the vertex, edge, or face to be transformed is highlighted in gray.

the eight different types of branches. The eighth branch has $\alpha_1 = \alpha_2 = \alpha_3 = 0$, corresponding to $\beta_1 = \beta_2 = \beta_3 = 0$, but in this relatively trivial case both the Y and the Δ can effectively be collapsed to a single vertex.

The proof of the crucial theorem of [52] that we employ in the next section relies on three additional relatively simple moves that either have no analog in field theory or trivially preserve the essential content of the Landau equations. These are (d) the deletion of a “tadpole” (edges that connect a vertex or terminal to itself), (e) the deletion of a “hanging propagator” (a vertex of degree one and the edge connected to it), and (f) the contraction of an edge connected to a terminal of degree one (called “FP assignment” [87]). The last of these is strictly speaking not completely trivial at the level of the Landau equations; it just removes an otherwise uninteresting bubble singularity.

4.3 Reduction of Planar Graphs

The reduction of general graphs under the operations reviewed in the previous section is a well-studied problem in the mathematical literature. When it is declared that a certain subset of vertices are to be considered terminals (which may not be removed by series or Y - Δ reduction) the corresponding problem is called *terminal Y - Δ reducibility*. Aspects of terminal Y - Δ reducibility have been studied in [88, 89, 90, 91, 87, 92], including an application to Feynman diagrams in [93]. For our purpose the key result comes from the Ph.D. thesis of I. Gitler [52], who proved that any planar 2-connected graph with m terminals lying on the same face can be reduced to a graph of the kind shown in Fig. 4.2, which we call *ziggurat* graphs, or to a minor thereof. We denote the m -terminal ziggurat graph by \mathcal{T}_m , and note that a *minor* of a graph \mathcal{G} is any graph that can be obtained from \mathcal{G} by any sequence of edge contractions and/or edge deletions.

At the level of Landau equations an edge contraction corresponds, as discussed above, to a relaxation (setting the associated α_j to zero), while an edge deletion corresponds to setting the associated q_j to zero. It is clear that the Landau singularities associated to any minor of a graph \mathcal{G} are a subset of those associated to \mathcal{G} . Consequently

we don't need to worry about explicitly enumerating all minors of \mathcal{T}_m ; their Landau singularities are already contained in the set of singularities of \mathcal{T}_m itself.

It is conventional to discuss scattering amplitudes for a fixed number n of external particles, each of which carries some momentum p_i that in massless theories satisfies $p_i^2 = 0$. The total momentum flowing into each terminal is not arbitrary, but must be a sum of one or more null vectors. The momenta carried by these individual particles are denoted graphically by attaching a total of n external edges to the terminals, with at least one per terminal. In this way it is clear that any Landau graph with $m \leq n$ terminals is potentially relevant to finding the Landau singularities of an n -particle amplitude. However, it is also clear that if $m < n$ then \mathcal{T}_m is a minor of \mathcal{T}_n , so again the Landau singularities of the former are a subset of those of the latter. Therefore, to find the Landau singularities of an n -particle amplitude it suffices to find those of the n -terminal ziggurat graph \mathcal{T}_n with precisely one external edge attached to each terminal. We call this the *n -particle ziggurat graph* and finally summarize:

The first-type Landau singularities of an n -particle scattering amplitude in any massless planar field theory are a subset of those of the n -particle ziggurat graph.

While the Landau singularities of the ziggurat graph exhaust the set of singularities that may appear in any massless planar theory, we cannot rule out the possibility that in certain special theories the actual set of singularities may be smaller because of nontrivial cancellation between the contributions of different Landau graphs to a given amplitude. We return to this important point in Sec. 4.6.

Let us also emphasize that Y - Δ reduction certainly changes the number of faces of a graph, so the above statement does not hold at fixed loop order L ; rather it is an all-order relation about the full set of Landau singularities of n -particle amplitudes at any finite order in perturbation theory. Since the n -particle ziggurat graph has $L = \lfloor (n-2)^2/4 \rfloor$ faces, we can however predict that a single computation at only $\lfloor (n-2)^2/4 \rfloor$ -loop order suffices to expose all possible Landau singularities of any n -particle amplitude.

In fact this bound is unnecessarily high. Gitler's theorem does not imply that ziggurat graphs cannot be further reduced to graphs of lower loop order, and it is easy to see

that in general this is possible. For example, as shown in Fig. 4.3, the six-terminal graph can be reduced by a sequence of Y - Δ reductions and one FP assignment to a particularly beautiful three-loop wheel graph whose 6-particle avatar we display in Fig. 4.4. Zigurat graphs with more than six terminals can also be further reduced, but we have not been able to prove a lower bound on the loop order that can be obtained for general n .

4.4 Landau Analysis of the Wheel

In this section we analyze the Landau equations for the graph shown in Fig. 4.4. The six external edges carry momenta p_1, \dots, p_6 into the graph, subject to $\sum_i p_i = 0$ and $p_i^2 = 0$ for each i . Using momentum conservation at each vertex, the momentum q_j carried by each of the twelve edges can be expressed in terms of the six p_i and three other linearly independent momenta, which we can take to be l_r , for $r = 1, 2, 3$, assigned as shown in the figure. Initially we consider the leading Landau singularities, for which we impose the twelve on-shell conditions

$$\begin{aligned}
(l_1 - p_1)^2 = l_1^2 = (l_1 + p_2)^2 &= 0, \\
(l_2 - p_3)^2 = l_2^2 = (l_2 + p_4)^2 &= 0, \\
(l_3 - p_5)^2 = l_3^2 = (l_3 + p_6)^2 &= 0, \\
(l_1 + p_2 - l_2 + p_3)^2 &= 0, \\
(l_2 + p_4 - l_3 + p_5)^2 &= 0, \\
(l_3 + p_6 - l_1 + p_1)^2 &= 0.
\end{aligned} \tag{4.4}$$

So far we have not needed to commit to any particular spacetime dimension. We now fix $D = 4$, which simplifies the analysis because for generic p_i there are precisely 16 discrete solutions for the l_r 's, which we denote by $l_r^*(p_i)$. To enumerate and explicitly exhibit these solutions it is technically helpful to parameterize the momenta in terms of momentum twistor variables [55], in which case the solutions can be associated with on-shell diagrams as described in [3]. Although so far the analysis is still applicable to

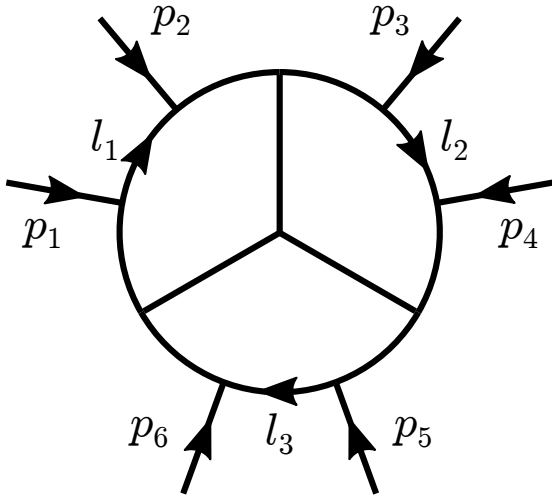


FIGURE 4.4: The three-loop six-particle wheel graph. The leading first-type Landau singularities of this graph exhaust all possible first-type Landau singularities of six-particle amplitudes in any massless planar field theory, to any finite loop order.

general massless planar theories, we note that in the special context of SYM theory, two cut solutions have MHV support, twelve NMHV, and two NNMHV.

With these solutions in hand, we next turn our attention to the Kirchhoff conditions

$$\begin{aligned}
 0 &= \alpha_1(l_1 - p_1) + \alpha_2 l_1 + \alpha_3(l_1 + p_2) + \\
 &\quad \alpha_{10}(l_3 + p_6 - l_1 + p_1) + \alpha_{11}(l_1 + p_2 - l_2 + p_3), \\
 0 &= \alpha_4(l_2 - p_3) + \alpha_5 l_2 + \alpha_6(l_2 + p_4) + \\
 &\quad \alpha_{11}(l_1 + p_2 - l_2 + p_3) + \alpha_{12}(l_2 + p_4 - l_3 + p_5), \\
 0 &= \alpha_7(l_3 - p_5) + \alpha_8 l_3 + \alpha_9(l_3 + p_6) + \\
 &\quad \alpha_{12}(l_2 + p_4 - l_3 + p_5) + \alpha_{10}(l_3 + p_6 - l_1 + p_1).
 \end{aligned} \tag{4.5}$$

Nontrivial solutions to this 12×12 linear system exist only if the associated *Kirchhoff determinant* $K(p_i, l_r)$ vanishes. By evaluating this determinant on each of the solutions $l_r = l_r^*(p_i)$ the condition for the existence of a non-trivial solution to the Landau equations can be expressed entirely in terms of the external momenta p_i . Using variables u, v, w, y_u, y_v, y_w that are very familiar in the literature on six-particle amplitudes (their definition in terms of the p_i 's can be found for example in [20]), we find that

$K(p_i, l_r^*(p_i)) = 0$ can only be satisfied if an element of the set

$$S_6 = \{u, v, w, 1-u, 1-v, 1-w, \frac{1}{u}, \frac{1}{v}, \frac{1}{w}\} \quad (4.6)$$

vanishes. We conclude that the three-loop $n = 6$ wheel graph has first-type Landau singularities on the locus

$$\mathcal{S}_6 \equiv \bigcup_{s \in S_6} \{s = 0\}. \quad (4.7)$$

It is straightforward, if somewhat tedious, to analyze all *subleading* Landau singularities corresponding to relaxations, as defined above. We refer the reader to [16, 17, 47] where this type of analysis has been carried out in detail in several examples. We find no additional first-type singularities beyond those that appear at leading order. Let us emphasize that this unusual feature does not occur for any of the examples in [16, 17, 47], which typically have many additional subleading singularities.

To summarize, we conclude that any six-particle amplitude in any four-dimensional massless planar field theory, at any finite loop order, can have first-type Landau singularities only on the locus \mathcal{S}_6 given by Eqs. (4.6) and (4.7), or a proper subset thereof.

4.5 Second-Type Singularities

The first-type Landau singularities that we have classified, which by definition are those encapsulated in the Landau equations (4.1), (4.2), do not exhaust all possible singularities of amplitudes in general quantum field theories. There also exist “second-type” singularities (see for example [58, 33]) which are sometimes called “non-Landauian” [27]. These arise in Feynman loop integrals as pinch singularities at infinite loop momentum and must be analyzed by a modified version of Eqs. (4.1), (4.2).

In the next section we turn our attention to the special case of SYM theory, which possesses a remarkable *dual conformal symmetry* [94, 95, 76] implying that there is no invariant notion of “infinity” in momentum space. As pointed out in [16], we therefore

expect that second-type singularities should be absent in any dual conformal invariant theory. Because ziggurat graphs are manifestly dual conformal invariant when $D = 4$, this would imply that the first-type Landau singularities of the ziggurat graphs should capture the entire “dual conformally invariant part” of the singularity structure of all massless planar theories in four spacetime dimensions. By this we mean, somewhat more precisely, the singularity loci that do not involve the infinity twistor.

4.6 Planar SYM Theory

In Sec. 4.3 we acknowledged that in certain special theories, the actual set of singularities of amplitudes may be strictly smaller than that of the ziggurat graphs due to cancellations. SYM theory has been shown to possess such rich mathematical structure that it would seem the most promising candidate to exhibit such cancellations. Contrary to this expectation, we now argue that:

Perturbative amplitudes in SYM theory exhibit first-type Landau singularities on *all* such loci that are possible in any massless planar field theory.

Moreover, our results suggest that this all-order statement is true separately in each helicity sector. Specifically: for any fixed n and any $0 \leq k \leq n - 4$, there is a finite value of $L_{n,k}$ such that the singularity locus of the L -loop n -particle N^k MHV amplitude is identical to that of the n -particle ziggurat graph for all $L \geq L_{n,k}$. In order to verify this claim, it suffices to construct an n -particle on-shell diagram with N^k MHV support that has the same Landau singularities as the n -particle ziggurat graph; or (conjecturally) equivalently, to write down an appropriate valid configuration of lines inside the amplituhedron [4] $\mathcal{A}_{n,k,L}$ for some sufficiently high L .

To see that this is plausible, note that in general the appearance of a given singularity at some fixed k and L can be shown to imply the existence of the same singularity at lower k but higher L by performing the opposite of a parallel reduction—doubling one or more edges of the relevant Landau graph to make bubbles (see for example Fig. 2 of [47]). For example, while one-loop MHV amplitudes do not have singularities of

three-mass box type, it is known by explicit computation [60] that two-loop MHV amplitudes do. Similarly, while two-loop MHV amplitudes do not have singularities of four-mass box type, we expect that three-loop MHV and two-loop NMHV amplitudes do. (To be clear, our analysis is silent on the question of whether the symbol alphabets of these amplitudes contain square roots; see the discussion in Sec. 7 of [53].)

It is indeed simple to check that the n -particle ziggurat graph can be converted into a valid on-shell diagram with MHV support by doubling *each* internal edge to form a bubble. Moreover, in this manner it is relatively simple to write an explicit mutually positive configuration of positive lines inside the MHV amplituhedron. However, we note that while this construction is sufficient to demonstrate the claim, it is certainly overkill; we expect MHV support to be reached at much lower loop level than this argument would require, as can be checked on a case by case basis for relatively small n .

4.7 Symbol Alphabets

Let us comment on the connection of our work to symbol alphabets. In general, the presence of some letter a in the symbol of an amplitude indicates that there exists some sheet on which the analytically continued amplitude has a branch cut from $a = 0$ to $a = \infty$. The symbols of all known six-particle amplitudes in SYM theory can be expressed in terms of a nine-letter alphabet [67] which may be chosen as [69]

$$A_6 = \{u, v, w, 1-u, 1-v, 1-w, y_u, y_v, y_w\}, \quad (4.8)$$

where $z = \{y_u, 1/y_u\}$ are the two roots of

$$u(1-v)(1-w)(z^2+1) = [u^2 - 2uvw + (1-v-w)^2] z \quad (4.9)$$

and y_v and y_w are defined by cycling $u \rightarrow v \rightarrow w \rightarrow u$. It is evident from Eq. (4.9) that y_u can attain the value 0 or ∞ only if $u = 0$ or $v = 1$ or $w = 1$. We therefore see that the singularity locus encoded in the hexagon alphabet A_6 is precisely equivalent to \mathcal{S}_6 given

by Eqs. (4.6) and (4.7). Indeed, the hypothesis that six-particle amplitudes in SYM theory do not exhibit singularities on any other loci at any higher loop order (which we now consider to be proven), and the apparently much stronger ansatz that the nine quantities shown in Eq. (4.8) provide a symbol alphabet for all such amplitudes, lies at the heart of a bootstrap program that has made possible impressive explicit computations to high loop order (see for example [69, 96, 70, 14, 72, 73, 20]). An analogous ansatz for $n = 7$ has similarly allowed for the computation of symbols of seven-particle amplitudes [21, 22].

Unfortunately, as the y_u, y_v, y_w letters demonstrate, the connection between Landau singularity loci and symbol alphabets is somewhat indirect. It is not possible to derive A_6 from \mathcal{S}_6 alone as knowledge of the latter only tells us about the locus where symbol letters vanish [23] or have branch points (see Sec. 7 of [53]). In order to determine what the symbol letters actually are away from these loci it seems necessary to invoke some other kind of structure; for example, cluster algebras may have a role to play here [18, 19].

4.8 Conclusion

We leave a number of open questions for future work. What is the minimum loop order L_n to which the n -particle ziggurat graph can be reduced? Can one characterize its Landau singularities for arbitrary n , generalizing the result for $n = 6$ in Sec. 4.4? Does there exist a similar framework for classifying second-type singularities, even if only in certain theories? The graph moves reviewed in Sec. 4.2 preserve the (sets of solutions to the) Landau equations even for non-planar graphs; are there results on non-planar Y - Δ reducibility (see for example [97, 98]) that may be useful for non-planar (but still massless) theories?

In Sec. 4.4 we saw that the wheel is a rather remarkable graph. The ziggurat graphs, and those to which they can be reduced, might warrant further study for their own sake. Intriguingly they generalize those studied in [99, 100] and are particular cases of the graphs that have attracted recent interest, for example in [101, 102], in the context of

“fishnet” theories. We have only looked at their singularity loci; it would be interesting to explore the structure of their cuts, perhaps in connection with the coaction studied in [30, 103, 104, 105, 106].

In the special case of SYM theory the technology might exist to address more detailed questions. For general n and k , what is the minimum loop order $L_{n,k}$ at which the Landau singularities of the n -particle N^k MHV amplitude saturate? Is there a direct connection between Landau singularities, zigurat graphs, and cluster algebras? For amplitudes of generalized polylogarithm type, now that we know (in principle) the relevant singularity loci, what are the actual symbol letters for general n , and can the symbol alphabet depend on k (even though the singularity loci do not)? How do Landau singularities manifest themselves in general amplitudes that are of more complicated (non-polylogarithmic) functional type?

Bibliography

- [1] Lars Brink, John H. Schwarz, and Joel Scherk. “Supersymmetric Yang-Mills Theories”. In: *Nucl. Phys.* B121 (1977), pp. 77–92. DOI: [10.1016/0550-3213\(77\)90328-5](https://doi.org/10.1016/0550-3213(77)90328-5).
- [2] Nima Arkani-Hamed et al. “The All-Loop Integrand For Scattering Amplitudes in Planar N=4 SYM”. In: *JHEP* 01 (2011), p. 041. DOI: [10.1007/JHEP01\(2011\)041](https://doi.org/10.1007/JHEP01(2011)041). arXiv: [1008.2958](https://arxiv.org/abs/1008.2958) [hep-th].
- [3] Nima Arkani-Hamed et al. *Grassmannian Geometry of Scattering Amplitudes*. Cambridge University Press, 2016. ISBN: 9781107086586, 9781316572962. DOI: [10.1017/CB09781316091548](https://doi.org/10.1017/CB09781316091548). arXiv: [1212.5605](https://arxiv.org/abs/1212.5605) [hep-th]. URL: <http://www.cambridge.org/us/academic/subjects/physics/theoretical-physics-and-mathematical-physics/grassmannian-geometry-scattering-amplitudes?format=HB&isbn=9781107086586>.
- [4] Nima Arkani-Hamed and Jaroslav Trnka. “The Amplituhedron”. In: *JHEP* 10 (2014), p. 030. DOI: [10.1007/JHEP10\(2014\)030](https://doi.org/10.1007/JHEP10(2014)030). arXiv: [1312.2007](https://arxiv.org/abs/1312.2007) [hep-th].
- [5] Nima Arkani-Hamed and Jaroslav Trnka. “Into the Amplituhedron”. In: *JHEP* 12 (2014), p. 182. DOI: [10.1007/JHEP12\(2014\)182](https://doi.org/10.1007/JHEP12(2014)182). arXiv: [1312.7878](https://arxiv.org/abs/1312.7878) [hep-th].
- [6] Yuntao Bai and Song He. “The Amplituhedron from Momentum Twistor Diagrams”. In: *JHEP* 02 (2015), p. 065. DOI: [10.1007/JHEP02\(2015\)065](https://doi.org/10.1007/JHEP02(2015)065). arXiv: [1408.2459](https://arxiv.org/abs/1408.2459) [hep-th].
- [7] Sebastian Franco et al. “Anatomy of the Amplituhedron”. In: *JHEP* 03 (2015), p. 128. DOI: [10.1007/JHEP03\(2015\)128](https://doi.org/10.1007/JHEP03(2015)128). arXiv: [1408.3410](https://arxiv.org/abs/1408.3410) [hep-th].

- [8] Thomas Lam. “Amplituhedron cells and Stanley symmetric functions”. In: *Commun. Math. Phys.* 343.3 (2016), pp. 1025–1037. DOI: [10.1007/s00220-016-2602-2](https://doi.org/10.1007/s00220-016-2602-2). arXiv: [1408.5531](https://arxiv.org/abs/1408.5531) [math.AG].
- [9] Nima Arkani-Hamed, Andrew Hodges, and Jaroslav Trnka. “Positive Amplitudes In The Amplituhedron”. In: *JHEP* 08 (2015), p. 030. DOI: [10.1007/JHEP08\(2015\)030](https://doi.org/10.1007/JHEP08(2015)030). arXiv: [1412.8478](https://arxiv.org/abs/1412.8478) [hep-th].
- [10] Yuntao Bai, Song He, and Thomas Lam. “The Amplituhedron and the One-loop Grassmannian Measure”. In: *JHEP* 01 (2016), p. 112. DOI: [10.1007/JHEP01\(2016\)112](https://doi.org/10.1007/JHEP01(2016)112). arXiv: [1510.03553](https://arxiv.org/abs/1510.03553) [hep-th].
- [11] Livia Ferro et al. “Towards the Amplituhedron Volume”. In: *JHEP* 03 (2016), p. 014. DOI: [10.1007/JHEP03\(2016\)014](https://doi.org/10.1007/JHEP03(2016)014). arXiv: [1512.04954](https://arxiv.org/abs/1512.04954) [hep-th].
- [12] Zvi Bern et al. “Evidence for a Nonplanar Amplituhedron”. In: *JHEP* 06 (2016), p. 098. DOI: [10.1007/JHEP06\(2016\)098](https://doi.org/10.1007/JHEP06(2016)098). arXiv: [1512.08591](https://arxiv.org/abs/1512.08591) [hep-th].
- [13] Daniele Galloni. “Positivity Sectors and the Amplituhedron”. In: (2016). arXiv: [1601.02639](https://arxiv.org/abs/1601.02639) [hep-th].
- [14] Lance J. Dixon et al. “Bootstrapping six-gluon scattering in planar N=4 super-Yang-Mills theory”. In: *PoS LL2014* (2014), p. 077. DOI: [10.22323/1.211.0077](https://doi.org/10.22323/1.211.0077). arXiv: [1407.4724](https://arxiv.org/abs/1407.4724) [hep-th].
- [15] John Golden and Marcus Spradlin. “A Cluster Bootstrap for Two-Loop MHV Amplitudes”. In: *JHEP* 02 (2015), p. 002. DOI: [10.1007/JHEP02\(2015\)002](https://doi.org/10.1007/JHEP02(2015)002). arXiv: [1411.3289](https://arxiv.org/abs/1411.3289) [hep-th].
- [16] Tristan Dennen, Marcus Spradlin, and Anastasia Volovich. “Landau Singularities and Symbolology: One- and Two-loop MHV Amplitudes in SYM Theory”. In: *JHEP* 03 (2016), p. 069. DOI: [10.1007/JHEP03\(2016\)069](https://doi.org/10.1007/JHEP03(2016)069). arXiv: [1512.07909](https://arxiv.org/abs/1512.07909) [hep-th].
- [17] Tristan Dennen et al. “Landau Singularities from the Amplituhedron”. In: *JHEP* 06 (2017), p. 152. DOI: [10.1007/JHEP06\(2017\)152](https://doi.org/10.1007/JHEP06(2017)152). arXiv: [1612.02708](https://arxiv.org/abs/1612.02708) [hep-th].

- [18] John Golden et al. “Motivic Amplitudes and Cluster Coordinates”. In: *JHEP* 01 (2014), p. 091. DOI: [10.1007/JHEP01\(2014\)091](https://doi.org/10.1007/JHEP01(2014)091). arXiv: [1305.1617](https://arxiv.org/abs/1305.1617) [hep-th].
- [19] James Drummond, Jack Foster, and Ömer Gürdoğan. “Cluster Adjacency Properties of Scattering Amplitudes in $N = 4$ Supersymmetric Yang-Mills Theory”. In: *Phys. Rev. Lett.* 120.16 (2018), p. 161601. DOI: [10.1103/PhysRevLett.120.161601](https://doi.org/10.1103/PhysRevLett.120.161601). arXiv: [1710.10953](https://arxiv.org/abs/1710.10953) [hep-th].
- [20] Simon Caron-Huot et al. “Bootstrapping a Five-Loop Amplitude Using Steinmann Relations”. In: *Phys. Rev. Lett.* 117.24 (2016), p. 241601. DOI: [10.1103/PhysRevLett.117.241601](https://doi.org/10.1103/PhysRevLett.117.241601). arXiv: [1609.00669](https://arxiv.org/abs/1609.00669) [hep-th].
- [21] James M. Drummond, Georgios Papathanasiou, and Marcus Spradlin. “A Symbol of Uniqueness: The Cluster Bootstrap for the 3-Loop MHV Heptagon”. In: *JHEP* 03 (2015), p. 072. DOI: [10.1007/JHEP03\(2015\)072](https://doi.org/10.1007/JHEP03(2015)072). arXiv: [1412.3763](https://arxiv.org/abs/1412.3763) [hep-th].
- [22] Lance J. Dixon et al. “Heptagons from the Steinmann Cluster Bootstrap”. In: *JHEP* 02 (2017), p. 137. DOI: [10.1007/JHEP02\(2017\)137](https://doi.org/10.1007/JHEP02(2017)137). arXiv: [1612.08976](https://arxiv.org/abs/1612.08976) [hep-th].
- [23] Juan Maldacena, David Simmons-Duffin, and Alexander Zhiboedov. “Looking for a bulk point”. In: *JHEP* 01 (2017), p. 013. DOI: [10.1007/JHEP01\(2017\)013](https://doi.org/10.1007/JHEP01(2017)013). arXiv: [1509.03612](https://arxiv.org/abs/1509.03612) [hep-th].
- [24] S. Mandelstam. “Determination of the pion - nucleon scattering amplitude from dispersion relations and unitarity. General theory”. In: *Phys. Rev.* 112 (1958), pp. 1344–1360. DOI: [10.1103/PhysRev.112.1344](https://doi.org/10.1103/PhysRev.112.1344).
- [25] Stanley Mandelstam. “Analytic properties of transition amplitudes in perturbation theory”. In: *Phys. Rev.* 115 (1959), pp. 1741–1751. DOI: [10.1103/PhysRev.115.1741](https://doi.org/10.1103/PhysRev.115.1741).
- [26] L. D. Landau. “On analytic properties of vertex parts in quantum field theory”. In: *Nucl. Phys.* 13 (1959), pp. 181–192. DOI: [10.1016/0029-5582\(59\)90154-3](https://doi.org/10.1016/0029-5582(59)90154-3).

- [27] R. E. Cutkosky. “Singularities and discontinuities of Feynman amplitudes”. In: *J. Math. Phys.* 1 (1960), pp. 429–433. DOI: [10.1063/1.1703676](https://doi.org/10.1063/1.1703676).
- [28] Zvi Bern et al. “Fusing gauge theory tree amplitudes into loop amplitudes”. In: *Nucl. Phys. B* 435 (1995), pp. 59–101. DOI: [10.1016/0550-3213\(94\)00488-Z](https://doi.org/10.1016/0550-3213(94)00488-Z). arXiv: [hep-ph/9409265](https://arxiv.org/abs/hep-ph/9409265) [hep-ph].
- [29] Zvi Bern, Lance J. Dixon, and David A. Kosower. “Progress in one loop QCD computations”. In: *Ann. Rev. Nucl. Part. Sci.* 46 (1996), pp. 109–148. DOI: [10.1146/annurev.nucl.46.1.109](https://doi.org/10.1146/annurev.nucl.46.1.109). arXiv: [hep-ph/9602280](https://arxiv.org/abs/hep-ph/9602280) [hep-ph].
- [30] Samuel Abreu et al. “From multiple unitarity cuts to the coproduct of Feynman integrals”. In: *JHEP* 10 (2014), p. 125. DOI: [10.1007/JHEP10\(2014\)125](https://doi.org/10.1007/JHEP10(2014)125). arXiv: [1401.3546](https://arxiv.org/abs/1401.3546) [hep-th].
- [31] Samuel Abreu, Ruth Britto, and Hanna Grönqvist. “Cuts and coproducts of massive triangle diagrams”. In: *JHEP* 07 (2015), p. 111. DOI: [10.1007/JHEP07\(2015\)111](https://doi.org/10.1007/JHEP07(2015)111). arXiv: [1504.00206](https://arxiv.org/abs/1504.00206) [hep-th].
- [32] Nima Arkani-Hamed et al. “Local Integrals for Planar Scattering Amplitudes”. In: *JHEP* 06 (2012), p. 125. DOI: [10.1007/JHEP06\(2012\)125](https://doi.org/10.1007/JHEP06(2012)125). arXiv: [1012.6032](https://arxiv.org/abs/1012.6032) [hep-th].
- [33] R. J. Eden et al. *The Analytic S-Matrix*. Cambridge University Press, 1966.
- [34] Freddy Cachazo, Peter Svrcek, and Edward Witten. “MHV vertices and tree amplitudes in gauge theory”. In: *JHEP* 09 (2004), p. 006. DOI: [10.1088/1126-6708/2004/09/006](https://doi.org/10.1088/1126-6708/2004/09/006). arXiv: [hep-th/0403047](https://arxiv.org/abs/hep-th/0403047) [hep-th].
- [35] Ruth Britto et al. “Direct proof of tree-level recursion relation in Yang-Mills theory”. In: *Phys. Rev. Lett.* 94 (2005), p. 181602. DOI: [10.1103/PhysRevLett.94.181602](https://doi.org/10.1103/PhysRevLett.94.181602). arXiv: [hep-th/0501052](https://arxiv.org/abs/hep-th/0501052) [hep-th].
- [36] Henriette Elvang and Yu-tin Huang. “Scattering Amplitudes”. In: (2013). arXiv: [1308.1697](https://arxiv.org/abs/1308.1697) [hep-th].

- [37] Nima Arkani-Hamed, Hugh Thomas, and Jaroslav Trnka. “Unwinding the Amplituhedron in Binary”. In: *JHEP* 01 (2018), p. 016. DOI: [10.1007/JHEP01\(2018\)016](https://doi.org/10.1007/JHEP01(2018)016). arXiv: [1704.05069](https://arxiv.org/abs/1704.05069) [hep-th].
- [38] Gerard 't Hooft and M. J. G. Veltman. “Scalar One Loop Integrals”. In: *Nucl. Phys.* B153 (1979), pp. 365–401. DOI: [10.1016/0550-3213\(79\)90605-9](https://doi.org/10.1016/0550-3213(79)90605-9).
- [39] Zvi Bern, Lance J. Dixon, and David A. Kosower. “Dimensionally regulated pentagon integrals”. In: *Nucl. Phys.* B412 (1994), pp. 751–816. DOI: [10.1016/0550-3213\(94\)90398-0](https://doi.org/10.1016/0550-3213(94)90398-0). arXiv: [hep-ph/9306240](https://arxiv.org/abs/hep-ph/9306240) [hep-ph].
- [40] Zvi Bern et al. “One loop n point gauge theory amplitudes, unitarity and collinear limits”. In: *Nucl. Phys.* B425 (1994), pp. 217–260. DOI: [10.1016/0550-3213\(94\)90179-1](https://doi.org/10.1016/0550-3213(94)90179-1). arXiv: [hep-ph/9403226](https://arxiv.org/abs/hep-ph/9403226) [hep-ph].
- [41] Zvi Bern et al. “One loop gauge theory amplitudes with an arbitrary number of external legs”. In: *Workshop on Continuous Advances in QCD Minneapolis, Minnesota, February 18-20, 1994*. 1994, pp. 3–21. arXiv: [hep-ph/9405248](https://arxiv.org/abs/hep-ph/9405248) [hep-ph]. URL: <http://www-public.slac.stanford.edu/sciDoc/docMeta.aspx?slacPubNumber=SLAC-PUB-6490>.
- [42] Andreas Brandhuber, Bill J. Spence, and Gabriele Travaglini. “One-loop gauge theory amplitudes in N=4 super Yang-Mills from MHV vertices”. In: *Nucl. Phys.* B706 (2005), pp. 150–180. DOI: [10.1016/j.nuclphysb.2004.11.023](https://doi.org/10.1016/j.nuclphysb.2004.11.023). arXiv: [hep-th/0407214](https://arxiv.org/abs/hep-th/0407214) [hep-th].
- [43] Zvi Bern et al. “All non-maximally-helicity-violating one-loop seven-gluon amplitudes in N=4 super-yang-Mills theory”. In: *Phys. Rev.* D71 (2005), p. 045006. DOI: [10.1103/PhysRevD.71.045006](https://doi.org/10.1103/PhysRevD.71.045006). arXiv: [hep-th/0410224](https://arxiv.org/abs/hep-th/0410224) [hep-th].
- [44] Ruth Britto, Freddy Cachazo, and Bo Feng. “Generalized unitarity and one-loop amplitudes in N=4 super-Yang-Mills”. In: *Nucl. Phys.* B725 (2005), pp. 275–305. DOI: [10.1016/j.nuclphysb.2005.07.014](https://doi.org/10.1016/j.nuclphysb.2005.07.014). arXiv: [hep-th/0412103](https://arxiv.org/abs/hep-th/0412103) [hep-th].
- [45] Zvi Bern, Lance J. Dixon, and David A. Kosower. “All Next-to-maximally-helicity-violating one-loop gluon amplitudes in N=4 super-Yang-Mills theory”. In: *Phys.*

- Rev. D* 72 (2005), p. 045014. DOI: [10.1103/PhysRevD.72.045014](https://doi.org/10.1103/PhysRevD.72.045014). arXiv: [hep-th/0412210](https://arxiv.org/abs/hep-th/0412210) [[hep-th](#)].
- [46] R. Keith Ellis and Giulia Zanderighi. “Scalar one-loop integrals for QCD”. In: *JHEP* 02 (2008), p. 002. DOI: [10.1088/1126-6708/2008/02/002](https://doi.org/10.1088/1126-6708/2008/02/002). arXiv: [0712.1851](https://arxiv.org/abs/0712.1851) [[hep-ph](#)].
- [47] Igor Prlina et al. “Boundaries of Amplituhedra and NMHV Symbol Alphabets at Two Loops”. In: *JHEP* 04 (2018), p. 049. DOI: [10.1007/JHEP04\(2018\)049](https://doi.org/10.1007/JHEP04(2018)049). arXiv: [1712.08049](https://arxiv.org/abs/1712.08049) [[hep-th](#)].
- [48] Jon Mathews. “Application of Linear Network Analysis to Feynman Diagrams”. In: *Phys. Rev.* 113 (1959), pp. 381–381. DOI: [10.1103/PhysRev.113.381](https://doi.org/10.1103/PhysRev.113.381).
- [49] Tai Tsun Wu. “Domains of Definition for Feynman Integrals over Real Feynman Parameters”. In: *Phys. Rev.* 123 (1961), pp. 678–689. DOI: [10.1103/PhysRev.123.678](https://doi.org/10.1103/PhysRev.123.678).
- [50] T. T. Wu. “Properties of Normal Thresholds in Perturbation Theory”. In: *Phys. Rev.* 123 (1961), pp. 689–691. DOI: [10.1103/PhysRev.123.689](https://doi.org/10.1103/PhysRev.123.689).
- [51] R. Bjorken and S. Drell. *Relativistic Quantum Fields*. McGraw-Hill, 1965.
- [52] Isidoro Gitler. *Delta-wye-delta transformations: algorithms and applications*. Ph.D. Thesis, University of Waterloo, 1991.
- [53] Igor Prlina et al. “All-Helicity Symbol Alphabets from Unwound Amplituhedra”. In: *JHEP* 05 (2018), p. 159. DOI: [10.1007/JHEP05\(2018\)159](https://doi.org/10.1007/JHEP05(2018)159). arXiv: [1711.11507](https://arxiv.org/abs/1711.11507) [[hep-th](#)].
- [54] Igor Prlina, Marcus Spradlin, and Stefan Stanojevic. “All-loop singularities of scattering amplitudes in massless planar theories”. In: *Phys. Rev. Lett.* 121.8 (2018), p. 081601. DOI: [10.1103/PhysRevLett.121.081601](https://doi.org/10.1103/PhysRevLett.121.081601). arXiv: [1805.11617](https://arxiv.org/abs/1805.11617) [[hep-th](#)].
- [55] Andrew Hodges. “Eliminating spurious poles from gauge-theoretic amplitudes”. In: *JHEP* 05 (2013), p. 135. DOI: [10.1007/JHEP05\(2013\)135](https://doi.org/10.1007/JHEP05(2013)135). arXiv: [0905.1473](https://arxiv.org/abs/0905.1473) [[hep-th](#)].

- [56] S. Coleman and R. E. Norton. “Singularities in the physical region”. In: *Nuovo Cim.* 38 (1965), pp. 438–442. DOI: [10.1007/BF02750472](https://doi.org/10.1007/BF02750472).
- [57] Stephen J. Parke and T. R. Taylor. “An Amplitude for n Gluon Scattering”. In: *Phys. Rev. Lett.* 56 (1986), p. 2459. DOI: [10.1103/PhysRevLett.56.2459](https://doi.org/10.1103/PhysRevLett.56.2459).
- [58] D. B. Fairlie et al. “Singularities of the Second Type”. In: *J. Math. Phys.* 3 (1962), p. 594. DOI: [10.1063/1.1724262](https://doi.org/10.1063/1.1724262).
- [59] D. B. Fairlie et al. “Physical sheet properties of second type singularities”. In: *Phys. Lett.* 3 (1962), p. 55. DOI: [10.1016/0031-9163\(62\)90200-7](https://doi.org/10.1016/0031-9163(62)90200-7).
- [60] S. Caron-Huot. “Superconformal symmetry and two-loop amplitudes in planar $N=4$ super Yang-Mills”. In: *JHEP* 12 (2011), p. 066. DOI: [10.1007/JHEP12\(2011\)066](https://doi.org/10.1007/JHEP12(2011)066). arXiv: [1105.5606](https://arxiv.org/abs/1105.5606) [hep-th].
- [61] Jacob L. Bourjaily and Jaroslav Trnka. “Local Integrand Representations of All Two-Loop Amplitudes in Planar SYM”. In: *JHEP* 08 (2015), p. 119. DOI: [10.1007/JHEP08\(2015\)119](https://doi.org/10.1007/JHEP08(2015)119). arXiv: [1505.05886](https://arxiv.org/abs/1505.05886) [hep-th].
- [62] Tristan Dennen. “Unpublished Notes”. In: ().
- [63] Zvi Bern, Lance J. Dixon, and Vladimir A. Smirnov. “Iteration of planar amplitudes in maximally supersymmetric Yang-Mills theory at three loops and beyond”. In: *Phys. Rev. D* 72 (2005), p. 085001. DOI: [10.1103/PhysRevD.72.085001](https://doi.org/10.1103/PhysRevD.72.085001). arXiv: [hep-th/0505205](https://arxiv.org/abs/hep-th/0505205) [hep-th].
- [64] Arthur E. Lipstein and Lionel Mason. “From d logs to dilogs the super Yang-Mills MHV amplitude revisited”. In: *JHEP* 01 (2014), p. 169. DOI: [10.1007/JHEP01\(2014\)169](https://doi.org/10.1007/JHEP01(2014)169). arXiv: [1307.1443](https://arxiv.org/abs/1307.1443) [hep-th].
- [65] K Chen. “Iterated path integrals”. In: *Bull. Amer. Math. Soc.* 83 (1977), pp. 831–879. DOI: [10.1090/S0002-9904-1977-14320-6](https://doi.org/10.1090/S0002-9904-1977-14320-6). eprint: [1008.2958](https://arxiv.org/abs/1008.2958).
- [66] A. B. Goncharov. “A simple construction of Grassmannian polylogarithms”. In: *arXiv:0908.2238v2 [math.AG]* (2009).

- [67] Alexander B. Goncharov et al. "Classical Polylogarithms for Amplitudes and Wilson Loops". In: *Phys. Rev. Lett.* 105 (2010), p. 151605. DOI: [10.1103/PhysRevLett.105.151605](https://doi.org/10.1103/PhysRevLett.105.151605). arXiv: [1006.5703](https://arxiv.org/abs/1006.5703) [hep-th].
- [68] Davide Gaiotto et al. "Pulling the straps of polygons". In: *JHEP* 12 (2011), p. 011. DOI: [10.1007/JHEP12\(2011\)011](https://doi.org/10.1007/JHEP12(2011)011). arXiv: [1102.0062](https://arxiv.org/abs/1102.0062) [hep-th].
- [69] Lance J. Dixon, James M. Drummond, and Johannes M. Henn. "Bootstrapping the three-loop hexagon". In: *JHEP* 11 (2011), p. 023. DOI: [10.1007/JHEP11\(2011\)023](https://doi.org/10.1007/JHEP11(2011)023). arXiv: [1108.4461](https://arxiv.org/abs/1108.4461) [hep-th].
- [70] Lance J. Dixon et al. "Hexagon functions and the three-loop remainder function". In: *JHEP* 12 (2013), p. 049. DOI: [10.1007/JHEP12\(2013\)049](https://doi.org/10.1007/JHEP12(2013)049). arXiv: [1308.2276](https://arxiv.org/abs/1308.2276) [hep-th].
- [71] Lance J. Dixon et al. "The four-loop remainder function and multi-Regge behavior at NNLLA in planar $N = 4$ super-Yang-Mills theory". In: *JHEP* 06 (2014), p. 116. DOI: [10.1007/JHEP06\(2014\)116](https://doi.org/10.1007/JHEP06(2014)116). arXiv: [1402.3300](https://arxiv.org/abs/1402.3300) [hep-th].
- [72] Lance J. Dixon and Matt von Hippel. "Bootstrapping an NMHV amplitude through three loops". In: *JHEP* 10 (2014), p. 065. DOI: [10.1007/JHEP10\(2014\)065](https://doi.org/10.1007/JHEP10(2014)065). arXiv: [1408.1505](https://arxiv.org/abs/1408.1505) [hep-th].
- [73] Lance J. Dixon, Matt von Hippel, and Andrew J. McLeod. "The four-loop six-gluon NMHV ratio function". In: *JHEP* 01 (2016), p. 053. DOI: [10.1007/JHEP01\(2016\)053](https://doi.org/10.1007/JHEP01(2016)053). arXiv: [1509.08127](https://arxiv.org/abs/1509.08127) [hep-th].
- [74] V. P. Nair. "A Current Algebra for Some Gauge Theory Amplitudes". In: *Phys. Lett. B* 214 (1988), p. 215. DOI: [10.1016/0370-2693\(88\)91471-2](https://doi.org/10.1016/0370-2693(88)91471-2).
- [75] L. F. Alday, D. Gaiotto, and J. Maldacena. "Thermodynamic Bubble Ansatz". In: *JHEP* 32 (1962), p. 1109. DOI: [10.1007/JHEP09\(2011\)032](https://doi.org/10.1007/JHEP09(2011)032).
- [76] J. M. Drummond et al. "Dual superconformal symmetry of scattering amplitudes in $N=4$ super-Yang-Mills theory". In: *Nucl. Phys. B* 317 (2010), p. 828. DOI: [10.1016/j.nuclphysb.2009.11.022](https://doi.org/10.1016/j.nuclphysb.2009.11.022).

- [77] G. F. Sterman and M. E. Tejeda-Yeomans. “Multiloop amplitudes and resummation”. In: *Phys. Lett. B* 48 (2003), p. 552. DOI: [10.1016/S0370-2693\(02\)03100-3](https://doi.org/10.1016/S0370-2693(02)03100-3).
- [78] J. L. Bourjaily, S. Caron-Huot, and J. Trnka. “Dual-Conformal Regularization of Infrared Loop Divergences and the Chiral Box Expansion”. In: *JHEP* 1 (2015), p. 1501. DOI: [10.1007/JHEP01\(2015\)001](https://doi.org/10.1007/JHEP01(2015)001).
- [79] D. A. Kosower, R. Roiban, and C. Vergu. “The Six-Point NMHV amplitude in Maximally Supersymmetric Yang-Mills Theory”. In: *Phys. Rev. D* 83 (2011). DOI: [10.1103/PhysRevD.83.065018](https://doi.org/10.1103/PhysRevD.83.065018).
- [80] S. N. Karp, L. K. Williams, and Y. X. Zhang. “Decompositions of amplituhedra”. In: *arXiv:1708.09525 [math.CO]* (2017).
- [81] J. L. Bourjaily, E. Hermann, and J. Trnka. “Prescriptive Unitarity”. In: *JHEP* 59 (2017), p. 1706. DOI: [10.1007/JHEP06\(2017\)059](https://doi.org/10.1007/JHEP06(2017)059). arXiv: [1704.05460 \[hep-th\]](https://arxiv.org/abs/1704.05460).
- [82] N. Arkani-Hamed et al. “Singularity Structure of Maximally Supersymmetric Scattering Amplitudes”. In: *Phys. Rev. Lett.* 26 (2014), p. 113. DOI: [10.1103/PhysRevLett.113.261603](https://doi.org/10.1103/PhysRevLett.113.261603). arXiv: [1410.0354 \[hep-th\]](https://arxiv.org/abs/1410.0354).
- [83] Z. Bern et al. “Logarithmic Singularities and Maximally Supersymmetric Amplitudes”. In: *JHEP* 202 (2015), p. 1506. DOI: [10.1007/JHEP06\(2015\)202](https://doi.org/10.1007/JHEP06(2015)202). arXiv: [1412.8584 \[hep-th\]](https://arxiv.org/abs/1412.8584).
- [84] Z. Bern et al. “Dual Conformal Symmetry, Integration-by-Parts Reduction, Differential Equations and the Nonplanar Sector”. In: *Phys. Rev. D.* 9 (2017), p. 96. DOI: [doi:10.1103/PhysRevD.96.096017](https://doi.org/10.1103/PhysRevD.96.096017). arXiv: [1709.06055 \[hep-th\]](https://arxiv.org/abs/1709.06055).
- [85] S. Franco et al. “Non-Planar On-Shell Diagrams”. In: *JHEP* 199 (2015), p. 1506. DOI: [doi:10.1007/JHEP06\(2015\)199](https://doi.org/10.1007/JHEP06(2015)199). arXiv: [1502.02034 \[hep-th\]](https://arxiv.org/abs/1502.02034).
- [86] J. L. Bourjaily et al. “Stratifying On-Shell Cluster Varieties: the Geometry of Non-Planar On-Shell Diagrams”. In: *JHEP* 3 (2015), p. 1610. DOI: [10.1007/JHEP10\(2016\)003](https://doi.org/10.1007/JHEP10(2016)003). arXiv: [1607.01781 \[hep-th\]](https://arxiv.org/abs/1607.01781).
- [87] I. Gitler and F. Sagols. “On terminal delta-wye reducibility of planar graphs”. In: *Networks* 57 (2011), p. 174.

- [88] I. Gitler and F. Sagols. "The use of wye-delta transformations in network simplification". In: *Oper. Res.* 8 (1960), p. 311.
- [89] T. A. Feo and J. S. Provan. "Delta-wye transformations and the efficient reduction of two-terminal planar graphs". In: *Oper. Res.* 41 (1993), p. 572.
- [90] Y. C. Verdière, I. Gitler, and D. Vertigan. "Réseaux électriques planaires II". In: *Comment. Math. Helv.* 71 (1996), p. 144.
- [91] D. Archdaecon et al. "Four-terminal reducibility and projective-planar wye-delta-wye-reducible graphs". In: *J. Graph Theory* 33 (2000), p. 83.
- [92] L. Demasi and B. Mohar. "Four terminal planar Delta-Wye reducibility via rooted $K_{2,4}$ minors". In: *Proceedings of the Twenty-Sixth Annual ACM-SIAM Symposium on Discrete Algorithms* (2015), p. 1728.
- [93] A. T. Suzuki. "Correspondence between the one-loop three-point vertex and the Y- and Δ - electric resistor networks". In: *Can. J. Phys.* 92 (2014), p. 131.
- [94] J. M. Drummond et al. "Magic identities for conformal four-point integrals". In: *JHEP* 64 (2007), p. 701.
- [95] L. F. Alday and J. M. Maldacena. "Gluon scattering amplitudes at strong coupling". In: *JHEP* 64 (2007), p. 706.
- [96] L. J. Dixon, J. M. Drummond, and Henn. "Analytic result for the two-loop six-point NMHV amplitude in $N=4$ super Yang-Mills theory". In: *JHEP* 24 (2012), p. 1201.
- [97] D. K. Wagner. "Delta-wye reduction of almost-planar graphs". In: *Discrete Appl. Math.* 158 (2015), p. 180.
- [98] I. Gitler and G. Sandoval-Angeles. "Delta-Wye Transformations and the Efficient Reduction of Almost-Planar Graphs". In: *ENDM* 129 (2017), p. 62.
- [99] J. L. Bourjaily et al. "Elliptic Double-Box Integrals: Massless Scattering Amplitudes beyond Polylogarithms". In: *Phys. Rev. Lett.* 12 (2018), p. 120.

-
- [100] J. L. Bourjaily et al. "Traintracks Through Calabi-Yaus: Amplitudes Beyond Elliptic Polylogarithms". In: *arXiv:1805.09326* (2018).
- [101] D. Chicherin et al. "Yangian Symmetry for Bi-Scalar Loop Amplitudes". In: *JHEP* 3 (2018), p. 1805.
- [102] B. Basso and L. J. Dixon. "Gluing Ladder Feynman Diagrams into Fishnets". In: *Phys. Rev. Lett.* 7 (2017), p. 119.
- [103] S. Abreu et al. "Cuts from residues: the one-loop case". In: *JHEP* 114 (2017), p. 1706.
- [104] S. Abreu et al. "Algebraic Structure of Cut Feynman Integrals and the Diagrammatic Coaction". In: *Phys. Rev. Lett.* 5 (2017), p. 119.
- [105] S. Abreu et al. "Diagrammatic Hopf algebra of cut Feynman integrals: the one-loop case". In: *JHEP* 90 (2017), p. 1712.
- [106] S. Abreu et al. "The diagrammatic coaction and the algebraic structure of cut Feynman integrals". In: *PoS RADCOR 2* (2018), p. 20017.